Implementation of Geostatistical Algorithms and Applications in Geological Media Simulation

(A thesis submitted for the degree of Diploma)

Vasileios Androulakis

DEPARTMENT OF MINERAL RESOURCES ENGINEERING
Technical University of Crete

<u>**Advisory Committee:**</u>

Professor D. T. Hristopoulos (supervisor), Dept. of Mineral Resources Engineering,TUC
Professor M. G. Galetakis, Dept. of Mineral Resources Engineering,TUC
Doctor D. Kourounis, Inst. of Computational Science,Universitá della Svizzera italiana, Switzerland

June, 2017

Acknowledgements

I would like to heartily thank my advising committee: my supervisor Professor D. T. Hristopulos, for the opportunity he gave me to work upon an intriguing topic and for the nice cooperation we have had during this work, Doctor D. Kourounis for the advice he provided me with, along with the Marmousi Model data, and Professor M. G. Galetakis for his usefull comments.

I would also like to express my gratitude to the members of the Geostatistics Laboratory of the Mineral Resources Engineering School of Technical University of Crete Mr Manolis Petrakis, Mrs Vicky Agou and Dr Andrew Pavlides for their invaluable help during this thesis.

Abstract

A commonly encountered problem in Geosciences is that of geological media simulation. The knownledge of the geological stratigraphy and of the physical properties of the strata, e.g. porosity, permeability, velocity of seismic waves, concentration of chemical elements or minerals, is of great importance for many disciplines such as hydrogeology, mining, petroleum engineering, geophysics and environmental restoration. The increasingly sophisticated data acquisition methods provide huge amounts of information about the spatial, temporal or spatiotemporal distribution of such physical attributes. However, they can not provide an extensive and complete image of the spatial distribution of the observable properties. This is due to the fact that such information is only available at a limited number of points which are randomly or regularly distributed in space. The mapping and graphical interpretation of these properties on regular grids in one, two, or three dimensions respectively, is more desirable and helpful.

Geostatistics provides various tools for deriving such maps and graphical interpretations via statistic and stochastic methods. The most widely used geostatistical tools are: i) Kriging and ii) Simulation.

In this thesis, such tools are applied to a geological media simulation problem. More explicitly, a known gridded dataset is sampled, both regularly and randomly, and it is reconstructed with geostatistical tools. Both the regular and the random sample contain 10,16% percentage of the original data. The first sample consists of 39 columns of the grid thus mimicking data obtained by well-logging drill-holes. The second sample involves randomly selected grid points. The original dataset is the Marmousi velocity model, a synthetic two-dimensional acoustic model developed in 1988 by the Institut Francais du Petrole (IFP), and used for a workshop on practical aspects of seismic data inversion at the 1990 EAEG (European Association of Exploration Geophysicists) meeting in Copenhagen. The Marmousi model was generated using a 2-D acoustic, finite-difference modelling program, so as to resemble an overall continental drift geological setting. The geometry is based on a geological profile through the North Quenguela trough in the Cuanza basin, which is located in north-western Angola along the Atlantic Coast of West Africa. The Marmousi model is characterized by high geological complexity: numerous large normal faults and tilted blocks,

resulting from the continental drift, complicate the structure towards its centre. The model also contains many reflectors, steep dips, and strong velocity variations in both the lateral and the vertical directions.

The purpose of this thesis is the exploratory application of geostatistical tools for the simulation of the above described geological section. The methods which are used herein are: i) Ordinary Kriging and ii) Directional Gradient Curvature (DGC) simulation method. Ordinary Kriging is selected because it is the most classic and widely used geostatistical tool. DGC is a novel, non-parametric, local simulation and gap-filling method, the comparison of which with the Ordinary Kriging can provide useful information. For the implementation of Kriging, software was developed in the MATLAB programming environment, while for the implementation of DGC simulation method software developed by the Geostatistics Laboratory (Technical University of Crete) was used. Several methods of parameter inference and anisotropy estimation have been used in connection with OK. The results of each method are evaluated and compared through proper validation measures (e.g. mean squared error, maximum reconstruction error, Pearson's correlation coefficient, Spearman's correlation coefficient).

The applied methods achieve relatively high correlation between the reconstructed field and the real data, i.e., 90-95%, for both samples. In the case of Kriging, the optimal performance is obtained by including separate estimation of anisotropy and data transformation to isotropy. Finally, the DGC simulation method has shown comparable, but slightly inferior, performance measures to OK estimation. We believe that this is due to the local nature of the latter in contrast with kriging, which accounts for correlations with longer range.

Περίληψη

Ένα ευρέως διαδεδομένο πρόβλημα στις Γεωεπιστήμες αποτελεί η προσομοίωση ενός γεωλογικού μέσου. Η ακριβής γνώση της γεωλογικής στρωματογραφίας και των ιδιοτήτων των στρωμάτων (π.χ. πορώδες, διαπερατότητα, ταχύτητα σεισμικών κυμάτων, συγκέντρωση χημικών στοιχείων και ορυκτών) είναι αντικείμενο κεφαλαιώδους σημασίας με εφαρμογές σε πολλά επιστημονικά πεδία, όπως η υδρογεωλογία, η μεταλλευτική, η μηχανική πετρελαίου, η γεωφυσική και η περιβαλλοντική αποκατάσταση. Τα σύγχρονα συστήματα συλλογής δεδομένων παρέχουν σημαντική ποσότητα πληροφορίας σχετικά με την χωρική, χρονική ή χωροχρονική μεταβολή τέτοιων φυσικών ιδιοτήτων. Παρόλα αυτά, δεν μπορούν να μας δώσουν μια ολοκληρωμένη εικόνα της κατανομής των ιδιοτήτων αυτών. Αυτό οφείλεται στο γεγονός ότι η πληροφορία αυτή είναι σε γεωαναφερόμενη μορφή (georeferenced), δηλ. συνδέεται με συγκεκριμένα μόνο σημεία του χώρου. Η χαρτογράφηση και η γραφική απεικόνιση αυτών των ιδιοτήτων σε κανονικά πλέγματα (στις 1, 2 και 3 διαστάσεις τουλάχιστον) είναι περισσότερο χρήσιμη και επιθυμητή.

Η γεωστατιστική παρέχει διάφορα εργαλεία για τον σχεδιασμό τέτοιων χαρτών και γραφικών απεικονίσεων μέσω στατιστικών και στοχαστικών μεθόδων. Τα πλέον ευρέως χρησιμοποιούμενα γεωστατιστικά εργαλεία είναι: α) η χωρική παρεμβολή με Kriging και β) η Προσομοίωση.

Στην παρούσα διπλωματική εργασία, τέτοιου είδους εργαλεία εφαρμόζονται για την επίλυση ενός προβλήματος προσομοίωσης γεωλογικού μέσου. Πιο συγκεκριμένα, ανακατασκευάζεται ένα πλεγματικό σύνολο δεδομένων (συνθετική ψηφιακή εικόνα) μέσω της γεωστατιστικής ανάλυσης δειγμάτων προερχόμενων από την αρχική εικόνα. Τα δείγματα που χρησιμοποιούνται είναι ένα κανονικό και ένα τυχαίο δείγμα. Και τα δύο αποτελούνται απο ένα ποσοστό σημείων που ανέρχεται στο 10,16% σου συνόλου των πλεγματικών σημείων της εικόνας. Το πρώτο περιλαμβάνει 39 στήλες του αρχικού πλέγματος με μια γεωμετρία που μιμείται δεδομένα από διαγραφίες γεωτρήσεων. Το δεύτερο δείγμα αποτελείται απο τυχαία επιλεγμένα σημεία του πλέγματος. Το αρχικό σύνολο δεδομένων είναι το μοντέλο ταχύτητας Marmousi, ένα συνθετικό ακουστικό μοντέλο δύο διαστάσεων που κατασκευάστηκε με βάση το γεωλογικό προφίλ της τάφρου North Quenguela, στην λεκάνη Cuanza, που βρίσκεται στην βορειοδυτική Αγκόλα και κατά μήκος της Ατλαντικής Ακτογραμμής της δυτικής Αφρικής. Το μοντέλο Marmousi χαρακτηρίζεται από μεγάλη γεωλογική πολυπλοκότητα: πολυάριθμα κανονικά ρήγματα και ανυψωμένα τεκτονικά κέρατα, τα οποία προκύπτουν από την μετακίνηση της γεωλογικής πλάκας, καθιστούν το κεντρικό τμήμα της δομής ιδιαίτερα περίπλοκο. Το μοντέλο περιέχει επίσης πολλές επιφάνειες ανάκλασης, απότομες βυθίσεις και μεγάλες διακυμάνσεις της ταχύτητας τόσο στην οριζόντια όσο και στην κατακόρυφη διεύθυνση.

Ο σκοπός της παρούσας διπλωματικής εργασίας είναι η διερευνητική εφαρμογή γεωστατιστικών μεθόδων για την προσομοίωση της παραπάνω ψηφιακής εικόνας του γεωλογικού μέσου. Οι μέθοδοι που χρησιμοποιήθηκαν είναι: α) το Κανονικό Kriging και β) η μέθοδος προσομοίωσης Κατευθυντικής Βαθμίδας και Καμπυλότητας (Directional Gradient Curvature (DGC)). Το Κανονικό Kriging χρησιμοποιείται καθώς είναι η πιο κλασική και ευρέως χρησιμοποιούμενη μέθοδος χωρικής παρεμβολής. Η μέθοδος DGC είναι μια καινοτόμα, μη-παραμετρική, τοπική μέθοδος προσομοίωσης και πλήρωσης κενών, η σύγκριση της οποίας με το Κανονικό Kriging θα μπορούσε να δώσει χρήσιμες πληροφορίες. Για την εφαρμογή του Kriging αναπτύχθηκε λογισμικό στο περιβάλλον προγραμματισμού MATLAB, ενώ για την εφαρμογή της μεθόδου προσομοίωσης DGC χρησιμοποιήθηκε λογισμικό που έχει αναπτυχθεί απο την ερευνητική Μονάδα Γεωστατιστικής (Πολυτεχνείο Κρήτης).

Διάφορες μέθοδοι για την εκτίμηση των παραμέτρων των εξεταζόμενων μοντέλων συνδιασποράς και την αντιμετώπιση της ανισοτροπίας υλοποιήθηκαν για την εφαρμογή του Κανονικού Kriging. Τα αποτελέσματα των διαφόρων μοντέλων και μεθόδων αξιολογούνται και συγκρίνονται μέσω κατάλληλων στατιστικών μέτρων (π.χ. μέσο τετραγωνικό σφάλμα, μέγιστο σφάλμα ανακατασκευής, συντελεστής συσχέτισης Pearson, συντελεστής συσχέτισης Spearman).

Οι μέθοδοι που χρησιμοποιήθηκαν επιτυγχάνουν υψηλή συσχέτιση, της τάξεως του 90-95%, μεταξύ των ανακατασκευασμένων και των πραγματικών δεδομένων και για τα δύο δείγματα. Επιπλέον, από την αξιολόγηση και τη σύγκριση αυτών προκύπτει ότι οι μέθοδοι εκτίμησης των παραμέτρων των εξεταζόμενων μοντέλων με τις καλύτερες επιδόσεις είναι εκείνες που περιλαμβάνουν τον μετασχηματισμό σε ισοτροπικές συντεταγμένες. Τέλος, η μέθοδος προσομοίωσης DGC επιτυγχάνει συγκρίσιμα αλλά ελαφρώς κατώτερα αποτελέσματα (της τάξεως του 89%) από αυτά του Κανονικού Kriging. Αυτό θεωρούμε ότι οφείλεται στον περιορισμό της τελευταίας μεθόδου να διακρίνει μόνο τοπικές συσχετίσεις σε αντίθεση με το Kriging, το οποίο λαμβάνει υπόψη του συσχετίσεις μεγαλύτερης ακτίνας.

Εκτεταμένη Περίληψη

Ένα ευρέως διαδεδομένο πρόβλημα στις Γεωεπιστήμες αποτελεί η προσομοίωση ενός γεωλογικού μέσου. Η ακριβής γνώση της γεωλογικής στρωματογραφίας και των ιδιοτήτων των στρωμάτων (π.χ. πορώδες, διαπερατότητα, ταχύτητα σεισμικών κυμάτων, συγκέντρωση χημικών στοιχείων και ορυκτών) είναι αντικείμενο κεφαλαιώδους σημασίας με εφαρμογές σε πολλά επιστημονικά πεδία, όπως η υδρογεωλογία, η μεταλλευτική, η μηχανική πετρελαίου, η γεωφυσική και η περιβαλλοντική αποκατάσταση. Τα σύγχρονα συστήματα συλλογής δεδομένων παρέχουν σημαντική ποσότητα πληροφορίας σχετικά με την χωρική, χρονική ή χωροχρονική μεταβολή τέτοιων φυσικών ιδιοτήτων. Παρόλα αυτά, δεν μπορούν να μας δώσουν μια ολοκληρωμένη εικόνα της κατανομής των ιδιοτήτων αυτών. Αυτό οφείλεται στο γεγονός ότι η πληροφορία αυτή είναι σε γεωαναφερόμενη μορφή (georeferenced), δηλ. συνδέεται με συγκεκριμένα μόνο σημεία του χώρου. Η χαρτογράφηση και η γραφική απεικόνιση αυτών των ιδιοτήτων σε κανονικά πλέγματα (στις 1, 2 και 3 διαστάσεις τουλάχιστον) είναι περισσότερο χρήσιμη και επιθυμητή.

Η γεωστατιστική παρέχει διάφορα εργαλεία για τον σχεδιασμό τέτοιων χαρτών και γραφικών απεικονίσεων μέσω στατιστικών και στοχαστικών μεθόδων. Τα πλέον ευρέως χρησιμοποιούμενα γεωστατιστικά εργαλεία είναι: α) η χωρική παρεμβολή με Kriging και β) η Προσομοίωση.

Στην παρούσα διπλωματική εργασία, τέτοιου είδους εργαλεία εφαρμόζονται για την επίλυση ενός προβλήματος προσομοίωσης γεωλογικού μέσου. Πιο συγκεκριμένα, ανακατασκευάζεται ένα πλεγματικό σύνολο δεδομένων (συνθετική ψηφιακή εικόνα) μέσω της γεωστατιστικής ανάλυσης δειγμάτων προερχόμενων από την αρχική εικόνα. Τα δείγματα που χρησιμοποιούνται είναι ένα κανονικό και ένα τυχαίο δείγμα. Και τα δύο αποτελούνται απο ένα ποσοστό σημείων που ανέρχεται στο 10,16% σου συνόλου των πλεγματικών σημείων της εικόνας. Το πρώτο περιλαμβάνει 39 στήλες του αρχικού πλέγματος με μια γεωμετρία που μιμείται δεδομένα από διαγραφίες γεωτρήσεων. Το δεύτερο δείγμα αποτελείται απο τυχαία επιλεγμένα σημεία του πλέγματος. Το αρχικό σύνολο δεδομένων είναι το μοντέλο ταχύτητας Marmousi, ένα συνθετικό ακουστικό μοντέλο δύο διαστάσεων που αναπτύχθηκε το 1988 από το Ινστιτούτο Πετρελαίου της Γαλλίας (Institut Francais du Petrole). Το μοντέλο αυτό χρησιμοποιήθηκε για τις εργαστηριακές ανάγκες ενός συνεδρίου της EAEG (European Association of Exploration Geophysicists) για την αντιστροφή σεισμικών δεδομένων που διεξήχθη στην Κοπεγχάγη το 1990. Το μοντέλο Marmousi κατασκευάστηκε με βάση το γεωλογικό προφίλ της τάφρου North Quenguela, στην λεκάνη Cuanza, που βρίσκεται στην βορειοδυτική Αγκόλα και κατά μήκος της Ατλαντικής Ακτογραμμής της δυτικής Αφρικής. Το μοντέλο Marmousi χαρακτηρίζεται από μεγάλη γεωλογική πολυπλοκότητα: πολυάριθμα κανονικά ρήγματα και ανυψωμένα τεκτονικά κέρατα, τα οποία προκύπτουν από την μετακίνηση της γεωλογικής πλάκας, καθιστούν το κεντρικό τμήμα της δομής ιδιαίτερα περίπλοκο. Το μοντέλο περιέχει επίσης πολλές επιφάνειες ανάκλασης, απότομες βυθίσεις και μεγάλες διακυμάνσεις της ταχύτητας τόσο στην οριζόντια όσο και στην κατακόρυφη διεύθυνση.

Ο σκοπός της παρούσας διπλωματικής εργασίας είναι η διερευνητική εφαρμογή γεωστατιστικών μεθόδων για την προσομοίωση της παραπάνω ψηφιακής εικόνας του γεωλογικού μέσου. Οι μέθοδοι που χρησιμοποιήθηκαν είναι: α) το Κανονικό Kriging και β) η μέθοδος προσομοίωσης Κατευθυντικής Βαθμίδας και Καμπυλότητας (Directional Gradient Curvature (DGC)). Το Κανονικό Kriging χρησιμοποιείται καθώς είναι η πιο κλασική και ευρέως χρησιμοποιούμενη μέθοδος χωρικής παρεμβολής. Η μέθοδος DGC είναι μια καινοτόμα, μη-παραμετρική, τοπική μέθοδος προσομοίωσης και πλήρωσης κενών, η σύγκριση της οποίας με το Κανονικό Kriging θα μπορούσε να δώσει χρήσιμες πληροφορίες. Για την εφαρμογή του Kriging αναπτύχθηκε λογισμικό στο περιβάλλον προγραμματισμού MATLAB, ενώ για την εφαρμογή της μεθόδου προσομοίωσης DGC χρησιμοποιήθηκε λογισμικό που έχει αναπτυχθεί απο την Ερευνητική Μονάδα Γεωστατιστικής (Πολυτεχνείο Κρήτης).

Στην περίπτωση του Κανονικού Kriging, τα βήματα της γεωστατιστικής ανάλυσης είναι τα εξής:

1. Προκαταρκτική Ανάλυση,
2. Εκτίμηση Παραμέτρων,
3. Επιλογή Βέλτιστου Μοντέλου (Διασταυρωτική Επιβεβαίωση),
4. Χωρική Εκτίμηση, και
5. Αξιολόγηση Απόδοσης

Στο βήμα της Εκτίμησης Παραμέτρων χρησιμοποιήθηκαν πέντε παραλλαγές για την εκτίμηση των παραμέτρων των εξεταζόμενων μοντέλων. Οι παραλλαγές αυτές διαφέρουν μεταξύ τους στον τρόπο εκτίμησης της ανισοτροπίας (παραμετρική ή μη παραμετρική εκτίμηση) καθώς και στην εφαρμογή ή μη μετασχηματισμού των δεδομένων σε ισοτροπικά. Τα μοντέλα συνδιασποράς που μελετώνται είναι τα: α) Γενικευμένο Εκθετικό, β) Γκαουσιανό, γ) Σφαιρικό, δ) Mátern και ε) Σπαρτιάτικο. Οι παραλλαγές για την εκτίμηση των παραμέτρων, οι οποίες έχουν ονομαστεί αυθαίρετα, είναι οι εξής:

- **DirVar0**: Δεν επιχειρείται εκτίμηση των παραμέτρων της ανισοτροπίας εκ των προτέρων. Ως εκ τούτου χρησιμοποιούνται σε όλα τα στάδια τηε ανάλυσης ανισοτροπικές συναρτήσεις βαριογραμμάτων, οι οποίες περιέχουν τον μέγιστο αριθμό αγνώστων παραμέτρων.
- **DirVar1**: Αρχικά, εκτιμώνται οι παράμετροι της ανισοτροπίας για καθένα απο τα εξεταζόμενα μοντέλα συνδιασποράς με την χρήση κατευθυντικών βαριογραμμάτων. Εν συνεχεία, οι παράμετροι αυτές εισάγονται στην αντίστοιχη ανισοτροπική συνάρτηση βαριογράμματος, ελαττώνοντας τον αριθμό των αγνώστων παραμέτρων κατά τρεις για κάθε μοντέλο. Οι νέες ανισοτροπικές συναρτήσεις βαριογραμμάτων (με λιγότερους βαθμούς ελευθερίας) χρησιμοποιούνται για την εκτίμηση των υπόλοιπων παραμέτρων.
- **DirVar2**: Αρχικά, εκτιμώνται οι παράμετροι της ανισοτροπίας για καθένα απο τα εξεταζόμενα μοντέλα συνδιασποράς με την χρήση κατευθυντικών βαριογραμμάτων. Στη συνέχεια, οι παράμετροι αυτές χρησιμοποιούνται για τον μετασχηματισμό του αρχικού ανισοτροπικού συστήματος συντεταγμένων σε ένα νέο ισοτροπικό σύστημα. Αυτό γίνεται για καθένα απο τα πέντε μοντέλα συνδιασποράς. Μετά τον μετασχηματισμό του συστήματοε συντεταγμένων εκτιμώνται οι παράμετροι των αντίστοιχων ισοτροπικών συναρτήσεων συνδιασποράς.
- **CHI1**: Αρχικά, εκτιμώνται οι παράμετροι της ανισοτροπίας για καθένα απο τα εξεταζόμενα μοντέλα συνδιασποράς με την χρήση της Εσσιανής ταυτότητας της συνδιασποράς. Εν συνεχεία, οι παράμετροι αυτές εισάγονται στην αντίστοιχη ανισοτροπική συνάρτηση βαριογράμματος, ελαττώνοντας τον αριθμό των αγνώστων παραμέτρων κατά τρεις για κάθε μοντέλο. Οι νέες ανισοτροπικές συναρτήσεις βαριογραμμάτων (με λιγότερους βαθμούς ελευθερίας) χρησιμοποιούνται για την εκτίμηση των υπόλοιπων παραμέτρων.
- **CHI2**: Αρχικά, εκτιμώνται οι παράμετροι της ανισοτροπίας για καθένα απο τα εξεταζόμενα μοντέλα συνδιασποράς με την χρήση της Εσσιανής ταυτότητας της συνδιασποράς. Στη συνέχεια, οι παράμετροι αυτές χρησιμοποιούνται για τον μετασχηματισμό του αρχικού ανισοτροπικού συστήματος συντεταγμένων σε ένα νέο ισοτροπικό σύστημα. Αυτό γίνεται για καθένα απο τα πέντε μοντέλα συνδιασποράς. Μετά τον μετασχηματισμό του συστήματοε συντεταγμένων εκτιμώνται οι παράμετροι των αντίστοιχων ισοτροπικών συναρτήσεων συνδιασποράς.

Η επιλογή του βέλτιστου μοντέλου γίνεται με την εφαρμογή διασταυρωτικής επιβεβαίωσης (LOOCV). Τα αποτελέσματα των διαφόρων μοντέλων αξιολογούνται και συγκρίνονται μέσω κατάλληλων στατιστικών μέτρων (π.χ. μέσο τετραγωνικό σφάλμα, μέγιστο σφάλμα ανακατασκευής, συντελεστής συσχέτισης Pearson, συντελεστής συσχέτισης Spearman). Η τελική επιλογή του μοντέλου γίνεται βάσει ενός συντελεστή, ο οποίος υπολογίζεται για κάθε εξεταζόμενο μοντέλο και συνδυάζει τις τιμές του μέσου τετραγωνικού σφάλματος και των συντελεστών συσχέτισης Pearson και Spearman.

Τα αποτελέσματα της παρούσας διπλωματικής εργασίας υποδυκνείουν ότι τα γεωστατιστικά εργαλεία είναι ιδιαίτερα χρήσιμα σε περιπτώσεις όπου τα διαθέσιμα δεδομένα περιέχουν ικανή πληροφορία για την εκάστοτε μελετώμενη φυσική ιδιότητα. Επομένως, η Γεωστατιστική θα μπορούσε να χρησιμοποιηθεί για την υποβοήθηση των υφιστάμενων γεωφυσικών μεθόδων για την προσομοίωση γεωλογικών δομών.

Τα μέτρα αξιολόγησης, και για τους δύο τύπους δειγματοληψίας, δείχνουν ότι όλες οι μέθοδοι που εφαρμόσθηκαν επιτυγχάνουν υψηλή συσχέτιση, της τάξεως του 90-95%, μεταξύ των ανακατασκευασμένων και των πραγματικών δεδομένων. Επιπλέον, από την σύγκριση των μεθόδων προκύπτει ότι το Κανονικό Kriging λειτουργεί με μεγαλύτερη αποτελεσματικότητα όταν το αρχικό ανισοτροπικό σύστημα συντεταγμένων μετασχηματίζεται σε ισοτροπικό. Όσον αφορά τα μοντέλα συνδιασποράς που εξετάστηκαν, από τα αποτελέσματα δεν υποδεικνύεται η υπεροχή κάποιου εξ αυτών στην ικανότητα περιγραφής των χωρικών συσχετίσεων της υπό μελέτη ιδιότητας έναντι των υπολοίπων. Τέλος, η μέθοδος προσομοίωσης DGC επιτυγχάνει συγκρίσιμα, αλλά ελαφρώς κατώτερα, αποτελέσματα (της τάξεως του 89%) από αυτά του Κανονικού Kriging. Αυτό θεωρούμε ότι οφείλεται στον περιορισμό της τελευταίας μεθόδου να διακρίνει μόνο τοπικές συσχετίσεις σε αντίθεση με το Kriging, το οποίο λαμβάνει υπόψη του συσχετίσεις μεγαλύτερης ακτίνας.

Contents

List of Figures

List of Tables

Nomenclature

Roman Symbols

A Subset domain of Ω

$c_z(\boldsymbol{s},\boldsymbol{s'})$ Covariance of the random field Z between the points $(\boldsymbol{s},\boldsymbol{s'})$

D Subset domain of $\mathbb{R}^n$

$\mathbb{E}[\cdot]$ Expectation operator

$F_z(z_s;\boldsymbol{s})$ Cumulative probability function of the *event* z_s of the random field Z

$f_z(z_s;\boldsymbol{s})$ Probability density function of the *event* z_s of the random field Z

$\gamma_z(\boldsymbol{s},\boldsymbol{s'})$ Variogram of the random field Z between the points $(\boldsymbol{s},\boldsymbol{s'})$

$F_z(z_s,z_{s'};\boldsymbol{s},\boldsymbol{s'})$ Joint cumulative distribution function of the random field Z at the two points $(\boldsymbol{s},\boldsymbol{s'})$

$f_z(z_s,z_{s'};\boldsymbol{s},\boldsymbol{s'})$ Joint probability density function of the random field Z at the two points $(\boldsymbol{s},\boldsymbol{s'})$

$m_z^n(\boldsymbol{s})$ Raw statistical moment of order n of the random field Z at the point $\boldsymbol{s}$

$m_z^n(\boldsymbol{s},\boldsymbol{s'})$ Raw 2D statistical moment of order n of the random field Z between the points $(\boldsymbol{s},\boldsymbol{s'})$

$m_{z,c}^n(\boldsymbol{s})$ Central statistical moment of order n of the random field Z at the point $\boldsymbol{s}$

$m_{z,c}^n(\boldsymbol{s},\boldsymbol{s'})$ Central 2D statistical moment of order n of the random field Z between the points $(\boldsymbol{s},\boldsymbol{s'})$

P Probability function on A

$\rho_z(\boldsymbol{s},\boldsymbol{s'})$ Correlation of the random field Z between the points $(\boldsymbol{s},\boldsymbol{s'})$

$\boldsymbol{s}$,$\boldsymbol{u}$ Position vectors of points belonging in D

$Z(\cdot)$ Scalar spatial random field

$z(\cdot)$ Single realization of the scalar spatial random field Z

$\hat{Z}(\cdot)$ Estimate of the random variable $Z(\cdot)$

z_j Single realization of the scalar spatial random field Z at the j-th point $\boldsymbol{s_j}$ of the domain D, i.e $z_j \equiv z(\boldsymbol{s_j})$

z_s Single realization of the scalar spatial random field Z at the point $\boldsymbol{s}$, i.e $z_s \equiv z(\boldsymbol{s})$

Greek Symbols

Ω Sample space of a probability field

ω State of the sample space of a probability field

Introduction

Geostatistics, since its empirical development by Matheron and Krige in the early 1960s (Cressie, 1990; Krige, 1951; Matheron, 1971) and the subsequent theoretical enhancement, was widely adopted by diverse scientific and engineering fields such as mining (Galetakis, 1998; Goovaerts, 1997; Pavlides et al., 2015) and petroleum engineering (Deutsch, 2002; Kelkar and Perez, 2002), hydrogeology (Mariethoz and Renard, 2010; Papadopoulou et al., 2009; Varouchakis and Hristopulos, 2013), meteorology (Agou, 2016; Bargaoui and Chebbi, 2009; Liu et al., 2010), atmospheric science (Žukovič and Hristopulos, 2013a), remote sensing (Žukovič and Hristopulos, 2013b), environmental and earth sciences (Christakos, 1992; Varouchakis et al., 2015), and material science (Greene, 1992). The widespread utility and success of the tools provided by Geostatistics is due to the growing demand for efficient analysis of the increasing amount of data being gathered by the sophisticated acquisition methods of the last decades.

A common problem in Geosciences is that of geological media modelling, i.e. the mapping of properties of the geological stratas' (e.g. mineral or pollutant concenteration, porosity, permeability, seismic waves velocity, resistivity). The graphical representation of these properties' spatial, temporal or spatiotemporal distribution can improve the understanding of the environmental parameters affecting the geological systems of interest and the decision-making for the scientists and engineers.

In this thesis we present an application of geostatistical methods in a problem of geological media modelling. Random and regular samples of the Marmousi Model (Bourgeois et al., 1990; Versteeg and Grau, 1990), a synthetic, two dimensional, acoustic model released at the workshop of 52nd EAEG meeting in 1990, are used as data. For the reconstruction of the original dataset, two methods are employed: i) Kriging estimation and ii) Directional Gradient Curvature (DGC) simulation method (Žukovič and Hristopulos, 2013a). Several methods regarding the parameter inference and anisotropy estimation of the data (i.e. parametric - non parametric anisotropy parameter inference) and the transformation of the data to isotropic or not, are investigated in the case of OK. To evaluate the performance of the

OK and the DGC simulation, proper validation measures are calculated for each method and compared.

This thesis is structured as follows: In the first chapter a brief definition of Geostatistics is given. The second chapter comprises basic notions of random fields, which constitute the primary tool of Geostatistics. The third and fourth chapters present the kriging and the simulation methods, respectively. The fifth chapter describes the commonly followed steps of data analysis. The sixth focuses on the case study of this thesis, concerning the application of geostatistical methods in the above described geological media modelling. Finally, in the seventh chapter the conclusions of the thesis are presented.

Chapter 1

Spatial Interpolation and Geostatistics

Assume that at two points of a 2D space, $\boldsymbol{s_1}(x_1, y_1)$ and $\boldsymbol{s_2}(x_2, y_2)$, the values of a physical variable, $Z(\boldsymbol{s_1})$ and $Z(\boldsymbol{s_2})$, respectively, are measured and known. Assume a third point in the same space, $\boldsymbol{u}(x_3, y_3)$, at which the value of the physical variable is unknown, $Z(\boldsymbol{u}) =?$. The principle of spatial continuity (also known as the 1st Law of Geography Tobler (1970)) indicates that physical phenomena are not randomly distributed in space but exhibit spatial correlation. As such, the information provided by the known values can be used to produce an estimation for the missing value, i.e. $\hat{Z}(\boldsymbol{u}) = f(Z(\boldsymbol{s_1}), Z(\boldsymbol{s_2}))$. This simple problem, illustrated in Fig. 1.1, is frequently encountered in spatial interpolation. It commonly arises due to lack of practicality, accesibility, financing or time (or a combination of them) demanded for an exhaustive sampling or due to malfunctions of the sampling equipment.

In practice the unknown values are usually nodes of a regular, numerical grid which covers the area of interest. The data set which provides the necessary information for the estimation of the missing values comprises hundreds or even thousands of known values. Thus, the estimation of the missing values results in mapping the distribution of the investigated physical variable in the whole area (see Fig. 1.1).

The various methods of spatial interpolation can be divided into two broad categories, the **deterministic** and the **stochastic** methods. The first category includes methods which use mathematical functions to calculate the values at the investigated locations based on the values of neighboring data. Some of these methods are Thiessen polygons (also known as Dirichlet or Voronoi diagrams), Natural Neighboors Method, Distance Weighted Methods, (Fuzzy) k-Nearest Neighboors, Moving Average Methods and Trend Surface Analysis (Barnett, 1981; Burrough et al., 2013).

The stochastic methods combine mathematical and statistical tools to estimate the unknown values and also assess the uncertainty of these estimations. They can be applied in mathematical modelling of spatial, temporal and spatiotemporal correlated data.

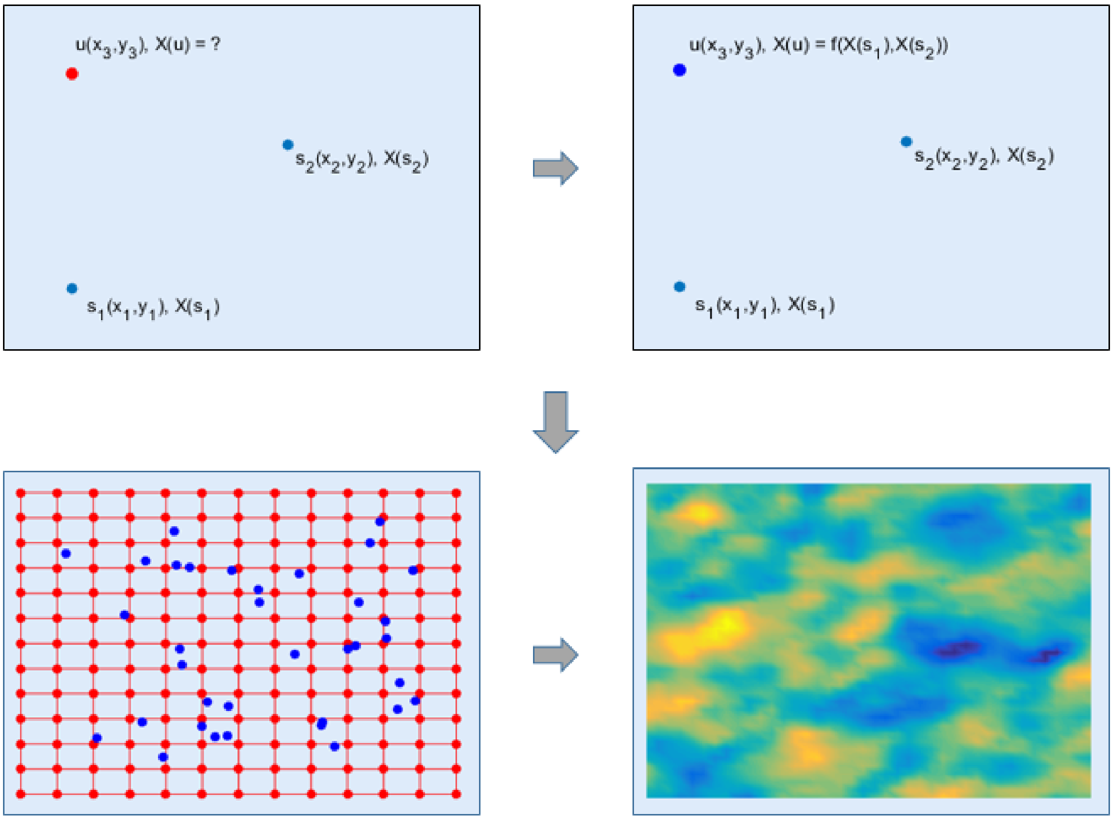

Figure 1.1 Graphical interpretation of Spatial Interpolation problems

The stochastic methods can be further divided into **Estimation processes** and **Simulation processes**. The estimation processes aim to determine the optimal value at the points of interest under one optimization criterion (e.g. minimizing the mean square error or maximizing the likelihood). Simulation processes, on the other hand, are intended to produce many of the possible states (alternative scenarios) of the field which satisfactorily agree with the existing statistical limitations resulting from the training sample (e.g. mean, standard deviation, variogram). Geostatistics belong to the stochastic methods (Lantuéjoul, 2013).

Frequently, the advantages of deterministic methods are the simplicity and ease of implementation, and the small computational cost. Disadvantages include lack of flexibility and uncertainty assessment. The stochastic methods, on the contrary, are more flexible, provide uncertainty assessment and higher accuracy. The limitations of them are related to the high computational cost and the possible big number of parameters needed to be tunned (Chilès and Delfiner, 2012; Lantuéjoul, 2013).

Chapter 2

Random Fields

2.1 Random Field

Random Fields (RFs) comprise the primary tool of Geostatistics. Generally, a random field is a set of random values that describe the distribution of a physical property in an n-dimensional space. Each of these values is attributed to a particular point in the n-dimensional space and at every point of this space the possible values follow a probability distribution function (pdf). The pdf can be the same or differ from one point to the other. The distribution of the random variable throughout the field can be described from the joint probability distribution function (j-pdf), i.e. the j-pdf describes the correlations between different points. As such, the value at one point can be written as a function of the values of other points, especially of the most adjacent ones (principle of spatial continuity). This spatial dependence (correlation) is the special feature that differentiates RFs from totally random (uncorrelated) processes.

A more strictly mathematical definition of random field is the following: "*Given a domain $D \subset \mathbb{R}^n$ (with a positive volume) and a probability space (Ω, A, P), a random field is a function of two variables $Z(\boldsymbol{s}, \omega)$ such that for each $\boldsymbol{s} \in D$ the section $Z(\boldsymbol{s}, \cdot)$ is a random variable on (Ω, A, P). Each of the functions $Z(\cdot, \omega)$ defined on D as the section of the RF at $\omega \in \Omega$ is a realization of the RF.*" Herein, for brevity and simplicity, RF is denoted by $Z(\boldsymbol{s})$, and with the lowercase $z(\boldsymbol{s})$ is denoted a single realization of the RF at the point $\boldsymbol{s}$ (Chilès and Delfiner, 2012).

A probability space (also known as probability field) is a mathematical triplet (Ω, A, P) consisting of:

• the sample space (or space of elementary events) Ω, which is a non-empty set of all possible events of a model

• the σ-algebra A, which is a set of subsets of Ω , called events, and

• the probability measure $P: A \to [0,1]$, which is a function on A, satisfying the condition $P(\Omega) = 1$ (Kolmogorov, 1960).

Depending on their properties the Random Fields can be classified into various categories. Markov random fields (MRF) (Kindermann, 1980; Rozanov, 1982), and Gaussian random fields (GaRF) (Adler and Taylor, 2007; Khoshnevisan, 2002) represent some of the major amongst these categories.

2.2 Probability Functions

2.2.1 1D Probability Functions

The one-dimensional (point) *probability density function (pdf)* at a point $\boldsymbol{s}$ of a random field, denoted as $f_z(z_s;\boldsymbol{s})$, describes the possible situations of the field at that specific point. In other words, the pdf gives the interval probability of the *event* z_s

$$f_z(z_s;\boldsymbol{s}) = P(z_s) = P(z_1 \leq z_s \leq z_2). \tag{2.1}$$

Similarly can be defined the *cumulative distribution function (cdf)* at the point $\boldsymbol{s}$ of the random field, $F_z(z_s;\boldsymbol{s})$, as

$$F_z(z_s;\boldsymbol{s}) = P(z_s \leq z_1). \tag{2.2}$$

From Eq. (2.1) and (2.2), if $F_z(z_s;\boldsymbol{s})$ is differentiable in z_s, follows that

$$f_z(z_s;\boldsymbol{s}) = F_z(z_2;\boldsymbol{s_2}) - F_z(z_1;\boldsymbol{s_1}) = \frac{d}{dx}F_z(z_s;\boldsymbol{s}). \tag{2.3}$$

Conversely, if $f_z(z_s;\boldsymbol{s})$ exists, it is valid that

$$F_z(z_s;\boldsymbol{s}) = \int_{-\infty}^{z_s} f_z(v;\boldsymbol{s})\, dv. \tag{2.4}$$

Some commonly used pdf are shown in Table 2.1.

2.2.2 2D Probability Functions

The two-dimensional probability functions of a random field,i.e. the *joint probability density function (j-pdf)*, $f_z(z_s, z_{s'};\boldsymbol{s},\boldsymbol{s'})$, and the *joint cummulative distribution function (j-cdf)*, $F_z(z_s, z_{s'};\boldsymbol{s},\boldsymbol{s'})$, describe the correlations between the possible situations of the field at two points. Specifically, they give respectively the interval and the cummulative probabilities of

Table 2.1 Common used probability density functions

Model	Probability Density Function
Uniform	$f_z(z_s;\boldsymbol{s}) = \begin{cases} \frac{1}{(b-a)}, & z_s \in [a,b] \\ 0, & z_s \notin [a,b] \end{cases}$
Exponential	$f_z(z_s;\boldsymbol{s}) = \begin{cases} b^{-1}exp(-b^{-1}x), & z_s \geq 0 \\ 0, & z_s < 0 \end{cases}$
Gaussian	$f_z(z_s;\boldsymbol{s}) = (\sqrt{2\pi}\sigma)^{-1}exp(-\frac{(x-m)^2}{2\sigma^2})$

the appearance both of the *events* $z_s, z_{s'}$

$$f_z(z_s, z_{s'};\boldsymbol{s},\boldsymbol{s'}) = P(z_1 \leq z_s \leq z_2) \cap P(z_3 \leq z_{s'} \leq z_4), \tag{2.5}$$

$$F_z(z_s, z_{s'};\boldsymbol{s},\boldsymbol{s'}) = P(z_s \leq z_1) \cap P(z_{s'} \leq z_2). \tag{2.6}$$

Note that Eqs. (2.5) and (2.6) are reciprocally linked

$$f_z(z_s, z_{s'};\boldsymbol{s},\boldsymbol{s'}) = \frac{\partial^2}{\partial z_s \partial z_{s'}} F_z(z_s, z_{s'};\boldsymbol{s},\boldsymbol{s'}), \tag{2.7}$$

$$F_z(z_s, z_{s'};\boldsymbol{s},\boldsymbol{s'}) = \int_{-\infty}^{z_s}\int_{-\infty}^{z_{s'}} f_z(v, v';\boldsymbol{s},\boldsymbol{s'})\, dv dv'. \tag{2.8}$$

2.3 Statistical Moments

The probability functions describe completely a random field, but they cannot always be easily and accurately defined. Thus, it is more convenient to work with the statistical moments, which contain partial (but sufficient) information about the random field and can be more easily estimated from the data. The Statistical Moments comprise a set of deterministic quantities, which represent average values (expectations), on all the possible states of the RF, of various combinations of the field's values in one or more locations.

In practical applications, the statistical moments of interest are those of low order (up to 4th-order), since the increase in the order implies harder estimation. Low-order moments are **mean, variance, skewness** and **kurtosis** for one-dimensional pdfs, while for joint pdfs

covariance and **variogram** are the main low-order moments (Casella and Berger, 2001; Kitanidis, 1997; Papoulis and Pillai, 2002; Thijssen, 2016). An analytic description of them is presented in the following sections.

2.3.1 1D Statistical Moments

The *raw statistical moment of order n* for a continuum variable is defined according to the equation

$$m_z^n(\boldsymbol{s}) = \mathbb{E}[Z^n(\boldsymbol{s})] = \int_{-\infty}^{\infty} z_s^n f_z(z_s;\boldsymbol{s})\, dz_s, \tag{2.9}$$

where $\mathbb{E}[\cdot]$ denotes the expectation operator.

To estimate the raw statistical moments of a **sample**, the following equation is used

$$\hat{m}_z^n \equiv \overline{z^n} = \frac{1}{M}\sum_{j=1}^{M} z_j^n, \tag{2.10}$$

where M the size of the sample.

Another class of statistical moments is the central statistical moments, which represent the expectation values of the field's *fluctuations* around the mean value (see 2.3.1), $Z'(\boldsymbol{s}) = Z(\boldsymbol{s}) - m_z(\boldsymbol{s})$, i.e. they provide a measure of *dispersion* around the mean.

The *central statistical moments of order n* for a continuum variable and a sample are given by

$$m_{z,c}^n(\boldsymbol{s}) = \mathbb{E}[(Z(\boldsymbol{s}) - m_z(\boldsymbol{s}))^n] = \mathbb{E}[(Z'(\boldsymbol{s}))^n] = \int_{-\infty}^{\infty} (z_s - m_z(\boldsymbol{s}))^n f_z(z_s;\boldsymbol{s})\, dz_s, \tag{2.11}$$

and

$$\hat{m}_{z,c}^n \equiv \overline{z'^n} = \frac{1}{M}\sum_{j=1}^{M} (z_j - m_z(\boldsymbol{s_j}))^n, \tag{2.12}$$

respectively.

Similar equations can be derived for the estimation of raw and central statistical moments in the case of discrete variables by replacing the integrals with summations.

Mean Value

The mean value is the 1st order statistical moment

$$m_z(\boldsymbol{s}) = \mathbb{E}[Z(\boldsymbol{s})], \tag{2.13}$$

and represents a measure of the central tendency of the probability distribution.

The mean value may not be independent of the position $\boldsymbol{s}$ due to possible spatial dependence of the one-dimensional pdf. It is common practice to model the $m_z(\boldsymbol{s})$ with a deterministic trend function and, subtracting it from the field values, to statistically process the fluctuations.

Variance

The variance is the 2st order central statistical moment

$$\sigma_z^2(\boldsymbol{s}) \equiv m_{z,c}^2(\boldsymbol{s}) = \mathbb{E}[(Z(\boldsymbol{s}) - m_z(\boldsymbol{s}))^2] = \mathbb{E}[(Z'(\boldsymbol{s}))^2], \tag{2.14}$$

and measures the dispersion from the center of the distribution. Its positive square root is the *standard deviation* σ.

Skewness

The skewness is the standardized 3rd order central statistical moment

$$s_z(\boldsymbol{s}) = \frac{1}{\sigma_z^3}\mathbb{E}[(Z(\boldsymbol{s}) - m_z(\boldsymbol{s}))^3] = \frac{1}{\sigma_z^3}\mathbb{E}[(Z'(\boldsymbol{s}))^3], \tag{2.15}$$

and measures the assymetry of the distribution. Right skewed ($\equiv$ right tail longer) distributions have positive skewness, while the left skewed ones have negative skewness. A symmetric distribution (i.e. gaussian) has $s_z(\boldsymbol{s}) = 0$.

Kurtosis

The kurtosis is the standardized 4th order central statistical moment

$$k_z(\boldsymbol{s}) = \frac{1}{\sigma_z^4}\mathbb{E}[(Z(\boldsymbol{s}) - m_z(\boldsymbol{s}))^4] = \frac{1}{\sigma_z^3}\mathbb{E}[(Z'(\boldsymbol{s}))^4], \tag{2.16}$$

and measures the heaviness of the tail of the distribution, compared to the normal distribution of the same variance. Gaussian distribution has $k_z(\boldsymbol{s}) = 3$, distributions with narrower peaks, called *leptokurtic*, have $k_z(\boldsymbol{s}) > 3$, and distributions with wider peaks, called *platykurtic*, have $k_z(\boldsymbol{s}) < 3$.

2.3.2 2D Statistical Moments

Covariance

The covariance is a 2nd order central 2D statistical moment

$$\begin{aligned} c_z(\boldsymbol{s},\boldsymbol{s'}) &= \mathbb{E}[(Z(\boldsymbol{s})-m_z(\boldsymbol{s}))(Z(\boldsymbol{s'})-m_z(\boldsymbol{s'}))] \\ &= \mathbb{E}[Z(\boldsymbol{s})Z(\boldsymbol{s'})]-m_z(\boldsymbol{s})m_z(\boldsymbol{s'}) \\ &= \mathbb{E}[Z'(\boldsymbol{s})Z'(\boldsymbol{s'})], \end{aligned} \tag{2.17}$$

and describes the quantitative dependence of the field's fluctuations between two different points. Higher absolute values indicate a higher dependence (correlation) and vice versa. Positive covariance implies variables with similar behaviors, i.e. increasing or decreasing of the one variable's values correspond to also increasing or decreasing, respectively, of the other variable's values. In the opposite case, negative covariance implies variables with opposite behaviors, i.e. increasing of the one variable's values correspond to decreasing of the other variable's values.

The covariance is dependent on the distance $\boldsymbol{r}=\boldsymbol{s'}-\boldsymbol{s}$ between the two points $\boldsymbol{s}$ and $\boldsymbol{s'}$. When the distance between the two points is ∞, the covariance is zero. As the distance decreases the covariance is increasing and when distance tends to zero, i.e. $\boldsymbol{s}\equiv\boldsymbol{s'}$, the covariance takes the maximum possible value, which is equal to the variance of the random field at that point

$$c_z(\boldsymbol{s},\boldsymbol{s}) = \sigma_z^2(\boldsymbol{s}). \tag{2.18}$$

Thus, the Eq. (2.17) can be rewritten as

$$c_z(\boldsymbol{s},\boldsymbol{s}+\boldsymbol{r}) \equiv c_z(\boldsymbol{s},\boldsymbol{r}) = \mathbb{E}[Z'(\boldsymbol{s})Z'(\boldsymbol{s}+\boldsymbol{r})]. \tag{2.19}$$

The standardization of the covariance by dividing it with the product of standard deviations at the two points (or with the variance if $\sigma_z(\boldsymbol{s})=\sigma_z(\boldsymbol{s'})$) gives a more accurate and meritocratic measure of the spatial dependences, which is called **correlation coefficient**

$$\rho_z(\boldsymbol{s},\boldsymbol{s'}) = \frac{c_z(\boldsymbol{s},\boldsymbol{s'})}{\sigma_z(\boldsymbol{s})\sigma_z(\boldsymbol{s'})} \in [-1,1]. \tag{2.20}$$

or, taking into account the dependence of covariance on $\boldsymbol{r}=\boldsymbol{s'}-\boldsymbol{s}$,

$$\rho_z(\boldsymbol{s},\boldsymbol{r}) = \frac{c_z(\boldsymbol{s},\boldsymbol{r})}{\sigma_z(\boldsymbol{s})\sigma_z(\boldsymbol{s}+\boldsymbol{r})} \in [-1,1]. \tag{2.21}$$

A graphical interpretation of the effect of different data distributions on the correlation coefficient can be seen in Fig. 2.1 where several sets of (x,y) points with estimated correlation coefficient are plotted. It can be noted that the correlation reflects the noisiness and direction of a linear relationship (top row), but not the slope of that relationship (middle), nor many aspects of nonlinear relationships (bottom).

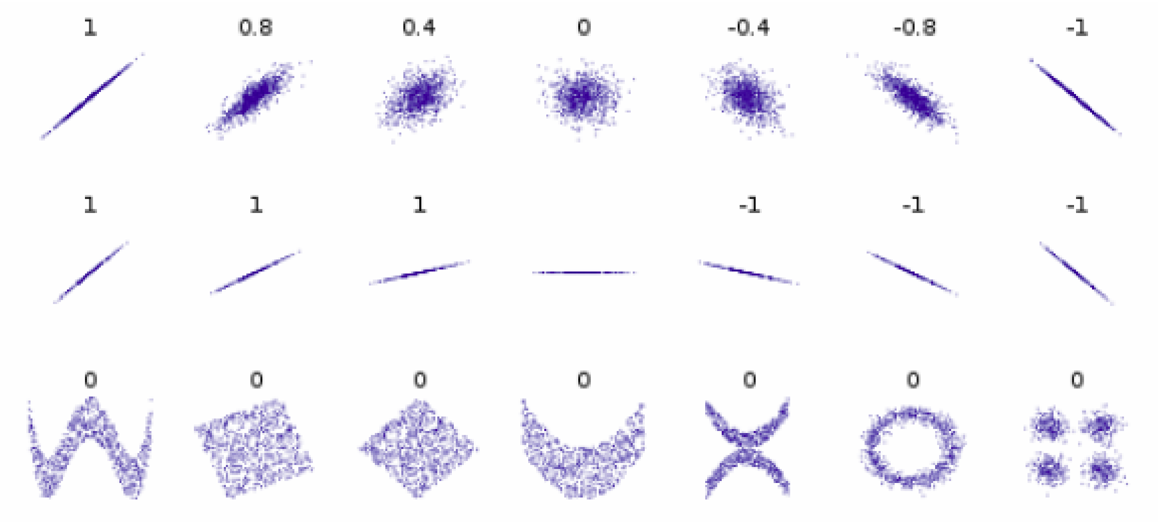

Figure 2.1 Several sets of (x, y) points, with the Pearson correlation coefficient of x and y for each set [https://en.wikipedia.org/wiki/Correlation_and_dependence]

Variogram

The variogram is also a 2nd order central 2D statistical moment

$$\begin{aligned}\gamma_z(\boldsymbol{s},\boldsymbol{s'}) &= \frac{1}{2}\mathbb{E}[(Z'(\boldsymbol{s})-Z'(\boldsymbol{s'}))^2] \\ &= \frac{1}{2}\mathrm{Var}[Z'(\boldsymbol{s})-Z'(\boldsymbol{s'})],\end{aligned} \tag{2.22}$$

and like the covariance describes the spatial dependence of the field's fluctuations between two different points.

Similarly to covariance, variogram is dependent on the distance between the two points ($\boldsymbol{r}=\boldsymbol{s'}-\boldsymbol{s}$). When $\|\boldsymbol{r}\|=0$, $\gamma_z(\boldsymbol{s},\boldsymbol{s'})=0$ and as $\|\boldsymbol{r}\|$ increases, the same does $\gamma_z(\boldsymbol{s},\boldsymbol{s'})$. However, variogram, in contrast with the covariance, does not require the *a priori* knowledge of the mean value of the RF, since by differencing the values of the RF the stochastic trends are removed. Therefore, it holds that

$$\gamma_z(\boldsymbol{s},\boldsymbol{s'}) \equiv \gamma_z(\boldsymbol{r}) = \frac{1}{2}\mathbb{E}[(Z'(\boldsymbol{s})-Z'(\boldsymbol{s}+\boldsymbol{r}))^2]. \tag{2.23}$$

Basic Parameters of the 2D Statistical Moments

In order to define the 2D Statistical Moments (i.e. covariance, correlation and variogram) and describe a random field, the following two parameters have to be determined:

- **covariance** (σ_z^2), which measures the width of the fields variations, and
- **correlation length** (ξ), which normalizes the distance ($\|\boldsymbol{r}\|$) such that the covariance can be also expressed as function of a dimensionless distance (h) instead of ξ.

2.4 Stationarity, Ergodicity and Isotropy

Except from the statistical moments, there are some properties of the RFs, such as **stationarity, ergodicity and isotropy**, which are of great importance for stochastic analysis.

2.4.1 Stationarity

Stationarity (or Homogeneity) implies that the probabilistic behavior of a stochastic process is independent of the position in space or time or spacetime. In practice, because strict stationarity is very difficult to establish, a weakened version of it is used (Chilès and Delfiner, 2012; Shumway and Stoffer, 2011).

Definition 2.1. *A random field $Z(\boldsymbol{s})$ is called weakly or 2nd-order stationary, if it is a finite variance process such that*

(i) the mean value is constant and does not depend on position in space,
$\mathbb{E}[Z(\boldsymbol{s})] = m_z, \forall \boldsymbol{s} \in D$, *and*

(ii) the covariance, $c_z(\boldsymbol{s},\boldsymbol{s}')$, defined in (2.17) depends only on $\boldsymbol{r} = \boldsymbol{s}' - \boldsymbol{s}$,
$c_z(\boldsymbol{s},\boldsymbol{s}') = c_z(\boldsymbol{r}), \forall \boldsymbol{s},\boldsymbol{s}' \in D$.

One important consequence of 2nd-order stationarity of a random field is that the covariance and the variogram of it are related

$$\gamma_z(\boldsymbol{r}) = \sigma_z^2 - c_z(\boldsymbol{r}), \tag{2.24}$$

where σ_z^2 is the constant variance $\forall \boldsymbol{s} \in D$.

2.4.2 Ergodicity

Ergodicity attributes stochastic processes that their average behavior over time remains identical to that over space. Therefore it follows that ergodic processes are perforce stationary (without the reverse being true). From practical aspect, ergodicity implies that a single sample is sufficient for the estimation of the statistical properties (i.e. moments) of a random process (Yaglom, 1987).

Since the analysis of random fields is restricted to the study of 2nd-order moments (as already mentioned) the ergodic behavior of a stationary RF can sufficiently be established by demonstrating that the mean and covariance functions are ergodic (Chilès and Delfiner, 2012).

2.4.3 Isotropy & Anisotropy

A stochastic process is called isotropic if its attributes are independent of spatial direction, i.e. it exhibits uniform behavior in all orientations. For a stationary random field, isotropy means that its covariance and variogram can be expressed as functions of the modulus of the vector $\boldsymbol{r}$ instead of the simple vector, i.e.

$$c_z(\boldsymbol{r}) = c_z(\|\boldsymbol{r}\|), \tag{2.25}$$

and

$$\gamma_z(\boldsymbol{r}) = \gamma_z(\|\boldsymbol{r}\|). \tag{2.26}$$

Generally, there are two types of anisotropy, **zonal anisotropy** and **range or elliptical anisotropy**. In the first case, the random field exhibits directional dependent variance (σ_z^2). In the later case the directionally dependent attribute of the field is the correlation length (ξ).

Zonal anisotropy can be modelled simply as the superposition of n number of random fields, where n the dimensionality of the field. On the contrary, modelling range anisotropy is more complicated, as the model's parameters include n number of correlation lengths $\xi_1, \xi_2, ..., \xi_n$ (one for each dimension) and $m = \frac{n}{2} = \frac{n!}{2(n-2)!}$ number of rotation angles $\phi_1, \phi_2, ..., \phi_m$ (one for each plane containing two of the n axes). It is obvious that isotropy is a subcategory of range anisotropy, where $\xi_1 = \xi_2 = ... = \xi_n$ and $\phi_1 = \phi_2 = ... = \phi_m$. For a homogeneous random field modelling anisotropy can be achieved with the computation of an anisotropic norm of the distance, i.e. the covariance can be expressed as

$$c_z(\boldsymbol{r}) = c_z(\|\boldsymbol{r}\|_A), \tag{2.27}$$

where $\|\boldsymbol{r}\|_A$ is the anisotropic norm and is equivalent to the above mentioned dimensionless distance h.

The analytic computation of the anisotropic norm can be derived by using transformation matrices. Any random field can be considered as an anisotropic field, which has been derived from an initially isotropic one that was rescaled and rotated to its final elliptical form. In a 2D case, this can be mathematically depicted by using the following computations:

$$\begin{aligned}
\mathbf{r_{an}} &= \mathbf{R}\mathbf{S}\mathbf{r_{is}} \\
\Leftrightarrow \quad \begin{bmatrix} x' \\ y' \end{bmatrix} &= \begin{bmatrix} \cos\phi & -\sin\phi \\ \sin\phi & \cos\phi \end{bmatrix} \begin{bmatrix} \xi_1 & 0 \\ 0 & \xi_2 \end{bmatrix} \begin{bmatrix} x \\ y \end{bmatrix} \\
\Leftrightarrow \quad \begin{bmatrix} x' \\ y' \end{bmatrix} &= \begin{bmatrix} \xi_1\cos\phi & -\xi_2\sin\phi \\ \xi_1\sin\phi & \xi_2\cos\phi \end{bmatrix} \begin{bmatrix} x \\ y \end{bmatrix} \\
\Leftrightarrow \quad \mathbf{r_{an}} &= \mathbf{B}\mathbf{r_{is}},
\end{aligned} \tag{2.28}$$

where $\mathbf{r_{is}}$ the initial isotropic coordinations system, $\mathbf{r_{an}}$ the tranformed anisotropic coordinations system, $\mathbf{R}$ the rotation matrix, $\mathbf{S}$ the rescaling matrix, $\mathbf{B} = \mathbf{RS}$ the total tranformation matrix, ϕ the rotation angle measured counterclockwise between the horizontal axis of the coordinate system and the first met principal axis of the anisotropy ellipse, and ξ_1, ξ_2 the correlation lengths along each of the principal axes direction (ξ_1 refers to the direction of the rotation angle ϕ).

The anisotropic norm of the transformed (anisotropic) coordinations system, which is the point, is equivalent to the euclidean norm of the original isotropic coordinations system, i.e. $\|\mathbf{r_{an}}\|_A = \|\mathbf{r_{is}}\|$. Therefore, the inversion of the transformation, a graphical representation of which can also be seen in Fig. 2.2, and subsequently the calculation of the euclidean norm of the inverted (isotropic) coordinations system become necessary steps for the processing of an anisotropic field.

The transformation can be inverted as

$$\mathbf{r_{is}} = \mathbf{B^{-1}}\mathbf{r_{an}}, \tag{2.29}$$

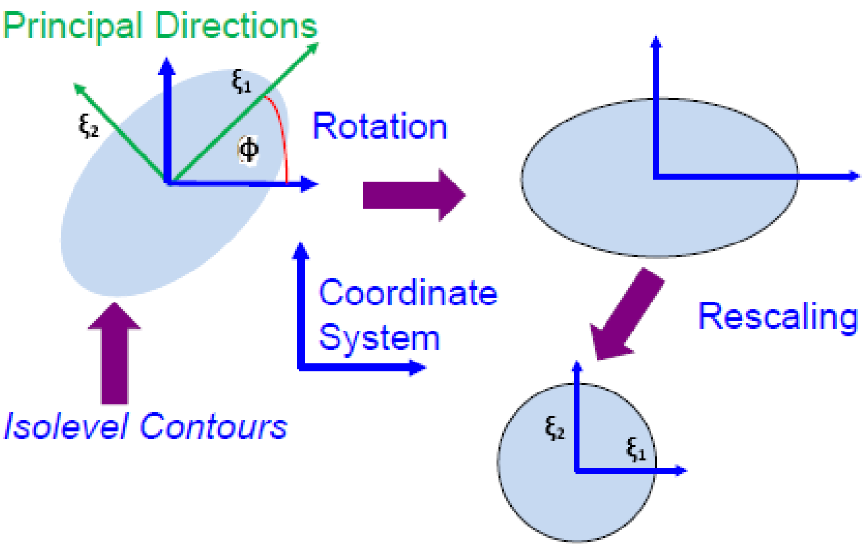

Figure 2.2 Inverse transformation of anisotropic coordinations system

where

$$
\begin{aligned}
\mathbf{B}^{-1} &= [\mathbf{RS}]^{-1} = \mathbf{S}^{-1}\mathbf{R}^{-1} \\
&= \begin{bmatrix} \xi_1 & 0 \\ 0 & \xi_2 \end{bmatrix}^{-1} \begin{bmatrix} \cos\phi & -\sin\phi \\ \sin\phi & \cos\phi \end{bmatrix}^{-1} \\
&= \frac{1}{\xi_1\xi_2} \begin{bmatrix} \xi_2 & 0 \\ 0 & \xi_1 \end{bmatrix} \frac{1}{cos^2\phi + sin^2\phi} \begin{bmatrix} \cos\phi & \sin\phi \\ -\sin\phi & \cos\phi \end{bmatrix} \\
&= \begin{bmatrix} \frac{1}{\xi_1} & 0 \\ 0 & \frac{1}{\xi_2} \end{bmatrix} \begin{bmatrix} \cos\phi & \sin\phi \\ -\sin\phi & \cos\phi \end{bmatrix} = \begin{bmatrix} \frac{\cos\phi}{\xi_1} & \frac{\sin\phi}{\xi_1} \\ \frac{-\sin\phi}{\xi_2} & \frac{\cos\phi}{\xi_2} \end{bmatrix}
\end{aligned} \tag{2.30}
$$

and the square of the euclidean norm of the inverted coordinations is, then, calculated as

$$
\begin{aligned}
h^2 &\equiv \|\mathbf{r_{an}}\|_A^2 \equiv \|\mathbf{r_{is}}\|^2 = \mathbf{r_{is}}^T\mathbf{r_{is}} \\
&= (\mathbf{B}^{-1}\mathbf{r_{an}})^T\mathbf{B}^{-1}\mathbf{r_{an}} = \mathbf{r_{an}}^T(\mathbf{B}^{-1})^T\mathbf{B}^{-1}\mathbf{r_{an}}.
\end{aligned} \tag{2.31}
$$

By setting $\mathbf{A} = (\mathbf{B^{-1}})^T\mathbf{B^{-1}}$ and substituting in Eq. (2.31) follows a more concise expression for the dimensioneless distance

$$h \equiv \|\mathbf{r_{an}}\|_A = \sqrt{\mathbf{r_{an}^T A r_{an}}}, \tag{2.32}$$

where A can be computed analytically by using the Eq. (2.30) as

$$\begin{aligned}
A &= (\mathbf{B^{-1}})^T\mathbf{B^{-1}} \\
&= \begin{bmatrix} \dfrac{\cos\phi}{\xi_1} & \dfrac{\sin\phi}{\xi_1} \\ \dfrac{-\sin\phi}{\xi_2} & \dfrac{\cos\phi}{\xi_2} \end{bmatrix}^T \begin{bmatrix} \dfrac{\cos\phi}{\xi_1} & \dfrac{\sin\phi}{\xi_1} \\ \dfrac{-\sin\phi}{\xi_2} & \dfrac{\cos\phi}{\xi_2} \end{bmatrix} \\
&= \begin{bmatrix} \dfrac{\cos\phi}{\xi_1} & \dfrac{-\sin\phi}{\xi_2} \\ \dfrac{\sin\phi}{\xi_1} & \dfrac{\cos\phi}{\xi_2} \end{bmatrix} \begin{bmatrix} \dfrac{\cos\phi}{\xi_1} & \dfrac{\sin\phi}{\xi_1} \\ \dfrac{-\sin\phi}{\xi_2} & \dfrac{\cos\phi}{\xi_2} \end{bmatrix} \\
&= \begin{bmatrix} \left(\dfrac{\cos\phi}{\xi_1}\right)^2 + \left(\dfrac{\sin\phi}{\xi_2}\right)^2 & \left(\dfrac{1}{\xi_1^2} - \dfrac{1}{\xi_2^2}\right)\cos\phi\sin\phi \\ \left(\dfrac{1}{\xi_1^2} - \dfrac{1}{\xi_2^2}\right)\cos\phi\sin\phi & \left(\dfrac{\sin\phi}{\xi_1}\right)^2 + \left(\dfrac{\cos\phi}{\xi_2}\right)^2 \end{bmatrix}.
\end{aligned} \tag{2.33}$$

Setting

$$A_1 = \left(\frac{\cos\phi}{\xi_1}\right)^2 + \left(\frac{\sin\phi}{\xi_2}\right)^2 \tag{2.34a}$$

$$A_2 = \left(\frac{\sin\phi}{\xi_1}\right)^2 + \left(\frac{\cos\phi}{\xi_2}\right)^2. \tag{2.34b}$$

$$A_{12} = \left(\frac{1}{\xi_1^2} - \frac{1}{\xi_2^2}\right)\cos\phi\sin\phi \tag{2.34c}$$

in Eq. (2.33) and combining with Eq. (2.32) it follows that

$$h \equiv \|\mathbf{r_{an}}\|_A = \sqrt{\mathbf{r_{an}^T A r_{an}}}$$
$$= \left(\begin{bmatrix} x' \\ y' \end{bmatrix}^T \begin{bmatrix} A_1 & A_{12} \\ A_{12} & A_2 \end{bmatrix} \begin{bmatrix} x' & y' \end{bmatrix} \right)^{1/2} \tag{2.35}$$
$$= \sqrt{A_1 x'^2 + 2A_{12}x'y' + A_2 y'^2}.$$

Note that in case of isotropic initial random field, i.e. $\xi_1 = \xi_2 = \xi$ and $\phi = 0$, it follows that $A_1 = A_2 = 1/\xi^2, A_12 = 0$ and the resulting dimensionless distance is

$$h = \sqrt{x'^2 + y'^2}/\xi = \|\mathbf{r}\|/\xi, \tag{2.36}$$

as it would be expected. Also, noticeable is the fact that an anisotropic field can be equivalently processed either as anisotropic by using the 2D dimensionless distance defined in Eq. (2.35) or as isotropic, using Eq. (2.36), after inverting the transformation effect.

Similar calculations can also be applied for 3-dimensional RFs, with the difference that three rotation angles (Euler angles) and three correlation lengths are needed in these cases to perform the inverse transformation. The corresponding 3D transformation matrix **B** is

$$\mathbf{B} = \begin{bmatrix} \xi_1 & 0 & 0 \\ 0 & \xi_2 & 0 \\ 0 & 0 & \xi_3 \end{bmatrix} \begin{bmatrix} \cos\phi_1 & -\sin\phi_1 & 0 \\ \sin\phi_1 & \cos\phi_1 & 0 \\ 0 & 0 & 1 \end{bmatrix} \begin{bmatrix} 1 & 0 & 0 \\ 0 & \cos\phi_2 & -\sin\phi_2 \\ 0 & \sin\phi_2 & \cos\phi_2 \end{bmatrix} \begin{bmatrix} \cos\phi_3 & -\sin\phi_3 & 0 \\ \sin\phi_3 & \cos\phi_3 & 0 \\ 0 & 0 & 1 \end{bmatrix}. \tag{2.37}$$

2.5 Permissible Covariance Functions

The covariance functions can not be any function, but have to meet some conditions. The conditions that determine the permissible covariance functions are provided by the Bochner's theorem.

Theorem 2.1. *A function $c_z(\boldsymbol{r})$ is a permissible covariance function, if the following conditions hold:*

(i) the integral $\widetilde{c_z}(\boldsymbol{k}) = \int c_z(\boldsymbol{r}) e^{-i\boldsymbol{kr}} d\boldsymbol{r}$ exists and is symmetric $\widetilde{c_z}(\boldsymbol{k}) = \widetilde{c_z}(-\boldsymbol{k})$,

(ii) it is non negative for all frequencies $\boldsymbol{k}$, and

(iii) is bounded for all frequencies $\boldsymbol{k}$.

The first condition implies that the Fourier transform of $c_z(\boldsymbol{r})$ (also called spectral density function of the random field) exists. Moreover, the symmetry of $c_z(\boldsymbol{r})$ ensures the positive semidefinitness of the covariance function, which is essential for the inversion of covariance matrices (see section 3). The second condition demands that $\widetilde{c_z}(\boldsymbol{k}) \geq 0 \quad \forall \boldsymbol{k} \in \mathbb{R}^n$. Finally, the third condition ensures the existence of the RF's variance (σ_z^2) (Bochner et al., 1959).

Table 2.2 Permissible Covariance Functions. $K_\nu(\cdot)$ denote the modified Bessel functions of the second kind of order ν, $\Gamma(\cdot)$ denote the Gamma function, h denotes the dimensionless distance, $\Delta = |\eta_1^2 - 4|^{1/2}$, $\beta_{1,2} = |2 \mp \eta_1|^{1/2}/2$, and $\omega_{1,2} = (|\eta_1 \mp \Delta|/2)^{1/2}$.

Model	**Covariance**
Nugget Effect	$c_z(h) = \begin{cases} \sigma_z^2, & h = 0 \\ 0, & h \neq 0 \end{cases}$
Generalized Exponential	$c_z(h) = \sigma_z^2 e^{-h^\nu}, \qquad 0 < \nu < 2$
Gaussian	$c_z(h) = \sigma_z^2 e^{-h^2}$
Spherical	$c_z(h) = \begin{cases} \sigma_z^2(1 - 1.5h + 0.5h^3), & 0 \leq h \leq 1 \\ 0, & h > 1 \end{cases}$
Cubic	$c_z(h) = \begin{cases} \sigma_z^2 \left(1 - 7h^2 + \frac{35}{4}h^3 - \frac{7}{2}h^5 + \frac{3}{4}h^7\right), & 0 \leq h \leq 1 \\ 0, & h > 1 \end{cases}$
Matérn (or Bessel-K)	$c_z(h) = \sigma_z^2 \frac{h^\nu K_\nu(h)}{2^{\nu-1}\Gamma(\nu)}, \qquad \nu > 0$
Generalized Cauchy	$c_z(h) = \sigma_z^2(1 + h^\alpha)^{-\nu/\alpha}, \qquad 0 < \alpha < 2, \quad \nu > 0$
Rational Quadratic	$c_z(h) = \sigma_z^2(1 + h^2)^{-\nu}, \qquad \nu > 0$
Exponential Sine	$c_z(h) = \sigma_z^2 \sin\left(\frac{\pi}{2} e^{-h}\right)$
Cardinal Sine	$c_z(h) = \sigma_z^2 \frac{\sin(h)}{h}$
Spartan (3D)	$c_z(h) = \begin{cases} \frac{\eta_0}{2\pi\Delta} e^{-h\beta_2} \left(\frac{\sin(h\beta_1)}{h}\right), & \lvert\eta_1\rvert < 2 \quad (\sigma_z^2 = \frac{\eta_0}{4\pi\sqrt{2+\eta_1}}), \\ \frac{\eta_0}{8\pi} e^{-h}, & \eta_1 = 2 \quad (\sigma_z^2 = \frac{\eta_0}{8\pi}), \\ \frac{\eta_0}{4\pi\Delta} \left(\frac{e^{-h\omega_1} - e^{-h\omega_2}}{h}\right), & \eta_1 > 2 \quad (\sigma_z^2 = \frac{\eta_0}{4\pi\Delta}(\omega_2 - \omega_1)) \end{cases}$

The mathematical expressions of some permissible covariance functions are shown in Table 2.2, while Fig. 2.3 depicts some graphs of them.

The model of Nugget Effect describes fluctuations that are spatially uncorrelated, such those that take place in distances shorter than the resolution of the sample or those resulting from errors of the sampling method.

The Generalized Exponential model characterizes distributions with abrupt spatial changes, i.e. the spatial correlation decreases rapidly with the increase of distance. The rapidity of the reduction increases with the decreasing of the value of the smoothness parameter ν. The most widely used model of the Generalized Exponential family is the one with $\nu = 1$; the Exponential model.

In contrast, the Gaussian model characterizes smoother spatial changes. However, a strong disadvandage of it is that it can lead to numerical instabilities in the covariance matrix calculation.

Spherical and Cubic models indicate RFs with even faster decreasing. Also, unlike the other models which asymptotically decline to zero when $h \to \infty$, they are zeroed for $h > 1$ (h denotes the dimensionless distance as defined in section 2.4.3).

Exponential Sine and Cardinal Sine models describe fluctuations with wavy and oscillatory behavior. The Generalized Cauchy model and the Rational Quadratic model, which is a subcase of the first, exhibit power-law dependence with different exponents in small and large scales (Chilès and Delfiner, 2012).

The Matérn or Bessel-K model is characterized by great flexibility since different values of the parameter ν correspond to different behaviors of the model. In Table 2.3 the special mathematical expressions of the Matérn model for different values of ν are presented (Chilès and Delfiner, 2012; Guttorp and Gneiting, 2006).

Finally, the Spartan model (SSRF) derives from the generalized Gibbs random fields theory. It differs from the other models since it is expressed through the parameters η_0 and η_1 instead of σ_z^2. The parameter η_0 is the scaling factor (defined the magnitude) of the covariance function, while the parameter η_1 (rigidity parameter) is related to the shape.The Spartan model, similar to the Matérn, exhibits great flexibility due to the different expressions obtained depending on the value of the parameter η_1. For $\eta_1 = 2$ the Spartan model is equivalent to the Exponential model, for $|eta_1| < 2$ it is similar to the product of Exponential and Cardinal Sine models and exhibits oscillatory behavior, and for $\eta_1 > 2$ a new form is obtained (Hristopulos and Elogne, 2007).

Furthermore, any combination (e.g. summation, multiplication, etc.) of permissible covariance functions leads to also permissible covariance function. The most commonly used combination is the summation of the nugget effect model with any of the other permissible models (Fig. 2.5). This combination enables the modelling of a data sample which contains errors due to the low resolution or the errors of the acquisition method or equipment.

Table 2.3 Special cases of Matérn model for different values of ν

ν	**Expression**	**Name**
$\nu = 1/3$	$c_z(h) = \sigma_z^2 2^{2/3} h^{1/3} K_{1/3}(h)/\Gamma(1/3)$	von Kármán
$\nu = 1/2$	$c_z(h) = \sigma_z^2 e^{-h}$	Exponential
$\nu = 1$	$c_z(h) = \sigma_z^2 h K_1(h)$	Whittle
$\nu = 3/2$	$c_z(h) = \sigma_z^2 (1+h) e^{-h}$	Modified Exponential
$\nu = 2$	$c_z(h) = \sigma_z^2 \frac{h^2}{2} K_2(h)$	-
$\nu = 5/2$	$c_z(h) = \sigma_z^2 (1+h+\frac{1}{3}h^2) e^{-h}$	3rd order autoregressive
$\nu = 3$	$c_z(h) = \sigma_z^2 \frac{1}{8} h^3 K_3(h)$	-
$\nu = 7/2$	$c_z(h) = \sigma_z^2 \frac{h^{7/2} K_{7/2}(h)}{2^{5/2}\Gamma(7/2)}$	-

Having determined the permissible covariance models, it is possible to determine the corresponding variogram models, at least for stationary random fields, as Eq. (2.24) indicates. Examples of permissible variogram models are shown in Table 2.4 and plots in Fig. 2.4.

Table 2.4 Permissible Variogram Functions. $K_\nu(\cdot)$ denote the modified Bessel functions of the second kind of order ν, $\Gamma(\cdot)$ denote the Gamma function, h denotes the dimensionless distance, $\Delta = |\eta_1^2 - 4|^{1/2}$, $\beta_{1,2} = |2 \mp \eta_1|^{1/2}/2$, and $\omega_{1,2} = (|\eta_1 \mp \Delta|/2)^{1/2}$.

Model	**Variogram**
Nugget Effect	$\gamma_z(h) = \begin{cases} 0, & h = 0 \\ \sigma_z^2, & h \neq 0 \end{cases}$
Generalized Exponential	$\gamma_z(h) = \sigma_z^2 \left(1 - e^{-h^\nu}\right), \qquad 0 < \nu < 2$
Gaussian	$\gamma_z(h) = \sigma_z^2 \left(1 - e^{-h^2}\right)$
Spherical	$\gamma_z(h) = \begin{cases} \sigma_z^2 \left(1.5h - 0.5h^3\right), & 0 \leq h \leq 1 \\ \sigma_z^2, & h > 1 \end{cases}$
Cubic	$\gamma_z(h) = \begin{cases} \sigma_z^2 \left(7h^2 - \frac{35}{4}h^3 + \frac{7}{2}h^5 - \frac{3}{4}h^7\right), & 0 \leq h \leq 1 \\ \sigma_z^2, & h > 1 \end{cases}$
Matérn (or Bessel-K)	$\gamma_z(h) = \sigma_z^2 \left(1 - \frac{h^\nu K_\nu(h)}{2^{\nu-1}\Gamma(\nu)}\right), \qquad \nu > 0$
Generalized Cauchy	$\gamma_z(h) = \sigma_z^2 \left(1 - (1 + h^\alpha)^{-\nu/\alpha}\right), \qquad 0 < \alpha < 2, \quad \nu > 0$
Rational Quadratic	$\gamma_z(h) = \sigma_z^2 \left(1 - (1 + h^2)^{-\nu}\right), \qquad \nu > 0$
Exponential Sine	$\gamma_z(h) = \sigma_z^2 \left(1 - \sin\left(\frac{\pi}{2} e^{-h}\right)\right)$
Cardinal Sine	$\gamma_z(h) = \sigma_z^2 \left(1 - \frac{\sin(h)}{h}\right)$
Spartan (3D)	$\gamma_z(h) = \begin{cases} \frac{\eta_0}{2\pi} \left(\frac{1}{2\sqrt{2+\eta_1}} - \frac{1}{\Delta}\right) e^{-h\beta_2} \frac{\sin(h\beta_1)}{h}, & \lvert\eta_1\rvert < 2, \\ \frac{\eta_0}{8\pi} \left(1 - e^{-h}\right), & \eta_1 = 2, \\ \frac{\eta_0}{4\pi\Delta}(\omega_2 - \omega_1) \left(1 - \frac{e^{-h\omega_1} - e^{-h\omega_2}}{h(\omega_2 - \omega_1)}\right), & \eta_1 > 2 \end{cases}$

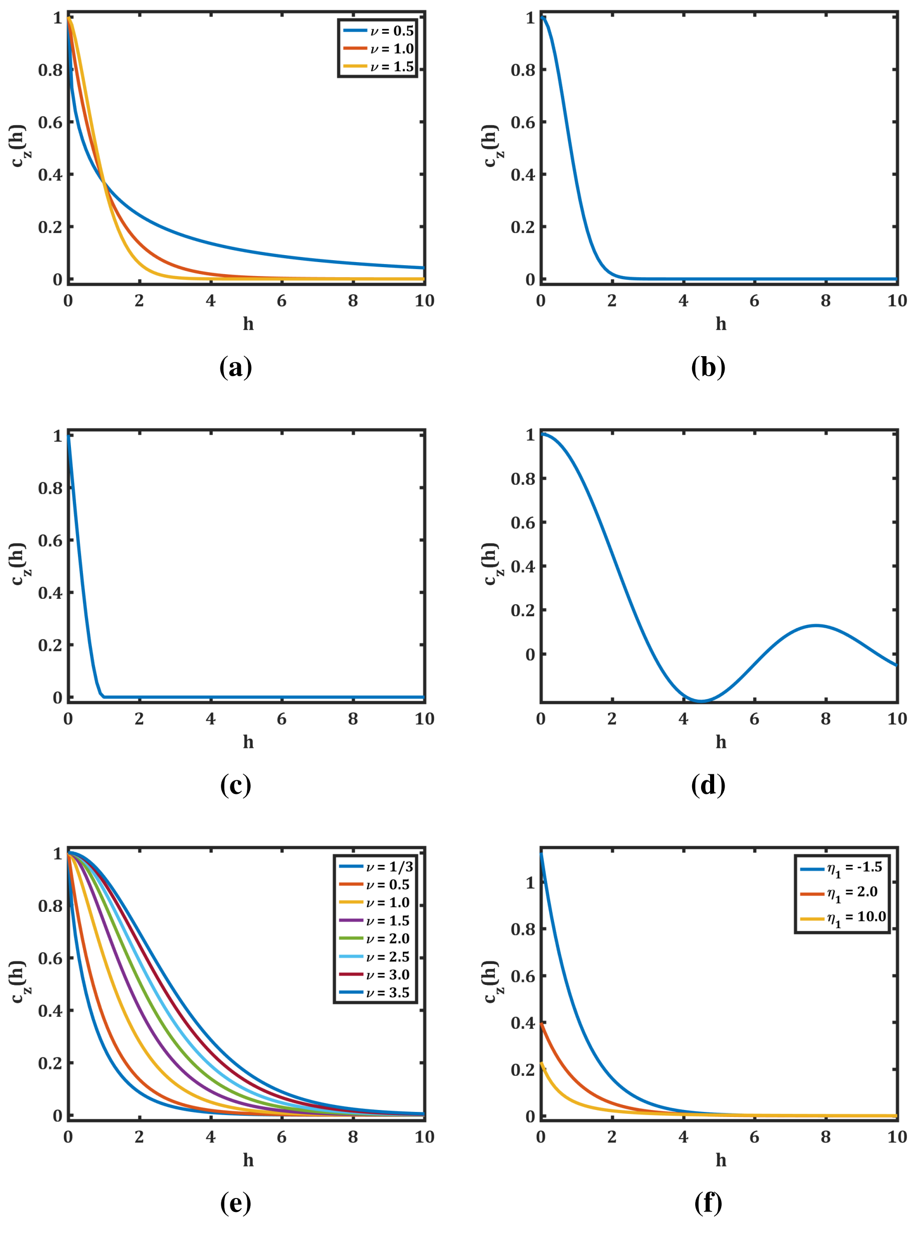

Figure 2.3 Permissible Covariance Models: a) Generalized Exponential; b) Gaussian; c) Spherical; d) Cardinal Sine; e) Matérn; f) Spartan (3D). The used parameters are $\sigma_z^2 = 1$, $\xi = 1$ and $\eta_0 = 10$ (h is the dimensionless distance $h = r/\xi$ where ξ the correlation length).

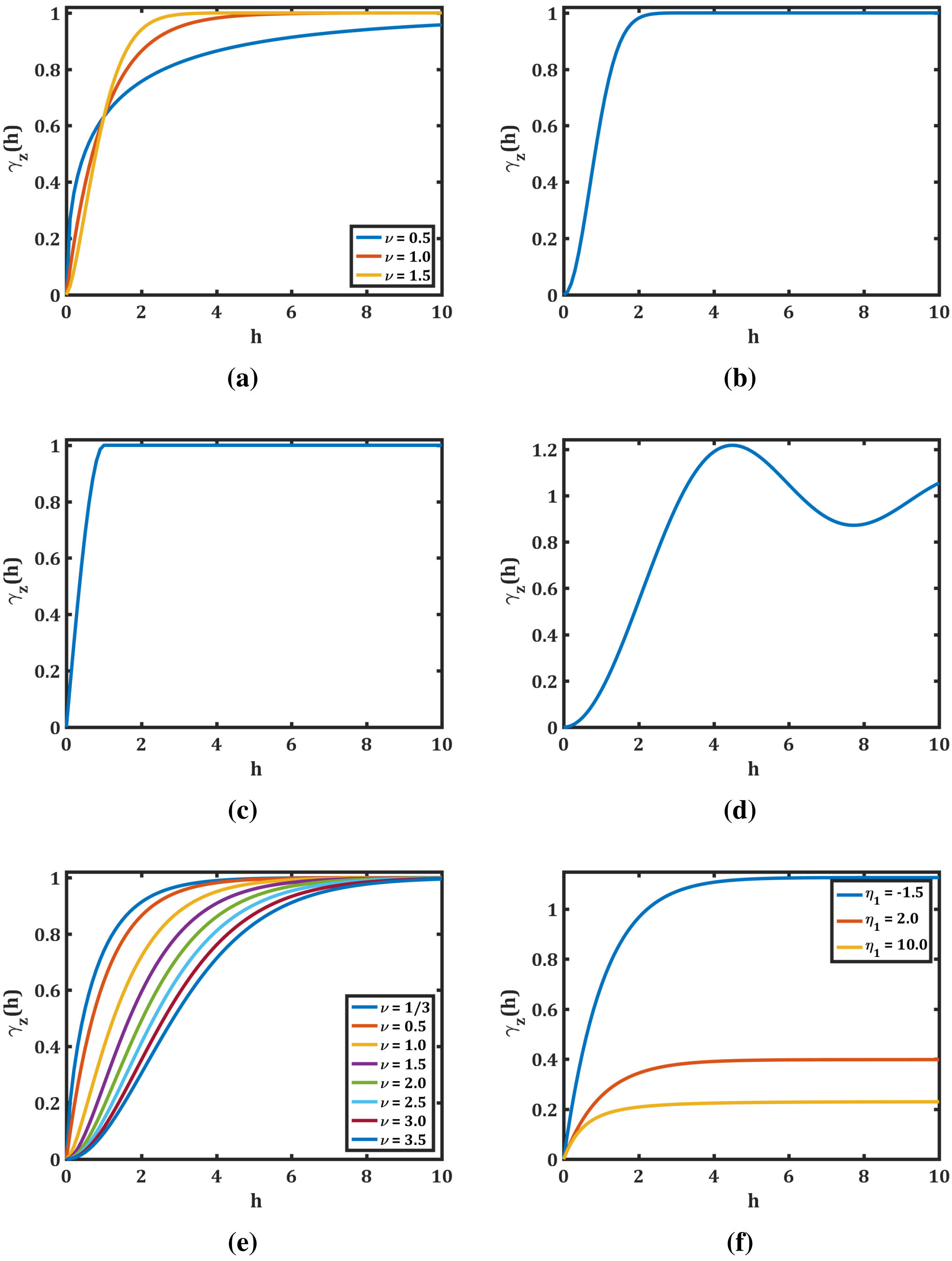

Figure 2.4 Variogram Models: a) Generalized Exponential; b) Gaussian; c) Spherical; d) Cardinal Sine; e) Matérn; f) Spartan (3D). The used parameters are $\sigma_z^2 = 1$, $\xi = 1$ and $\eta_0 = 10$ (h is the dimensionless distance $h = r/\xi$ where ξ the correlation length).

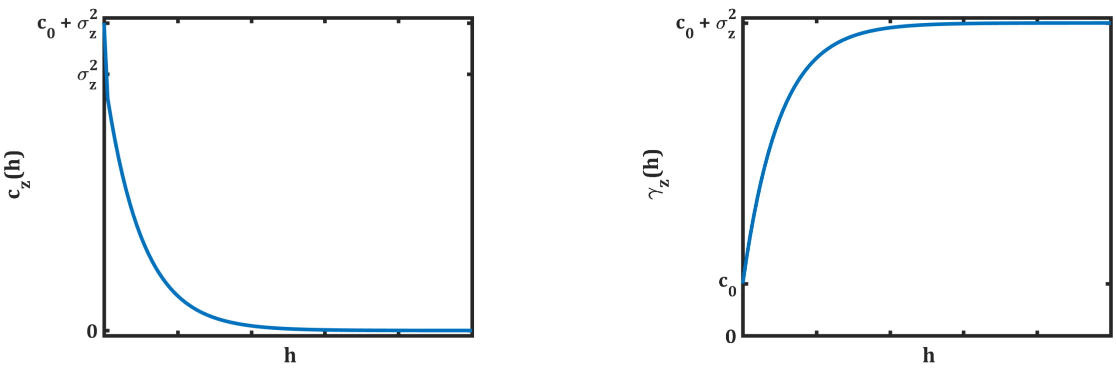

(a) **(b)**

Figure 2.5 Summation of Permissible Model with Nugget Effect: a) Covariance; b) Variogram.

2.6 Experimental Covariance and Variogram

In many cases, the computation of the experimental covariance or variogram from the data is necessary. The experimental variogram is computed as:

$$\hat{\gamma}_z(\mathbf{h}) = \frac{1}{2N(\mathbf{h})} \sum_{i=1}^{N(\mathbf{h})} \left[z(\mathbf{s_i}) - z(\mathbf{s_i} + \mathbf{h})\right]^2, \tag{2.38}$$

and the experimental covariance as:

$$\hat{C}_z(\mathbf{h}) = \frac{1}{2N(\mathbf{h})} \sum_{i=1}^{N(\mathbf{h})} \left[z(\mathbf{s_i})z(\mathbf{s_i} + \mathbf{h}) - \hat{m}_z(\mathbf{s_i} - \mathbf{h})\hat{m}_z(\mathbf{s_i} + \mathbf{h})\right], \tag{2.39}$$

where $N(\mathbf{h})$ is the number of pairs of data locations i which are separated by a vector $\mathbf{h}$. Hence, in a 2D anisotropic case the space is separated into cyclical sections defined from an upper and lower anglular limit and an upper and lower distance limit (see Fig. 2.6). For each of these sections the corresponding experimental variogram value $\hat{\gamma}_z(\mathbf{s_{c,k}})$ is calculated and attached to the center of it, $\mathbf{s_{c,k}}$. For isotropic 2D cases or 1D cases, only distance limits are applied and the experimental variogram values are attached to the center of the resulting distance sections (or lags).

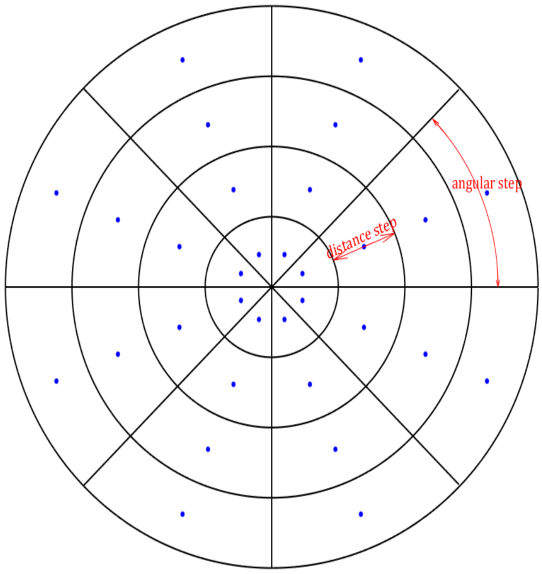

Figure 2.6 Space separation into cyclical sections

Chapter 3

Kriging

3.1 Basic Notions of Kriging

Kriging is the method developed by the South African engineer Danie G. Krige in 1951 while working on the evaluation of the Witwatersrand reef complex (South Africa) gold resources (Cressie, 1990; Krige, 1951). Kriging is the most commonly used geostatistical method of interpolation. The Kriging Estimator predicts the value of a random field $Z(\cdot)$ at a point $\mathbf{s_u}$, where no measurements are available, as a weighted average of n neighbooring values $(Z(\mathbf{s_1}), Z(\mathbf{s_2}), ..., Z(\mathbf{s_n}))$. The set of prediction points (S_u) comprises the nodes of a regular grid, which covers the area of interest. In this way, the estimation of the missing values leads to the mapping and the iso-level contour representation of the random field over it. The neighbooring points, where measurements are available, consist the sampling set (S_s). For the predictions ideally the whole sampling set is used. However, in the cases where the computational complexity is high, it is possible to use only a part of the dataset. This can be achieved by using only the sampling points within a user-defined kriging neighboorhood around the prediction point.

The generalized Kriging Estimator is mathematically expressed as:

$$\hat{Z}(\mathbf{u}) = m_z(\mathbf{u}) + \sum_{i=1}^{n(\mathbf{u})} \lambda_i \left[Z(\mathbf{s_i}) - m_z(\mathbf{s_i}) \right], \tag{3.1}$$

where λ_i are the linear weights of the sampling points and $n(\mathbf{u})$ is the number of the sampling points within the kriging neighboorhood of the prediction point $\mathbf{s_u}$.

The weights of the Kriging Estimator are calculated by considering three restrictions:

- the estimations must respect the real data; thus, the statistical information derived from the data (covariance or variogram model) is used,

- the variance of the error of the estimation must be minimized, and
- the unbiasedness constraint must be fullfilled.

The predictions given by the Kriging Estimator, due to the minimization of the variance of the estimation's error, are the best linear unbiased estimations (BLUE) (Goovaerts, 1997). Kriging, in contrast to other methods of interpolation, makes possible the quantification of the uncertainty of the estimations at each point, giving a validation tool for the estimations' reliability.

3.1.1 Error Variance

The error variance is given from the equation:

$$\sigma_E^2(\mathbf{u}) = Var\left[Z(\mathbf{u}) - \hat{Z}(\mathbf{u})\right]. \tag{3.2}$$

The minimization of it and therefore the obtainment of the optimal linear weights λ_i is achieved by setting to zero each of the $n(\mathbf{u})$ partial first derivatives of the error variance with respect to the weights, i.e.

$$\frac{\partial \sigma_E^2(\mathbf{u})}{\partial \lambda_i} = 0, \quad i = 1, \ldots, n(\mathbf{u}). \tag{3.3}$$

The restriction imposed by the *unbiasedness constraint*, under which the optimization must be done, ensures that the mean value of the error $\varepsilon(\mathbf{u}) = Z(\mathbf{u}) - \hat{Z}(\mathbf{u})$ is zeroed, i.e.

$$\mathbb{E}[\varepsilon(\mathbf{u})] = \mathbb{E}[Z(\mathbf{u}) - \hat{Z}(\mathbf{u}] = 0. \tag{3.4}$$

If it is not fulfilled by default from the Kriging Estimator (see section 3.2.2), it is imposed as an additional restriction for the linear weights (Chilès and Delfiner, 2012; Oliver and Webster, 2015).

3.2 Methods of Kriging

There are various methods of Kriging, with the following to be the most widely used:

- **Simple Kriging (SK)**, which applies when the mean value of the random field is constant and known.
- **Ordinary Kriging (OK)**, which applies when the mean value of the field is constant within the neighboorhood of the estimated point but unknown.

- **Universal Kriging (UK)**, which applies when the mean value of the field is not constant (depends on the location) and unknown.
- **Indicator Kriging (IK)**, which applies when the values of the random field can be sorted into categories by using threshold values.
- **Co-Kriging (CK)**, which applies when the values of the random field are correlated to more than one variables, i.e. in multivariate cases, where the cross-correlation functions between the variables must be taken into account.

Herein, only the first two methods of Kriging will be described in details.

3.2.1 Simple Kriging

Simple Kriging (SK) is applied when the mean value of the random field is known and constant throughout the area of interest, i.e. $\mathbb{E}[Z(\mathbf{s})] = m_z$. Replacing to Eq. (3.1), the expression for the Simple Kriging Estimator derives as:

$$\hat{Z}(\mathbf{u}) = m_z \left[1 - \sum_{i=1}^{n(\mathbf{u})} \lambda_i\right] + \sum_{i=1}^{n(\mathbf{u})} \lambda_i Z(\mathbf{s_i}). \tag{3.5}$$

The mean of the estimation's error is:

$$\begin{aligned}
\mathbb{E}[\varepsilon(\mathbf{u})] &= \mathbb{E}[Z(\mathbf{u}) - \hat{Z}(\mathbf{u})] \\
&= \mathbb{E}[Z(\mathbf{u}) - m_z \left[1 - \sum_{i=1}^{n(\mathbf{u})} \lambda_i\right] - \sum_{i=1}^{n(\mathbf{u})} \lambda_i Z(\mathbf{s_i})] \\
&= \mathbb{E}[Z(\mathbf{u})] - \mathbb{E}[m_z] + \sum_{i=1}^{n(\mathbf{u})} \lambda_i \mathbb{E}[m_z] - \sum_{i=1}^{n(\mathbf{u})} \lambda_i \mathbb{E}[Z(\mathbf{s_i})] \\
&= m_z - m_z + \sum_{i=1}^{n(\mathbf{u})} \lambda_i m_z - \sum_{i=1}^{n(\mathbf{u})} \lambda_i m_z = 0.
\end{aligned} \tag{3.6}$$

This means that the SK Estimator fulfills by construction the unbiassedness constraint and therefore no additional restriction has to be imposed to the error variance minimization.

The optimal linear weights λ_i are calculated by solving the linear equations system deriving from Eq. (3.3):

$$\sum_{i=1}^{n(\mathbf{u})} \lambda_j c_z(\mathbf{s_i} - \mathbf{s_j}) = c_z(\mathbf{s_i} - \mathbf{s_u}), \quad i, j = 1, ..., n(\mathbf{u}), \tag{3.7}$$

or in formulation of matrix equation:

$$\mathbf{C}_{i,j}\lambda_j = \mathbf{C}_{i,u}$$

$$\Leftrightarrow \begin{bmatrix} c_z(\mathbf{s_1}-\mathbf{s_1}) & \cdots & \cdots & c_z(\mathbf{s_1}-\mathbf{s_n}) \\ c_z(\mathbf{s_2}-\mathbf{s_1}) & \cdots & \cdots & c_z(\mathbf{s_2}-\mathbf{s_n}) \\ \vdots & \vdots & \vdots & \vdots \\ c_z(\mathbf{s_n}-\mathbf{s_1}) & \cdots & \cdots & c_z(\mathbf{s_n}-\mathbf{s_n}) \end{bmatrix} \begin{bmatrix} \lambda_1 \\ \lambda_2 \\ \vdots \\ \lambda_n \end{bmatrix} = \begin{bmatrix} c_z(\mathbf{s_1}-\mathbf{u}) \\ c_z(\mathbf{s_2}-\mathbf{u}) \\ \vdots \\ c_z(\mathbf{s_n}-\mathbf{u}) \end{bmatrix} \tag{3.8}$$

$$\Leftrightarrow \begin{bmatrix} \sigma_z^2 & \cdots & \cdots & c_z(\mathbf{s_1}-\mathbf{s_n}) \\ c_z(\mathbf{s_2}-\mathbf{s_1}) & \cdots & \cdots & c_z(\mathbf{s_2}-\mathbf{s_n}) \\ \vdots & \vdots & \vdots & \vdots \\ c_z(\mathbf{s_n}-\mathbf{s_1}) & \cdots & \cdots & \sigma_z^2 \end{bmatrix} \begin{bmatrix} \lambda_1 \\ \lambda_2 \\ \vdots \\ \lambda_n \end{bmatrix} = \begin{bmatrix} c_z(\mathbf{s_1}-\mathbf{u}) \\ c_z(\mathbf{s_2}-\mathbf{u}) \\ \vdots \\ c_z(\mathbf{s_n}-\mathbf{u}) \end{bmatrix},$$

where $\mathbf{C}_{i,j}$ represents the covariance matrix between the neighboors of the studied missing value, and $\mathbf{C}_{i,u}$ represents the covariance matrix between the neighboors and the missing value (Goovaerts, 1997). These covariance matrices are calculated using the variogram model, inferred from the real data, as indicated by Eq. (2.24).

The linear system has a solution if and only if the covariance function is permissible (semi-positive definite), which implies that the covariance matrix can be inverted. The solution is given by the following equation:

$$\lambda_j = \mathbf{C_{i,j}}^{-1}\mathbf{C_{i,u}}, \quad \forall j = 1,\ldots,n(\mathbf{u}), \tag{3.9}$$

and the error variance, which determines the uncertainty of the estimation, is calculated as:

$$\sigma^2_{E,SK}(\mathbf{u}) = \sigma_z^2 - \sum_{i=1}^{n(\mathbf{u})} \lambda_i c(\mathbf{s_i}-\mathbf{s_u}), \quad i = 1,\ldots,n(\mathbf{u}). \tag{3.10}$$

3.2.2 Ordinary Kriging

Ordinary Kriging (OK) is applied when the mean value of the random field is constant within the neighboorhood of the missing point but unknown. In this case, the Ordinary Kriging Estimator which derives from Eq. (3.1) is expressed as:

$$\hat{Z}(\mathbf{u}) = \sum_{i=1}^{n(\mathbf{u})} \lambda_i Z(\mathbf{s_i}). \tag{3.11}$$

The mean of the estimation's error is:

$$\begin{aligned}\mathbb{E}[\varepsilon(\mathbf{u})] &= \mathbb{E}[Z(\mathbf{u}) - \hat{Z}(\mathbf{u})] = \mathbb{E}[Z(\mathbf{u}) - \sum_{i=1}^{n(\mathbf{u})} \lambda_i Z(\mathbf{s_i})] \\ &= \mathbb{E}[Z(\mathbf{u})] - \sum_{i=1}^{n(\mathbf{u})} \lambda_i \mathbb{E}[Z(\mathbf{s_i})] = m_{\hat{z}} - \sum_{i=1}^{n(\mathbf{u})} \lambda_i m_z.\end{aligned} \tag{3.12}$$

Considering that the mean value of the estimations has, obviously, to be equal to the mean value of the random field, i.e. $m_{\hat{z}} \equiv m_z$ and setting the mean of the estimation's error to zero, as unbiasedness constraint imposes, Eq. (3.12) leads to the following:

$$\begin{aligned}&\mathbb{E}[\varepsilon(\mathbf{u})] = 0 \Leftrightarrow m_{\hat{z}} - \sum_{i=1}^{n(\mathbf{u})} \lambda_i m_z = 0 \Leftrightarrow m_z - \sum_{i=1}^{n(\mathbf{u})} \lambda_i m_z = 0 \Leftrightarrow m_z \left(1 - \sum_{i=1}^{n(\mathbf{u})} \lambda_i\right) = 0 \\ &\Leftrightarrow 1 - \sum_{i=1}^{n(\mathbf{u})} \lambda_i = 0 \Leftrightarrow \sum_{i=1}^{n(\mathbf{u})} \lambda_i = 1.\end{aligned} \tag{3.13}$$

The above result indicates that the OK Estimator, as opposed to the SK Estimator, is not unbiased by structure but the additional limitation of unit summed linear weights needs to be imposed to the error variance minimization. This is achieved by means of the *Lagrange multiplier method*, and one more partial derivative of the error variance is added to the linear equations system of Eq. (3.3), this with respect to the Lagrange multiplier, μ, i.e.

$$\frac{\partial \sigma_E^2(\mathbf{u})}{\partial \mu} = 0. \tag{3.14}$$

Therefore, the optimal linear weights λ_i of Ordinary Kriging are calculated by solving the following linear equations system:

$$\begin{aligned}&\sum_{i=1}^{n(\mathbf{u})} \lambda_j c_z(\mathbf{s_i} - \mathbf{s_j}) + \mu = c_z(\mathbf{s_i} - \mathbf{s_u}), \quad i, j = 1, \ldots, n(\mathbf{u}) \\ &\sum_{i=1}^{n(\mathbf{u})} \lambda_i = 1,\end{aligned} \tag{3.15}$$

or in formulation of matrix equation:

$$\begin{bmatrix} \sigma_z^2 & c_z(\mathbf{s_1}-\mathbf{s_2}) & \cdots & c_z(\mathbf{s_1}-\mathbf{s_n}) & 1 \\ c_z(\mathbf{s_2}-\mathbf{s_1}) & \sigma_z^2 & \cdots & c_z(\mathbf{s_2}-\mathbf{s_n}) & 1 \\ \vdots & \vdots & \vdots & \vdots & \vdots \\ c_z(\mathbf{s_n}-\mathbf{s_1}) & c_z(\mathbf{s_n}-\mathbf{s_2}) & \cdots & \sigma_z^2 & 1 \\ 1 & 1 & \cdots & 1 & 0 \end{bmatrix} \begin{bmatrix} \lambda_1 \\ \lambda_2 \\ \vdots \\ \lambda_n \\ \mu \end{bmatrix} = \begin{bmatrix} c_z(\mathbf{s_1}-\mathbf{u}) \\ c_z(\mathbf{s_2}-\mathbf{u}) \\ \vdots \\ c_z(\mathbf{s_n}-\mathbf{u}) \\ 1 \end{bmatrix}. \tag{3.16}$$

The error variance of the Ordinary Kriging estimation is calculated as:

$$\sigma^2_{E,OK}(\mathbf{u}) = \sigma_z^2 - \sum_{i=1}^{n(\mathbf{u})} \lambda_i c(\mathbf{s_i}-\mathbf{s_u}) - \mu, \quad i = 1,...,n(\mathbf{u}). \tag{3.17}$$

Comparing it with the error variance of the SK it follows that

$$\sigma^2_{E,OK}(\mathbf{u}) = \sigma^2_{E,SK}(\mathbf{u}) - \mu, \tag{3.18}$$

which, taking into account the always negative value of parameter μ, indicates that the uncertainty of OK is greater than this of SK. This is due to the assumption of unknown mean value that OK method makes, which leads to greater uncertainty.

Chapter 4

Stochastic Simulations

Stochastic Simulations is a widely used tool for estimating missing values of a random field in cases when the existing information is deemed inadequate for straightforward interpolation, for estimating the cdf of a variable from a dataset or for estimating error margins. In general, stochastic simulations generate a large number of realizations of the studied field, which emulate the characteristics of the observed realization (real data). By processing statistically these realizations the best estimation of the field, as well as the associated uncertainty can be derived.

The main difference between stochastic simulation and kriging is that the former aims to maintain the general characteristics of the data over local accuracy, while the later gives the estimation with the minimum error variance without deference to the global statistics.

There are several theoretically established and practically implemented stochastic simulation methods. They can be, broadly, categorized into *parametric* and *non-parametric* depending on the necessity or not of a priori knowledge of an explicit mathematical (parametric) model, as well as into *conditional* and *unconditional* depending on the placement or not of constraints on the values generated at sampling points, so as the simulation returns the known values (Webster and Oliver, 2007).

Herein, two methods will be briefly presented: i) Turning-Bands (TB) method, and ii) Directional Gradient-Curvature (DGC) method.

4.1 Turning-Bands Method

The Turning-Bands Method (Chentsov, 1957; Mantoglou and Wilson, 1982) is a parametric unconditional simulation method, which applies on second-order stationary, isotropic and Gaussian random fields.

The general procedure of the TB method is described by the following steps:

1. Performance, if needed, of suitable transformations of the data values, aiming to the fulfilment of stationarity, isotropy and normality preconditions. Data values are assumed to transform from the z-space to the y-space.
2. Computation and modelling of the covariance $c_s(h)$ of the y-space data.
3. Determination of a regular square or cubic grid, in two or three dimensions, respectively, covering the study area.
4. Generation of L number of random lines (bands) around an arbitrary origin of the grid (usually a centroid located at the grid center) with the corresponding direction vectors **e** uniformly distributed on the unit circle or sphere. The number of the bands is controlled by the modeler.
5. Generation, for each line, of a second-order stationary unidimensional discrete process with zero mean and covariance function $c_s(l_i)$, where l_i is the coordinate on the corresponding line. Due to the discrete line process, a set of bands is defined from the limits of each discretized segment, which turn, as the lines turn; hence the name 'turning bands method'.
6. Orthogonal projection of the regular grid's nodes $\mathbf{s_g}$ to each line and assignment to them the corresponding values of the one dimensional discrete process. As a result derives the generation of L independent unidimensional realizations (one for each line) with covariance function $c_s(l_i)$, i.e. at every node of the regular grid there are L values $z_i(l_i)$ assigned from the L unidimensional realizations (simulations).
7. Assignment to each node the value $z(\mathbf{s_g})$ given by

$$z(\mathbf{s_g}) = \frac{1}{\sqrt{L}} \sum_{i=1}^{L} z_i(l_i), \quad i = 1, ..., L, \tag{4.1}$$

   as the realization of the two- or three- dimensional random field.
8. Estimation of the uncertainty of each node's value as

$$\sigma^2(\mathbf{s_g}) = Var[z_i(l_i) z_j(l_j)], \quad i, j = 1, ..., L. \tag{4.2}$$

9. Back-transform the simulated y-space values to the simulated z-space values.

4.2 Directional Gradient-Curvature method

The Directional Gradient-Curvature (DGC) method, established by Žukovič and Hristopulos (2013a,b), is a novel tool for non-parametric conditional simulations designed for reconstructing missing grid data. It is based on the matching of the normalised squared gradient and curvature of the sample and entire domain data using conditional Monte Carlo simulations. Direction-dependent information (e.g. non-stationarity, anisotropy) is captured by using the local information of the immediate neighboorhood centered at each missing point. The DGC method can be used to model complex structured random fields without requiring a parametric formulation of it. In addition, the necessary user input is minimal.

In order to reduce the computational cost of the method, the sample's continuously valued field $Z(\mathbf{s_s})$ is transformed to an integer valued indicator field $I_s \equiv I(\mathbf{s_s})$ by means of threshold levels. Thus, the reconstruction of missing data is reduced to a spatial classification problem. The number of classes N_c is defined according to the desirable resolution and accuracy of the application. Generally, increasing N_c leads to more accurate estimations. In low resolution applications a small number of classes (i.e. $N_c = 8$) is sufficient. At the limit $N_c \to \infty$ the DGC method approximates continuous interpolation. Consequently, the reconstruction of the missing data is rendered equivalent to assigning a class label $I_g \equiv I(\mathbf{s_g})$ at each point $\mathbf{s_g}$ of the mapping grid.

The local square gradient and curvature terms in an arbitrary direction $\mathbf{e_n}$ with corresponding lattice step α_n are given by

$$G_n(I;\mathbf{s_i}) = \frac{\left[I(\mathbf{s_i}+\alpha_n\mathbf{e_n}) - I(\mathbf{s_i})\right]^2}{\alpha_n^2}, \quad n = 1,...,d, \tag{4.3}$$

$$C_n(I;\mathbf{s_i}) = \frac{\left[I(\mathbf{s_i}+\alpha_n\mathbf{e_n}) + I(\mathbf{s_i}-\alpha_n\mathbf{e_n}) - 2I(\mathbf{s_i})\right]^2}{\alpha_n^4}, \quad n = 1,...,d. \tag{4.4}$$

The average of these terms, for each direction e_n, is taken over the grid, so as to normalise them.

The estimated indicator index of the grid nodes $\hat{I}_g$ are derived through the minimization of the following objective function:

$$U(I_g|I_s) = \sum_{n=1}^{d}\left[w_1\phi(\overline{G}_n(I_g),\overline{G}_n(I_s)) + w_2\phi(\overline{C}_n(I_g),\overline{C}_n(I_s))\right], \tag{4.5}$$

$$\phi(x,x') = \begin{cases}(1-x/x')^2, & x' \neq 0\\ x^2, & x' = 0\end{cases}, \tag{4.6}$$

where $\overline{G}_n(I_g)$ and $\overline{G}_n(I_s)$ represent the normalized squared gradient and curvature, respectively, terms in one direction, defined as averages over the grid, w_1, w_2 are weights of the gradient and the curvature ($w_1, w_2 \geq 0$, $w_1 + w_2 = 1$), and d is the number of directions used.

The main steps of the DGC method can be summarized as follows:

1. Definition of the number of simulations M, the number of classes N_c, the size of the neighboorhood, the residual cost function tolerance tol and the maximum number of Monte Carlo steps i_{max} (optional).
2. Discretization of $Z(s_s)$ to obtain the sample class identity field I_s.
3. Calculation of the sample directional normalised squared gradient and curvature $\overline{G}_n(I_g), \overline{G}_n(I_s)$, $n = 1,.,d$.
4. For each simulation:
   (a) Assignment of initial values $\hat{I}_g^{(0)}$ to the prediction points $\mathbf{s_g}$, by majority rule, based on the prevailing value of each point's sample neighbors. If no majority is reached up to the defined neighborhood, the initial value is assigned (i) randomly from the range of the labels with tie votes or (ii) from the entire range of labels 1,.,Nc, if majority is not reached due to absence of sampling points within the neighborhood.
   (b) Calculation of the initial energy values $\overline{G}_n(I_g^{(0)}), \overline{G}_n(I_s(0))$, $n = 1,.,d$, and the objective function $U^{(0)} = U(\hat{I}_g^{(0)}|I_s)$.
   (c) Definition for each grid node of the state (amongst the possible states) that minimizes the objective function. An iterative process is followed starting from the initial state and generating a new state by randomly adding ± 1 to the previous. The updating of class identity states uses the "greedy" Monte Carlo (MC) method (Papadimitriou and Steiglitz, 1982). If the objective function of the new state is less than the one of the initial state, it is accepted else the initial state is kept and the nest grid node is investigated.
5. Evaluation of the statistics from the simulations.

The Directional Gradient-Curvature (DGC) model is inspired by Spartan spatial random fields (SSRF) (Hristopulos and Elogne, 2007), which are based on short-range interactions between the field values. The DGC method do not strictly belong neither to the interpolation methods nor to the conditional simulation mathods. Interpolation methods provide a single optimal estimation of the missing values. Conditional simulation sample the entire data and try to reconstruct the joint conditional probability density function of the missing data. On the other hand, DGC takes account only the data that corresponds to local minima of the objective function. The stochastic nature of the DGC derives from the multiple realizations that it returns (Žukovič and Hristopulos, 2013a).

Chapter 5

Data Analysis

Real data processing in Geostatistics is a demanding problem and consists of many succesive steps. There is not a standard procedure applying to every data set, but each researcher can follow different way depending on the data and the final purpose of the analysis.

In Geostatistics every data set is considered as a single realization of a random field, summed with a trend model and an independent gaussian fluctuation, i.e.

$$Z(\mathbf{s}) = m_z(\mathbf{s}) + Z'(\mathbf{s}) + \varepsilon(\mathbf{s}), \tag{5.1}$$

where $Z(\mathbf{s})$ the total random field which coincides with the real data at the sample's points, $m_z(\mathbf{s})$ the global trend model, $Z'(\mathbf{s})$ a random field with zero mean value corresponding to the fluctuations (also called residuals) of the field $Z(\mathbf{s})$ around the trend and $\varepsilon(\mathbf{s})$ the error.

It is common practice in geostatistical analysis to initially evaluate and remove the trend model and then process the residuals. More specific, a general and widely accepted procedure for data analysis includes the following indicative steps (Goovaerts, 1997):

1. Preliminary Analysis
2. Parameter Inference
3. Model Selection
4. Spatial Prediction
5. Performance Assessment

In the following sections a brief description of each step is presented.

5.1 Preliminary Analysis

Preliminary analysis of data aims to examine some basic statistical properties before any other analysis tool is applied.

Normality

To assess whether a data set comes from a normal (Gaussian) distribution, often the normal probability plot of it is examined. This plot displays the theoretical quantiles of a normal distribution (x axis) versus the experimental quantiles of the studied data (y axis). Therefore, the normality of the data set can be assessed visually; if the resulting plot coincides with a theoretical straight line (corresponding with the normal distribution) or deviates to a small extend from it, the data is deemed Gaussian. Normal probability plot can also be used to identify and remove outliers.

In the case of non-gaussian data set suitable transformations have to be implemmented to it, so as to transform the data to a new data set with approximately normal distribution. The most widely used transformation is the Box-Cox Power transformation (Box and Cox, 1964). The one parametric Box-Cox transformation for a variable x is defined as:

$$x^{(\lambda)} = \begin{cases} \dfrac{x^{\lambda}-1}{\lambda}, & \lambda \neq 0 \\ \ln(x), & \lambda = 0 \end{cases}, \tag{5.2}$$

and the two parametric Box-Cox transformation, which can also handle negative values of x, is defined as:

$$x^{(\lambda_1,\lambda_2)} = \begin{cases} \dfrac{(x+\lambda_2)^{\lambda_1}-1}{\lambda}, & \lambda_1 \neq 0 \\ \ln(x+\lambda_2), & \lambda_1 = 0 \end{cases}. \tag{5.3}$$

The optimum parameters λ_1, λ_2 are usually calculated by maximizing the Log-Likelihood Function (LLF), or minimizing the negative LLF (see also section 5.2.1. Note that Box-Cox transformation cannot restore the normality for each data set. In such cases, other more complex non-linear transformations may have to be applied. A common practice is to assume gaussianity of the transformed dataset after applying the Box-Cox transformation in order to avoid such complex transformations.

Trend Removal

The trend function $m_z(\mathbf{s})$, which represents the deterministic part of the random field $Z(\mathbf{s})$, is usually modelled by low-order polynomials of the coordinations of the sample's points. Alternatively, if the data exhibits periodicity a combination of the linear with the periodic model (sinusoidal) can be used. In Table 5.1 are shown some common trend functions for 2D cases.

Table 5.1 Common trend models

Model	**Trend Function(2D)**
Mean	$m_z(\boldsymbol{s}) = a_0$
Linear	$m_z(\boldsymbol{s}) = a_0 + a_1 x + a_2 y$
Quadratic	$m_z(\boldsymbol{s}) = a_0 + a_1 x + a_2 y + a_3 xy + a_4 x^2 + a_5 y^2$
Cubic	$m_z(\boldsymbol{s}) = a_0 + a_1 x + a_2 y + a_3 xy + a_4 x^2 + a_5 y^2 + a_6 x^2 y + a_7 xy^2 + a_7 x^3 + a_8 y^3$
Quartic	$m_z(\boldsymbol{s}) = a_0 + a_1 x + a_2 y + a_3 xy + a_4 x^2 + a_5 y^2 + a_6 x^2 y + a_7 xy^2 + a_8 x^3 + a_9 y^3 + a_{10} x^2 y^2 + a_{11} x^3 y + a_{12} xy^3 + a_{13} x^4 + a_{14} y^4$
Linear+Periodic	$m_z(\boldsymbol{s}) = a_0 + a_1 x + a_2 y + \sum_{j=1}^{n} \{a_{4(j-1)+3} \cos 2\pi f_{x,j} x + a_{4(j-1)+4} \sin 2\pi f_{x,j} x + a_{4(j-1)+5} \cos 2\pi f_{y,j} y + a_{4(j-1)+6} \sin 2\pi f_{y,j} y\}$

The linear coefficients a_i are usually estimated by means of *Multiple Linear Regression (MLR)*. The MLR method estimates the coefficients a_i of the independent variables, also called regressors, of a linear model of order p (in this case the coordinations x_i and y_i) that give the least square error between the investigated model and the dependent variable or regressand ($Z(\boldsymbol{s_i})$) by solving the linear equations system:

$$\boldsymbol{Z}(\boldsymbol{s_i}) = \boldsymbol{C}a, \tag{5.4}$$

where $\boldsymbol{Z}(\boldsymbol{s_i}) = \begin{bmatrix} Z(\boldsymbol{s_1}) \\ Z(\boldsymbol{s_2}) \\ \vdots \\ Z(\boldsymbol{s_n}) \end{bmatrix}$, $a = \begin{bmatrix} a_1 \\ a_2 \\ \vdots \\ a_n \end{bmatrix}$, and $\boldsymbol{C} = \begin{bmatrix} x_1^{k=0}y_1^{l=0} & x_1^{k=1}y_1^{l=0} & x_1^{k=0}y_1^{l=1} & \cdots & x_1^k y_1^l \\ x_2^{k=0}y_2^{l=0} & x_2^{k=1}y_2^{l=0} & x_2^{k=0}y_2^{l=1} & \cdots & x_2^k y_2^l \\ \vdots & \vdots & \vdots & \cdots & \vdots \\ x_n^{k=0}y_n^{l=0} & x_n^{k=1}y_n^{l=0} & x_n^{k=0}y_n^{l=1} & \cdots & x_n^k y_n^l \end{bmatrix}$, $(k+l \leq p)$.

The dominant frequencies of the data, $f_{x,i}, f_{y,i}$, in x and y directions, respectively, for the periodic model are estimated by means of *Fast Fourier Transformation (FFT)*. The squaring of the FFT of the data results to the magnitudes of the frequencies in the spectral domain. Consequently, these magnitudes and the corresponding frequencies are sorted in descending order of the magnitude, for both x and y directions. The first elements of the resulting frequencies lists (the number of which is defined by the modeler) are the desirable quantities.

The selection of the best trend model is done by means of Information Criteria, e.g. Akaike Information Criterion (AIC), corrected Akaike Information Criterion (AICc), Bayesian Information Criterion (BIC) (Akaike, 1974; Schwarz, 1978), or Least Squared Error (LSE).

5.2 Parameter Inference

In the next step of the data analysis, a number of theoretical models for examination is choosen and the optimum parameters of them $\boldsymbol{\theta}_i = [\theta_1, \theta_2, ..., \theta_n]_i$, which give the best fitting to the data, are estimated. The estimation of these parameters is achieved by minimizing an objective functional, which typically matches an experimentally calculated term from the available data with the corresponding theoretical term of the investigated model. The most widely used methods for the parameter inference are: i) the Covariance-Variogram Fitting (CVF), ii) the Maximum Likelihood Estimation (MLE) and iii) the Method of Moments (MoM).

It is also possible to estimate some of the model's parameters with different methods and then use one of the above methods to estimate the remaining parameters. This is usually applied in the case of anisotropic data, where the parameters of anisotropy are firstly estimated. In this way, the computational cost of the optimization steps is reduced significantly and the reliability of the results is improved. The classic Directional CVF (DCVF) method and the more modern Covariance Hessian Identity (CHI) method are some methods for estimating the parameters of anisotropy from a data set.

5.2.1 Common Methods of Parameter Inference

Covariance-Variogram Fitting (CVF)

Covariance-Variogram Fitting (CVF) estimates the optimum parameters by minimizing one error function between the experimentally calculated covariance or variogram and the corresponding theoretical quantity, which derive from the investigated model. The error functions can have various expressions. For example it can be the net sum of the squared error for the variogram fitting:

$$f_{er}(\theta) = \sum_{k=1}^{N_c} \left[\hat{\gamma}_z(\mathbf{s_{c,k}}) - \gamma_z(\mathbf{s_{c,k}};\theta)\right]^2, \tag{5.5}$$

the sum of the squared error weighted with the corresponding theoretical variogram value:

$$f_{er}(\theta) = \sum_{k=1}^{N_c} \frac{\left[\hat{\gamma}_z(\mathbf{s_{c,k}}) - \gamma_z(\mathbf{s_{c,k}};\theta)\right]^2}{\gamma_z^2(\mathbf{s_{c,k}};\theta)}, \tag{5.6}$$

the the sum of the squared error divided by the corresponding number of pairs:

$$f_{er}(\theta) = \sum_{k=1}^{N_c} \frac{\left[\hat{\gamma}_z(\mathbf{s_{c,k}}) - \gamma_z(\mathbf{s_{c,k}};\theta)\right]^2}{n(\mathbf{s_{c,k}})}, \tag{5.7}$$

or the combination of the last two errors:

$$f_{er}(\theta) = \sum_{k=1}^{N_c} \frac{1}{n(\mathbf{s_{c,k}})} \frac{\left[\hat{\gamma}_z(\mathbf{s_{c,k}}) - \gamma_z(\mathbf{s_{c,k}};\theta)\right]^2}{\gamma_z^2(\mathbf{s_{c,k}};\theta)}, \tag{5.8}$$

where $\hat{\gamma}_z(\mathbf{s_{c,k}})$ the experimental variogram values at the centers of the cyclical sections (see section 2.6), $\gamma_z(\mathbf{s_{c,k}};\theta)$ the theoretical variogram values at the centers of the cyclical sections given by the investigated model with parameters θ, N_c the number of cyclical sections, and $n(\mathbf{s_{c,k}})$ the number of pairs of data included into the kth cyclical section. Similar equations can be derived for the case of covariance fitting.

In practice, the angular sections are allocated between the semicycle and the separation vectors $\mathbf{h}$ of the pairs corresponding to diametrically opposite directions, i.e. to angles ϕ and $\phi+\pi$, are considered as identical. This follows from the ellipsoid representation of anisotropy. Also, note that for the minimization of the error the rotation angle ϕ is restricted between $-\pi/2$ and $\pi/2$ in order to avoid equivalent solutions (Olea, 2006).

Maximum Likelihood Estimation (MLE)

The Maximum Likelihood Estimation, proposed by Fisher (1997) estimates optimum parameters by maximizing the likelihood the known realization (real data) can be produced by a given parameter set. In practice, this is achieved by minimizing the negative log-likelihood function (NLLF). The basic concepts of the MLE method as described by Pardo-Igúzquiza (1998) are briefly represented below.

The joint pdf of n experimental multivariate Gaussian data with zero mean can be expressed as:

$$f_z(\mathbf{z};\theta) = (2\pi)^{-n/2}|\mathbf{C}|^{-n/2}\exp\{-\frac{1}{2}\mathbf{z}\mathbf{C}^{-1}\mathbf{z}\}, \tag{5.9}$$

where n the number of experimental data, $\mathbf{C}$ the nxn covariance matrix of the data,$|\cdot|$ denotes the determinant, and θ the $mx1$ vector of parameters that defines the covariance matrix.

The NLLF of the data given the parameters θ, then, is expressed as:

$$L(\sigma_z^2,\theta';\mathbf{z}) = \frac{n}{2}\ln(2\pi)+n\ln(\sigma)+\frac{1}{2}\ln(|A|)+\frac{1}{2\sigma_z^2}\mathbf{z}\mathbf{A}^{-1}\mathbf{z}, \tag{5.10}$$

where θ' the covariance parameters without the variance, and $\mathbf{A}=\mathbf{C}/\sigma_z^2$ the correlation matrix.

Replacing in Eq. (5.10) the ML estimate of the variance:

$$\hat{\sigma}_z^2 = \frac{1}{n}\mathbf{z}\mathbf{A}^{-1}\mathbf{z}, \tag{5.11}$$

the NLLF becomes:

$$L(\hat{\sigma}_z^2,\theta';\mathbf{z}) = \frac{n}{2}\left(\ln(2\pi)+1-\ln(n)\right)+\frac{1}{2}\ln(|A|)+\frac{n}{2}\mathbf{z}\mathbf{A}^{-1}\mathbf{z}. \tag{5.12}$$

The covariance parameters θ' are estimated as the values that minimize the Eq. (5.12), while the variance $\hat{\sigma}_z^2$ is subsequently estimated according to Eq. (5.11).

Method of Moments (MoM)

The Method of Moments (MoM) estimates the parameters of a model by relating the sample moments to the parameters of interest and solving the resulting system (Bowman and Shenton, 2004). More specifically the k unknown parameters $\theta_1, \theta_2, ..., \theta_k$ defining the pdf $f_z(z;\theta)$ of a random variable Z are estimated as the solution of the system consisting of the k first moments of the variable, which can be expressed as functions of θ, i.e.

$$\begin{aligned} \hat{\mu}_1 &\equiv \mathbb{E}[z(\mathbf{s_i}] = \frac{1}{n}\sum_{i=1}^{n} z(\mathbf{s_i}) = g_1(\theta) \\ \hat{\mu}_2 &\equiv \mathbb{E}[z^2(\mathbf{s_i}] = \frac{1}{n}\sum_{i=1}^{n} z^2(\mathbf{s_i}) = g_2(\theta) \\ &\vdots \\ \hat{\mu}_k &\equiv \mathbb{E}[z^k(\mathbf{s_i})] = \frac{1}{n}\sum_{i=1}^{n} z^k(\mathbf{s_i}) = g_k(\theta). \end{aligned} \tag{5.13}$$

5.2.2 Estimation of Anisotropy

Directional Covariance-Variogram Fitting (DCVF)

Directional CVF is a method for estimating the parameters of anisotropy (ϕ, ξ_1, ξ_2) of a field. In this method, like in the CVF, the space is divided into cyclical sections defined from angular and distance limits, and the experimental variogram corresponding to these sections are computed from the data, referred to the centers $(\phi_{c,i}, \xi_{c,i})$ of them. However, in this case, the theoretical model, in its isotropic form, is fitted separately to each of the j number of angular sections. Thus, j number of parameter vectors θ, corresponding to the j angular sections, and consequently same number of (ξ, ϕ) pairs are obtained. The estimation of the anisotropy parameters follows from the fitting of an ellipse to these pairs. The lenghts of the ellipsis major axes correspond to the (ξ_1, ξ_2) parameters, while the angle between the first met, while rotating counter-clockwise, major axis of the theoretical ellipsis and the horizontal plane corresponds to the rotation angle.

Covariance Hessian Identity (CHI)

The CHI offers a fast, non-parametric and non-iterative method for estimating the anisotropic parameters of a 2D random field (Chorti and Hristopulos, 2008; Hristopulos, 2002; Petrakis, 2012; Petrakis and Hristopulos, 2012). It is based on linking the second-order derivatives of the covariance function with the ensemble average of the *Gradient Kronecker Product*

(GKP) of the data. More specifically, according to Swerling (1962), the CHI of the covariance function and the sample-estimated expectation of GKP are related via the following expression:

$$Q_{ij} \equiv \mathbb{E}\left[\frac{\partial Z(\mathbf{s})}{\partial s_i}\frac{\partial Z(\mathbf{s})}{\partial s_j}\right] = \frac{\partial^2 c_z(\mathbf{h})}{\partial h_i \partial h_j}\bigg|_{h=(0,0)}, \tag{5.14}$$

where Q_{ij} represents a tensor. Obviously, this is valid only for differentiable random fields. For non-differentiable randoms fields numerical approximations of the derivatives can be estimated (Chorti and Hristopulos, 2008).

In the case of a 2D, differentiable and homogeneous random field, the explicit equations for the elements of the CHI derive by expressing the covariance function in terms of the ratio of the correlation lengths $R = \xi_1/\xi_2$ and the rotation angle ϕ:

$$Q_{11} = \frac{\sigma_z^2 \zeta^2}{\xi_1^2}\left(\cos^2\phi + R^2 \sin^2\phi\right), \tag{5.15}$$

$$Q_{22} = \frac{\sigma_z^2 \zeta^2}{\xi_1^2}\left(R^2\cos^2\phi + \sin^2\phi\right), \tag{5.16}$$

$$Q_{12} = Q_{21} = \frac{\sigma_z^2 \zeta^2}{\xi_1^2}\left[\sin\phi\cos\phi(1-R^2)\right]. \tag{5.17}$$

The anisotropic parameters R and ϕ are then estimated by minimizing the following objective function:

$$F(\phi, R) = \left[\frac{Q_{22}}{Q_{11}} - \frac{R^2 + \tan^2\phi}{1 + R^2\tan^2\phi}\right]^2 + \left[\frac{Q_{12}}{Q_{11}} - \frac{\tan^2\phi(1-R^2)}{1+R^2\tan^2\phi}\right]^2. \tag{5.18}$$

The constants ζ and ξ_1 remain undetermined from the optimization of the objective function. The first one is eliminated by the division, thus its value doesn't need to be determined. The second is usually of interest and can be determined from the experimental variogram.

5.3 Model Selection

After estimating the optimum parameters of a number of covariance models, an assessment of their predictive accuracy is required in order to select one model, this with the best performance, for the following steps of data analysis. This is usually achieved by means of *Cross-Validation (CV)*.

Cross-Validation is a technique for providing information about how an estimated model will perform in a real problem. In general, CV is performed by partitioning a sample dataset into two subsets, called *training subset* and *validation subset*. The first subset is used as input for the estimation of the missing values of the second one. The estimator in this step is the same as the one which is intended to be applied in the next step of Spatial Prediction.

5.3.1 Common Types of Cross-Validation

The most commonly used types of CV is the exhaustive *Leave-p-out Cross-Validation (LpOCV)* and the non-exhaustive *k-fold Cross-Validation (k-fold CV)*. Exhaustive cross-validation methods compute all possible ways to divide the original sample into a training and a validation set (Geisser, 1975, 1993; Seni and Elder, 2010).

Leave-p-out Cross-Validation (LpOCV)

In LpOCV the validation set consists of p sample points of the sample dataset, while the remaining realizations are used as training set. The cross-validation process is repeated for every possible combination of p number of realizations and the results are then averaged to provide a single estimation. This method may lead to high computational cost. For this reason it is preferred in cases where the sample dataset is relatively small.

A particular case of LpOCV with $p = 1$, also called *Leave One Out Cross-Validation (LOOCV)* is preferred, due to its simplicity and its lower computational cost.

k-fold Cross-Validation (k-fold CV)

In k-fold CV the sample dataset is randomly divided into k equal sized subsets. It is apparent that this method requires a larger dataset than LOOCV. Then the CV process is repeated k times (the folds) using each time one of the k subsets as validation set and the remaining $k-1$ subsets as training set. The results, like to LpOCV, are also averaged to give the final estimation. The simplest variation of k-fold CV is the one with $k = 2$ (2-fold CV), while in the case of $k = n$ (the size of the sample dataset) the k-fold CV is exactly the LOOCV.

5.3.2 Measures of Cross-Validation Performance

Common validation measures

In order to assess the performance of the cross-validation, it is usefull to compute and compare validation measures for each model. Such measures are the Mean Absolute Error

(MAE), the Maximum Absolute Error ($MxAE$), the Mean Squared Error (MSE), the Root Mean Squared Error ($RMSE$), the Pearson's correlation coefficient (ρ) and the Spearman's correlation coefficient (r_S). The above mentioned errors measure the accuracy and precision of the predictions, while the Pearson's and Spearman's correlation coefficients provide a measure of the linear and non-linear, respectively the relationship between the real and the predicted data. These measures are calculated by the following equations:

$$MnAE = \frac{1}{N}\sum_{i=1}^{N}\left|\hat{z}(\mathbf{s}_i) - z(\mathbf{s}_i)\right|, \tag{5.19}$$

$$MxAE = max(\left|\hat{z}(\mathbf{s_i}) - z(\mathbf{s_i})\right|), \tag{5.20}$$

$$MSE = \frac{1}{N}\sum_{i=1}^{N}\left[\hat{z}(\mathbf{s}_i) - z(\mathbf{s}_i)\right]^2, \tag{5.21}$$

$$RMSE = \frac{1}{N}\sqrt{\sum_{i=1}^{N}\left[\hat{z}(\mathbf{s}_i) - z(\mathbf{s}_i)\right]^2}, \tag{5.22}$$

$$\bar{\rho}_{Z,\hat{Z}} = \frac{\sum_{i=1}^{N}\left[z(\mathbf{s}_i) - \overline{z(\mathbf{s}_i)}\right]\left[\hat{z}(\mathbf{s}_i) - \overline{\hat{z}(\mathbf{s}_i)}\right]}{\sqrt{\sum_{i=1}^{N}\left[z(\mathbf{s}_i) - \overline{z(\mathbf{s}_i)}\right]^2}\sqrt{\sum_{i=1}^{N}\left[\hat{z}(\mathbf{s}_i) - \overline{\hat{z}(\mathbf{s}_i)}\right]^2}}, \tag{5.23}$$

$$r_S = 1 - \frac{\sum_{i=1}^{N}(R_{z_i} - R_{\hat{z}_i})^2}{N(N^2-1)}, \tag{5.24}$$

where R_{z_i} denotes the rank of $z(\mathbf{s}_i)$ among all $z(\mathbf{s})$ values. The rank is computed by sorting the z values in ascending order; the rank of a given value is equal to its order of appearance in the sorted list.

These measures can be compared individually or to be combined to one kind of a coefficient, at the rate of which will the final choice be made. In this way, a more meritocratic measure that also enables a more automatic selection of a model derives. For instance, this coefficient could be of the form:

$$r_F = \frac{1}{relMSE_i^2}\rho_i r_{S,i} \in [0,1], \tag{5.25}$$

where i corresponds to the investigated models and $relMSE_i = MSE_i/min(MSE_i) > 1$ is the model's relative MSE. The $relMSE_i$ in the denominator is squared so as to equalize the product of the two correlation coefficients in the numerator. As the performance of the investigated model improves, the correlation coefficients increase and the *MSE* decreases. As the correlation coefficients increase so does the numerator of the r_F, converging to 1. As the *MSE* decreases, the *relMSE* and consequently the denominator of the r_F also decreases converging to 1. Thus, as the accuracy of the investigated model improves, the final coefficient increases converging to 1.

Classification measures

Except from the above validation measures it is often usefull to calculate some classification measures. This requires converting the continuum valued field into a discrete one by separating the continuum values into n equal bins and assigning n integer indicators to each one.

Discretizing both the original and the estimated values of the field, the performance of the classification of the unkwown values can be measured by calculating:

- the Pearson's and Spearman's correlation coefficients of the original and estimated indicators of the missing values, and
- the *misclassification rate* (MCR), i.e. the percent of the estimations that are not equal to the corresponding original indicators.

These measures can be estimated for both classification methods (e.g. DGC simulation method) and interpolation methods (e.g. Ordinary Kriging).

5.4 Spatial Prediction

In this step the desirable estimation method is applied in order to predict the missing values and to produce a map of the study area. Widely used estimation methods are the Kriging and the Stochatic Simulations, which have been described in Chapters 3 and 4, respectively.

The parametric estimation methods (e.g. Ordinary Kriging and Turning Bands Simulation) require as input the best model defined in the steps of Parameter inference and Model Selection. On the contrary, the non-parametric method of DGC simulation, does not need a pre-defined model, i.e. the steps 2 and 3 (Parameter inference and Model Selection) are skipped.

The uncertainty of the estimations is also evaluated in this step, usually by means of confidence intervals at some confidence level. The confidence interval at 95% confidence level of the estimations in the case of Ordinary Kriging is calculated as:

$$(\hat{z}(\mathbf{s}_i) - 1.96\sigma_{E,OK}(\mathbf{s}_i), \hat{z}(\mathbf{s}_i) + 1.96\sigma_{E,OK}(\mathbf{s}_i). \tag{5.26}$$

Chapter 6

Case Study: Marmousi Model

6.1 Description of the Data

6.1.1 Geologic Profile of the Data

The purpose of this thesis is the exploratory implementation of geostatistical tools for the simulation of geological media. The tools which have been used are: i) Ordinary Kriging and ii) DGC simulation method. For the implementation of Kriging software was developed in MATLAB programming environment, while for the implementation of Directional Gradient Curvature (DGC) simulation method software developed by the Geostatistics Laboratory (Technical University of Crete) is used. Several variations for parameter inference (parametric-non parametric) and anisotropy tackling (transform data to isotropic or not) have been used in OK.

More explicitly, a known gridded dataset is sampled, both randomly and regularly, and the reconstruction of it is subsequently attempted with the above mentioned methods. The original dataset is the Marmousi Model, a synthetic 2D acoustic model created in 1988 by the Institute Francais du Petrole (IFP), and used for the workshop on practical aspects of seismic data inversion at the 1990 EAEG meeting in Copenhagen. It was generated using a 2-D acoustic finite-difference modeling program, so as to resemble an overall continental drift geological setting. The geometry of the Marmousi is based on a profile through the North Quenguela trough in the Cuanza basin. The Cuanza basin is in northwestern Angola on the Atlantic Coast of West Africa and is about 300 km long north-south and 170 km wide east-west (Fig. 6.1).

The geological model of the basin consists, from top to bottom, of:

- Surface and subsurface sediments of Lower and Upper Cretaceous, Paleocene, Eocene, and Miocene strata.

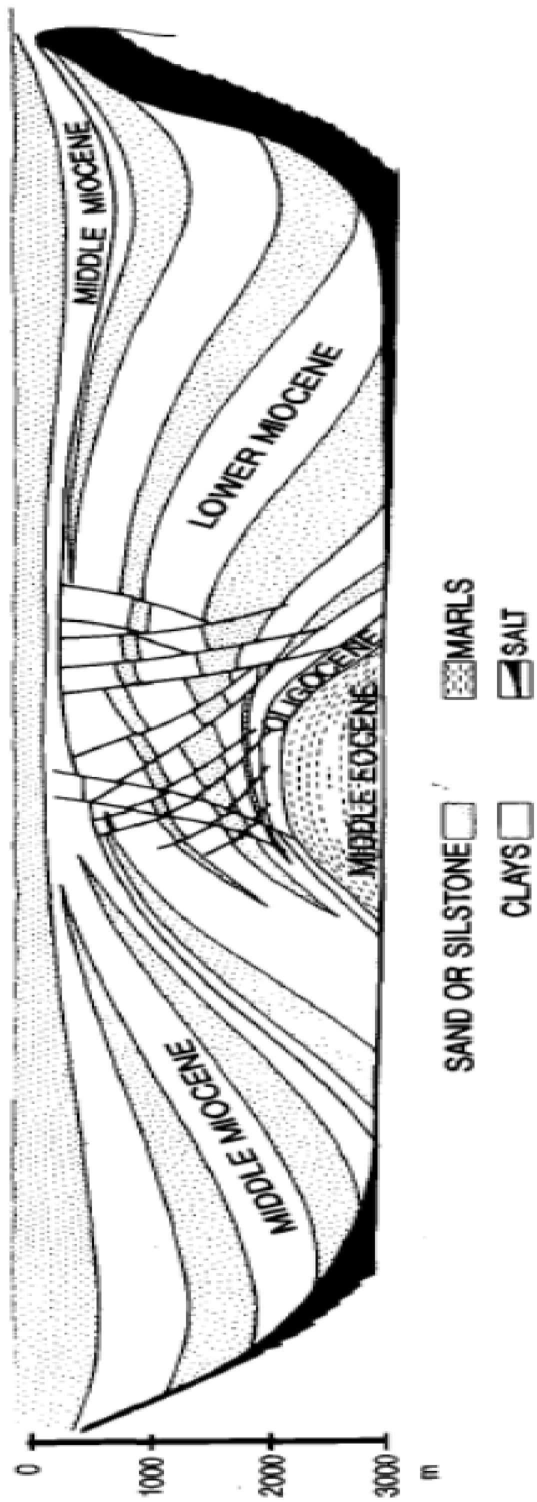

Figure 6.1 Profile through the North Quenguela trough in the Cuanza basin (Angola) after Verrier and Branco (1972)

- Early Cretaceous carbonate-evaporite (mainly salt) sequence and a Late Cretaceous and Tertiary argillaceous-arenaceous sequence.
- Precambrian crystalline basement, which is partly covered by extrusive rocks and granite-wash type sediments.

The post-Aptian (Early Cretaceous) tectonic process of the West Africa Salt Basin, has affected significantly the salt movements into the basin. As a result of the basinward tilt of the margin, the carbonate stratas of the Early Cretaceous and the overlying Upper Cretaceous sequence slid on the salt layer and broke up into smaller blocks. This process caused a mobilization of the salt and the formation of salt rollers, salt diapirs and a whole suite of raft tectonics structures such as turtlebacks, carbonate rafts and severe folding at the toe of the salt basin.

Occurrences of oil and gas have been reported in almost all of the stratigraphic units in the Cuanza basin, and there is major production from the Cretaceous rocks. These hydrocarbon occurrences are expected to be entraped into the folded carbonate and salt structures of the basin, due to the nature of the basement and the salt tectonics (Brognon and Verrier, 1966; Spathopoulos, 1996).

Based on this profile a geometric model was created using the MIMIC™ module of the SIERRA package. Then this model was transformed into a 2-D velocity/density grid (Fig. 6.2). The Marmousi model contains 158 horizontally layered horizons. Numerous large normal faults and tilted blocks, resulting from the continental drift, complicates the model towards its center. The model sits under approximately 32 m of water and is 9.2 km in length and 3 km in depth.The target zone is a reservoir located at a depth of about 2.5 km. The model contains many reflectors, steep dips, and strong velocity variations in both the lateral and the vertical direction (with a minimum velocity of 1500 m/s and a maximum of 5500 m/s) (Bourgeois et al., 1990; Irons, 2008; Versteeg and Grau, 1990).

6.1.2 Basic Notions and Assumptions for the Data

The data consists a 122x384 grid, i.e. 46848 values in total. This means that each cell of the grid corresponds to a 24,60x23,96 m (depth x length) space. The information mentioned in section 6.1.1 as well as the visualisation of the data (Fig. 6.2), indicate that the studied dataset is highly complexed and possibly non-stationary, as at least the anisotropy characteristics change significantly over the space. The geological section can be separated into three vertical bands. The left and right bands exhibit anisotropy which can be described by an ellipsis with an almost horizontal major axis, while in the central band the major axis turns to about 40°. For simplicity, in this thesis the field is arbitrarily assumed stationary and

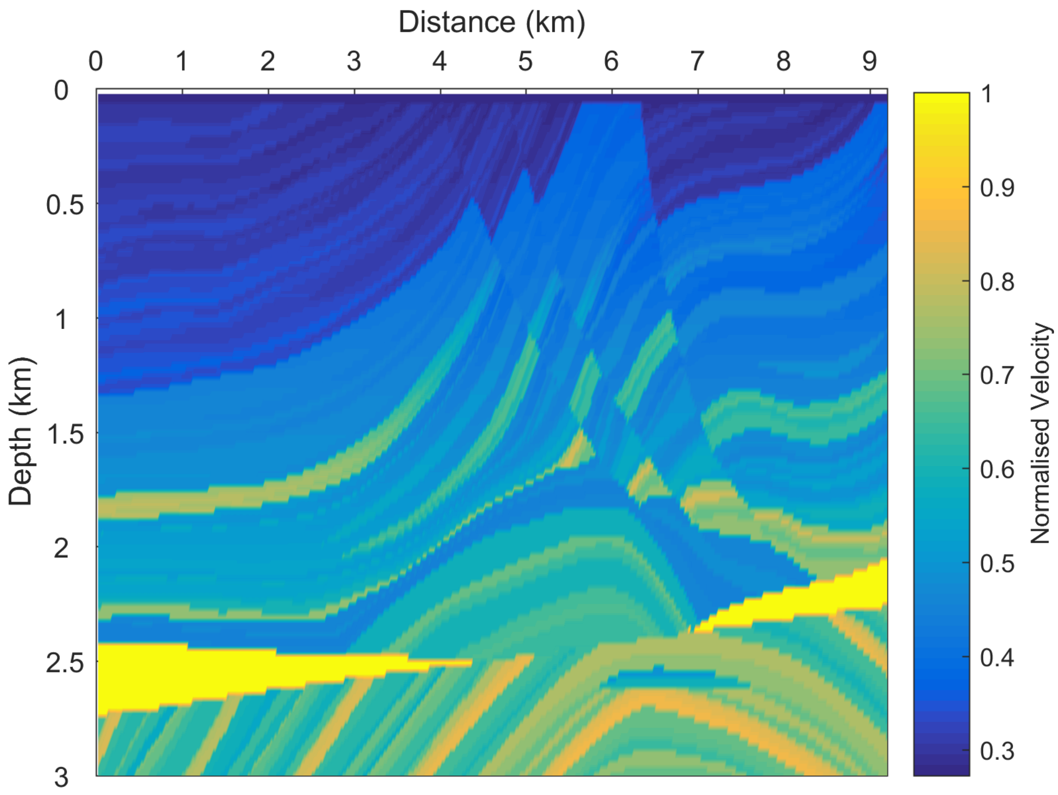

Figure 6.2 Normalised Marmousi Model (Velocity Model)

is modelled as such. However, the reliability and the performance of the final models are evaluated in the light of this complexity.

As mentioned above, two samples of the Marmousi Model are used, shown in Fig. 6.3. Both of the samples contain 4758 points, which correspond a 10,16% of the original data. The first sample consists of 39 columns of the grid, starting from the 3rd and selecting one per 10 columns until the end of the grid. The geometry of this sample resembles, in some way, to data obtained by well-logging drill-holes (which in this case is impractical as the distance of the sample's drill-holes corresponds only to 240 m).Hereafter, this sample is called regular. The second sample is sampled randomly in the 2D space.

In order to decrease the computational cost we normalise the original values dividing with the maximum of them (5500 m/s). In this way, the resulting values belong to [0,1]. For the same reasons, the coordinations of the data points used are not the real coordinations but the (i, j) indices of the 122x384 grid's nodes. The i index correspond to the depth of the point, while j index correspond to the distance alongside the geological section. This means that the i's take values from 1 to 122, with the 1 corresponding to the horizontal edge of the grid closer to the surface, and the j's take values from 1 to 384, with the 1 corresponding to the eastern vertical edge of the grid.

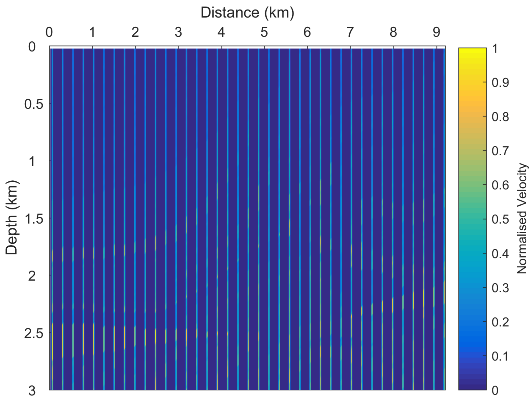

(a) Regular Sample: 4758 points (10,16% of the original data) containing 39 columns of the grid (starting from the 3rd and selecting one per 10 columns until the end of the grid.)

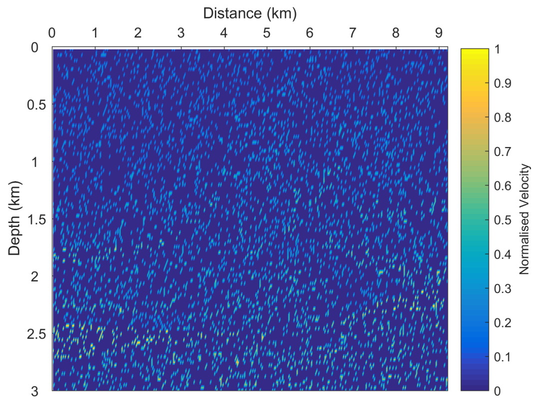

(b) Random Sample: 4758 points (10,16% of the original data) selected randomly from the original. data

Figure 6.3 Samples of original data

6.2 Methodology

Ordinary Kriging

For the implementation of Ordinary Kriging to the samples of Marmousi Model, the general procedure described in Chapter 5 is followed. The indicative steps of this procedure are the following:

1. Preliminary Analysis
2. Parameter Inference
3. Model Selection (LOOCV)
4. Spatial Prediction
5. Performance Assessment

For the analysis procedure the following variogram models have been used: 1) Generalized Exponential, 2) Gaussian, 3) Spherical, 4) Generalized Matern, 5) Spartan(3D).

In the step of Parameter Inference, five variations are used. These methods differed regarding anisotropy estimation (i.e. parametric versus non parametric) and data transformation (transform data to isotropic or not). A consice description of each variation, which are arbitrarily named, follows (see also Table 6.1):

- **DirVar0:** A priori anisotropy parameter inference is not attempted. Thus, the anisotropic variogram functions, which contain the maximum number of unknown parameters for each model, are used in the optimization procedure of the 2nd step as well as in the following steps.

Table 6.1 Description of the five variations of Parameter Inference step. DVF:Directional Variogram Fitting, CHI: Covariance Hessian Identity (P.I.: Parmaeter Inference).

Variation	**Anisotropy P.I. Method**	**Anisotropic Inversion**
DirVar0	–	NO
DirVar1	DVF	NO
DirVar2	DVF	YES
CHI1	CHI	NO
CHI2	CHI	YES

- **DirVar1:** Anisotropy parameter inference is initially applied for each model by means of Directional Variogram Fitting (DVF) (see section 5.2.2). Subsequently, the estimated parameters are inserted to the corresponding anisotropic variogram functions, reducing by three the number of unknown parameters for each model. The new anisotropic variogram functions (with lower degrees of freedom) are used in the optimization procedure of the 2nd step as well as in the following steps.
- **DirVar2:** Anisotropy parameter inference is initially applied for each model by means of DVF. Subsequently, the estimated paramaters are used in order to inverse anisotropic effect (see section 2.4.3) for each model separately. The step of *Parameter Inference* is then repeated using this time the isotropic variogram functions for each model. The isotropic variogram functions are used in the 2nd optimization procedure as well as in the following steps.
- **CHI1:** Anisotropy parameter inference is initially applied for each model by means of CHI (see section 5.2.2). Subsequently, the estimated paramaters are inserted to the corresponding anisotropic variogram functions, reducing by three the number of unknown parameters for each model. The new anisotropic variogram functions (with lower degrees of freedom) are used in the optimization procedure of the 2nd step as well as in the following steps.
- **CHI2:** Anisotropy parameter inference is initially applied for each model by means of CHI. Subsequently, the estimated paramaters are used in order to inverse anisotropic effect for each model separately. The step of *Parameter Inference* is then repeated using this time the isotropic variogram functions for each model. The isotropic variogram functions are used in the 2nd optimization procedure as well as in the following steps.

Also, the type of error used for the optimization in the step of *Parameter Inference* is the error function defined in Eq. (5.8).

Finally, in the Model Selection step where Leave-One-Out-Cross-Validation is applied the immediate neighboors are not taken into account in order to avoid overestimating the models. The risk of overestimation holds as OK generally assigns higher weights to the nearest neighboors and lower weights to the more distant ones. In the case of the regular sample, this means that for each estimation the data taken into account is all the columns except from the one containing the studied missing point.

Software for Ordinary Kriging

The above variations have been implemented to the investigated data by using software developed in the MATLAB programming environment. Specifically, 6 main functions were developed for:

i) detrending 2D data,
ii) calculating experimental anisotropic or isotropic variogram,
iii) fitting theoretical variogram model to the experimental variogram (parameter inference),
iv) estimating the anisotropic parameters of a random field with the directional variograms fitting method (DVF),
v) performing cross validation, and
vi) estimating the missing values with ordinary kriging, respectively.

Some auxiliary functions, for the computation of the covariance and variogram function and the construction of random fields, were also developed. These functions, along with a complete example of their application, are available in https://github.com/billisandr/geostats2D. For software testing purposes the above described analysis is implemented to a random sample of a synthetic dataset presented in section 6.3.

Software developed by D. T. Hristopulos for the estimation of 2D anisotropy parameters with the CHI method, which is available in http://www.geostatistics.tuc.gr/index.php?id=5677.

DGC Simulation method

The DGC Simulation method (section 4.2) is implemented to the two samples of Marmousi Model in an one-step procedure (the step of *Spatial Prediction*). For this method, software developed by Milan Žukovič and D. T. Hristopulos (which is currently unavailable online) was used.

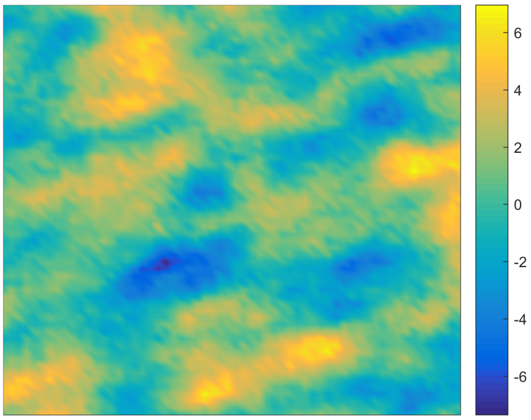

(a) Simulated Gaussian RF from Generalized Mátern covariance function with parameters $\sigma_z^2 = 4.00, \xi_1 = 3.00, R = 1.67, \phi = 20.0°, c_0 = 0.20$ and $\nu = 2.00$.No trend is added.

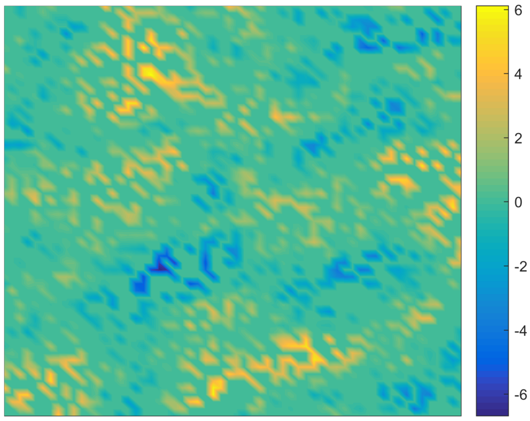

(b) Random Sample of synthetic RF: 1188 points (33% of the original synthetic data) selected randomly.

Figure 6.4 Synthetic RF and random sample

6.3 Synthetic Data Test

In this section, is presented the implementation of the developed functions to synthetic data so as to test the performance of them. Two variations of the analysis procedure, *DirVar0* and *DirVar1* (see Section 6.2), are used for the geostatistical analysis of synthetic data sampled randomly from a known constructed random field. The data are simulated from a Gaussian RF using a Generalized Mátern covariance function with parameters $\sigma_z^2 = 4.00, \xi_1 = 3.00, R = 1.67, \phi = 20.0°, c_0 = 0.20$ and $\nu = 2.00$ (without adding any trend). The size of the simulated random field is 60x60 and the sample consists of the 33% of the it (i.e. 1188 points of 3600). The simulated RF and the sample are shown in Fig. 6.4.

6.3.1 Preliminary Analysis

The statistics (Table 6.2) and the histograms (Fig. 6.5) of the sample and the original dataset show that the sample is representative of the original data, as well as that both of the datasets come from a gaussian distribution.

The normal probability plot of the sample (Fig. 6.6) also indicates that the data does come from a gaussian distribution. Moreover, the examined data are from structure gaussian and unbiased so there is no need for any transformations or trend removal.

Table 6.2 Original and sample datasets statistics

Dataset	Min	Max	Mean	Median	Variance	Skewness	Kurtosis
Original	-7.348	6.958	0.514	0.515	4.777	-0.074	3.020
Sample	-6.677	6.114	0.602	0.645	4.588	-0.164	3.121

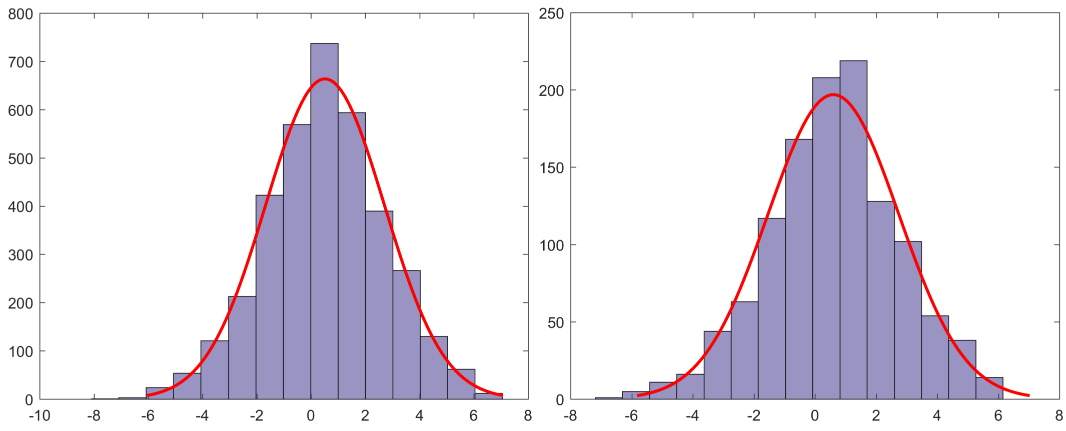

(a) Original **(b)** Random sample

Figure 6.5 Histograms of original and sample datasets

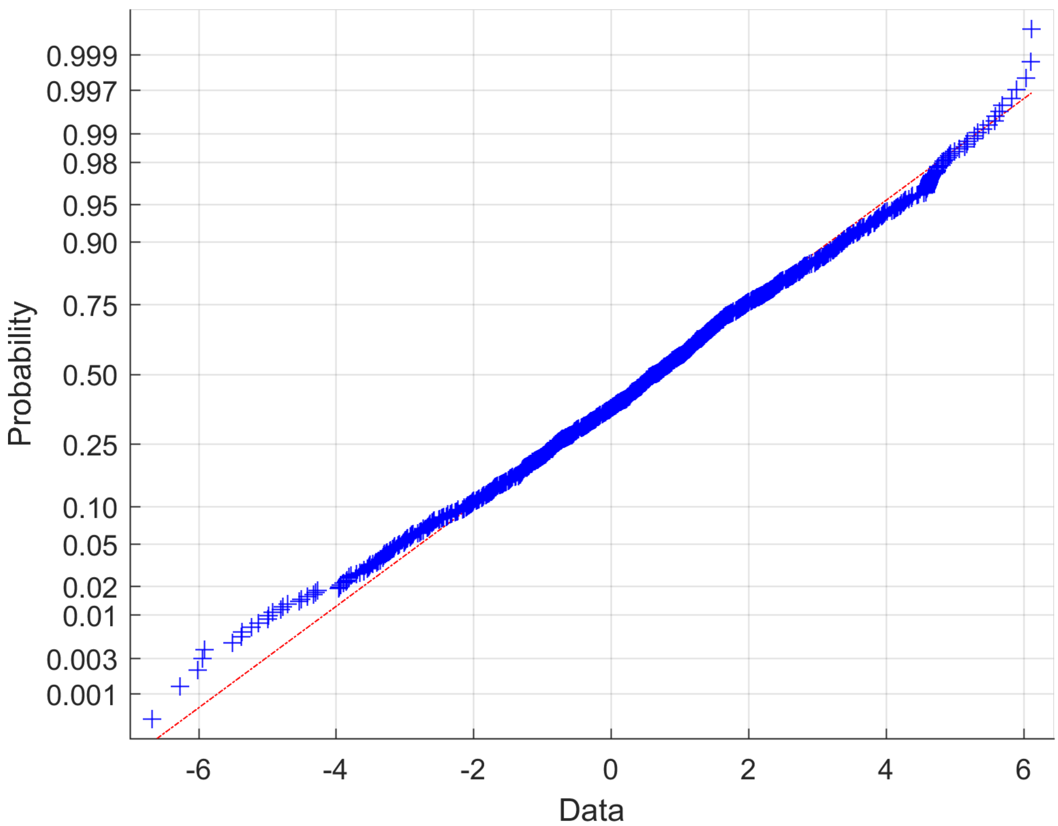

Figure 6.6 Normal probability plot of random sample

6.3.2 Calculation of Experimental Variogram

The experimental directional variograms with angular step 4° and 15° are shown in Fig. 6.7. These figures display clearly the anisotropic characteristics of the field. More specifically, it can be easily seen that the spatial correlation differs significantly from direction to direction; the variogram is stabilized around a maximum value (sill) in longer distances along the horizontal and almost horizontal directions than the other directions.

6.3.3 DirVar0

In the *DirVar0* method the investigated random field (transformed and detrended Marmousi model) is modeled by anisotropic variogram equations without estimating the anisotropy parameters in advance. Hence, the anisotropic variogram equations contain the maximum number of unknown parameters for each model. The parameter inference of these models is achieved through the minimization of the error function described by Eq. (5.8) between the experimental directional variograms and the choosen anisotropic theoretical models.

The initial values and the boundaries of the parameters for each model used in the optimization/parameter inference step are presented in Table 6.3, and the resulting optimum parameters are presented in Table 6.4. The estimated $sigma_z^2, \xi_1$ and ϕ for all the models except from Spartan are very close to the real, while the nugget effect (c_0) is estimated with good accuracy only from Generalized Exponential and Generalized Mátern models. From the estimated anisotropy ratios only the one deriving from the Generalized Mátern is closer to the real, while the other models give highly underestimated ratios. From the above derives that the most close to the reality model is the Generalized Mátern, which is the one used for the simulation of the synthetic data. The only erroneous estimation made from this model is the estimation of the smoothness parameter ν, which is undererestimated.

The scores of the LOOCV, presented in Table 6.5, confirm the above observations as they clarify that the Generalized Mátern model has the best performance, followed by Spartan and Generalized Exponential.

A visualisation of the the selected theoretical model's fitting to the experimental variogram is interpretted in Fig. 6.8, in which the directional experimental variograms of the field on the directions $0°, 30°, 60°, 90°, 120°$, and $150°$ are plotted against the theoretical model (the rest directional variograms in directions $15°, 45°, 75°, 105°, 135°$, and $165°$ can be found in Appendix A). It can be seen that the best anisotropic model fits well to the directional experimetnal variograms.

The estimation of the field values derived from OK with the best model is shown in Fig. 6.9. A scatter diagram of original and estimated values of the field, as well as their

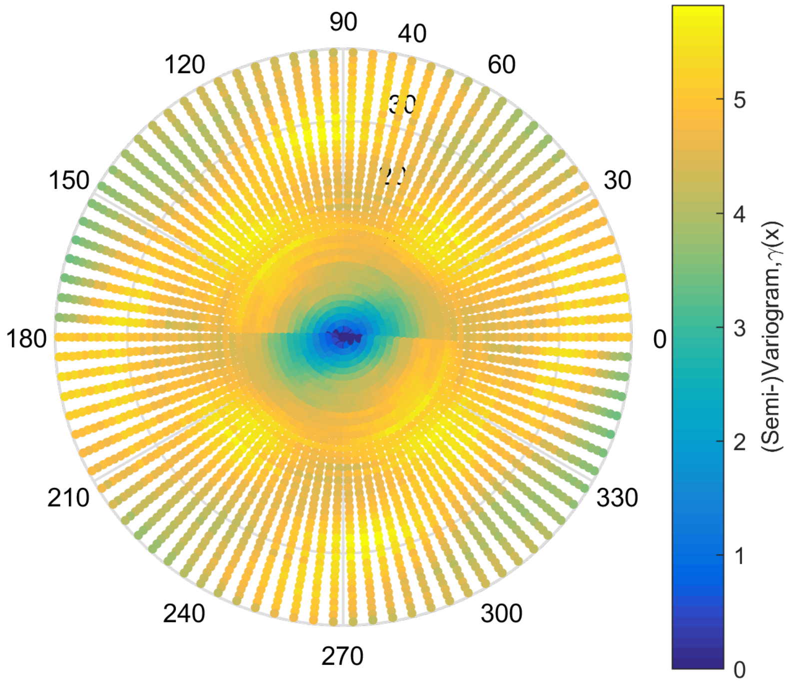

(a) 4° angular step

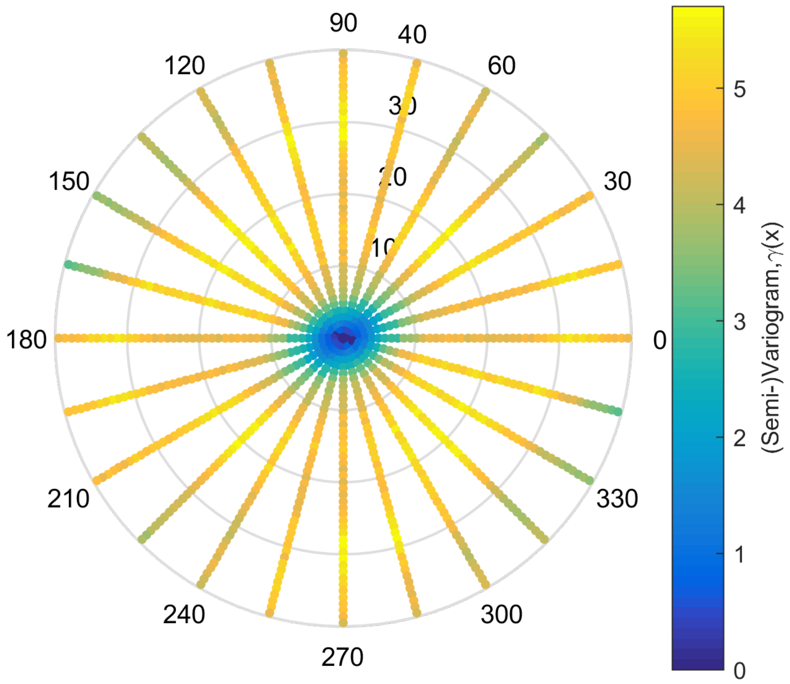

(b) 15° angular step

Figure 6.7 Directional experimental variograms of the synthetic data. For both cases the angular tolerance is 20°, the maximum distance taken into account is the 20% of the grid's diagonal which is equivalent to about 16, and is divided into 45 distance lags.

Table 6.3 Initial values and boundaries of the parameters for optimization step, where $\hat{g}_{max}(\equiv$ maximum value of experimental variogram$) = 5.7026$, $d_{max} \simeq 16$, $b = [\sigma_z^2 = \hat{g}_{max}, \xi_1 = d_{max}1/3, R = 0.5, \phi = 10°, c_0 = \hat{g}_{max}/100]$, $b_{sp} = [\eta_0 = 1000, \xi_1 = d_{max}1/3, R = 0.5, \phi = 10°, c_0 = \hat{g}_{max}/100]$, $b_b = [\sigma_z^2 \in [0, 1.5\hat{g}_{max}], \xi_1 \in [0, d_{max}], R \in [0, 30], \phi \in [-90°, 90°], c_0 \in [0, \hat{g}_{max}/5]]$,$b_{sp,b} = [\eta_0 \in [0, \infty], \xi_1 \in [0, 1.5d_{max}], R \in [0, 30], \phi \in [-90°, 90°], c_0 \in [0, \hat{g}_{max}/5]]$.

Model	Initial Values	Boundaries
Gen. Exponential	$[b, \nu = 1.5]$	$[b_b, \nu \in (0, 2)]$
Gaussian	$[b]$	$[b_b]$
Spherical	$[b]$	$[b_b]$
Gen. Matérn	$[b]$	$[b_b]$
Spartan	$[b_{sp}, \eta_1 = 1]$	$[b_{sp,b}, \eta_1 \in (-2, \infty)]$

Table 6.4 Optimum Parameters of the examined variogram models

Model	σ_z^2	ξ_1	R	ϕ	c_0	ν
Gen. Exponential	4.965	1.694	0.203	−65.2°	0.167	1.494
Gaussian	4.427	1.703	0.213	−66.0°	0.456	–
Spherical	4.840	1.519	0.095	−64.4°	0.000	–
Gen. Matérn	4.945	1.694	0.429	−65.2°	0.260	1.525
	η_0	ξ_1	R	ϕ	c_0	η_1
Spartan	165.129	0.625	0.081	−27.1°	0.000	2.000

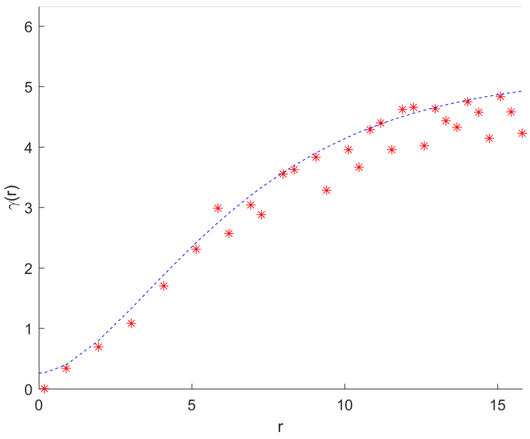

(a) 0°

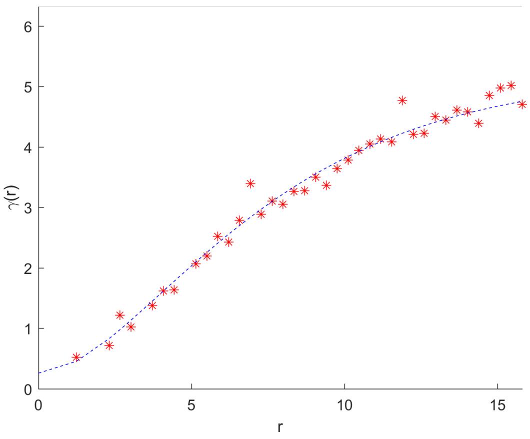

(b) 30°

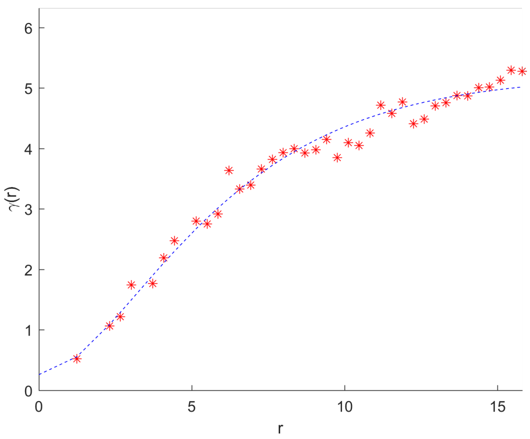

(c) 60°

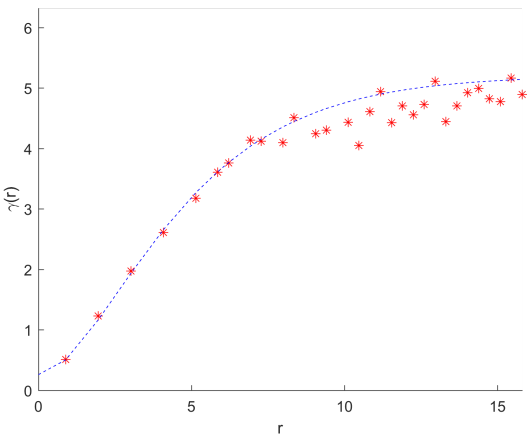

(d) 90°

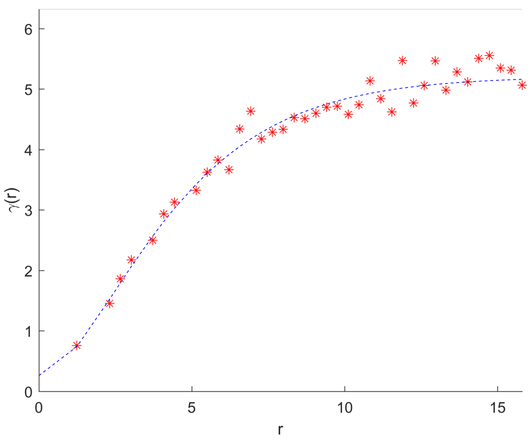

(e) 120°

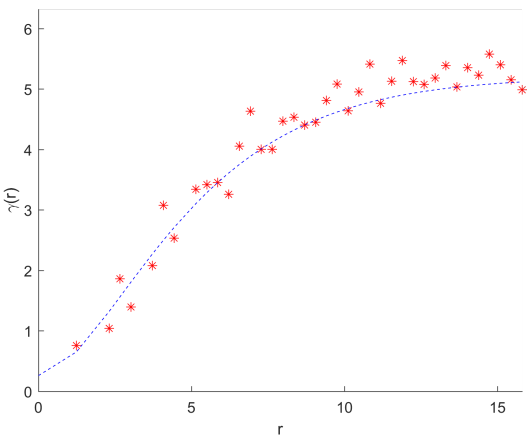

(f) 150°

Figure 6.8 Fitting of the best theoretical model to the directional experimental variograms of the field. The best model is a Gen. Mátern with parameters $\sigma_z^2 = 4.945, \xi_1 = 1.694, R = 0.429, \phi = -65.2°, c_0 = 0.260, \nu = 1.525$. The experimental variogram is calculated with angular tolerance 20°, 45 distance lags and taking into account maximum distance equivalent to about 16.

Table 6.5 Leave-One-Out Cross Validation Scores

Model	MeanAE	MaxAE	MSE	RMSE	R_p	R_{sp}	r_F
Gen. Exponential	1.171	4.790	2.217	1.489	0.736	0.721	0.156
Gaussian	1.171	4.780	2.216	1.489	0.736	0.721	0.156
Spherical	1.171	4.773	2.216	1.489	0.736	0.721	0.156
Gen. Matérn	0.855	3.566	1.201	1.096	0.885	0.866	0.766
Spartan	1.142	4.488	2.109	1.452	0.754	0.738	0.181

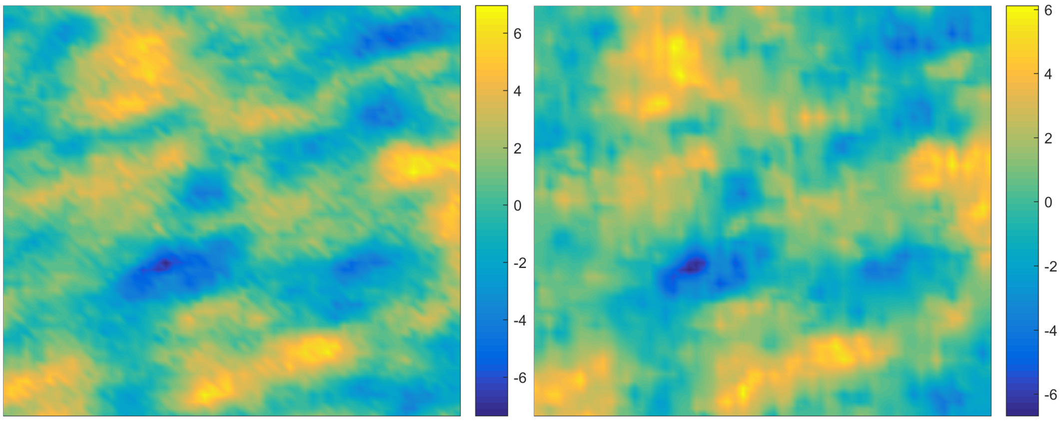

(a) Original Stochastic Component **(b)** Estimated Stochastic Component

Figure 6.9 Original and Estimation of the field. The model used is a Gen. Mátern with parameters $\sigma_z^2 = 4.945, \xi_1 = 1.694, R = 0.429, \phi = -65.2°, c_0 = 0.260, \nu = 1.525$.

histograms can be seen in Fig. 6.10. In general, the estimations follow the original values achieving a good proximity to the original distribution. In Table 6.6 the measures of the estimation performance for the three best models are presented. From these measures it can be observed that the first model's performance is much better than others two, which is almost identical. In addition, Fig. 6.11 maps the confidence interval width of the estimations, i.e. it depicts the spatial distribution of the uncertainty. The uncertainty is zero at the known points, while it increases up to 4.7 gradually with the distance of the missing points from the known locations.

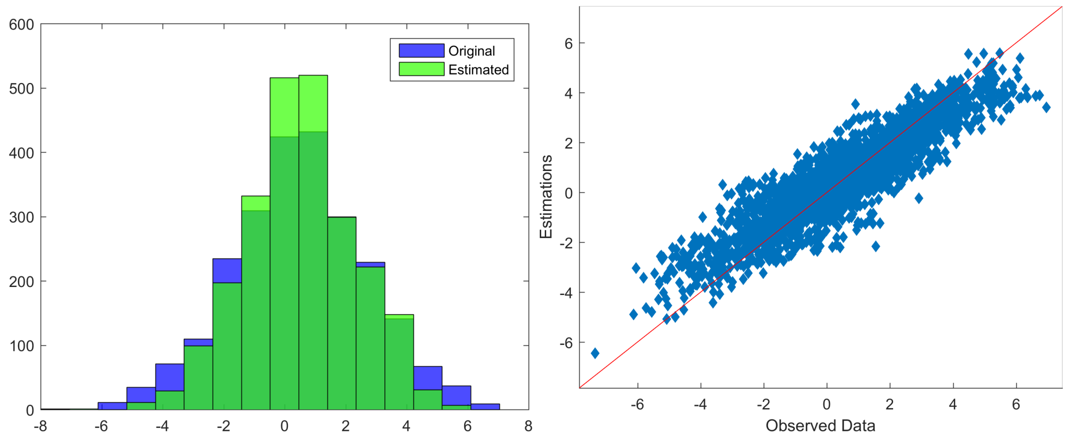

Figure 6.10 Histograms and Scatter plot of original and estimated values of the field's stochastic component. The model used is a Gen. Mátern with parameters $\sigma_z^2 = 4.945, \xi_1 = 1.694, R = 0.429, \phi = -65.2°, c_0 = 0.260, \nu = 1.525$.

Table 6.6 Ordinary Kriging Scores

Model	MeanAE	MaxAE	MSE	RMSE	R_p	R_{sp}	r_F
Gen. Mátern	0.737	3.713	0.904	0.951	0.907	0.897	0.813
Spartan	1.194	5.198	2.239	1.496	0.752	0.743	0.091
Gen. Exponential	1.197	5.037	2.254	1.501	0.750	0.742	0.089

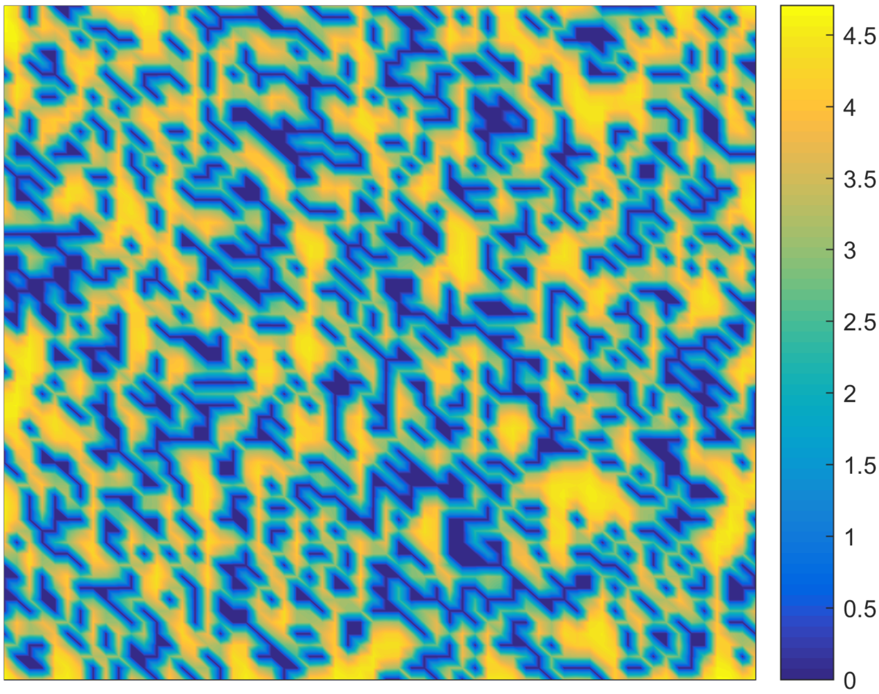

Figure 6.11 Uncertainty of the total field's estimation

6.3.4 DirVar1

In the *DirVar1* method the investigated random field is modeled by anisotropic variogram equations after estimating the anisotropy parameters of them. The anisotropy parameters are estimated by means of DVF (see section 5.2.2). Subsequently, the estimated parameters are replaced to the corresponding anisotropic variogram functions, reducing by three the number of unknown parameters for each model. The parameter inference of the models with the lower degrees of freedom is achieved through the minimization of the error function between the experimental directional variograms and the chosen anisotropic theoretical models.

The initial values and the boundaries of the parameters for each isotropic model used in the anisotropy parameter inference step with DVF method are as specified in Table 6.3 without considering the anisotropy parameters R and ϕ. The anisotropy parameters for each model are estimated by fitting an ellipse to the resulting pairs of (ϕ, ξ) of each model.The fitting of the ellipses to the pairs of (ϕ, ξ) of each model are depicted in Fig. 6.12, while the estimated anisotropy parameters for all models are given in Table 6.7.

All the investigated models, except from the Spartan, indicate that the major axis of the anisotropy ellipsis lies on between 0° and 47°. These estimations are relatively close to the used anisotropy angle of 20° for the construction of the synthetic random field. The Spartan model diverges significantly from the other models and gives the direction of the major

Table 6.7 Anisotropy parameters of the examined variogram models estimated with DVF method

Model	Anisotropy Parameters		
	ξ_1	R	ϕ
Gen. Exponential	4.867	0.563	$-58.5°$
Gaussian	4.874	0.653	$-65.5°$
Spherical	11.557	0.743	$-90.0°$
Gen. Matérn	1.846	0.342	$-42.3°$
Spartan	3.858	0.536	$15.3°$

Table 6.8 Optimum Parameters of the variogram models with the lower degrees of freedom

Model	σ_z^2	c_0	ν
Gen. Exponential	4.248	0.201	1.533
Gaussian	4.232	0.196	–
Spherical	4.285	0.162	–
Gen. Matérn	4.066	0.418	2.832
	η_0	c_0	η_1
Spartan	108.431	0.000	1.759

axis on 105°. This is probably due to minimization miscalculations caused by inappropriate objective function (very smooth or possible local minima), inappropriate initial values, etc. As for the estimated anisotropy ratios the Generalized Mátern converges to a lower value from the real, while the rest models converge to closer values. Finally, the minor axis of the ellipsis anisotropy is best estimated by the Generalized Mátern while the other models give much higher values and especially the Spherical. Anyway, more reliable conclusions can be drawn after the cross validation procedure.

By replacing the estimated anisotropy parameters to the anisotropic variogram models and minimizing the error function (Eq. (5.8)) of the "new" models and the experimental directional variograms the rest parameters are estimated, as presented in Table 6.8.

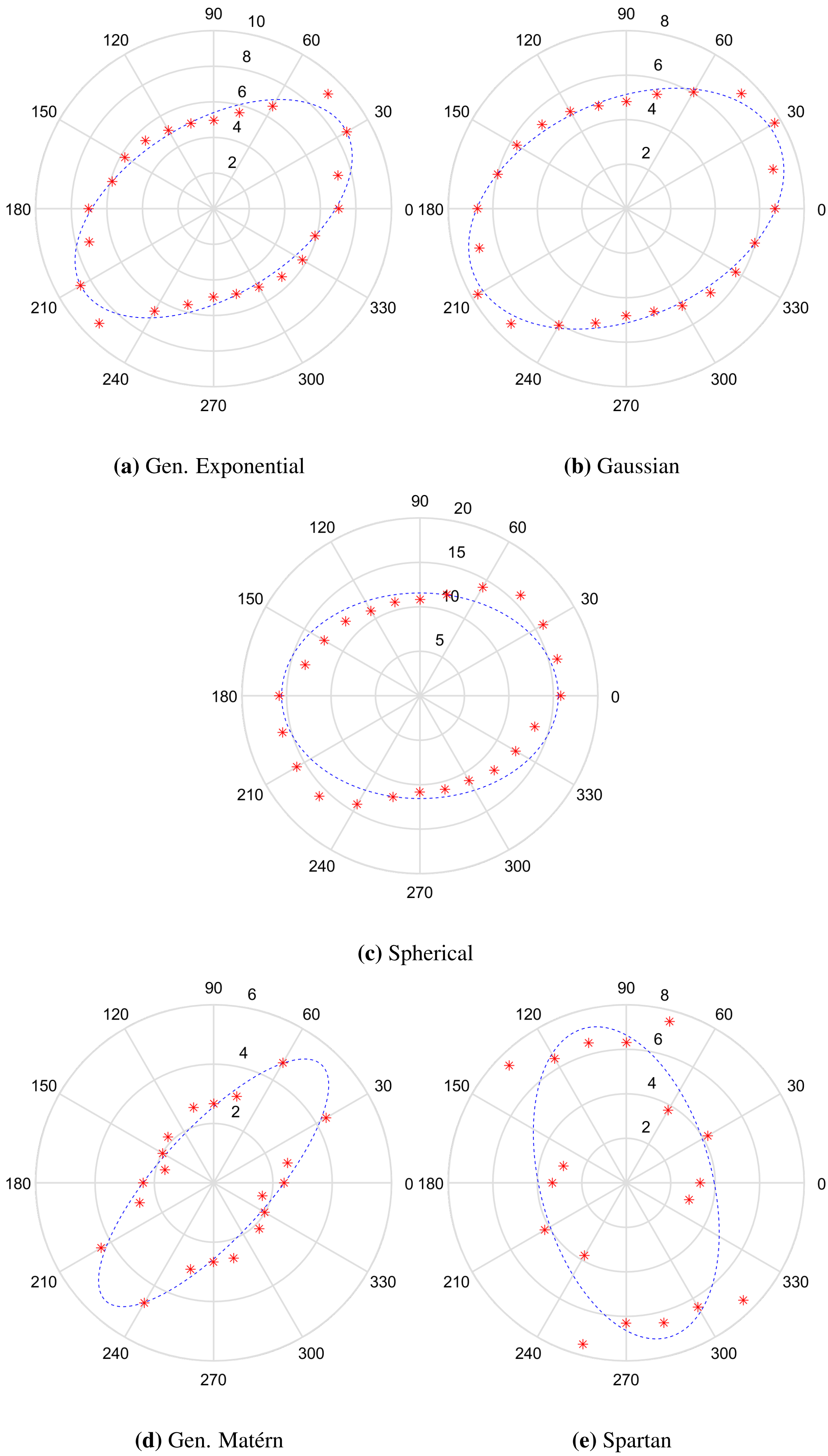

(a) Gen. Exponential

(b) Gaussian

(c) Spherical

(d) Gen. Matérn

(e) Spartan

Figure 6.12 Fitting of ellipses to the pairs (ϕ, ξ) of the examined variogram models

Table 6.9 Leave-One-Out Cross Validation Scores

Model	MeanAE	MaxAE	MSE	RMSE	R_p	R_{sp}	r_F
Gen. Exponential	1.079	4.319	1.888	1.374	0.794	0.773	0.228
Gaussian	1.098	4.316	1.948	1.396	0.785	0.764	0.209
Spherical	1.275	5.642	2.626	1.621	0.664	0.654	0.083
Gen. Matérn	0.812	7.452	1.149	1.072	0.873	0.868	0.758
Spartan	13.851	4177.341	16826.381	129.717	0.034	0.296	0.000

After the parameter inference Leave-One-Out Cross Validation (LOOCV) is applied in order to define the best models. The scores of the LOOCV, presented in Table 6.9, give as best model the Generalized Mátern, followed by the Generalized Exponential and the Gaussian.

The fitting of the best model to the experimental variogram along the directions of $0°, 30°, 60°, 90°, 120°$, and $150°$ is interpretted in Fig. 6.13 (the rest directional variograms in directions $15°, 45°, 75°, 105°, 135°$, and $165°$ can be found in Appendix A). As it can be seen the best theoretical variogram model fits well to the experimental directional variograms.

Implementing OK with the determined best model, the resulting estimation of the field is as shown in Fig. 6.14. The scatter diagram and histograms of the original and the estimated values are illustrated in Fig. 6.15, and the measures of the estimation performance for the three best models are presented in Table 6.10. In general, the estimations reproduce the original field quite well as it be seen from the histograms. As for the models' performance the Gen. Mátern achieved significantly higher measures than the other two which have similar measures. Finally, Fig. 6.16 shows the spatial distribution of the ordinary kriging estimations uncertainty. The uncertainty is zero at the known points, while it increases up to 4.7 gradually with the distance of the missing points from the known points.

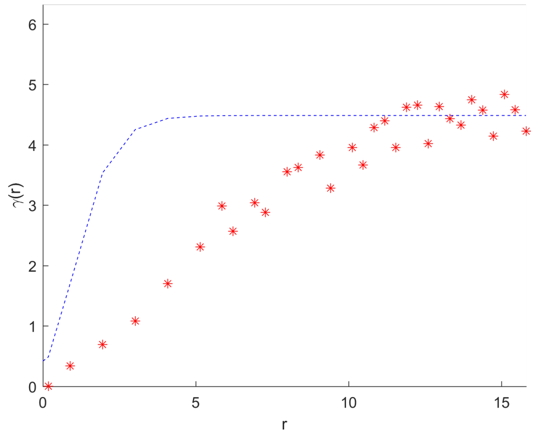

(a) 0°

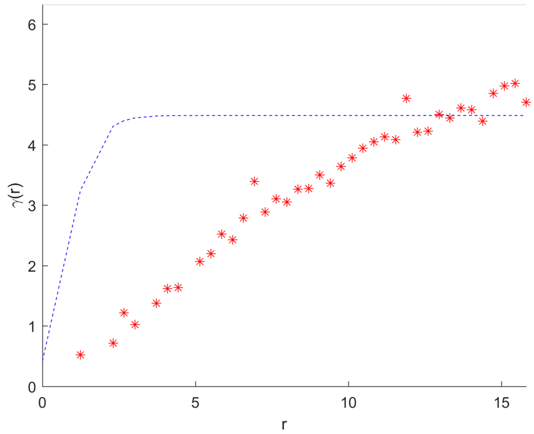

(b) 30°

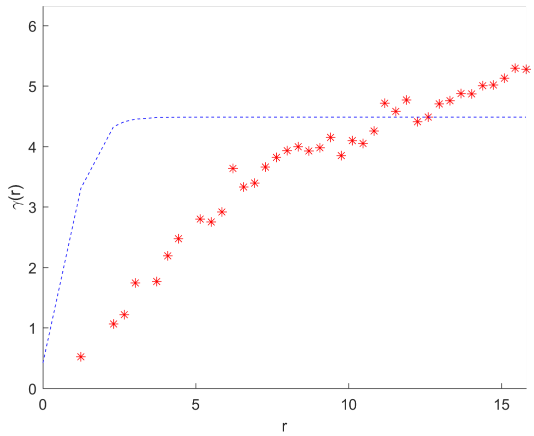

(c) 60°

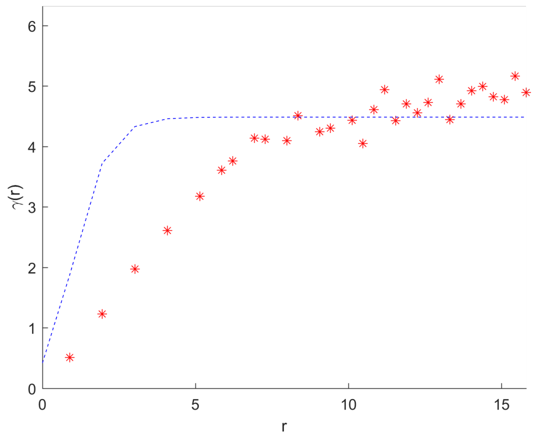

(d) 90°

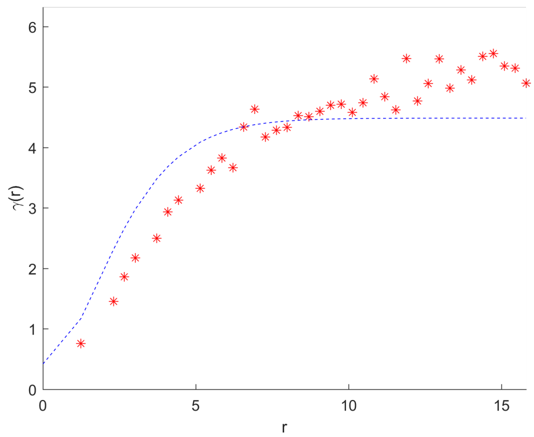

(e) 120°

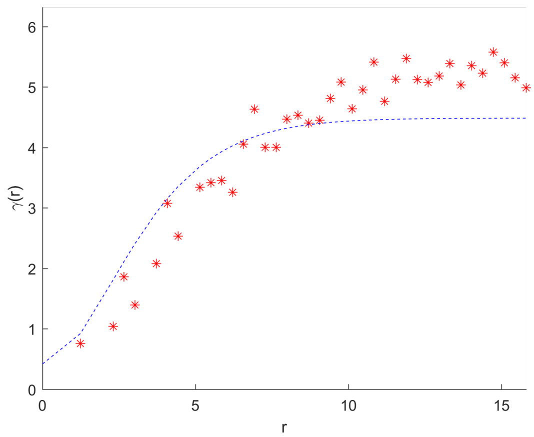

(f) 150°

Figure 6.13 Fitting of the best theoretical model to the experimental directional variograms of the field. The best model is a Gen. Mátern with parameters $sigma_z^2 = 4.066, \xi_1 = 1.846, R = 0.432, \phi = -42.3°, c_0 = 0.418, \nu = 2.832$. The experimental variogram is calculated with angular tolerance 20°, 45 distance lags and taking into account maximum distance equivalent to about 80.

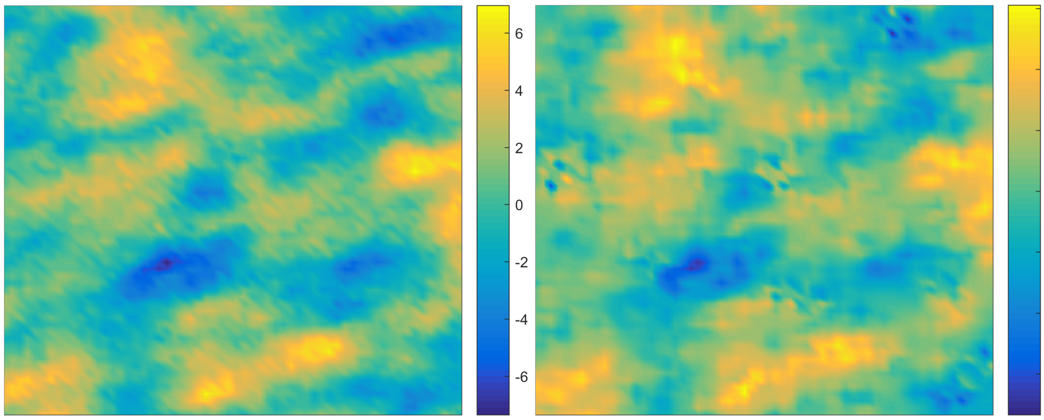

(a) Original Stochastic Component **(b)** Estimated Stochastic Component

Figure 6.14 Original and Estimation of the stochastic component of the field. The model used is a Gen. Mátern with parameters $sigma_z^2 = 4.066, \xi_1 = 1.846, R = 0.432, \phi = -42.3°, c_0 = 0.418, \nu = 2.832$.

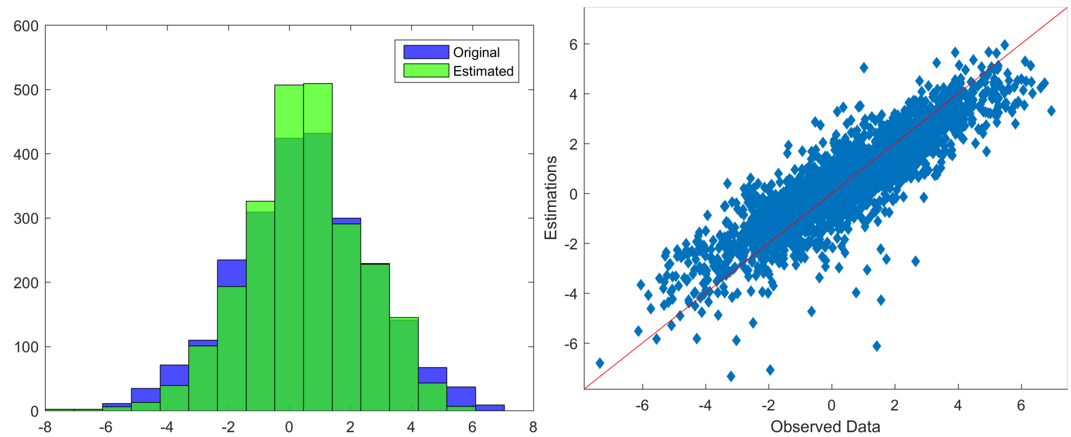

Figure 6.15 Histograms and Scatter plot of original and estimated values of the field's stochastic component.The model used is a Gen. Mátern with parameters $sigma_z^2 = 4.066, \xi_1 = 1.846, R = 0.432, \phi = -42.3°, c_0 = 0.418, \nu = 2.832$.

Table 6.10 Ordinary Kriging Scores

Model	MeanAE	MaxAE	MSE	RMSE	R_p	R_{sp}	r_F
Gen. Matérn	0.798	7.558	1.115	1.056	0.878	0.878	0.771
Gen. Exponential	0.952	4.324	1.489	1.220	0.852	0.841	0.402
Gaussian	0.903	4.331	1.357	1.165	0.857	0.849	0.491

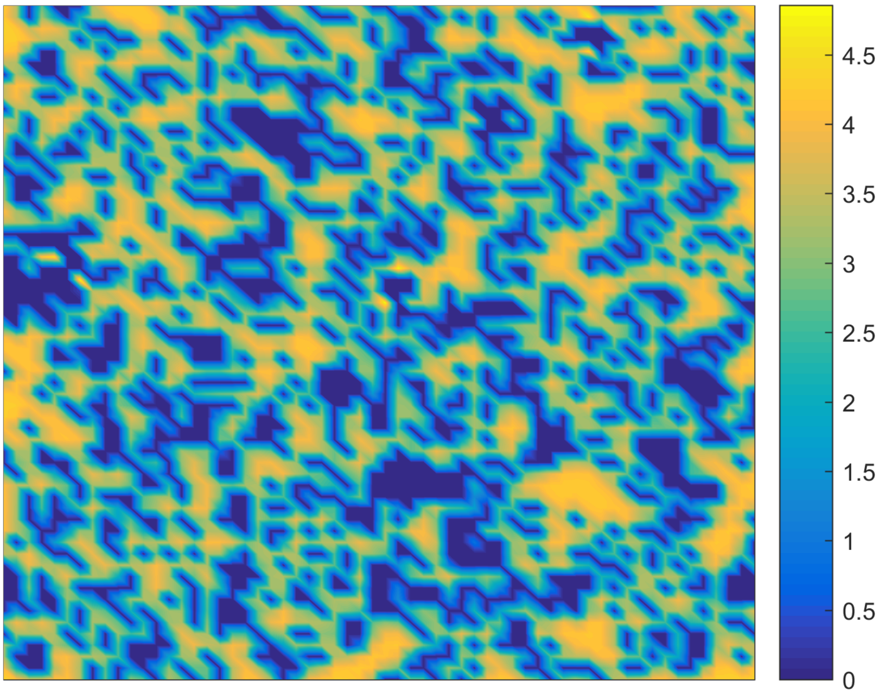

Figure 6.16 Uncertainty of the total field's estimation

6.3.5 Synopsis

The above described analysis of the simple synthetic dataset indicates that the developed codes can handle succesively such datasets and provide relatively reliable and acurrate results.

In the next sections these codes are applied to a more complex dataset.

6.4 Regular Sample of Marmousi Model

6.4.1 Ordinary Kriging

Preliminary Analysis

It is essential to examine whether the sample is representative of original data. From the statistics of both the sample and the original datasets (Table 6.11) as well as the histograms of them (Fig. 6.17), it is clear that the sample is totally representative of the original dataset.

The normal probability plot of the sample (Fig. 6.18), however, indicates that the data does not come from a gaussian distribution. Thus, Box-Cox transformation is necessary to be applied to the sample dataset. The best Box-Cox transformation is attained when $\lambda = -0.2606$. The statistics of the transformed values can be seen in Table 6.12, while the histogram and the normal probability plot of them are presented in Fig. 6.19). It is

Table 6.11 Original and sample datasets statistics

Dataset	Min	Max	Mean	Median	Variance	Skewness	Kurtosis
Original	0.273	1.000	0.514	0.475	0.030	0.824	3.277
Sample	0.273	1.000	0.514	0.473	0.030	0.823	3.270

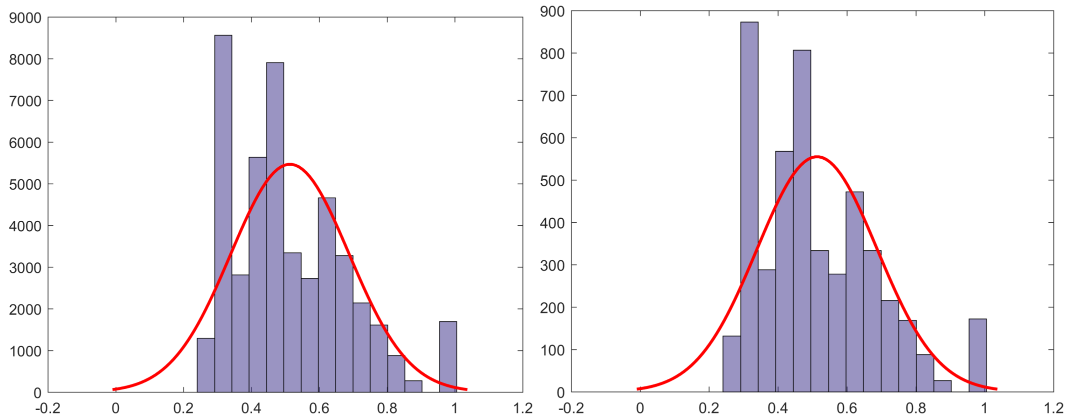

(a) Original **(b)** Regular sample

Figure 6.17 Histograms of original and sample datasets

clear that the Box-Cox transformation does not provides a truly gaussian dataset, but the transformed dataset is closer to the gaussian distribution than the original sample. Thus, no further actions are taken and the analysis proceeds under the assumption that the transformed dataset resembles sufficiently a dataset obtained from a gaussian distribution.

After transforming the regular sample's values, the next step is the removal of any possible trend. The trend models described in Section 5.1 (see Table 5.1) have been tested. The parameters of these models are inferred by means of multilinear regression of the transformed normalised velocities field on the (i, j) indices of the sample points. The complete expressions of the resulting trend functions are given in Table 6.13, while the normal probability plots of the fluctuations of each model are shown in Fig. 6.20. The best model is choosen as the one resulting in fluctuations which are closer to the gaussian distribution. This model, as can be seen from Fig. 6.20, is the linear trend model.

Table 6.12 Transformed (Box-Cox with $\lambda = -0.2606$) dataset statistics

Min	Max	Mean	Median	Variance	Skewness	Kurtosis
-1.546	0.000	-0.810	-0.826	0.157	0.025	2.127

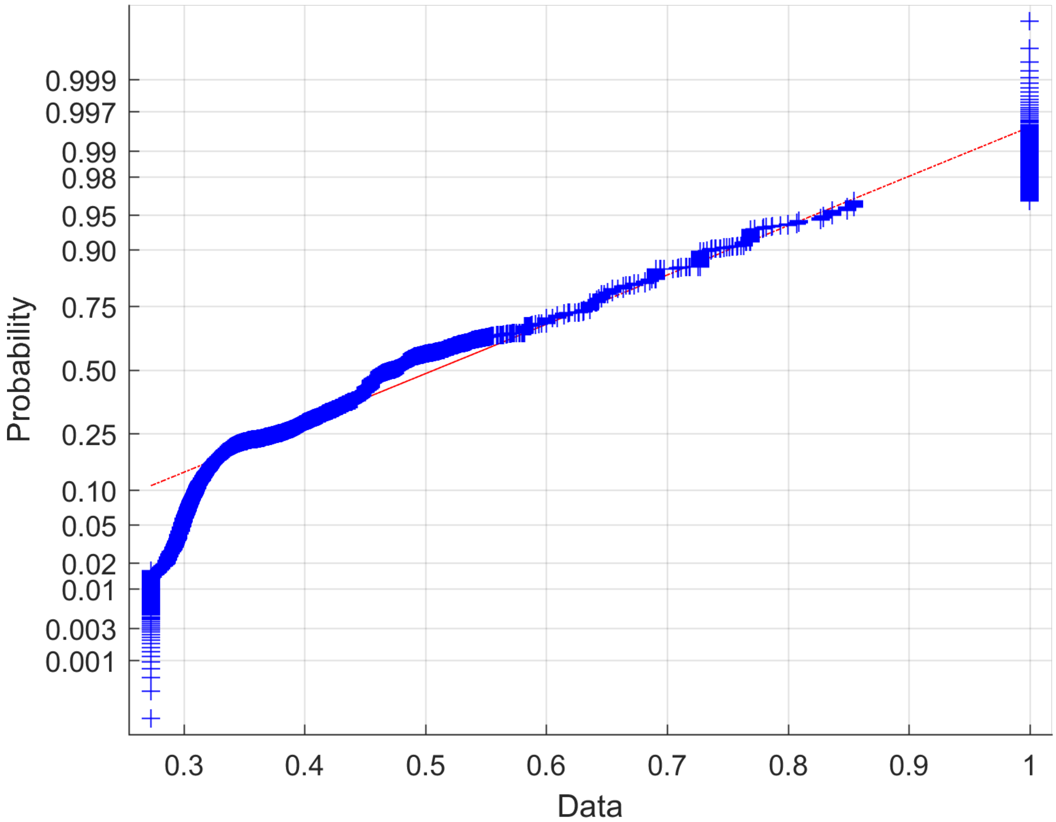

Figure 6.18 Normal probability plot of regular sample

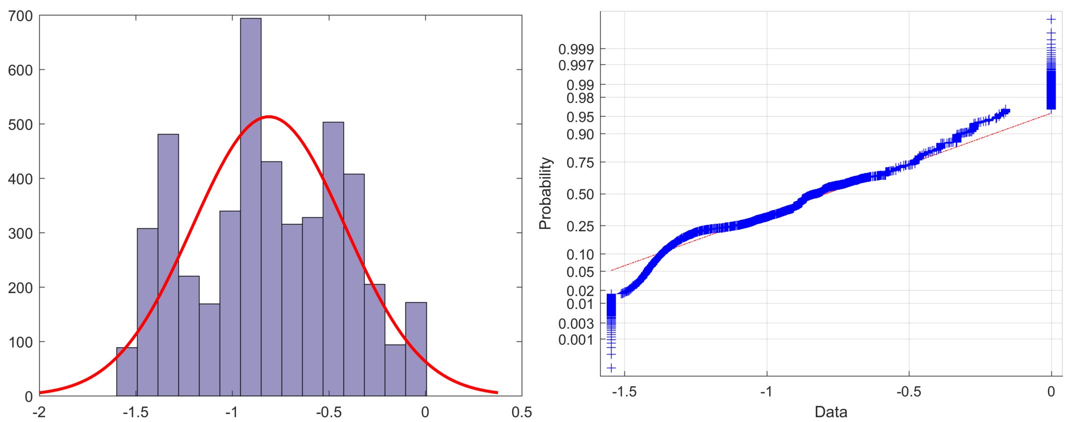

(a) Histogram **(b)** Normal probability plot

Figure 6.19 Histogram and normal probability plot of the transformed regular sample. The transformation applied is the Box-Cox with $\lambda = -0.2606$.

Table 6.13 Estimated trend models (regular sample)

Model	**Estimated Trend Function**
Mean	$m_z(\boldsymbol{s}) = -0.8105$
Linear	$m_z(\boldsymbol{s}) = -0.3044 + 5.1258 \cdot 10^{-4}x - 0.0098y$
Quadratic	$m_z(\boldsymbol{s}) = -0.3316 + 1.6886 \cdot 10^{-4}x - 0.0065y + 5.1848 \cdot 10^{-6}xy + 6.4395 \cdot 10^{-8}x^2 - 3.5533 \cdot 10^{-5}y^2$
Cubic	$m_z(\boldsymbol{s}) = -0.2066 - 0.0022x - 0.0066y + 4.3039 \cdot 10^{-5}xy + 8.3445 \cdot 10^{-6}x^2 - 1.0253 \cdot 10^{-4}y^2 - 4.8771 \cdot 10^{-8}x^2y - 1.5470 \cdot 10^{-7}xy^2 - 9.1203 \cdot 10^{-9}x^3 + 5.2494 \cdot 10^{-7}y^3$
Quartic	$m_z(\boldsymbol{s}) = -0.2760 - 0.0043x + 0.0074y + 1.4800 \cdot 10^{-5}xy + 3.5298 \cdot 10^{-5}x^2 - 4.8234 \cdot 10^{-4}y^2 - 1.0227 \cdot 10^{-7}x^2y + 7.4577 \cdot 10^{-7}xy^2 - 1.1655 \cdot 10^{-7}x^3 + 3.8748 \cdot 10^{-6}y^3 + 8.4378 \cdot 10^{-10}x^2y^2 - 8.6842 \cdot 10^{-11}x^3y - 6.6459 \cdot 10^{-9}xy^3 + 1.4608 \cdot 10^{-10}x^4 - 8.4033 \cdot 10^{-9}y^4$
Linear+Periodic	$m_z(\boldsymbol{s}) = -0.3661 + 5.1253 \cdot 10^{-4}x - 0.0088y + 0.0033\cos 2\pi 0.0256x - 0.0029\sin 2\pi 0.0256x - 0.0524\cos 2\pi 0.0082y + 0.0520\sin 2\pi 0.0082y - 4.2847 \cdot 10^{-4}\cos 2\pi 0.0513x + 0.0032\sin 2\pi 0.0513x - 0.0025\cos 2\pi 0.0164y + 0.0211\sin 2\pi 0.0164y$

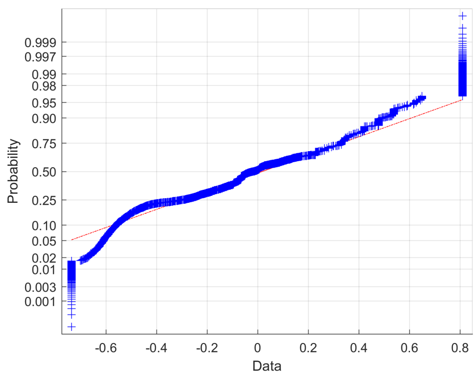

(a) Mean

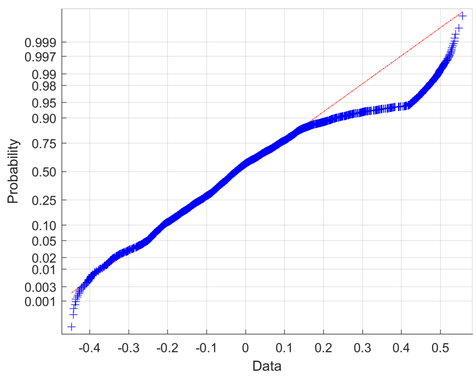

(b) Linear model

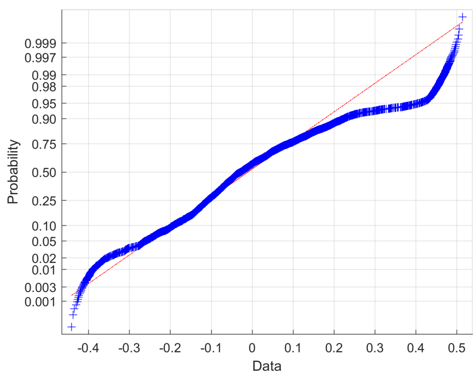

(c) Quadratic model

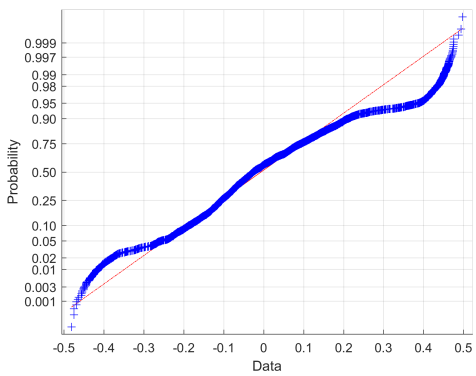

(d) Cubic model

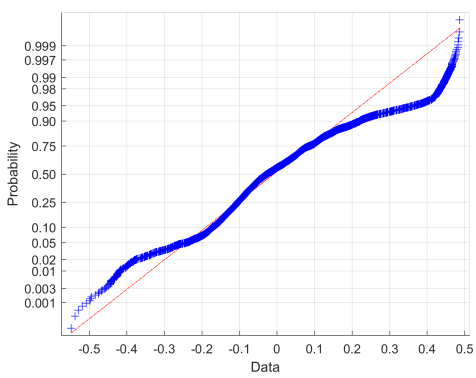

(e) Quartic model

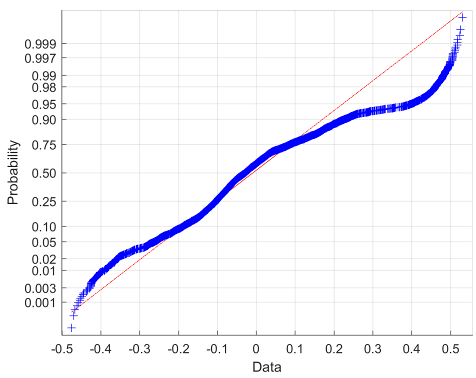

(f) Periodic model

Figure 6.20 Normal probability plots of the fluctuations resulting from the estimated trend models.

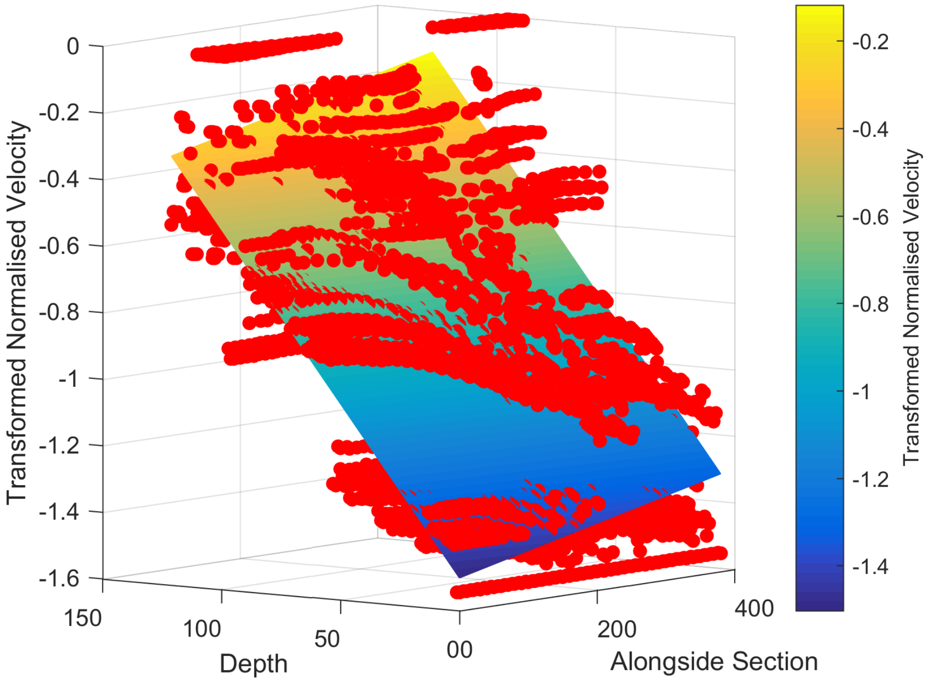

Figure 6.21 Multilinear regression of the transformed normalised velocities field on the indices (i, j) of the sample points. The trend equation is given by $m_z(\boldsymbol{s}) = -0.3044 + 5.1258 \cdot 10^{-4}x - 0.0098y$.

Table 6.14 Transformed and detrended dataset statistics

Min	Max	Mean	Median	Variance	Skewness	Kurtosis
-0.446	0.557	0.000	-0.025	0.033	0.744	3.745

In Fig. 6.21 the multilinear regression of the transformed normalised velocities field on the indices (i, j) of the sample points is depicted, while in Fig. 6.22 is plotted the histogram of the transformed and detrended data (i.e. the fluctuations), and in Table 6.14 are evaluated the statistics of them. Finally, in Fig. 6.23 is presented the transformed and detrended Marmousi model, in order to obtain an inspection of the random field, which we intend to regenerate hereinafter with the five variations of the analysis procedure, described in Section 6.2.

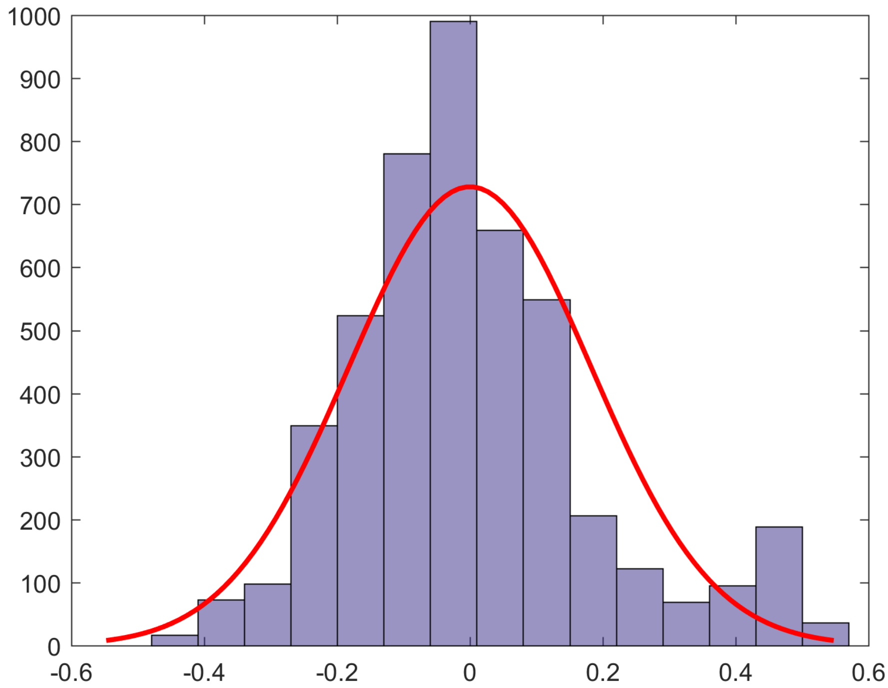

Figure 6.22 Histogram of transformed and detrended sample dataset

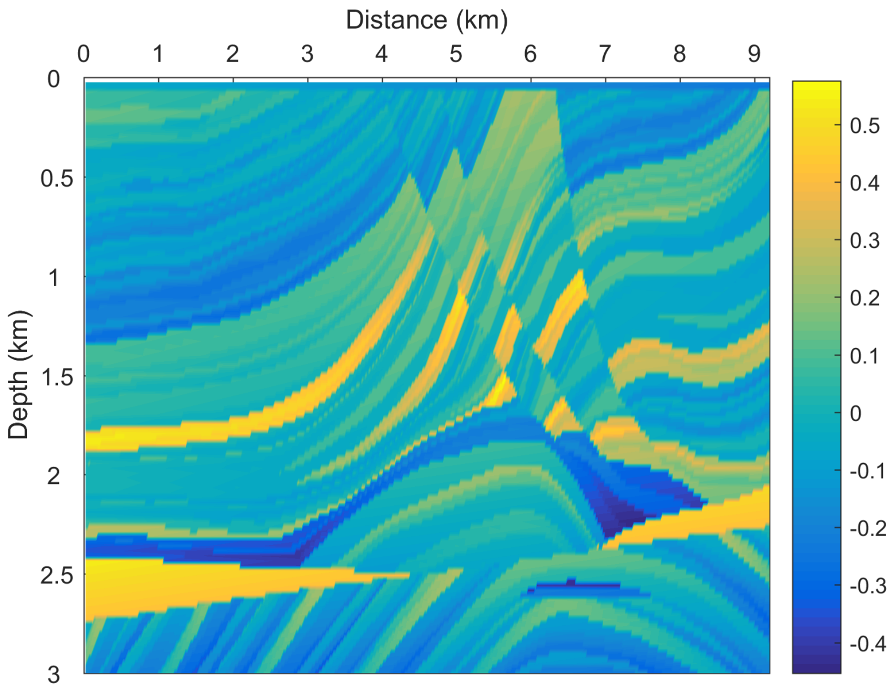

Figure 6.23 Transformed and detrended Marmousi model

Calculation of Experimental Variogram

The experimental directional variograms with angular step 4° and 15° are shown in Fig. 6.24. These figures display clearly the significant anisotropic characteristics of the field (as it is highly expected for such geological data). More specifically, it can be easily seen that the spatial correlation differs significantly from direction to direction; the variogram is stabilized around a maximum value (sill) in much more longer distances along the horizontal and almost horizontal directions than the other directions.

The experimental variograms with the smaller angular step (4°) have been calculated only in order to provide a clearer visualization of the anisotropy of the field, while the directional experimental variograms with the higher angular step (15°) are used in practice in the following steps. We avoid to use the exprimental variograms with the small angular step due to the higher computational cost that they will lead the further analysis.

DirVar0

In the *DirVar0* method the investigated random field (transformed and detrended Marmousi model) is modeled by anisotropic variogram equations without estimating the anisotropy parameters in advance. Hence, the anisotropic variogram equations contain the maximum number of unknown parameters for each model. The parameter inference of these models is achieved through the minimization of the error function described by Eq. (5.8) between the experimental directional variograms and the choosen anisotropic theoretical models.

The initial values and the boundaries of the parameters for each model used in the optimization step are presented in Table 6.15, and the resulting optimum parameters are presented in Table 6.16. The investigated models' parameters generally agree, with only exception the anisotropy ratios which exhibit relatively high discrepancies. However, the correctness of them cannot be evaluated before the cross validation procedure.

After the parameter inference, the best model is selected by means of Leave-One-Out Cross Validation (LOOCV). In order to obtain the estimations of the original field (normalised velocities) on the dataset locations and to compare them with the original values, the kriged values are back-transformed in two steps:

a)) the corresponding trend values at the known points are added to the estimations of the stochastic component (detrended and transformed normalised velocities), and

b)) the Box-Cox transformation is inverted.

The performance of the models is evaluated by calculating the validation measures described in Section 5.3.2, and the best model is chosen based on the coefficient expressed by Eq.

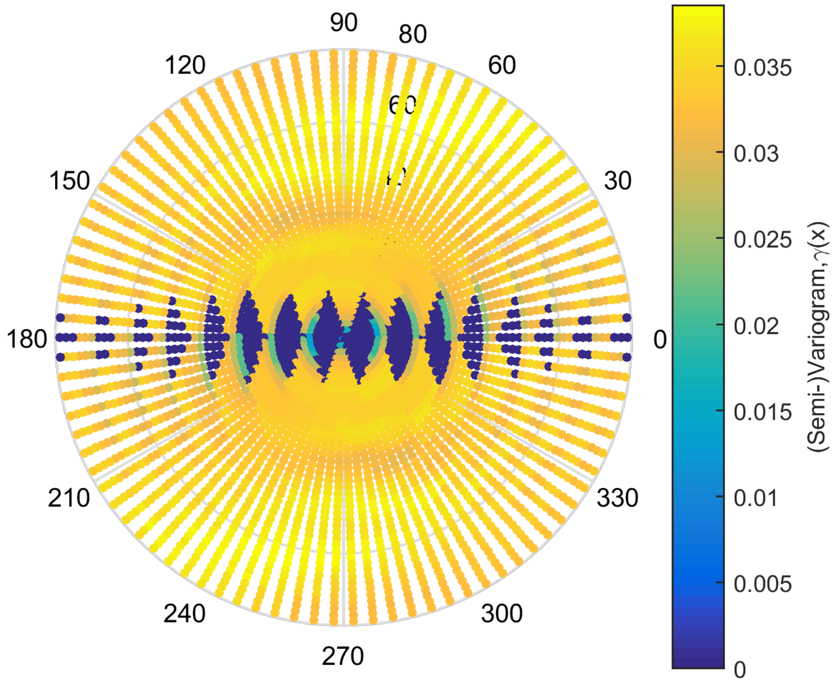

(a) 4° angular step

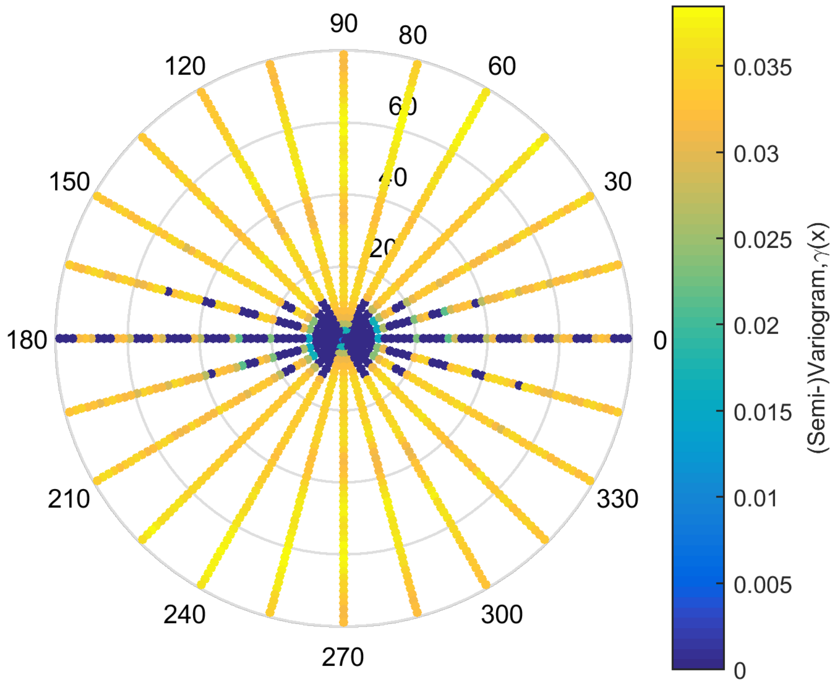

(b) 15° angular step

Figure 6.24 Directional experimental variograms of the field. For both cases the angular tolerance is 20°, the maximum distance taken into account is the 20% of the grid's diagonal which is equivalent to about 80, and is divided into 45 distance lags.

Table 6.15 Initial values and boundaries of the parameters for optimization step, where $\hat{g}_{max}$($\equiv$ maximum value of experimental variogram) $= 0.0384$, $d_{max} \simeq 80$, $b = [\sigma_z^2 = \hat{g}_{max}, \xi_1 = d_{max}2/3, R = 0.5, \phi = 10°, c_0 = \hat{g}_{max}/100]$, $b_{sp} = [\eta_0 = 1000, \xi_1 = d_{max}2/3, R = 0.5, \phi = 10°, c_0 = \hat{g}_{max}/100]$, $b_b = [\sigma_z^2 \in [0, 1.5\hat{g}_{max}], \xi_1 \in [0, 1.5d_{max}], R \in [0, 30], \phi \in [-90°, 90°], c_0 \in [0, \hat{g}_{max}/5]]$, $b_{sp,b} = [\eta_0 \in [0, \infty], \xi_1 \in [0, 1.5d_{max}], R \in [0, 30], \phi \in [-90°, 90°], c_0 \in [0, \hat{g}_{max}/5]]$.

Model	**Initial Values**	**Boundaries**
Gen. Exponential	$[b, \nu = 1.5]$	$[b_b, \nu \in (0, 2)]$
Gaussian	$[b]$	$[b_b]$
Spherical	$[b]$	$[b_b]$
Gen. Matérn	$[b]$	$[b_b]$
Spartan	$[b_{sp}, \eta_1 = 1]$	$[b_{sp,b}, \eta_1 \in (-2, \infty)]$

Table 6.16 Optimum Parameters of the investigated variogram models

Model	σ_z^2	ξ_1	R	ϕ	c_0	ν
Gen. Exponential	0.035	8.745	0.340	−83.8°	0.000	0.756
Gaussian	0.026	5.879	0.253	−85.3°	0.008	–
Spherical	0.026	7.657	0.109	−84.4°	0.008	–
Gen. Matérn	0.034	8.847	0.210	−83.8°	0.000	0.300
	η_0	ξ_1	R	ϕ	c_0	η_1
Spartan	4.257	8.306	0.085	−84.0°	0.000	88.809

Table 6.17 Leave-One-Out Cross Validation Scores (see section 5.3.2

Model	MnAE	MxAE	MSE	RMSE	R_p	R_{sp}	r_F
Gen. Exponential	0.051	0.395	0.006	0.079	0.894	0.927	0.617
Gaussian	0.051	0.393	0.006	0.078	0.896	0.928	0.640
Spherical	0.048	0.372	0.005	0.073	0.910	0.934	0.850
Gen. Matérn	0.050	0.384	0.006	0.076	0.902	0.931	0.723
Spartan	0.049	0.375	0.005	0.073	0.909	0.934	0.829

(5.25). As can be seen from the validation measures of the LOOCV presented in Table 6.17 the best model is the Spherical, followed by the Spartan and the Generalized Matérn models.

A visualisation of the the selected theoretical model's fitting to the experimental variogram is interpretted in Fig. 6.25, in which the directional experimental variograms of the field on the directions $0°, 30°, 60°, 90°, 120°$, and $150°$ are plotted against the theoretical model (while the rest directional variograms in directions $15°, 45°, 75°, 105°, 135°$, and $165°$ can be found in Appendix A). The best anisotropic model fits fairly well to the directional experimetnal variograms.

In the next step, Ordinary Kriging is applied to the sample stochastic component field, using the three best models and an arbitrarily defined rectangular neighboorhood of size 22x4. This neighboorhood is selected so as to ensure that neighboors from at least two drill-holes away on both sides will be included. Only the results of the first model is presented in detail, while the other two are used only for comparison.

The estimation of the stochastic component of the field (i.e the transformed and detrended normalised velocities) given by the best model is shown in Fig. 6.26. A scatter diagram of original and estimated values of the stochastic component, as well as their histograms can be seen in Fig. 6.27. Finally , in Table 6.18 the measures of the stochastic component estimation performance for the three best models are presented.

By adding the trend to the estimations of the stochastic component of the field and inverting the Box-Cox transformation, the estimation of the total field, which is shown in Fig. 6.28, is derived. As for the stochastic component, a scatter diagram of the original and the estimated values of the total field, as well as their histograms can be seen in Fig. 6.29. In general, the estimations follow the original values without achieving satisfying proximity of the total distribution. Both the tails of the distribution as the middle of it exhibit significant discrepancies.

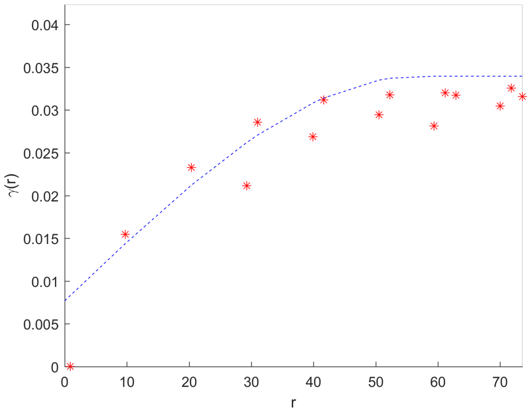

(a) 0°

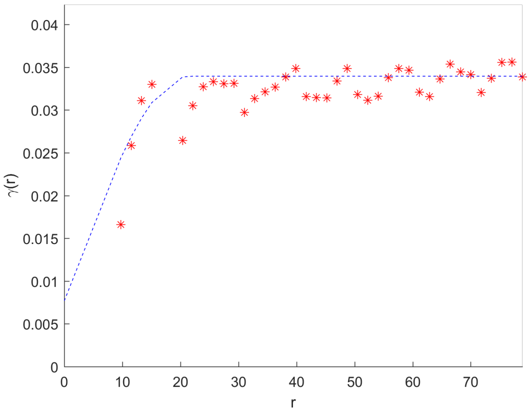

(b) 30°

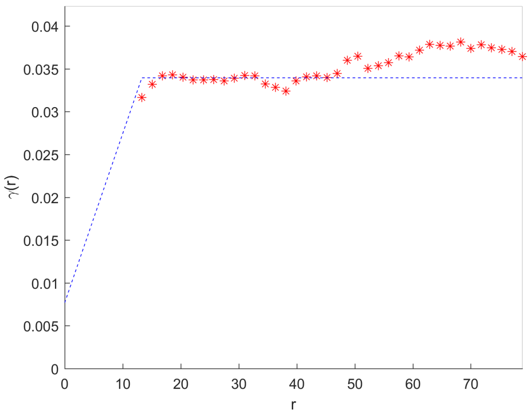

(c) 60°

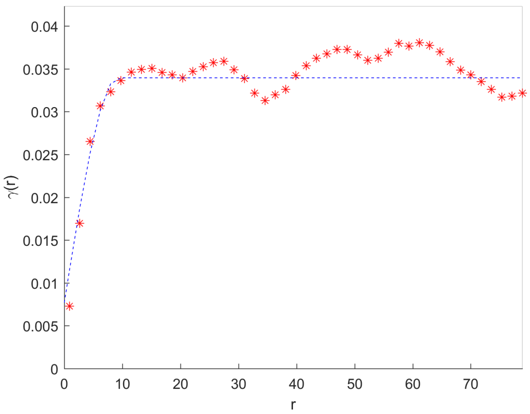

(d) 90°

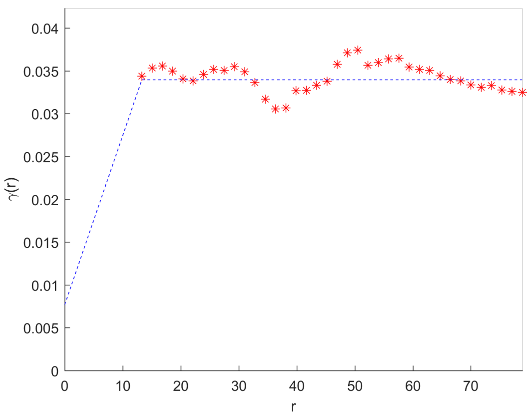

(e) 120°

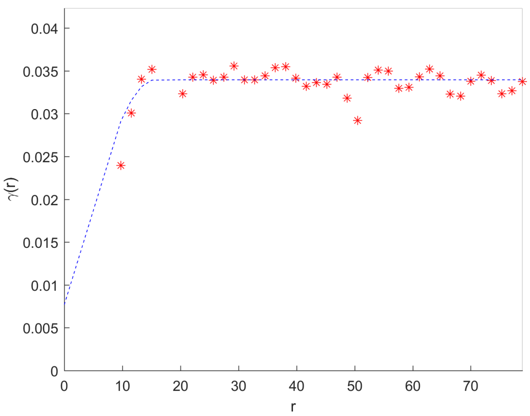

(f) 150°

Figure 6.25 Fitting of the best theoretical model to the directional experimental variograms of the field. The best model is a Spherical with parameters $\sigma_z^2 = 0.026, \xi_1 = 7.657, R = 0.109, \phi = -84.4°, c_0 = 0.008$. The experimental variogram is calculated with angular tolerance 20°, 45 distance lags and taking into account maximum distance equivalent to about 80.

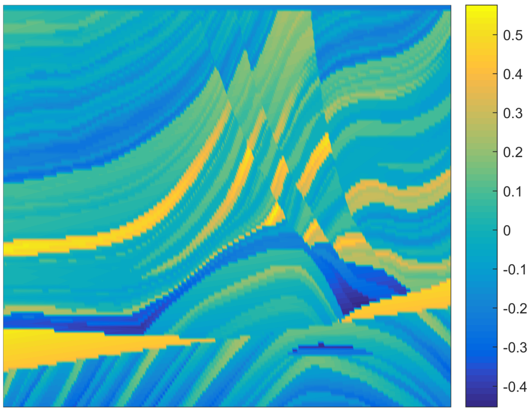

(a) Original Stochastic Component

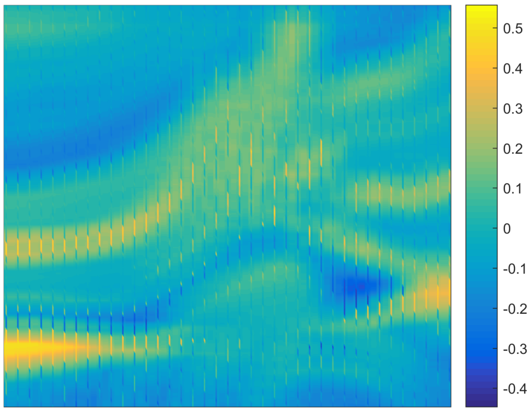

(b) Estimated Stochastic Component

Figure 6.26 Original and Estimation of the stochastic component of the field. The model used is the Spherical with parameters $\sigma_z^2 = 0.026, \xi_1 = 7.657, R = 0.109, \phi = -84.4°, c_0 = 0.008$.

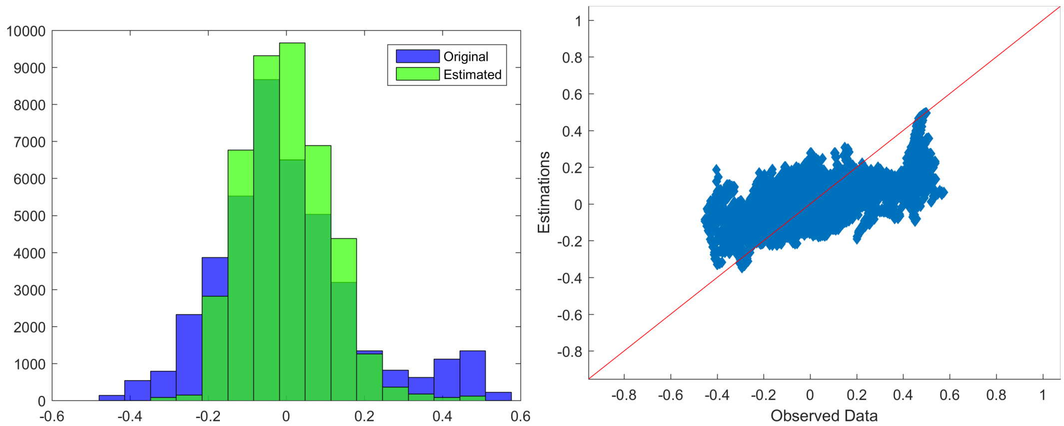

Figure 6.27 Histograms and Scatter plot of original and estimated values of the field's stochastic component. The model used is the Spherical with parameters $\sigma_z^2 = 0.026, \xi_1 = 7.657, R = 0.109, \phi = -84.4°, c_0 = 0.008$.

Table 6.18 Ordinary Kriging Scores

Model	MnAE	MxAE	MSE	RMSE	R_p	R_{sp}	r_F
Spherical	0.094	0.579	0.016	0.127	0.732	0.723	0.530
Spartan	0.094	0.580	0.016	0.127	0.728	0.720	0.512
Gen. Matérn	0.097	0.589	0.017	0.132	0.700	0.697	0.413

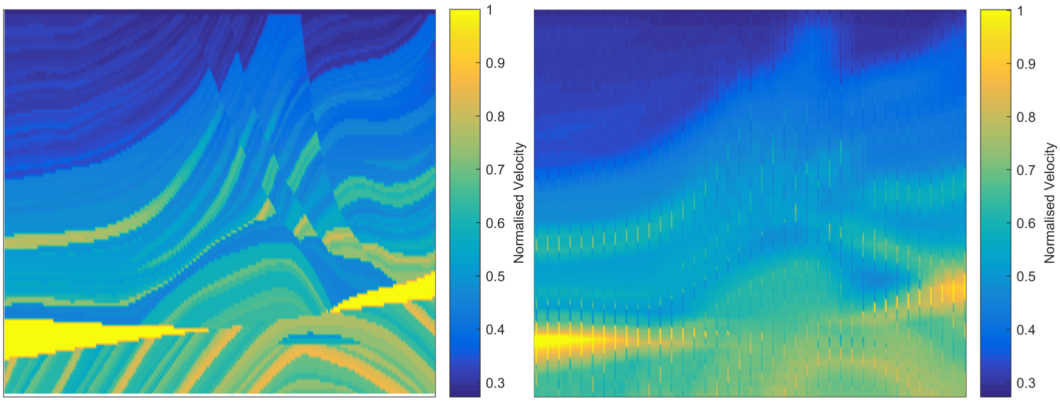

(a) Original Total Field

(b) Estimated Total Field

Figure 6.28 Original and estimated total field

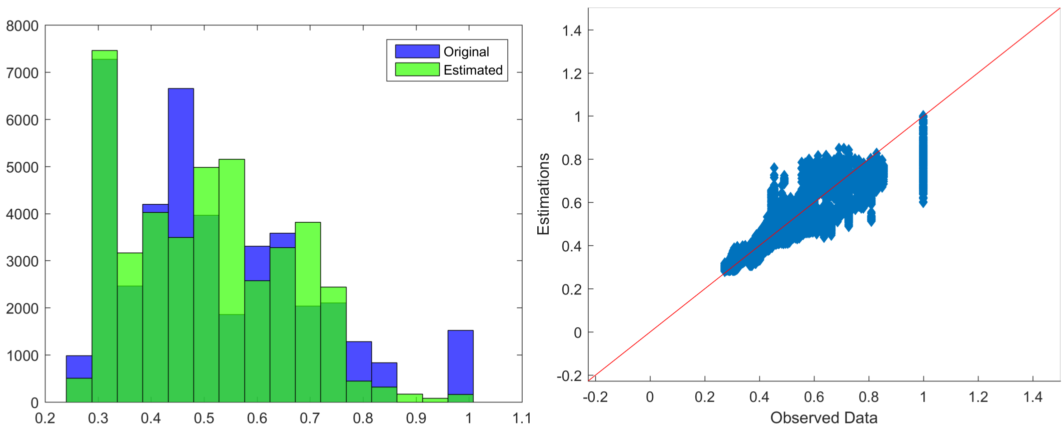

Figure 6.29 Histograms and Scatter plot of original and estimated values (total field)

In Table 6.19 the measures of the total field (i.e. normalised velocities) estimation performance for the three best models are presented. From these measures it can be observed that the two first models' performance is almost identical, while the third one follows closely. In addition, Fig. 6.30 maps the confidence interval width of the estimations, i.e. it depicts the spatial distribution of the uncertainty. The uncertainty is zero at the known locations, while at the investigated points it is equal to 0.37 with slightly smaller values at the edges. This can be explained by the fact that the number of the neighboors taken into account by the ordinary kriging estimations is the same for all the missing points, except for the edges of the field where it decreases, due to the regularity of the sample.

In Table 6.20 are presented the classification measures (see section 5.3.2) for the cases of 4 and 16 classes. By increasing the number of classes, the correlation coefficients increase,

Table 6.19 Total Field Estimation Scores

Model	MnAE	MxAE	MSE	RMSE	R_p	R_{sp}	r_F
Spherical	1.317	1.867	1.803	1.343	0.935	0.943	0.881
Spartan	1.317	1.866	1.803	1.343	0.934	0.942	0.880
Gen. Matérn	1.317	1.865	1.803	1.343	0.930	0.938	0.872

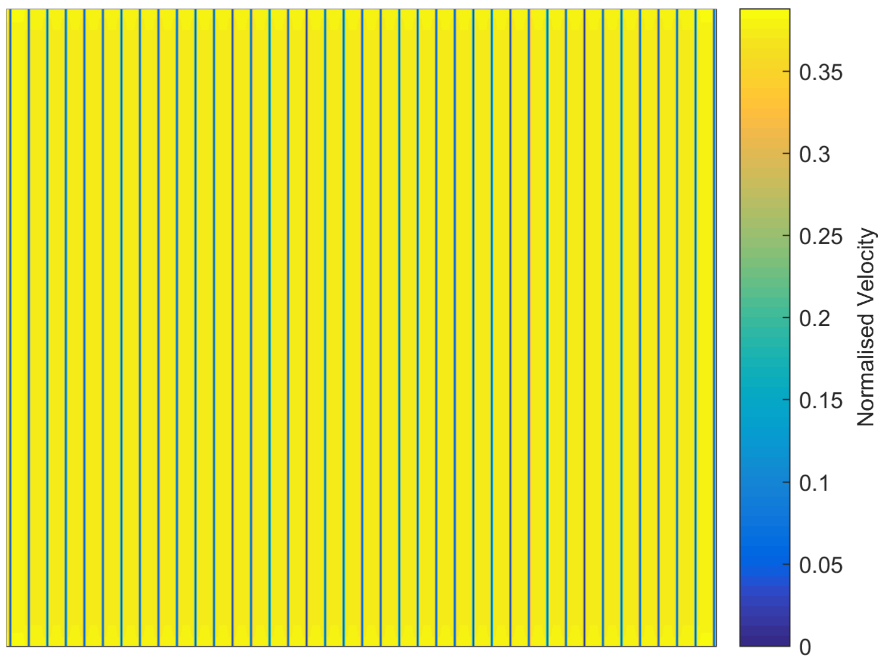

Figure 6.30 Uncertainty of the total field's estimation

Table 6.20 Classification Measures

	4 classes			16 classes		
Model	R_p	R_{sp}	**MCR**	R_p	R_{sp}	**MCR**
Spherical	0.860	0.873	0.220	0.916	0.936	0.584
Spartan	0.859	0.873	0.222	0.914	0.936	0.584
Gen. Matérn	0.852	0.867	0.227	0.906	0.931	0.588

while the MCR decreases. The increasing of the N_c leads to a more complex model, which closer to the reality. That is the reason of the correlation coefficients' improvement. On the contrary, the misclassification rate's deterioration can be attributed to the thinning of the binning, which incommodes the interpolation.

DirVar1

In the *DirVar1* method the investigated random field is modeled by anisotropic variogram equations after estimating the anisotropy parameters of them. The anisotropy parameters are estimated by means of DVF (see section 5.2.2). Subsequently, the estimated parameters are replaced to the corresponding anisotropic variogram functions, reducing by three the number of unknown parameters for each model. The parameter inference of the models with the lower degrees of freedom is achieved through the minimization of the error function between the experimental directional variograms and the chosen anisotropic theoretical models.

The initial values and the boundaries of the parameters for each isotropic model used in the anisotropy parameter inference step with DVF method are as specified in Table 6.15 without considering the anisotropy parameters R and ϕ. The anisotropy parameters for each model are estimated by fitting an ellipse to the resulting pairs of (ϕ, ξ) of each model. The fitting of the ellipses to these pairs for the 5 models are depicted in Fig. 6.31, while the estimated anisotropy parameters for all models are given in Table 6.21. In general, the investigated models' fitting show that the major axis of the anisotropy ellipsis is either on the almost horizontal direction ($0°$) or on the direction of about $30-40°$. This results agree with the intuitive estimations of the anisotropy angle mentioned at section 6.1.2. The non-stationarity of the field is also indicated by the strong dependence of the correlation length values' on the direction as it is illustrated in Fig. 6.31. For all the models the correlation lengths on the vertical or almost vertical directions are significantly smaller than these on the other directions. These rapid changes may also affect negatively the optimization procedure.

Table 6.21 Anisotropy parameters of the investigated variogram models estimated with DVF method

Model	Anisotropy Parameters		
	ξ_1	R	ϕ
Gen. Exponential	3.981	0.264	$-90.0°$
Gaussian	4.827	0.298	$-90.0°$
Spherical	11.550	0.397	$-90.0°$
Gen. Matérn	2.987	0.145	$-90.0°$
Spartan	40.338	0.307	$-50.9°$

Table 6.22 Optimum Parameters of the variogram models with the lower degrees of freedom

Model	σ_z^2	c_0	ν
Gen. Exponential	0.033	0.000	1.012
Gaussian	0.026	0.008	–
Spherical	0.026	0.007	–
Gen. Matérn	0.031	0.002	0.700
	η_0	c_0	η_1
Spartan	0.832	0.000	1.928

As regards the variations on the estimated anisotropy ratios, no reliable conclusions can be drawn before the cross validation procedure.

By replacing the estimated anisotropy parameters to the anisotropic variogram models and minimizing the error function of the new models and the experimental directional variograms the rest parameters are estimated, as presented in Table 6.22. The common parameters generally agree for all the investigated models.

After the parameter inference Leave-One-Out Cross Validation (LOOCV) is applied in order to define the best models. The validation measures of the LOOCV, presented in Table 6.23, give as best model the Spartan, followed by the Generalized Mátern and the Generalized Exponential models.

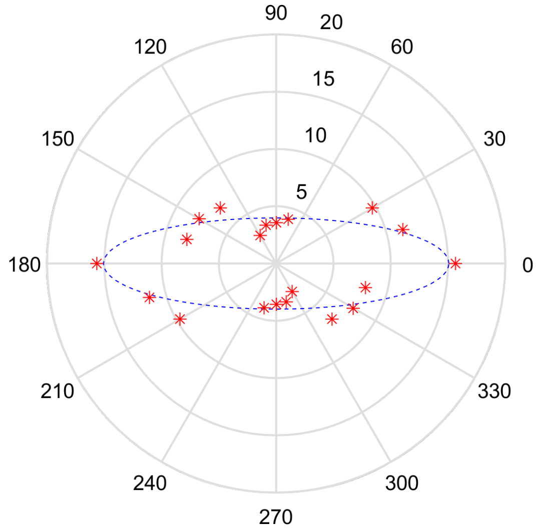

(a) Gen. Exponential

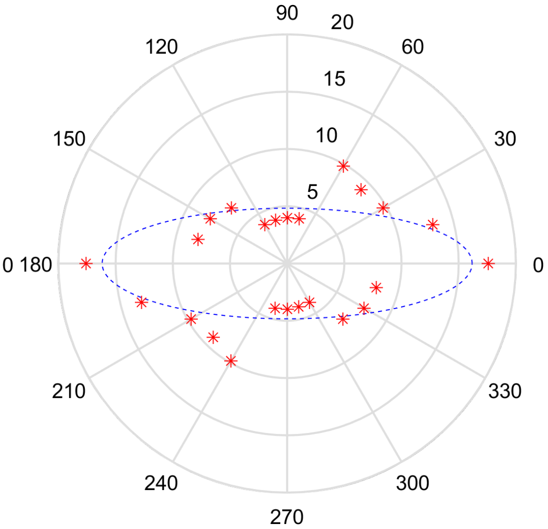

(b) Gaussian

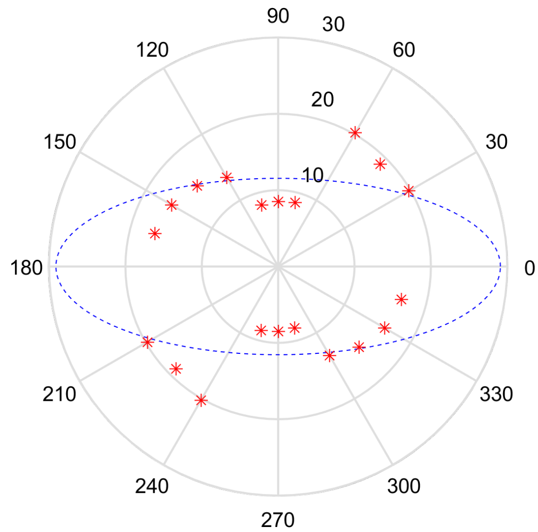

(c) Spherical

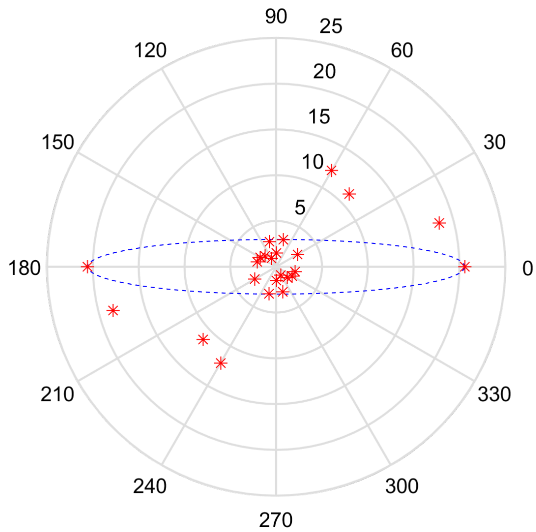

(d) Gen. Matérn

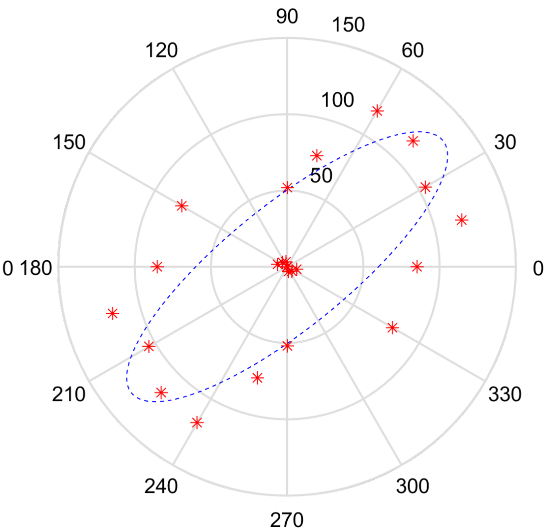

(e) Spartan

Figure 6.31 Fitting of ellipses to the pairs (ϕ, ξ) of the investigated variogram models

Table 6.23 Leave-One-Out Cross Validation Scores (see section 5.3.2

Model	MnAE	MxAE	MSE	RMSE	R_p	R_{sp}	r_F
Gen. Exponential	0.053	0.401	0.007	0.081	0.887	0.923	0.562
Gaussian	0.055	0.420	0.007	0.086	0.872	0.914	0.437
Spherical	0.054	0.411	0.007	0.083	0.880	0.919	0.502
Gen. Matérn	0.053	0.401	0.007	0.081	0.887	0.923	0.562
Spartan	0.049	0.372	0.005	0.074	0.908	0.933	0.848

Table 6.24 Ordinary Kriging Scores

Model	MnAE	MxAE	MSE	RMSE	R_p	R_{sp}	r_F
Spartan	0.094	0.676	0.017	0.129	0.716	0.709	0.507
Gen. Matérn	0.104	0.605	0.020	0.142	0.631	0.641	0.273
Gen. Exponential	0.104	0.605	0.020	0.142	0.632	0.642	0.276

The fitting of the best model to the experimental variogram along selected directions is interpretted in Fig. 6.32 (the rest directional variograms can be found in Appendix A). As it can be seen the best theoretical variogram model diverges significantly from the experimental directional variograms. This can be attributed to minimization miscalculations, i.e. inappropiate objective function (very smooth or possible local minima), inappropriate initial values or to the fields complexity (as mentioned above). Thus, the analysis is continued without taking any further action.

Implementing OK with the determined best model, the resulting estimation of the stochastic component of the field (i.e the transformed and detrended normalised velocities) is as shown in Fig. 6.33. The scatter diagram and histograms of the original and the estimated values of the stochastic component are illustrated in Fig. 6.34, and the measures of the stochastic component estimation performance for the three best models are presented in Table 6.24.

The resulting estimation of the total field, after the trend addition and Box-Cox transformation inversion, is as shows Fig. 6.35, and the correspomding scatter diagram and histograms are shown in Fig. 6.36. In general, the estimations follow the original values

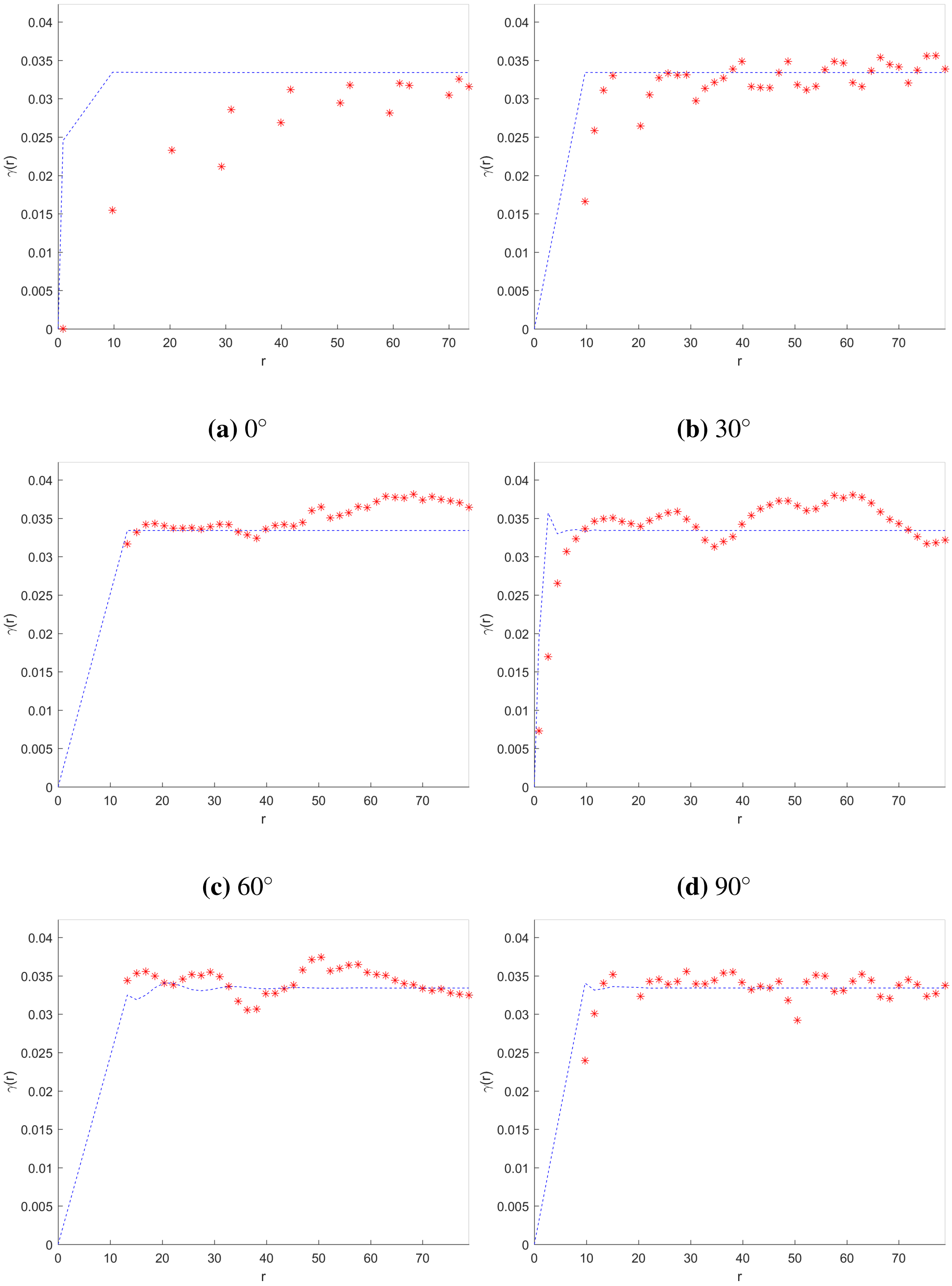

(a) 0° **(b)** 30°
(c) 60° **(d)** 90°
(e) 120° **(f)** 150°

Figure 6.32 Fitting of the best theoretical model to the experimental directional variograms of the field. The best model is a Spartan with parameters $\eta_0 = 0.832, \xi_1 = 40.338, R = 0.307, \phi = -50.9°, c_0 = 0.000, \eta_1 = 1.928$. The experimental variogram is calculated with angular tolerance 20°, 45 distance lags and taking into account maximum distance equivalent to about 80.

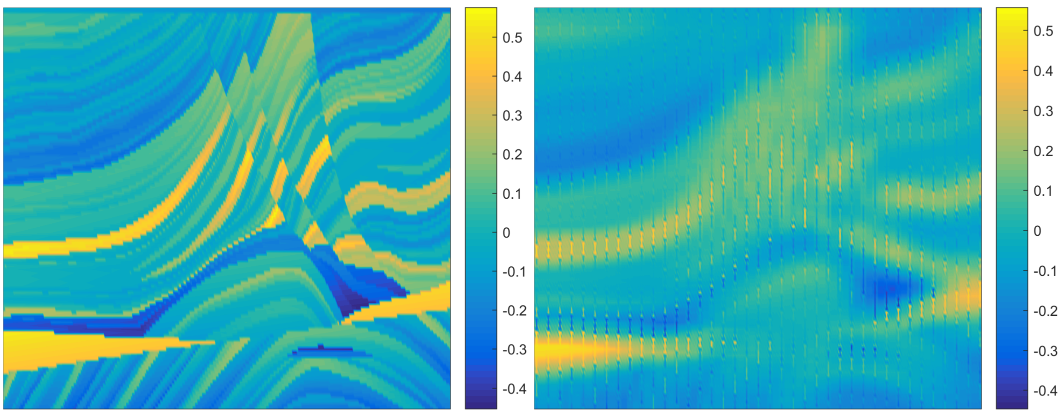

(a) Original Stochastic Component (b) Estimated Stochastic Component

Figure 6.33 Original and Estimation of the stochastic component of the field. The model used is a Spartan with parameters $\eta_0 = 0.832, \xi_1 = 40.338, R = 0.307, \phi = -50.9°, c_0 = 0.000, \eta_1 = 1.928$.

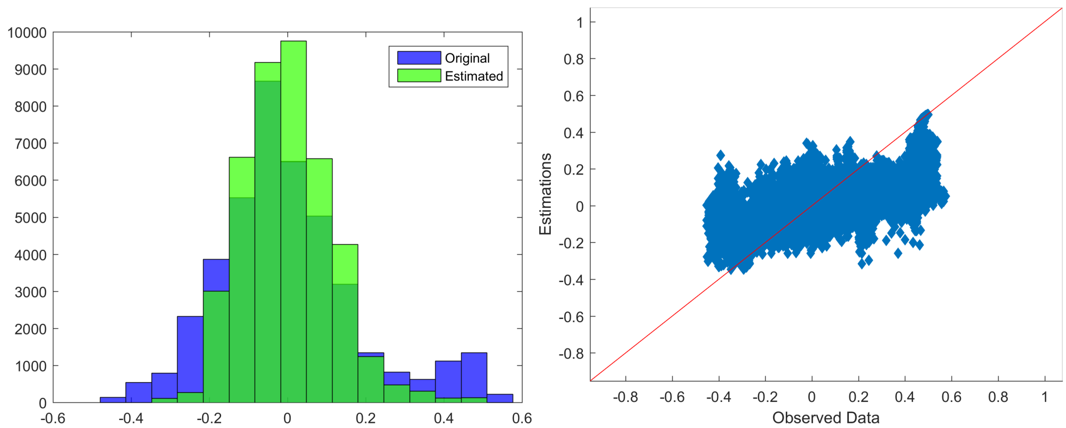

Figure 6.34 Histograms and Scatter plot of original and estimated values of the field's stochastic component.The model used is a Spartan with parameters $\eta_0 = 0.832, \xi_1 = 40.338, R = 0.307, \phi = -50.9°, c_0 = 0.000, \eta_1 = 1.928$.

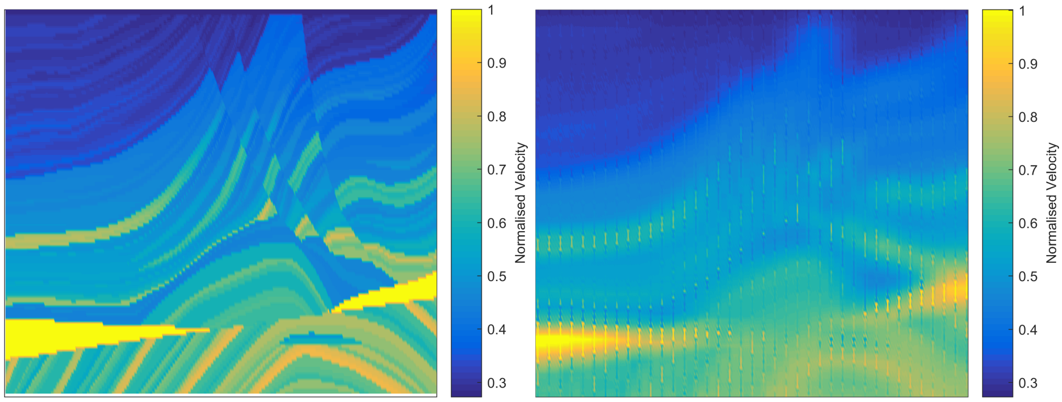

(a) Original Total Field **(b)** Estimated Total Field

Figure 6.35 Original and estimated total field

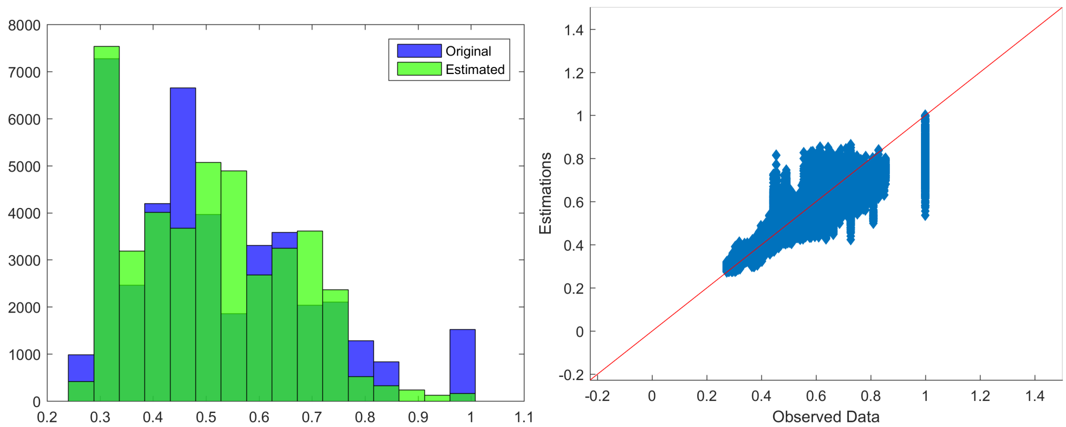

Figure 6.36 Histograms and Scatter plot of original and estimated values (total field)

without, however, achieving satisfying proximity of the total distribution; both the tails of the distribution as the middle of it exhibit significant discrepancies. The measures of the total field (i.e. normalised velocities) estimation performance for the three best models, presented in Table 6.25, show that the first model has significantly better performance than the other two which have almost the same validation measures. Finally, Fig. 6.37 shows the spatial distribution of the ordinary kriging estimations uncertainty. The uncertainty is zero at the drill-holes (known points), while increases from $\simeq 0.30$ near the drill-holes to 0.37 at great distance between the drill-holes.

Also, in Table 6.26 are presented the classification measures for the cases of 4 and 16 classes. The same observations, as in *DirVar0*, apply.

Table 6.25 Total Field Estimation Scores

Model	MnAE	MxAE	MSE	RMSE	R_p	R_{sp}	r_F
Spartan	1.317	1.869	1.803	1.343	0.932	0.940	0.876
Gen. Matérn	1.317	1.863	1.804	1.343	0.918	0.927	0.851
Gen. Exponential	1.317	1.863	1.804	1.343	0.918	0.928	0.851

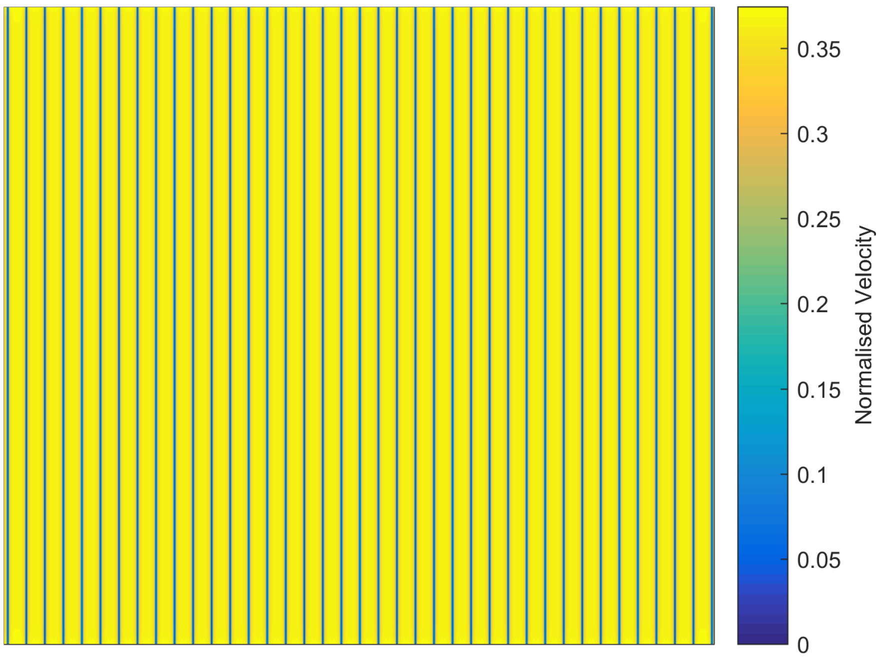

Figure 6.37 Uncertainty of the total field's estimation

Table 6.26 Classification Measures

	4 classes			16 classes		
Model	R_p	R_{sp}	**MCR**	R_p	R_{sp}	**MCR**
Spartan	0.856	0.871	0.219	0.912	0.934	0.578
Gen. Matérn	0.840	0.859	0.235	0.889	0.921	0.600
Gen. Exponential	0.840	0.859	0.235	0.889	0.921	0.600

DirVar2

In the *DirVar2* method the anisotropy parameters are also estimated by means of DVF (see section 5.2.2) in advance, as in the *DirVar1* variation, but in this case these parameters are used for rescalling and rotating the original anisotropic coordinations system to a new isoropic coordinations system. Subsequently, the field is modeled by isotropic variogram equations following a similar to the previous variations procedure (i.e. parameter inference by minimizing the error function, LOOCV and OK).

Therefore, the 5 sets of anisotropy parameters estimated in the *DirVar1* method (see Table 6.21) are used for the inversion of the anisotropic effect, giving equal number of new coordination systems. Each system corresponds to a variogram model with the isotropic form of which it is tested in the following steps. Before this, however, it is necessary to examine whether the new systems are actually isotropic or have retained anisotropic characteristics. This is dependent on the reliability of the anisotropy parameters estimation. For this purpose, the experimental directional variograms for each coordinations system are calculated, and subsequently the new anisotropy parameters are estimated by means of DVF. The results are shown in Table 6.27, while in Fig. 6.38 are displayed the experimental directional variograms of the new coordination systems. The results show that despite small improvement (indicated by the proximity of the new corralation length to 1 and the new anisotropy angle to 0) the anisotropic effect remains at relatively high levels as indicated by the very small increase of the anisotropy ratios. Nevertheless, analysis procedure continues by assuming the new coordinations systems as isotropic.

By minimizing the error function of the isotropic variogram functions of the models and the corresponding experimental omnidirectional (isotropic) variograms of the new coordinations systems (see Fig. 6.39) the parameters of the isotropic models are estimated, as presented in Table 6.28. The common parameters are generally close for all the investigated models.

The Leave-One-Out Cross Validation (LOOCV) for the estimated models gives the validation measures presented in Table 6.29. As best model derives the Generalized Exponential, followed by Generalized Mátern and Spartan. As it can be seen from Fig. 6.39), though, all the models except Spartan (probably due to optimization miscalculations) fit fairly well to their corresponding experimental omnidirectional variograms.

The estimation of the stochastic component of the field (i.e the transformed and detrended normalised velocities) resulting from OK is as shown in Fig. 6.40. The scatter diagram and histograms of the original and the estimated values of the stochastic component are, also, shown in Fig. 6.41, and the measures of the stochastic component estimation performance for the three best models are presented in Table 6.30. The resulting estimation of the total

Table 6.27 Anisotropy parameters of the new coordinations systems

Model	Anisotropy Parameters		
	ξ_1	R	ϕ
Gen. Exponential	0.833	0.432	5.2°
Gaussian	0.822	0.468	0.0°
Spherical	0.832	0.324	6.1°
Gen. Matérn	1.598	0.235	11.3°
Spartan	0.826	0.445	0.0°

Table 6.28 Optimum Parameters of the isotropic variogram models

Model	σ_z^2	ξ	c_0	ν
Gen. Exponential	0.033	1.031	0.000	0.948
Gaussian	0.025	1.002	0.007	–
Spherical	0.025	1.083	0.007	–
Gen. Matérn	0.033	1.425	0.000	0.405
	η_0	ξ	c_0	η_1
Spartan	0.045	0.081	0.000	-1.989

Table 6.29 Leave-One-Out Cross Validation Scores (see section 5.3.2

Model	MnAE	MxAE	MSE	RMSE	R_p	R_{sp}	r_F
Gen. Exponential	0.025	0.350	0.002	0.048	0.962	0.974	0.937
Gaussian	0.032	0.364	0.003	0.053	0.953	0.967	0.609
Spherical	0.031	0.362	0.003	0.052	0.955	0.969	0.647
Gen. Matérn	0.028	0.370	0.002	0.048	0.961	0.972	0.881
Spartan	0.025	0.361	0.002	0.048	0.961	0.974	0.874

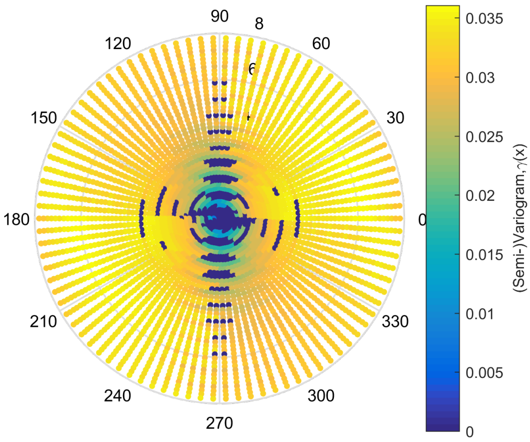

(a) Gen. Exponential

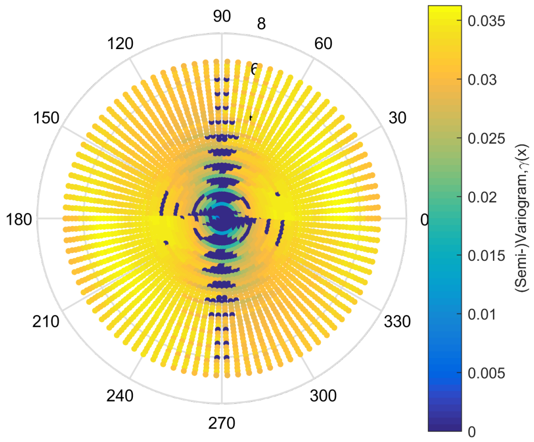

(b) Gaussian

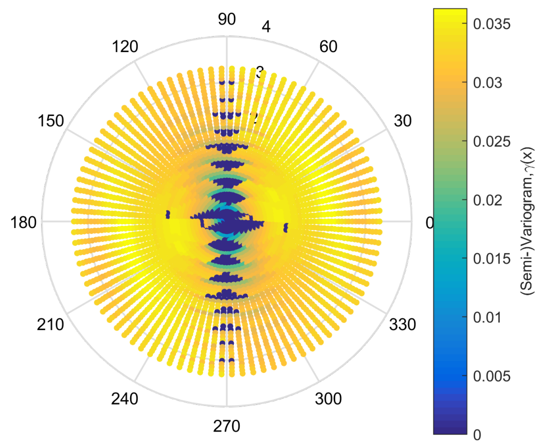

(c) Spherical

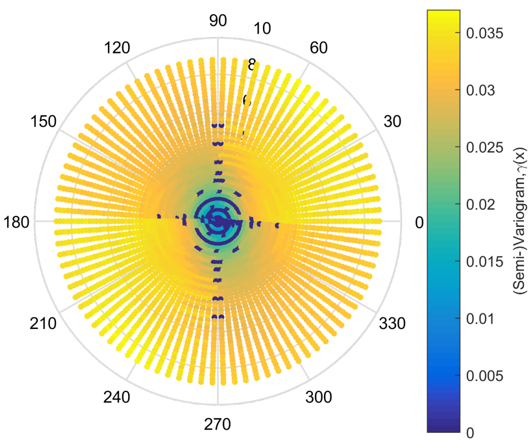

(d) Gen. Matérn

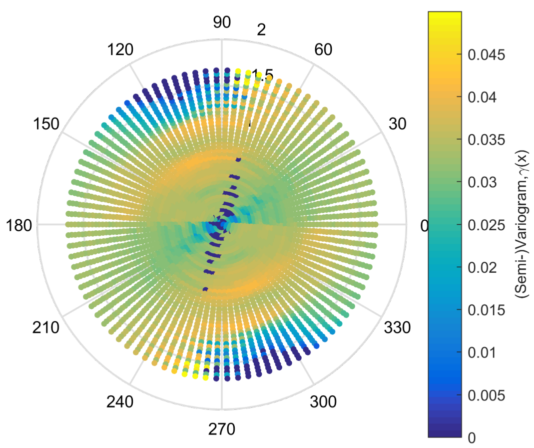

(e) Spartan

Figure 6.38 Experimental directional variograms of the new coordinations systems

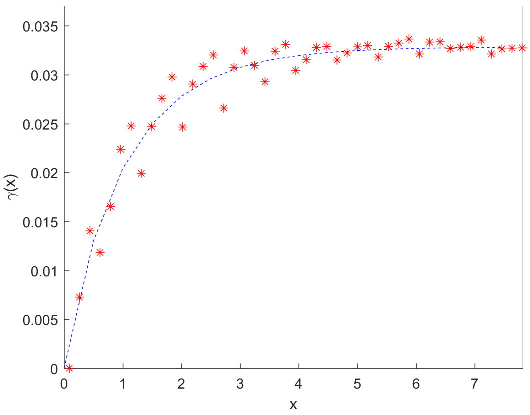

(a) Gen. Exponential

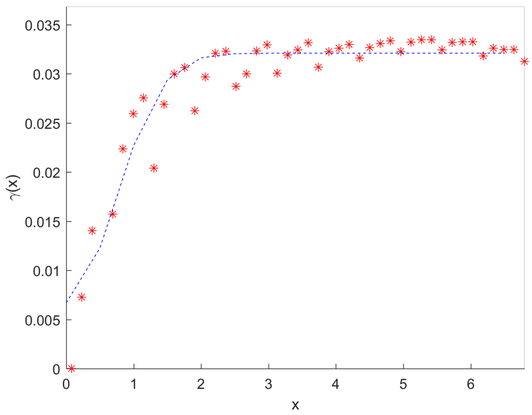

(b) Gaussian

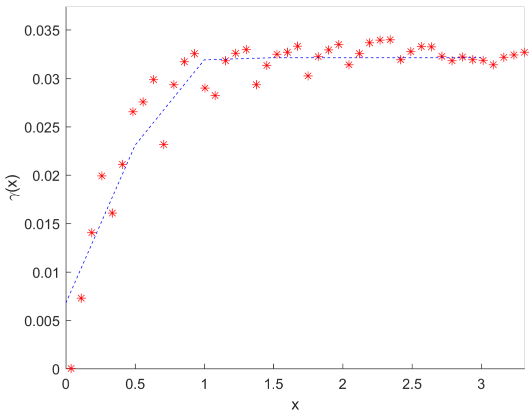

(c) Spherical

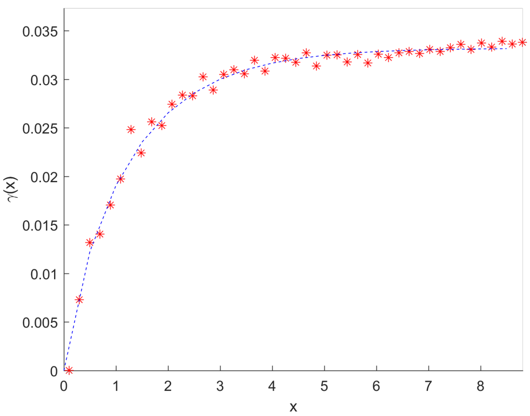

(d) Gen. Matérn

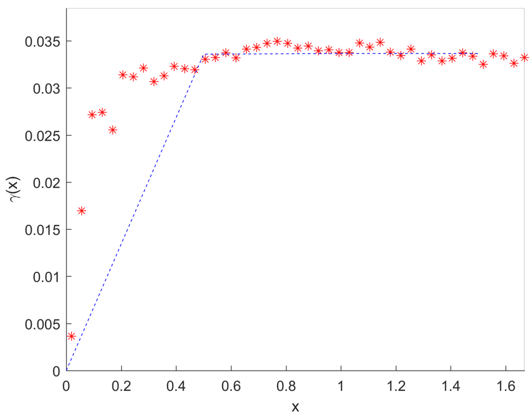

(e) Spartan

Figure 6.39 Fitting of the theoretical models to the corresponding experimental omnidirectional variograms of the new coordinations systems.

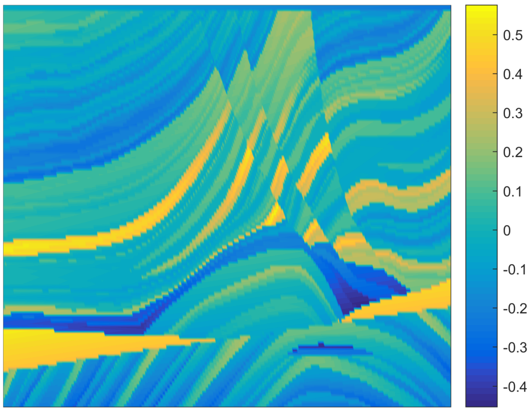

(a) Original Stochastic Component

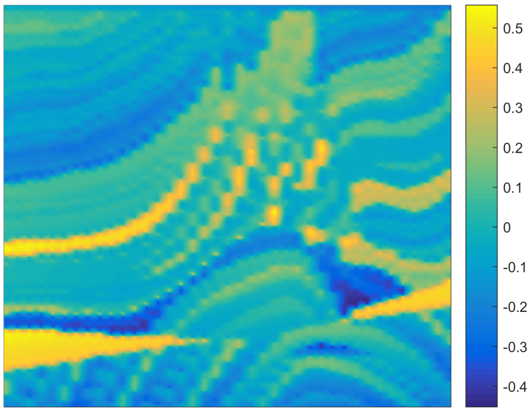

(b) Estimated Stochastic Component

Figure 6.40 Original and Estimation of the stochastic component of the field. The model used is a Gen. Exponential with parameters $\sigma_z^2 = 0.033, \xi = 1.031, c_0 = 0.000, \nu = 0.948$.

Table 6.30 Ordinary Kriging Scores

Model	MnAE	MxAE	MSE	RMSE	R_p	R_{sp}	r_F
Gen. Exponential	0.044	0.681	0.005	0.073	0.916	0.907	0.831
Gen. Matérn	0.046	0.661	0.006	0.074	0.914	0.905	0.783
Spartan	0.066	0.658	0.009	0.094	0.875	0.867	0.286

field, after the trend addition and Box-Cox transformation inversion, is as shows Fig. 6.42, and the correspomding scatter diagram and histograms are shown in Fig. 6.43. In general, the estimations follow the original values achieving a very good proximity of the total distribution. The measures of the total field (i.e. normalised velocities) estimation performance for the three best models, presented in Table 6.31, show that their performance is almost identical. Also, the spatial distribution of the ordinary kriging estimations uncertainty is shown in Fig. 6.44. The uncertainty (as expected from theory) increases gradually from $\simeq 0.00$ near the drill-holes to 0.20 at great distance between the drill-holes, and exhibits the same patern all over the examined space due to the regularity of the sample.

Finally, in Table 6.32 are presented the classification measures for the cases of 4 and 16 classes. The results show that for all models the measures increase as the number of classes increase, while the best model has the higher performance rates for any number of classes.

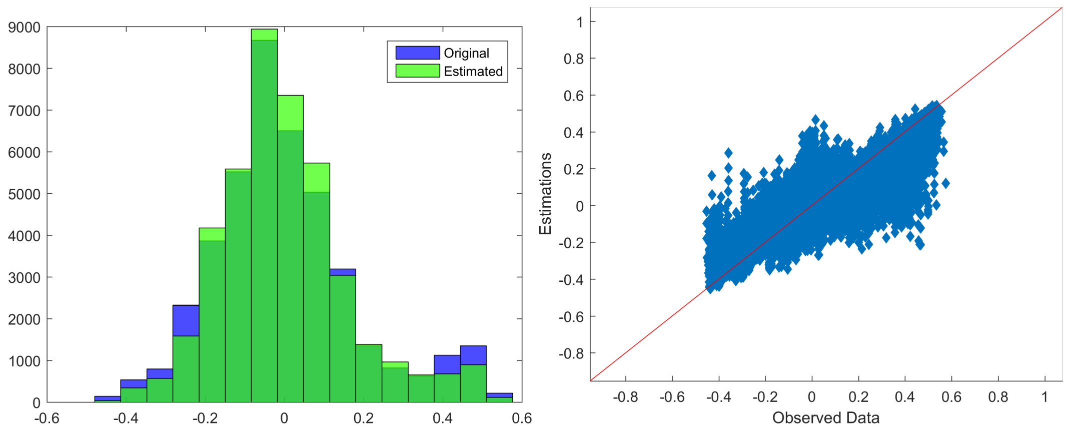

Figure 6.41 Histograms and Scatter plot of original and estimated values of the field's stochastic component. The model used is a Gen. Exponential with parameters $\sigma_z^2 = 0.033, \xi = 1.031, c_0 = 0.000, \nu = 0.948$.

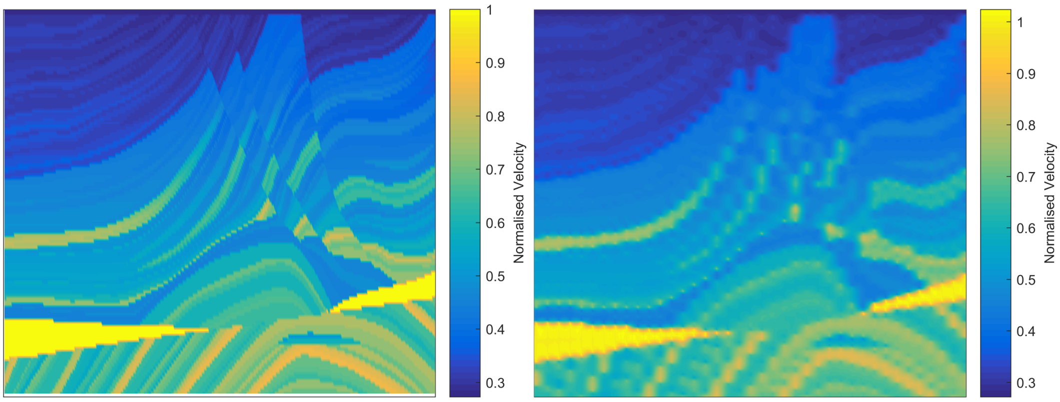

(a) Original Total Field

(b) Estimated Total Field

Figure 6.42 Original and estimated total field

Table 6.31 Total Field Estimation Scores

Model	MnAE	MxAE	MSE	RMSE	R_p	R_{sp}	r_F
Gen. Exponential	1.321	1.843	1.803	1.343	0.960	0.979	0.938
Gen. Matérn	1.321	1.843	1.803	1.343	0.960	0.979	0.938
Spartan	1.318	1.867	1.801	1.342	0.961	0.970	0.932

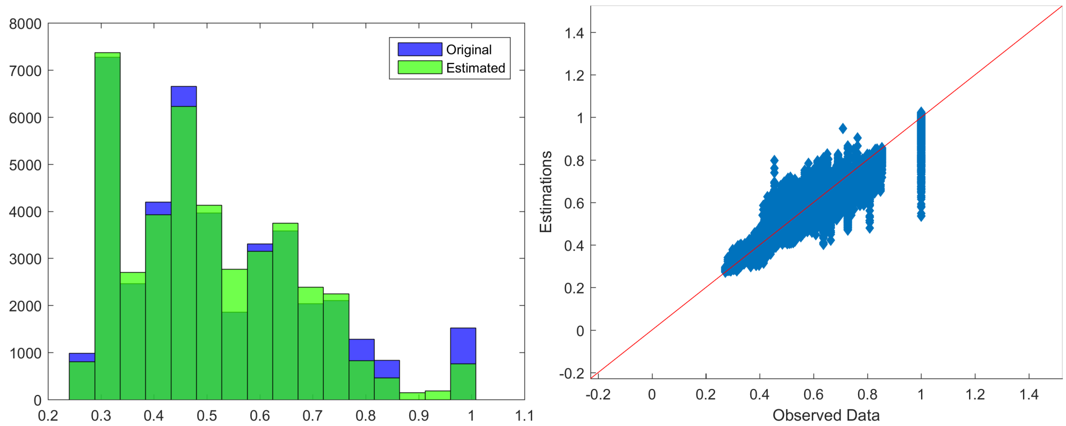

Figure 6.43 Histograms and Scatter plot of original and estimated values (total field)

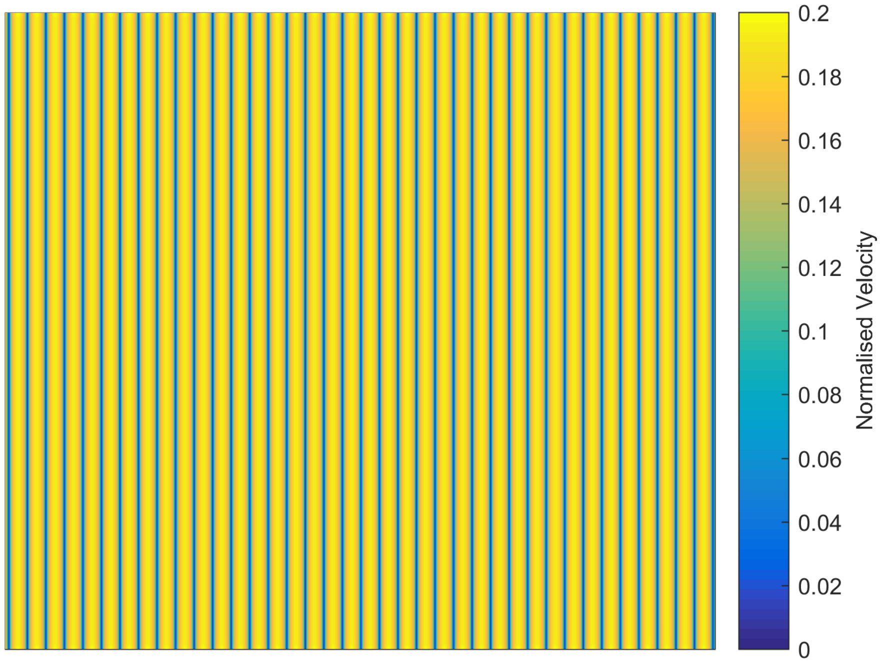

Figure 6.44 Uncertainty of the total field's estimation

Table 6.32 Classification Measures

	4 classes			16 classes		
Model	R_p	R_{sp}	**MCR**	R_p	R_{sp}	**MCR**
Gen. Exponential	0.929	0.930	0.116	0.972	0.975	0.317
Gen. Matérn	0.927	0.929	0.119	0.971	0.975	0.330
Spartan	0.891	0.899	0.173	0.953	0.963	0.464

CHI1

In the *CHI1* method the investigated random field is modeled by anisotropic variogram equations after estimating the anisotropy parameters. The anisotropy parameters in this case are estimated by means of CHI (see section 5.2.2) and are the same for all the models. Subsequently, the estimated parameters are replaced to the corresponding anisotropic variogram functions, reducing by two the number of unknown parameters for each model (in the previous variations the parameters were reduced by three) as the CHI method estimates only R and ϕ. The parameter inference of the models with the lower degrees of freedom is achieved through the minimization of the error function between the experimental directional variograms and the chosen anisotropic theoretical models.

The estimated anisotropy parameters are given in Table 6.33. The parameters captured by the CHI estimator indicates that the major axis of the anisotropy ellipsis is almost horizontal and is also significantly greater ($\simeq$ 10 times) than the minor axis.

By replacing the estimated anisotropy parameters to the anisotropic variogram models and minimizing the error function of the new models and the experimental directional variograms the rest parameters for each model are estimated, as presented in Table 6.34. The estimated values of the variance and the nugget effect are very close but the correlation lengths differ depending on the model. The correlation length of the Spherical model is significantly higher from the other models.

The Leave-One-Out Cross Validation (LOOCV) gives as best model the Spherical, followed by Spartan and Generalized Exponential.

Table 6.33 Anisotropy parameters of the investigated variogram models estimated with CHI method

R	ϕ
0.108	$-88.5°$

Table 6.34 Optimum Parameters of the variogram models with the lower degrees of freedom

Model	σ_z^2	ξ	c_0	ν
Gen. Exponential	0.033	4.994	0.000	1.098
Gaussian	0.028	8.471	0.006	–
Spherical	0.033	79.760	0.000	–
Gen. Matérn	0.029	1.074	0.004	3.500
	η_0	ξ	c_0	η_1
Spartan	0.841	5.032	0.000	2.000

Table 6.35 Leave-One-Out Cross Validation Scores (see section 5.3.2

Model	MnAE	MxAE	MSE	RMSE	R_p	R_{sp}	r_F
Gen. Exponential	0.052	0.398	0.006	0.080	0.889	0.924	0.678
Gaussian	0.053	0.407	0.007	0.082	0.884	0.921	0.622
Spherical	0.050	0.386	0.006	0.077	0.900	0.930	0.837
Gen. Matérn	0.053	0.404	0.007	0.082	0.885	0.922	0.635
Spartan	0.052	0.398	0.006	0.080	0.890	0.925	0.691

Table 6.36 Ordinary Kriging Scores

Model	MnAE	MxAE	MSE	RMSE	R_p	R_{sp}	r_F
Spherical	0.099	0.588	0.018	0.133	0.692	0.689	0.476
Spartan	0.103	0.602	0.020	0.140	0.645	0.652	0.344
Gen. Exponential	0.103	0.602	0.020	0.141	0.640	0.648	0.333

The fitting of the best model to the experimental variogram on selected directions is interpretted in Fig. 6.45 (the rest directional variograms can be found in Appendix A). As it can be seen the best theoretical variogram model diverges significantly from the experimental directional variograms. This can be attributed to minimization miscalculations, i.e. inappropiate objective function (very smooth or possible local minima), inappropriate initial values or to the fields complexity. Thus, the analysis proceeds without taking any further action.

Implementing OK with the determined best model, the resulting estimation of the stochastic component of the field (i.e the transformed and detrended normalised velocities) is as shown in Fig. 6.46. The scatter diagram and histograms of the original and the estimated values of the stochastic component are illustrated in Fig. 6.47, and the measures of the stochastic component estimation performance for the three best models are presented in Table 6.36.

The resulting estimation of the total field, after the trend addition and Box-Cox transformation inversion, is as shows Fig. 6.48, and the correspomding scatter diagram and histograms are shown in Fig. 6.49. In general, the estimations follow the original values without, however, achieving satisfying proximity of the total distribution; both the tails of the distribution as the middle of it exhibit significant discrepancies. The measures of the total field (i.e. normalised velocities) estimation performance for the three best models, presented in Table 6.37, show that the first model has significantly better performance than the other two which have almost the same validation measures. Finally, Fig. 6.50 shows the spatial distribution of the ordinary kriging estimations uncertainty. The uncertainty is zero at the known locations, while at the investigated points it is equal to 0.37 with slightly smaller values at the edges.

Also, in Table 6.38 are presented the classification measures for the cases of 4 and 16 classes. The same comments, as in *DirVar2*, apply.

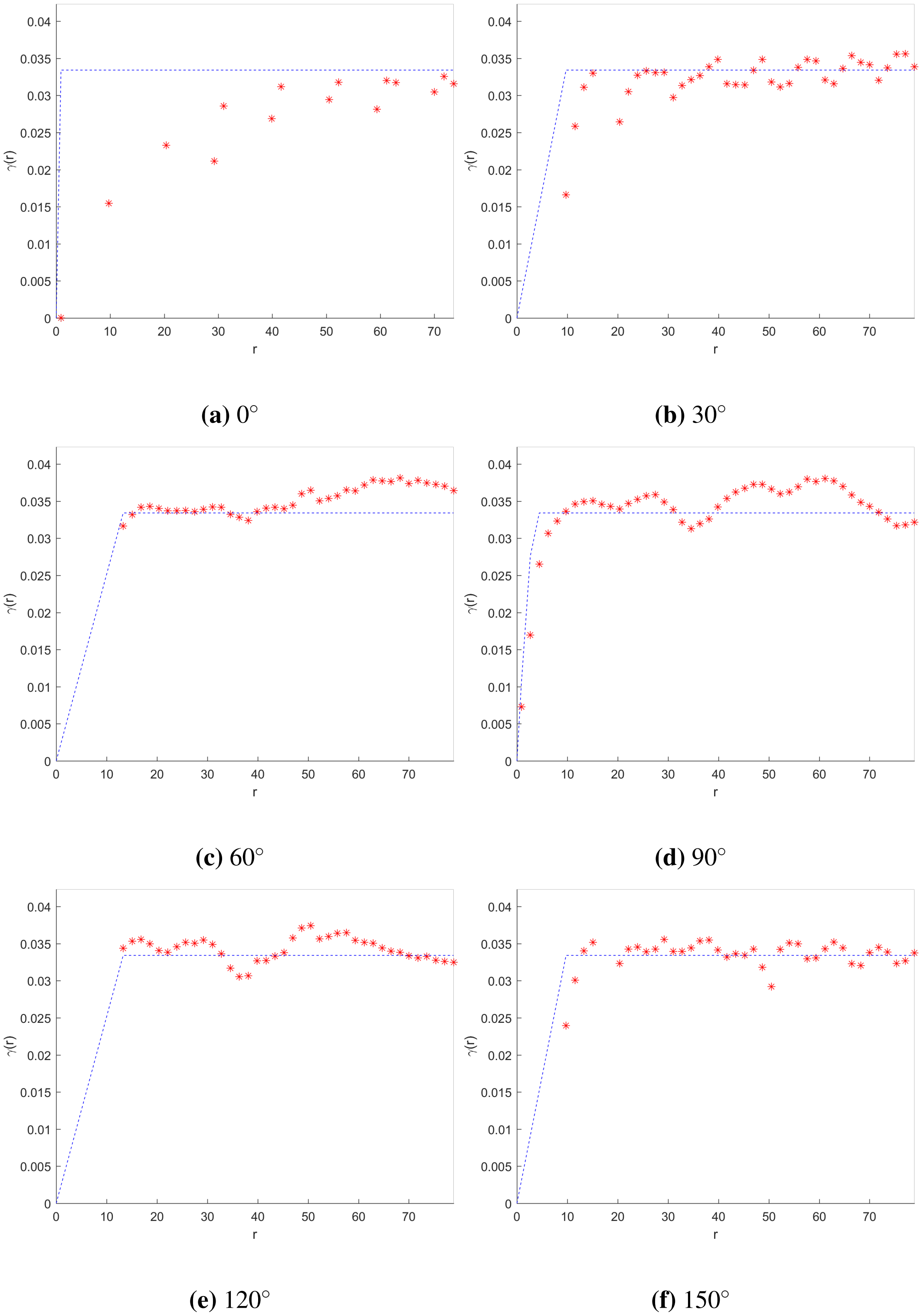

(a) 0° **(b)** 30° **(c)** 60° **(d)** 90° **(e)** 120° **(f)** 150°

Figure 6.45 Fitting of the best theoretical model to the experimental directional variograms of the field. The best model is a Spherical with parameters $\sigma_z^2 = 0.033, \xi_1 = 79.760.338, R = 0.108, \phi = -88.5°, c_0 = 0.000$. The experimental variogram is calculated with angular tolerance 20°, 45 distance lags and taking into account maximum distance equivalent to about 80.

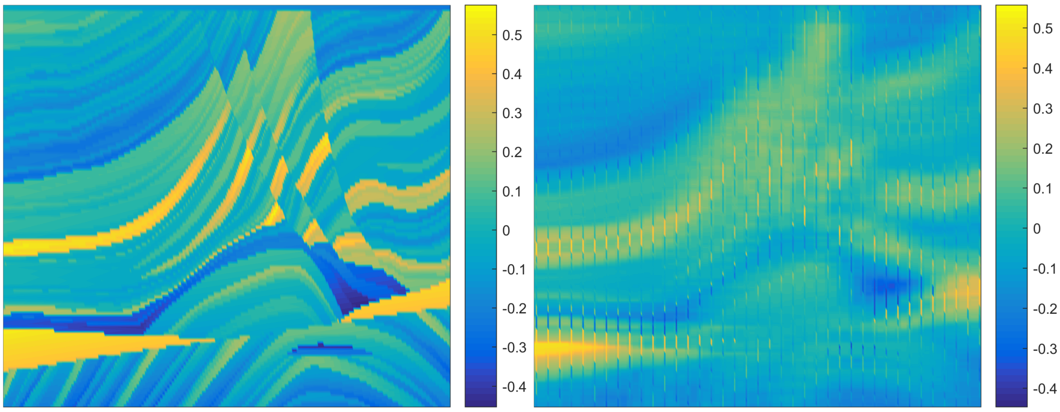

(a) Original Stochastic Component **(b)** Estimated Stochastic Component

Figure 6.46 Original and Estimation of the stochastic component of the field. The model used is a Spherical with parameters $\sigma_z^2 = 0.033, \xi_1 = 79.760.338, R = 0.108, \phi = -88.5°, c_0 = 0.000$.

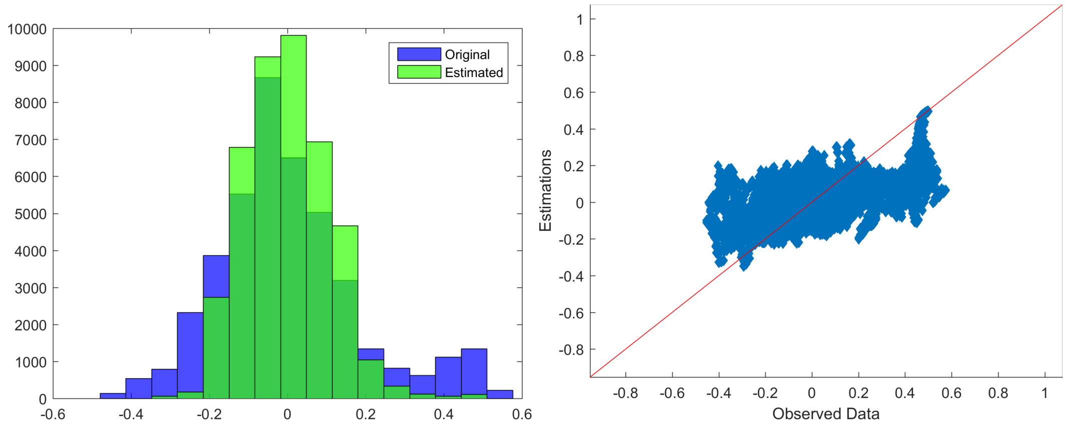

Figure 6.47 Histograms and Scatter plot of original and estimated values of the field's stochastic component. The model used is a Spherical with parameters $\sigma_z^2 = 0.033, \xi_1 = 79.760.338, R = 0.108, \phi = -88.5°, c_0 = 0.000$.

Table 6.37 Total Field Estimation Scores

Model	MnAE	MxAE	MSE	RMSE	R_p	R_{sp}	r_F
Spherical	1.317	1.865	1.803	1.343	0.929	0.937	0.870
Spartan	1.317	1.864	1.804	1.343	0.920	0.930	0.855
Gen. Exponential	1.317	1.864	1.804	1.343	0.920	0.929	0.854

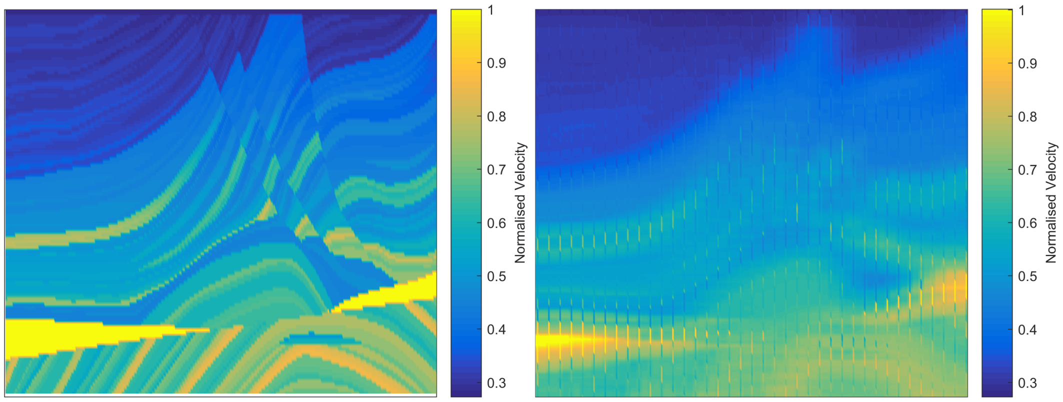

(a) Original Total Field **(b)** Estimated Total Field

Figure 6.48 Original and estimated total field

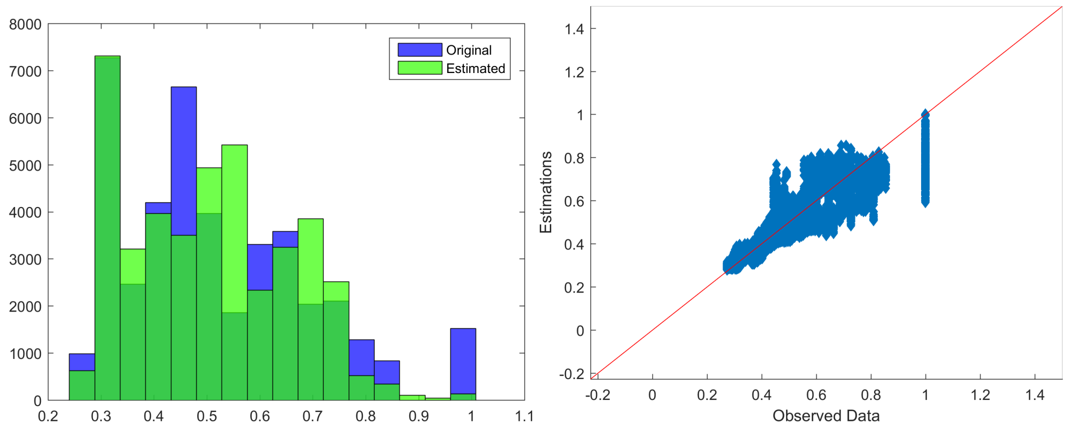

Figure 6.49 Histograms and Scatter plot of original and estimated values (total field)

Table 6.38 Classification Measures

	4 classes			16 classes		
Model	R_p	R_{sp}	**MCR**	R_p	R_{sp}	**MCR**
Spherical	0.848	0.864	0.228	0.904	0.929	0.591
Spartan	0.842	0.860	0.234	0.892	0.923	0.598
Gen. Exponential	0.841	0.860	0.235	0.891	0.922	0.599

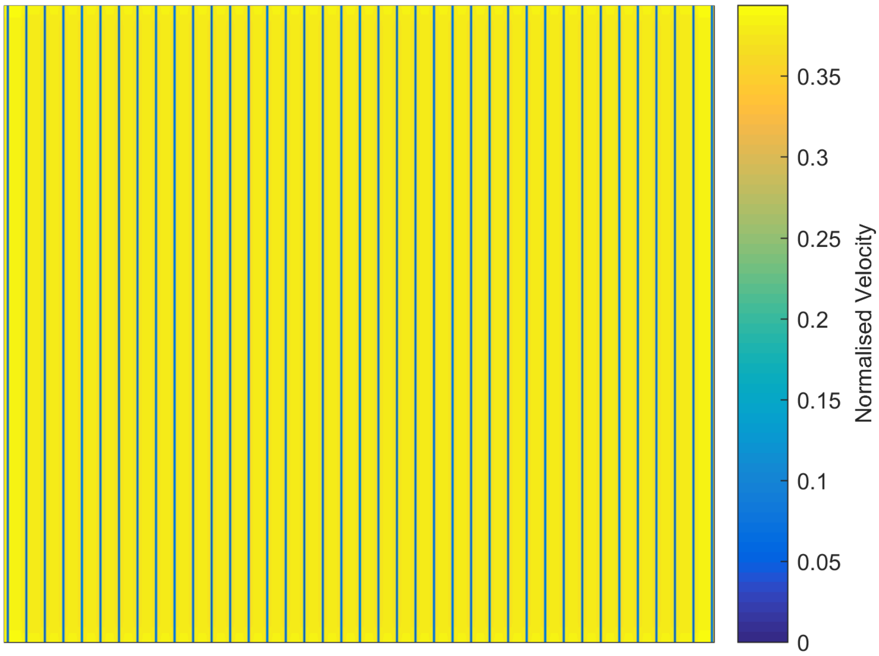

Figure 6.50 Uncertainty of the total field's estimation

CHI2

In the *CHI2* method the anisotropy parameters are also estimated by means of CHI in advance, as in the *CHI1* variation, but in this case these parameters are used for rescalling and rotating the original anisotropic coordinations system to a new isoropic coordinations system. Subsequently, the field is modeled by isotropic variogram equations following a similar to the previous variations procedure (i.e. parameter inference by minimizing the error function, LOOCV and OK).

Therefore, the 1 set of anisotropy parameters estimated in the *CHI1* variation (see Table 6.33) is used for the inversion of the anisotropic effect, giving a new coordination systems. In order to invert the original coordination system it is assumed that $\xi_1 = R$, as long as the CHI method estimates only R and ϕ. Subsequently, the new system is modeled using the 5 isotropic variogram models. Before this, however, it is necessary to examine whether the new system is actually isotropic or have retained anisotropic characteristics. This is obviously dependent on the reliability of the anisotropy parameters estimation. For this purpose, the experimental directional variograms of the new coordinations system is calculated, and then the new anisotropy parameters are estimated by means of DVF (see section 5.2.2) using the 5 variogram models. The results are shown in Table 6.39, while in Fig. 6.51 is displayed the experimental directional variograms of the new coordinations system. All the models give increased anisotropy ratio relatively to the original one, but only

Table 6.39 Anisotropy parameters of the new coordinations systems

Model	Anisotropy Parameters		
	ξ_1	R	ϕ
Gen. Exponential	35.297	0.394	6.1°
Gaussian	33.661	0.738	16.6°
Spherical	73.440	0.899	12.4°
Gen. Matérn	42.206	0.465	19.8°
Spartan	47.751	0.535	22.0°

Table 6.40 Optimum Parameters of the isotropic variogram models

Model	σ_z^2	ξ	c_0	ν
Gen. Exponential	0.033	32.950	0.000	0.776
Gaussian	0.026	36.473	0.007	–
Spherical	0.026	91.788	0.007	–
Gen. Matérn	0.034	48.7994	0.000	0.322
	η_0	ξ	c_0	η_1
Spartan	9.687	328.725	0.001	467.369

the two of them recognize it as almost isotropic (i.e. Gaussian and Spherical). Nevertheless, analysis procedure continues by assuming the new coordinations system as isotropic.

By minimizing the error function of the isotropic variogram functions of the models and the corresponding experimental omnidirectional (isotropic) variogram of the new coordinations system (see Fig. 6.52) the parameters of the isotropic models are estimated, as presented in Table 6.40. All the models fit well to the experimental omnidirectional variogram. Also, the estimated parameters are very close, except from the correlation lengths which differ significantly depending on the model; the Spartan model is attributed by the extremely large value of about 329, the Spherical model by the lower value of about 92 while the rest models' correlation length range from 32 to 49.

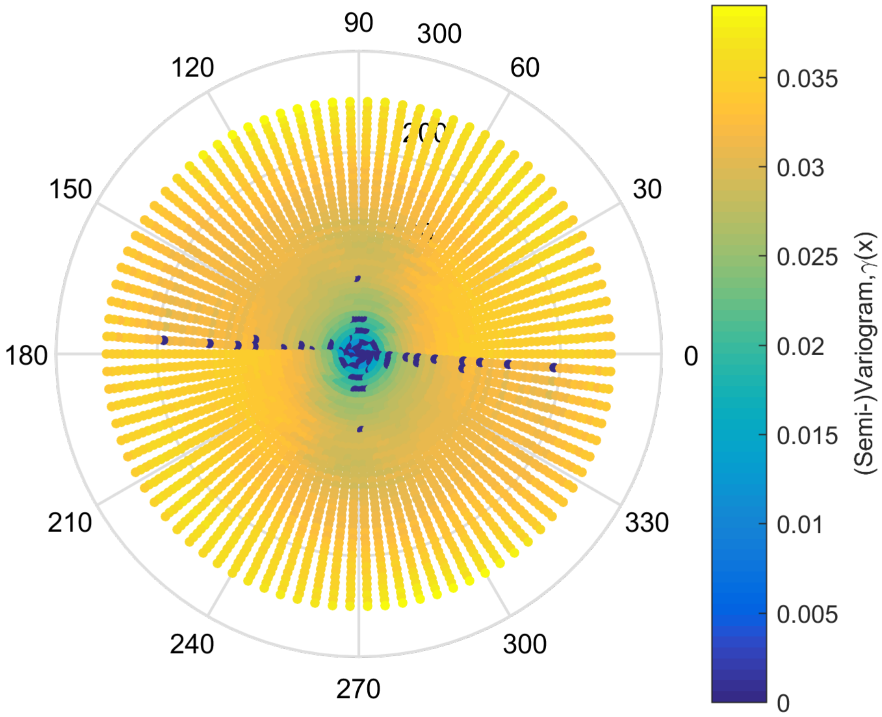

Figure 6.51 Experimental directional variograms of the new coordinations system

The Leave-One-Out Cross Validation (LOOCV) for the estimated models gives the validation measures presented in Table 6.41. As best model derives the Spartan, followed by Generalized Exponential and Generalized Mátern. As it can be seen from Fig. 6.52), the above mentioned models are those that fit better to the experimental omnidirectional variogram.

The estimation of the stochastic component of the field (i.e the transformed and detrended normalised velocities) resulting from OK is as shown in Fig. 6.53. The scatter diagram and histograms of the original and the estimated values of the stochastic component are shown in Fig. 6.54, and the measures of the stochastic component estimation performance for the three best models are presented in Table 6.42. The resulting estimation of the total field, after the trend addition and Box-Cox transformation inversion, is as shows Fig. 6.55, and the correspomding scatter diagram and histograms are shown in Fig. 6.56. In general, the estimations follow the original values achieving a very good proximity of the total distribution. The measures of the total field (i.e. normalised velocities) estimation performance for the three best models, presented in Table 6.43, show that their performance is almost identical. Also, the spatial distribution of the ordinary kriging estimations uncertainty is shown in Fig. 6.57. The uncertainty (as expected from theory) increases quickly from $\simeq 0.00$ near the

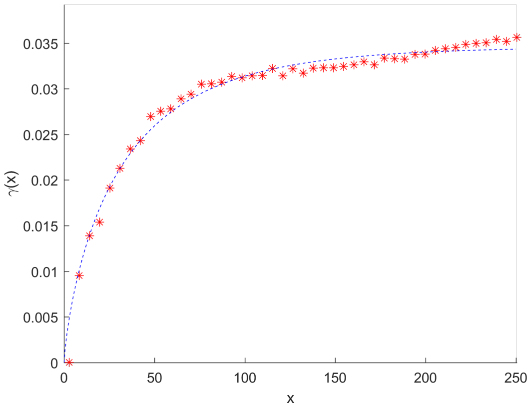

(a) Gen. Exponential

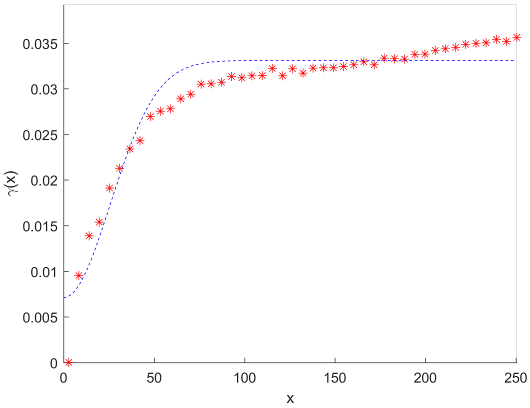

(b) Gaussian

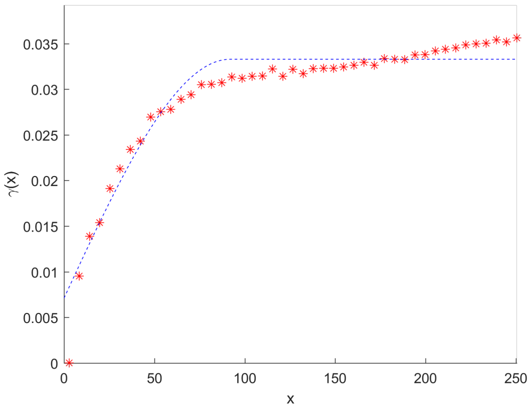

(c) Spherical

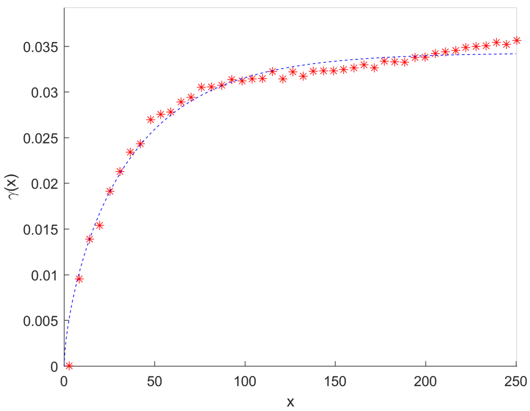

(d) Gen. Matérn

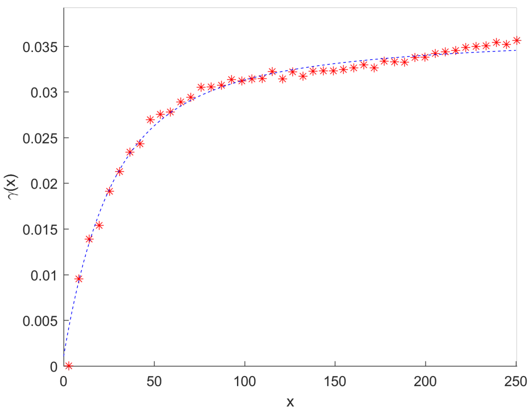

(e) Spartan

Figure 6.52 Fitting of the theoretical models to the corresponding experimental omnidirectional variograms of the new coordinations systems.

Table 6.41 Leave-One-Out Cross Validation Scores (see section 5.3.2

Model	MnAE	MxAE	MSE	RMSE	R_p	R_{sp}	r_F
Gen. Exponential	0.030	0.346	0.002	0.049	0.960	0.968	0.897
Gaussian	0.034	0.346	0.003	0.054	0.951	0.960	0.604
Spherical	0.032	0.344	0.003	0.052	0.955	0.964	0.724
Gen. Matérn	0.030	0.346	0.002	0.050	0.959	0.967	0.876
Spartan	0.030	0.347	0.002	0.049	0.960	0.968	0.930

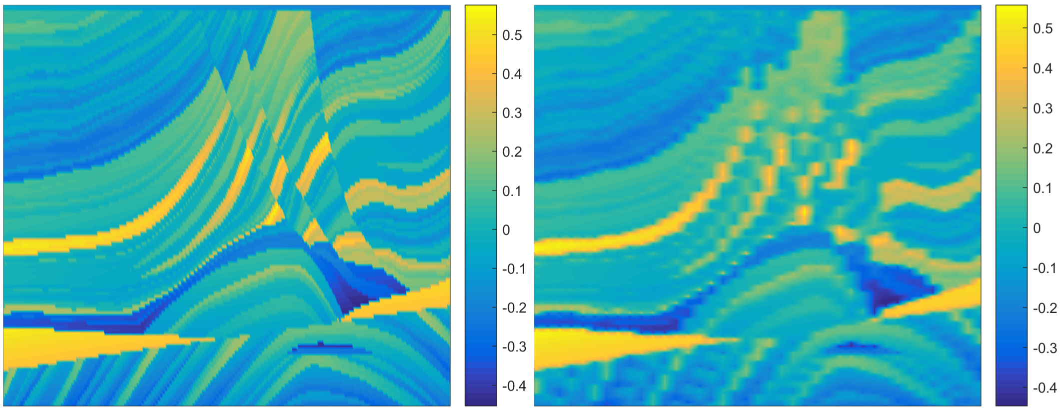

(a) Original Stochastic Component **(b)** Estimated Stochastic Component

Figure 6.53 Original and Estimation of the stochastic component of the field. The model used is a Spartan with parameters $\eta_0 = 9.687, \xi = 328.725, c_0 = 0.001, \eta_1 = 467.369$.

drill-holes to $\simeq 0.20$ at great distance between the drill-holes, and exhibits the same patern all over the exained space due to the regularity of the sample.

Finally, in Table 6.44 are presented the classification measures for the cases of 4 and 16 classes. The results show that for all models have almost identical performance, while the measures increase as the number of classes increase.

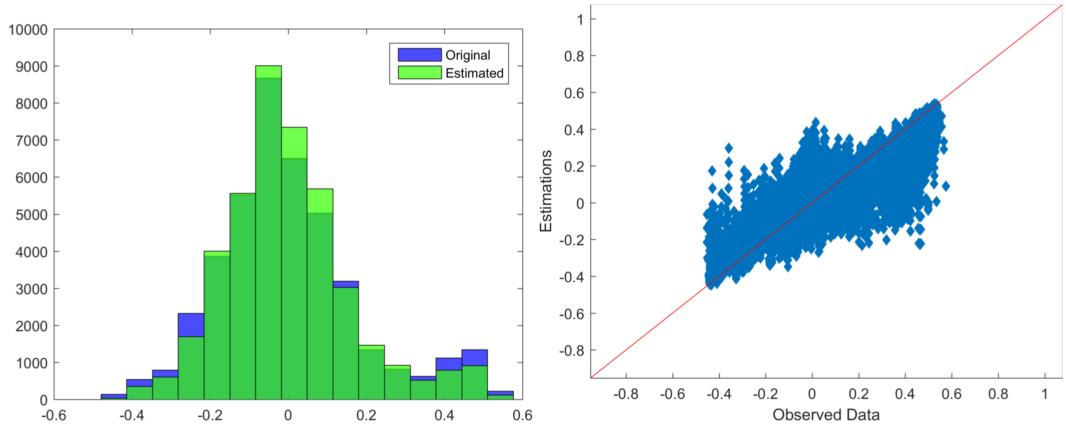

Figure 6.54 Histograms and Scatter plot of original and estimated values of the field's stochastic component. The model used is a Spartan with parameters $\eta_0 = 9.687, \xi = 328.725, c_0 = 0.001, \eta_1 = 467.369$.

Table 6.42 Ordinary Kriging Scores

Model	MnAE	MxAE	MSE	RMSE	R_p	R_{sp}	r_F
Spartan	0.040	0.695	0.005	0.072	0.920	0.908	0.835
Gen. Exponential	0.041	0.703	0.005	0.072	0.920	0.908	0.831
Gen. Matérn	0.042	0.691	0.005	0.072	0.919	0.908	0.819

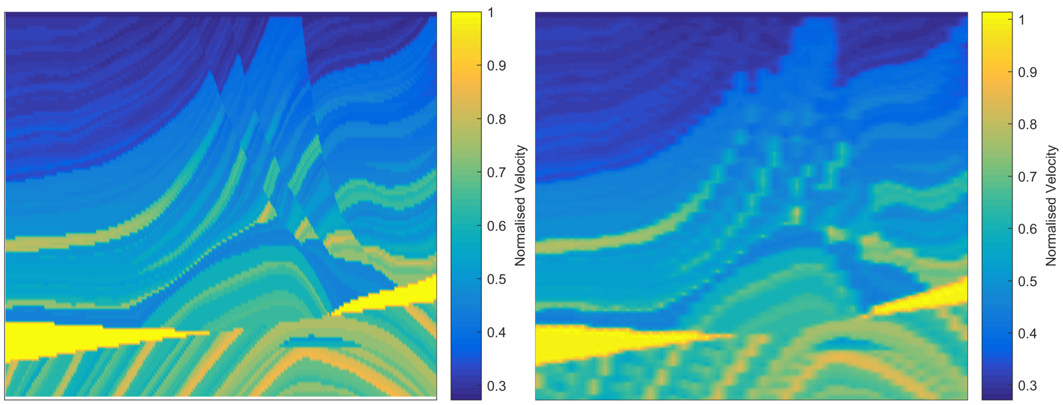

(a) Original Total Field **(b)** Estimated Total Field

Figure 6.55 Original and estimated total field

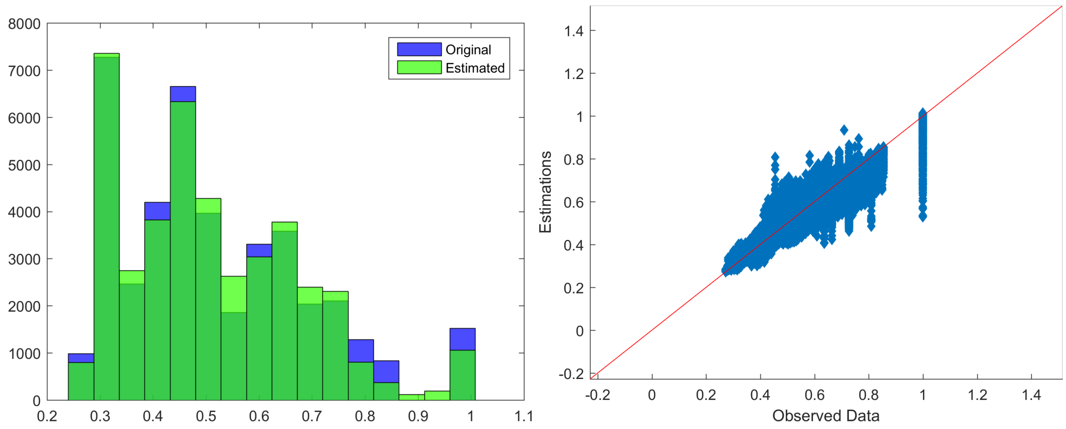

Figure 6.56 Histograms and Scatter plot of original and estimated values (total field)

Table 6.43 Total Field Estimation Scores

Model	MnAE	MxAE	MSE	RMSE	R_p	R_{sp}	r_F
Spartan	1.321	1.839	1.803	1.343	0.959	0.980	0.940
Gen. Exponential	1.321	1.839	1.803	1.343	0.960	0.980	0.940
Gen. Matérn	1.321	1.839	1.803	1.343	0.960	0.980	0.940

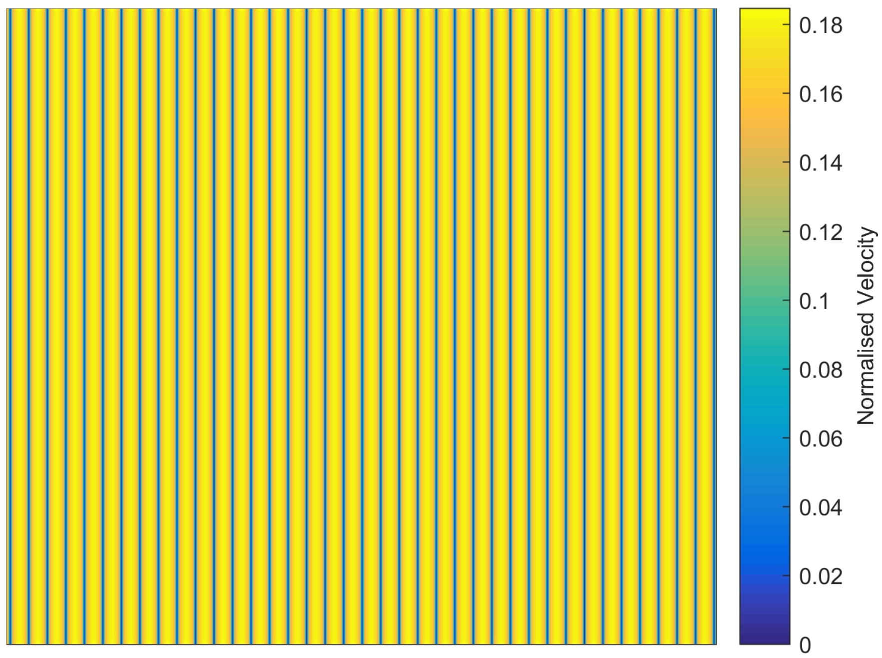

Figure 6.57 Uncertainty of the total field's estimation

Table 6.44 Classification Measures

	4 classes			16 classes		
Model	R_p	R_{sp}	**MCR**	R_p	R_{sp}	**MCR**
Spartan	0.930	0.931	0.114	0.974	0.976	0.295
Gen. Exponential	0.930	0.932	0.114	0.974	0.976	0.295
Gen. Matérn	0.929	0.931	0.115	0.974	0.976	0.302

6.4.2 DGC Simulation

The DGC simulation method is applied to the original dataset (i.e normalised velocities) in one step. The simulation is calculated using 4, 16 and 100 classes; in the first two case the result is a classification while in the third the procedure approximates an interpolation. The number of simulations calculated for each case is 10 and the mean of them is the final results, which are interpretted in Figs. 6.58, 6.59, and 6.60 along with the histograms of the original and the estimated data and the distribution of the uncertainty of the estimations. The neighboorhood used for the DGC simulation procedure is the same as the one used in OK, i.e 22x4. Finally, some measures of the DGC simulation performance are summarized in Table 6.45. The classification results show that the increasing of the number of classes from 4 to 16 leads to lower errors and higher correlation coefficient. This can be explained by the fact that the field is described better by a more complex model. The misclassification rate, on the contrary, increases with the increasing of the N_c due to the thinning of the bins which affects negatively the accuracy of the estimations. On the other hand, the results obtained by increasing the number of classes to 100 show that the interpolation performance is relatively close to the classification with $N_c = 16$, with slightly higher errors and smaller correlation but significantly higher MCR than the later.

Table 6.45 DGC Validation Measures

Classes	MnAE	RMSE	R_p	MCR
4	0.071	0.090	0.858	0.193
16	0.043	0.072	0.915	0.465
100	0.045	0.079	0.894	0.915

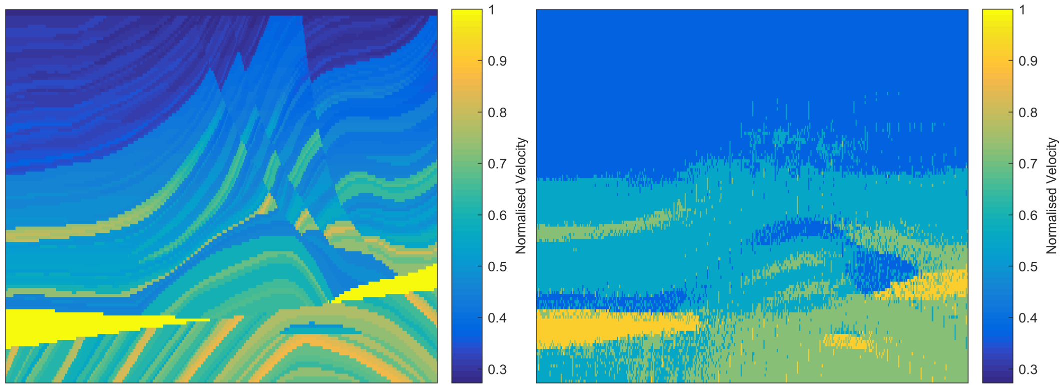

(a) Original **(b)** Estimated

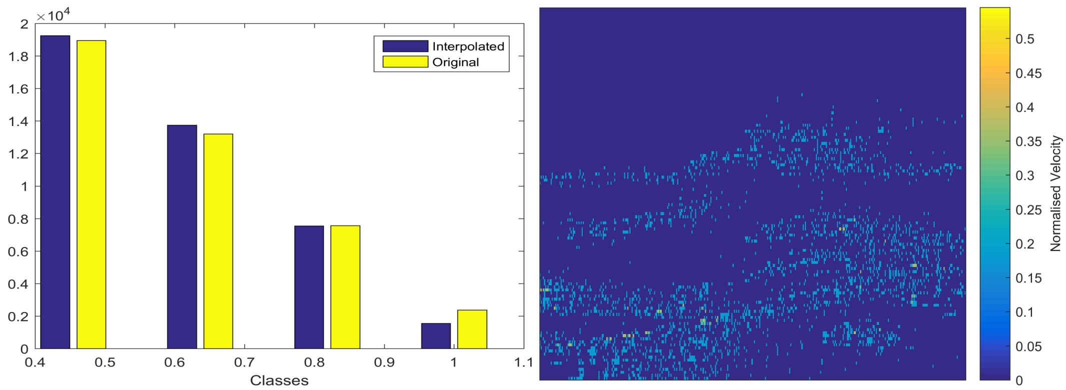

(c) Histograms **(d)** 95% Confidence interval width

Figure 6.58 Results of DGC simulation with 4 classes

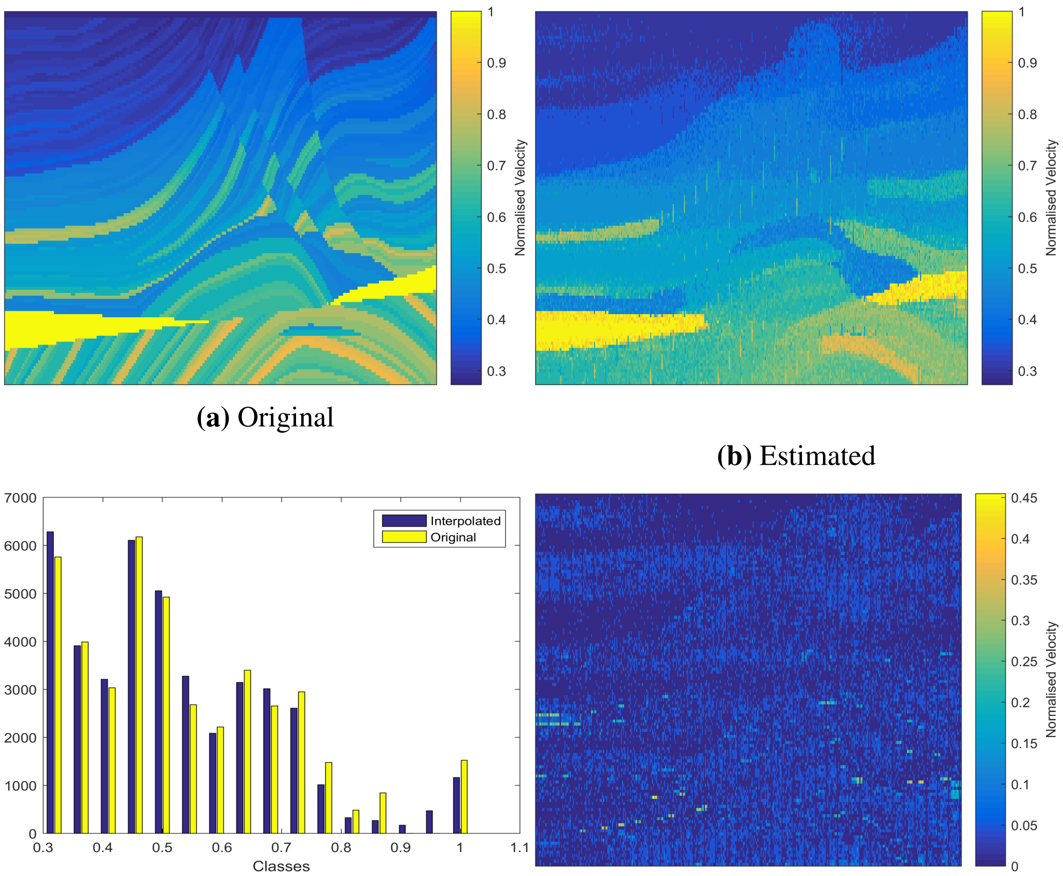

(a) Original

(b) Estimated

(c) Histograms

(d) 95% Confidence interval width

Figure 6.59 Results of DGC simulation with 16 classes

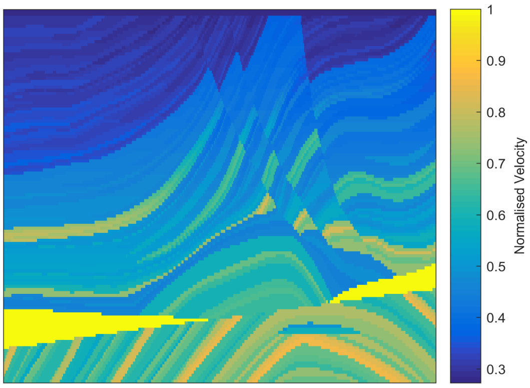

(a) Original

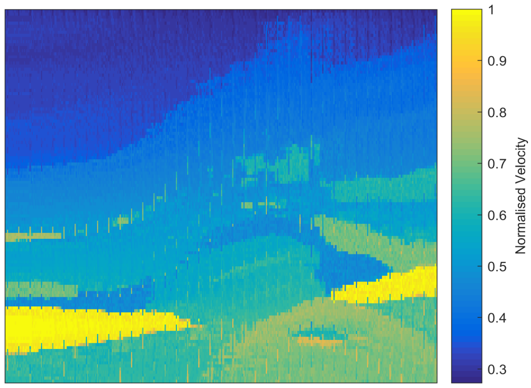

(b) Estimated

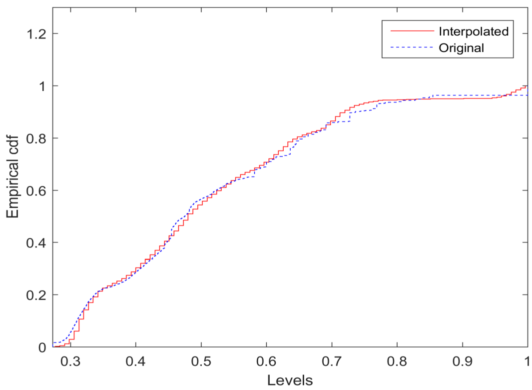

(c) Empirical cdf

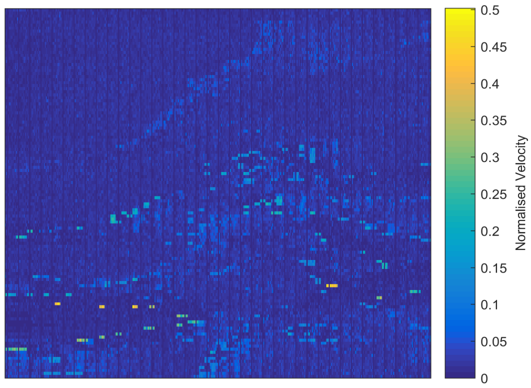

(d) 95% Confidence interval width

Figure 6.60 Results of DGC simulation with 100 classes

6.4.3 Synopsis

The results of the methods applied to the analysis of the investigated field's regular sample are summarized in Table 6.46. These results show that the best methods for the reconstruction of the Marmousi model are the variations *DirVar2* and *CHI2*, which exhibit equal performance. As regards the investigated models, no one shows significantly better performance. However, the Spartan model is always amongst the three best models. The DGC simulation method has shown comparative performance rates to those of OK estimation, but slightly lower from the later. Notable is also the fact that in all methods the increase of the number of classes results to the improvement of the estimations as indicated by the increase of the correlation coefficients. However, in the DGC method the increase of the classes leads also to the worsening of the misclassification rate, as the complexity of the procedure increases.

Table 6.46 Summarized results for the regular sample

		Interpolation			4 Classes		16 Classes	
Method	**Model**	**MnAE**	**RMSE**	R_p	R_p	**MCR**	R_p	**MCR**
DirVar0	**Spherical**	1.317	1.343	0.935	0.860	0.220	0.916	0.584
	Spartan	1.317	1.343	0.934	0.859	0.222	0.914	0.584
	Gen. Matérn	1.317	1.343	0.930	0.852	0.227	0.906	0.588
DirVar1	**Spartan**	1.317	1.343	0.932	0.856	0.219	0.912	0.578
	Gen. Matérn	1.317	1.343	0.918	0.840	0.235	0.889	0.600
	Gen. Expon.	1.317	1.343	0.918	0.840	0.235	0.889	0.600
DirVar2	**Gen. Expon.**	1.321	1.343	0.960	0.929	0.116	0.972	0.317
	Gen. Matérn	1.321	1.343	0.960	0.927	0.119	0.971	0.330
	Spartan	1.318	1.342	0.961	0.891	0.173	0.953	0.464
CHI1	**Spherical**	1.317	1.343	0.929	0.848	0.228	0.904	0.591
	Spartan	1.317	1.343	0.920	0.842	0.234	0.892	0.598
	Gen. Expon.	1.317	1.343	0.920	0.841	0.235	0.891	0.599
CHI2	**Spartan**	1.321	1.343	0.959	0.930	0.114	0.974	0.295
	Gen. Expon.	1.321	1.343	0.960	0.930	0.114	0.974	0.295
	Gen. Matérn	1.321	1.343	0.960	0.929	0.115	0.974	0.302
DGC	–	0.045	0.079	0.894	0.858	0.193	0.915	0.465

6.5 Random Sample of Marmousi Model

The analysis of the random sample follows the same procedure as for the regular sample.

6.5.1 Ordinary Kriging

Preliminary Analysis

The statistics (Table 6.47) and the histograms (Fig. 6.61) of the sample and the original dataset show that the sample is totally representative of the original data.

The normal probability plot of the sample (Fig. 6.62), however, indicates that the data does not come from a gaussian distribution. Thus, Box-Cox transformation is necessary to be applied to the sample dataset. The best Box-Cox transformation is attained when $\lambda = -0.2944$. The statistics of the transformed values can be seen in Table 6.48, while the histogram and the normal probability plot of them are presented in Fig. 6.63. The Box-Cox transformation does not provides a truly gaussian dataset, but the transformed dataset is closer to the gaussian distribution than the original sample. However, no further actions are taken and the analysis procedure is continued under the assumption that the transformed dataset comes from a gaussian distribution.

After transforming the random sample's values, the next step is the removal of any possible trend. The trend models described in Section 5.1 (see Table 5.1) have been tested. The parameters of these models are inferred by means of multilinear regression of the transformed normalised velocities field on the (i, j) indices of the sample points. The complete expressions of the resulting trend functions are given in Table 6.49, while the normal probability plots of the fluctuations of each model are shown in Fig. 6.64. The best model is choosen as the one resulting in fluctuations which are closer to the gaussian distribution. This model, as can be seen from Fig. 6.64, is the linear trend model.

In Fig. 6.65 the multilinear regression of the transformed normalised velocities field on the indices (i, j) of the sample points is depicted, while in Fig. 6.66 is plotted the histogram of the transformed and detrended data (i.e. the fluctuations), and in Table 6.50 are evaluated the statistics of them. Finally, in Fig. 6.67 is presented the transformed and detrended

Table 6.47 Original and sample datasets statistics

Dataset	Min	Max	Mean	Median	Variance	Skewness	Kurtosis
Original	0.273	1.000	0.514	0.475	0.030	0.824	3.277
Sample	0.273	1.000	0.512	0.471	0.030	0.851	3.326

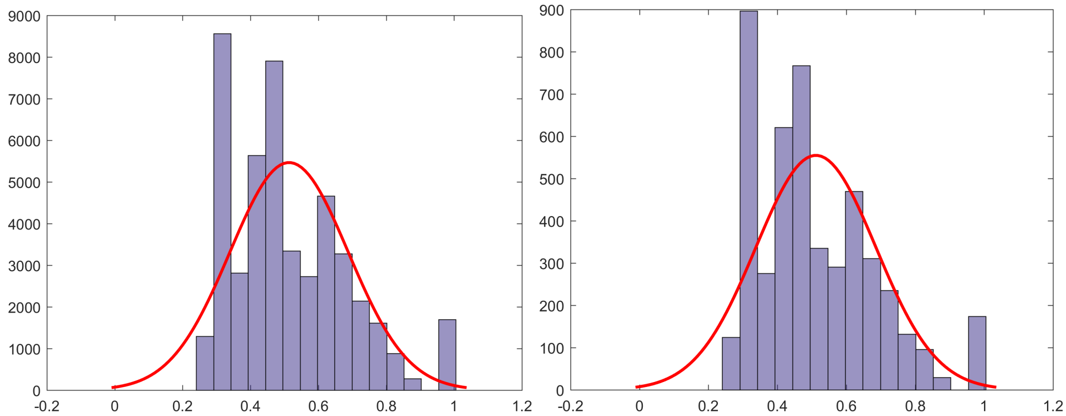

(a) Original

(b) Random sample

Figure 6.61 Histograms of original and sample datasets

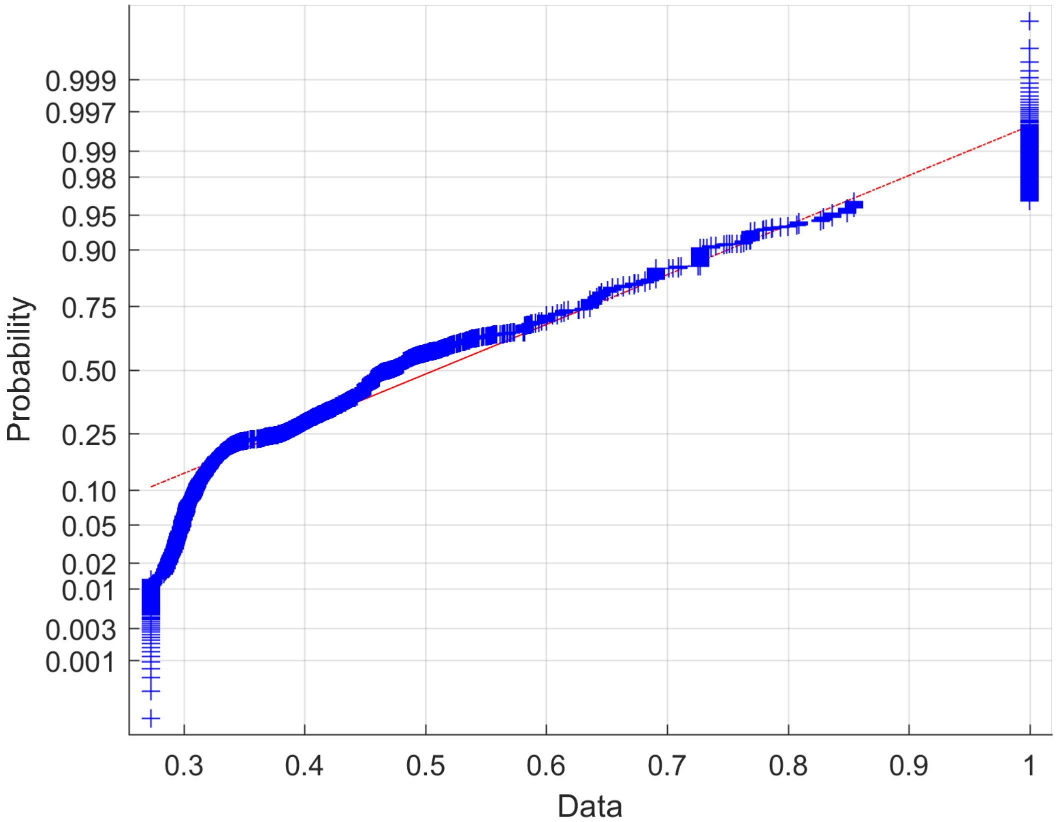

Figure 6.62 Normal probability plot of random sample

Table 6.48 Transformed (Box-Cox with $\lambda = -0.2606$) dataset statistics

Min	Max	Mean	Median	Variance	Skewness	Kurtosis
-1.583	0.000	-0.827	-0.844	0.164	0.028	2.126

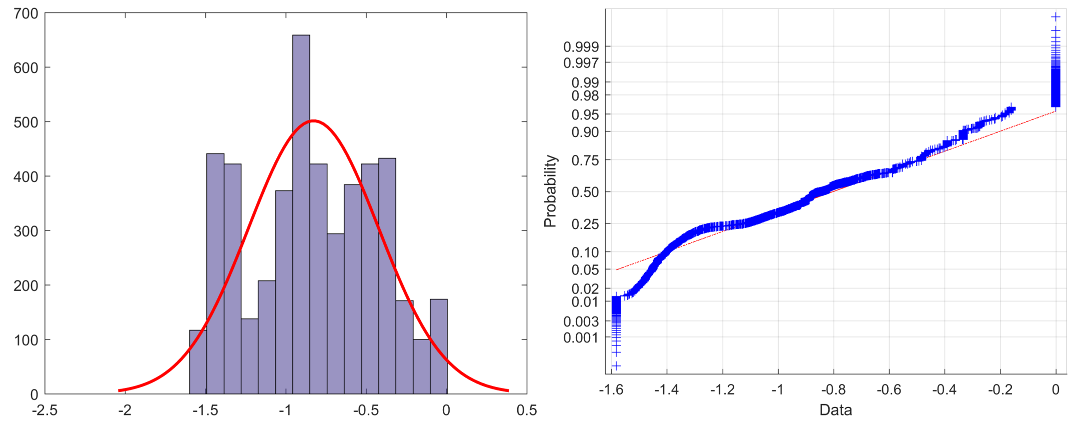

(a) Histogram **(b)** Normal probability plot

Figure 6.63 Histogram and normal probability plot of the transformed random sample. The transformation applied is the Box-Cox with $\lambda = -0.2944$.

Table 6.49 Estimated trend models (random sample)

Model	**Estimated Trend Function**
Mean	$m_z(\boldsymbol{s}) = -0.8271$
Linear	$m_z(\boldsymbol{s}) = -0.3023 + 5.2017 \cdot 10^{-4}x - 0.0101y$
Quadratic	$m_z(\boldsymbol{s}) = -0.3143 - 2.5325 \cdot 10^{-5}x - 0.0067y + 6.0531 \cdot 10^{-6}xy$ $+ 4.4887 \cdot 10^{-7}x^2 - 3.7038 \cdot 10^{-5}y^2$
Cubic	$m_z(\boldsymbol{s}) = -0.1126 - 0.0037x - 0.0085y + 5.4460 \cdot 10^{-5}xy + 1.5396 \cdot 10^{-5}x^2$ $- 9.0123 \cdot 10^{-5}y^2 - 6.7206 \cdot 10^{-8}x^2y$ $- 1.8463 \cdot 10^{-7}xy^2 - 1.8824 \cdot 10^{-8}x^3 + 4.8737 \cdot 10^{-7}y^3$
Quartic	$m_z(\boldsymbol{s}) = -0.1699 - 0.0068x + 0.0063y + 2.3499 \cdot 10^{-5}xy + 5.3995 \cdot 10^{-5}x^2$ $- 4.9044 \cdot 10^{-4}y^2 - 1.4725 \cdot 10^{-7}x^2y + 8.3151 \cdot 10^{-7}xy^2$ $- 1.6992 \cdot 10^{-7}x^3 + 3.9641 \cdot 10^{-6}y^3 + 7.9058 \cdot 10^{-10}x^2y^2$ $- 2.3328 \cdot 10^{-11}x^3y - 7.2008 \cdot 10^{-9}xy^3 + 1.9912 \cdot 10^{-10}x^4$ $- 8.4700 \cdot 10^{-9}y^4$
Linear+Periodic	$m_z(\boldsymbol{s}) = -0.3038 + 5.1872 \cdot 10^{-4}x - 0.0101y - 0.0036\cos 2\pi 0.0256x$ $- 0.0046\sin 2\pi 0.0256x - 0.0016\cos 2\pi 0.0656y + 0.0217\sin 2\pi 0.0656y$ $- 0.0041\cos 2\pi 0.3846x + 0.0026\sin 2\pi 0.3846x$ $- 0.0184\cos 2\pi 0.0738y + 0.0034\sin 2\pi 0.0738y$

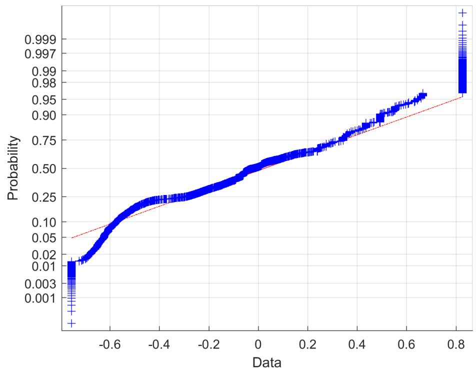

(a) Mean

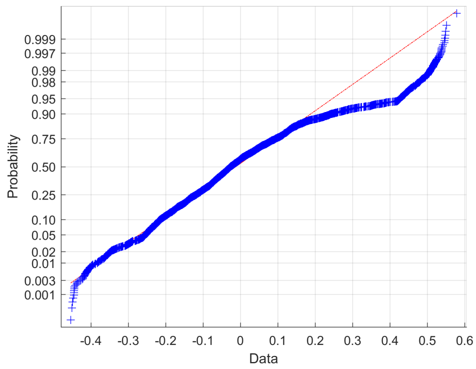

(b) Linear model

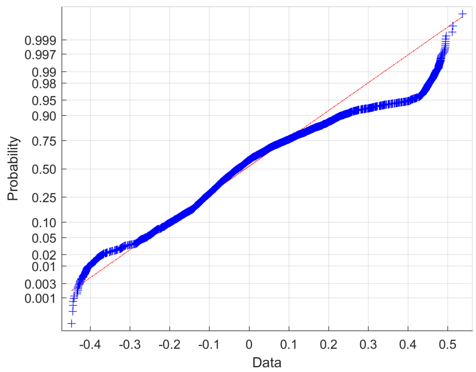

(c) Quadratic model

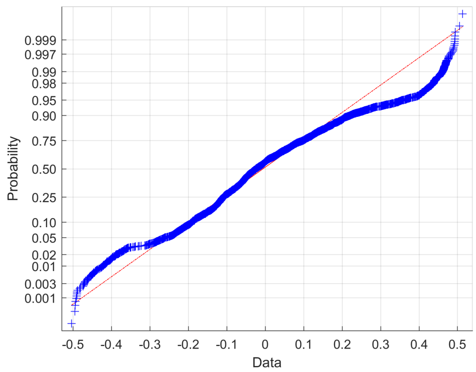

(d) Cubic model

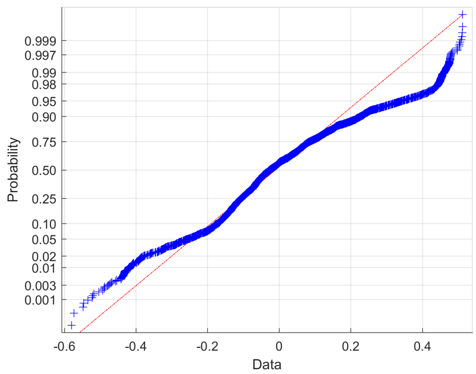

(e) Quartic model

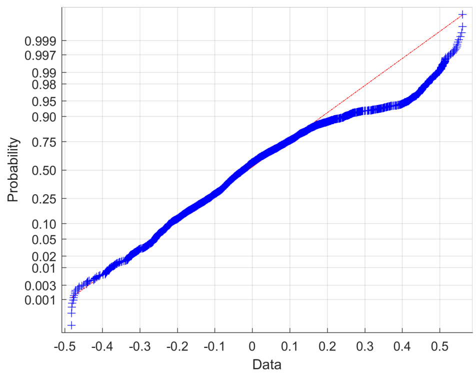

(f) Periodic model

Figure 6.64 Normal probability plots of the fluctuations resulting from the estimated trend models.

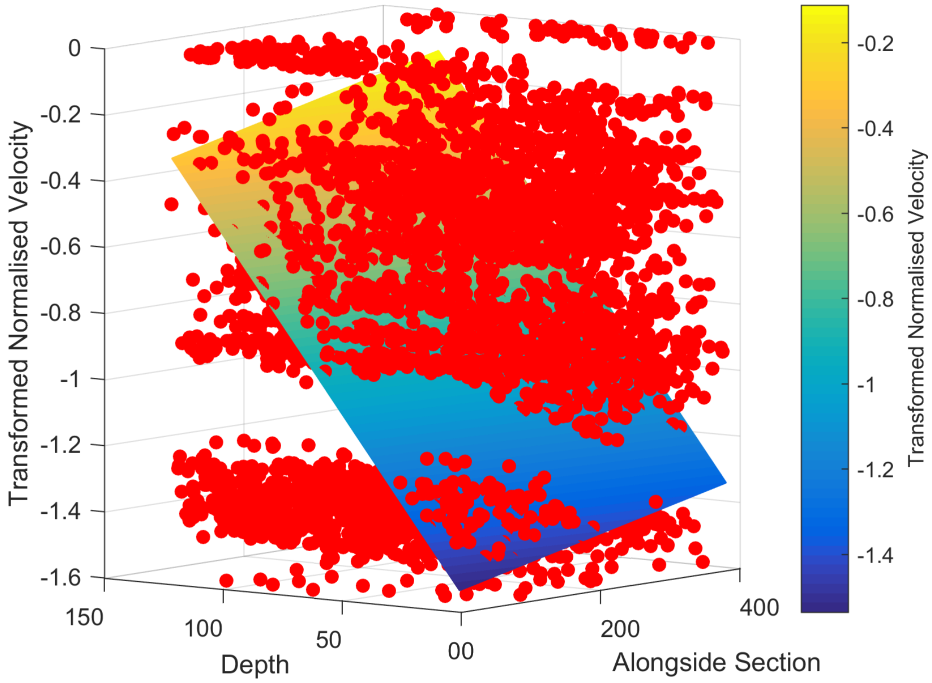

Figure 6.65 Multilinear regression of the transformed normalised velocities field on the indices (i, j) of the sample points. The trend equation is given by $m_z(\boldsymbol{s}) = -0.3023 + 5.2017 \cdot 10^{-4}x - 0.0101y$.

Table 6.50 Transformed and detrended dataset statistics

Min	Max	Mean	Median	Variance	Skewness	Kurtosis
-0.454	0.579	0.000	-0.027	0.035	0.714	3.660

Marmousi model, in order to obtain an inspection of the random field, which we intend to regenerate hereinafter with the five variations of the analysis procedure, described in Section 6.2.

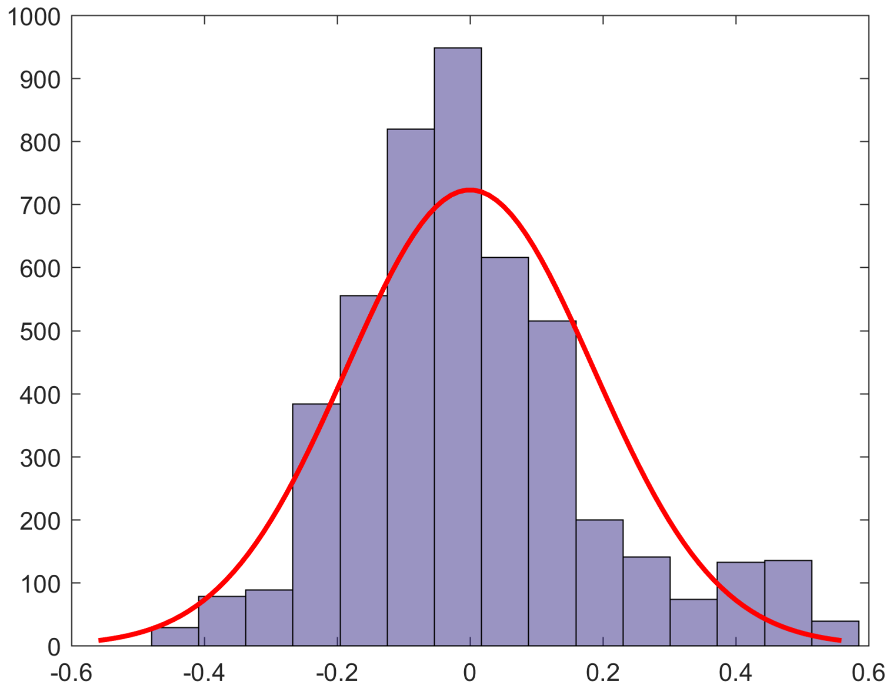

Figure 6.66 Histogram of transformed and detrended sample dataset

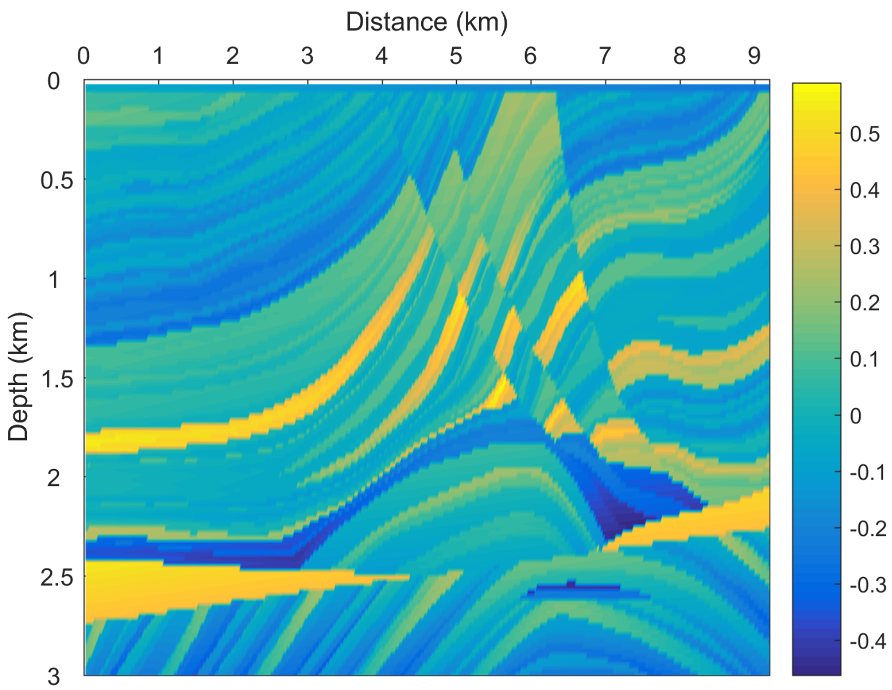

Figure 6.67 Transformed and detrended Marmousi model

Calculation of Experimental Variogram

The experimental directional variograms with angular step $4°$ and $15°$ are shown in Fig. 6.68. These figures display clearly the significant anisotropic characteristics of the field (as it is highly expected for such geological data). More specifically, it can be easily seen that the spatial correlation differs significantly from direction to direction; the variogram is stabilized around a maximum value (sill) in longer distances along the horizontal and almost horizontal directions than the other directions.

Again the experimental variograms with the smaller angular step ($4°$) have been calculated only in order to provide a clearer visualization of the anisotropy of the field, while the directional experimental variograms with the higher angular step ($15°$) are used in practice in the following steps. We avoid to use the exprimental variograms with the small angular step due to the higher computational cost that they will lead the further analysis.

DirVar0

The initial values and the boundaries of the parameters for each model used in the optimization step are presented in Table 6.51, and the resulting optimum parameters are presented in Table 6.52.

As can be seen from the validation measures of the LOOCV presented in Table 6.53 the best model is the Generalized Exponential, followed by Spartan and Spherical.

A visualisation of the the selected theoretical model's fitting to the experimental variogram is interpretted in Fig. 6.69, in which the directional experimental variograms of the field on the directions $0°, 30°, 60°, 90°, 120°$, and $150°$ are plotted against the theoretical model (the rest directional variograms can be found in A). The best anisotropic model fits fairly well to the directional experimental variograms.

The estimation derived from OK of the stochastic component of the field (i.e the transformed and detrended normalised velocities) given by the best model is shown in Fig. 6.70. A scatter diagram of original and estimated values of the stochastic component, as well as their histograms can be seen in Fig. 6.71. Finally , in Table 6.54 the measures of the stochastic component estimation performance for the three best models are presented.

By adding the trend to the estimations of the stochastic component of the field and inverting the Box-Cox transformation, the estimation of the total field, shown in Fig. 6.72, is derived. For the stochastic component, a scatter diagram of the original and the estimated values of the total field, as well as their histograms can be seen in Fig. 6.73. In general, the estimations follow the original values without achieving satisfying proximity of the

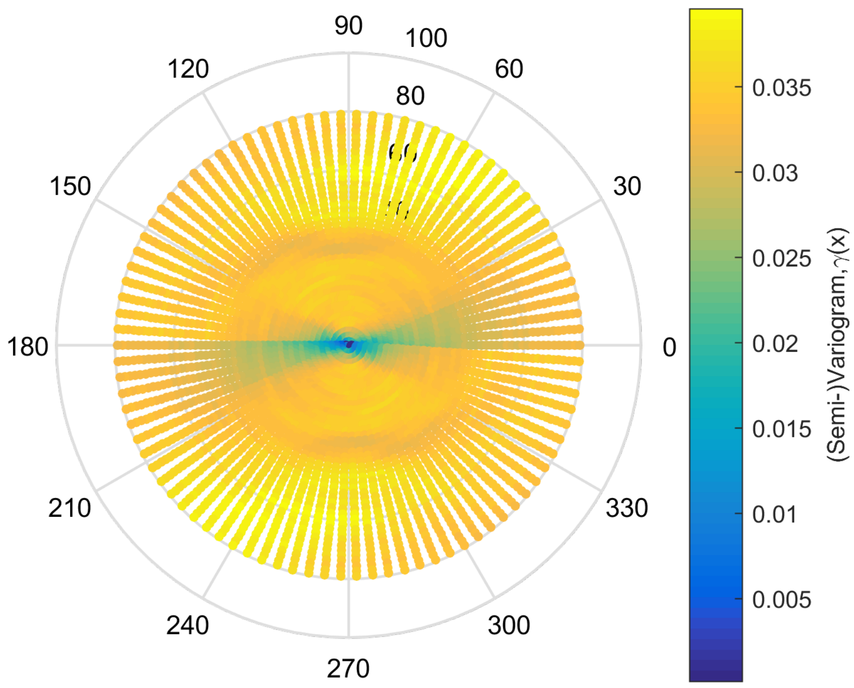

(a) 4° angular step

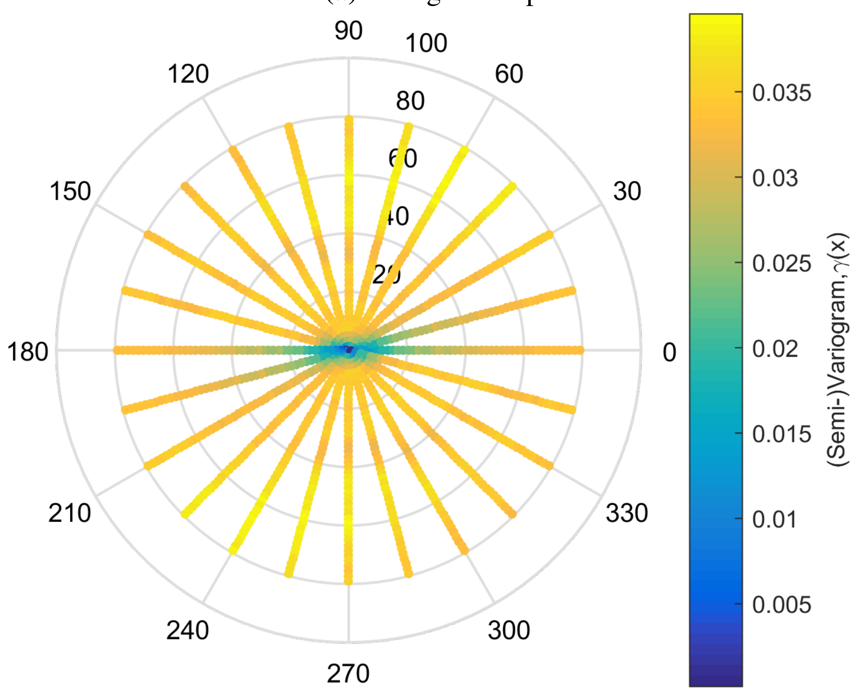

(b) 15° angular step

Figure 6.68 Directional experimental variograms of the field. For both cases the angular tolerance is 20°, the maximum distance taken into account is the 20% of the grid's diagonal which is equivalent to about 80, and is divided into 45 distance lags.

Table 6.51 Initial values and boundaries of the parameters for optimization step, where $\hat{g}_{max}$($\equiv$ maximum value of experimental variogram) $= 0.0384$, $d_{max} \simeq 80$, $b = [\sigma_z^2 = \hat{g}_{max}, \xi_1 = d_{max}2/3, R = 0.5, \phi = 10°, c_0 = \hat{g}_{max}/100]$, $b_{sp} = [\eta_0 = 1000, \xi_1 = d_{max}2/3, R = 0.5, \phi = 10°, c_0 = \hat{g}_{max}/100]$, $b_b = [\sigma_z^2 \in [0, 1.5\hat{g}_{max}], \xi_1 \in [0, 1.5d_{max}], R \in [0, 30], \phi \in [-90°, 90°], c_0 \in [0, \hat{g}_{max}/5]]$,$b_{sp,b} = [\eta_0 \in [0, \infty], \xi_1 \in [0, 1.5d_{max}], R \in [0, 30], \phi \in [-90°, 90°], c_0 \in [0, \hat{g}_{max}/5]]$.

Model	Initial Values	Boundaries
Gen. Exponential	$[b, \nu = 1.5]$	$[b_b, \nu \in (0, 2)]$
Gaussian	$[b]$	$[b_b]$
Spherical	$[b]$	$[b_b]$
Gen. Matérn	$[b]$	$[b_b]$
Spartan	$[b_{sp}, \eta_1 = 1]$	$[b_{sp,b}, \eta_1 \in (-2, \infty)]$

Table 6.52 Optimum Parameters of the investigated variogram models

Model	σ_z^2	ξ_1	R	ϕ	c_0	ν
Gen. Exponential	0.035	9.671	0.370	$-83.4°$	0.000	0.734
Gaussian	0.034	108.181	0.901	$-83.0°$	0.008	–
Spherical	0.027	8.663	0.116	$-83.9°$	0.008	–
Gen. Matérn	0.035	9.848	0.227	$-83.4°$	0.000	0.300
	η_0	ξ_1	R	ϕ	c_0	η_1
Spartan	5.094	9.852	0.082	$-83.5°$	0.000	123.852

Table 6.53 Leave-One-Out Cross Validation Scores (see section 5.3.2

Model	MnAE	MxAE	MSE	RMSE	R_p	R_{sp}	r_F
Gen. Exponential	0.045	0.405	0.005	0.070	0.917	0.945	0.866
Gaussian	0.052	0.392	0.007	0.076	0.895	0.928	0.640
Spherical	0.046	0.401	0.005	0.072	0.913	0.941	0.782
Gen. Matérn	0.046	0.391	0.005	0.072	0.912	0.941	0.781
Spartan	0.046	0.400	0.005	0.072	0.913	0.941	0.784

Table 6.54 Ordinary Kriging Scores

Model	MnAE	MxAE	MSE	RMSE	R_p	R_{sp}	r_F
Gen. Exponential	0.090	0.772	0.017	0.130	0.721	0.719	0.519
Spartan	0.096	0.582	0.017	0.131	0.719	0.711	0.488
Spherical	0.097	0.572	0.017	0.132	0.715	0.707	0.472

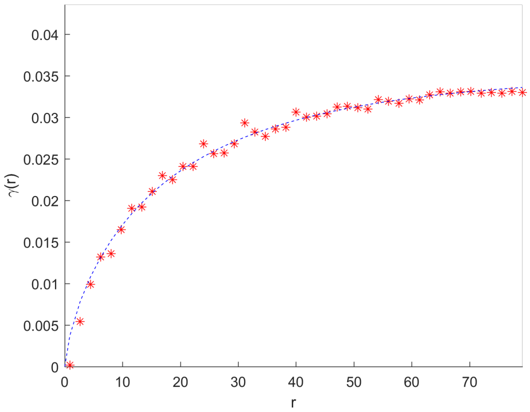

(a) 0°

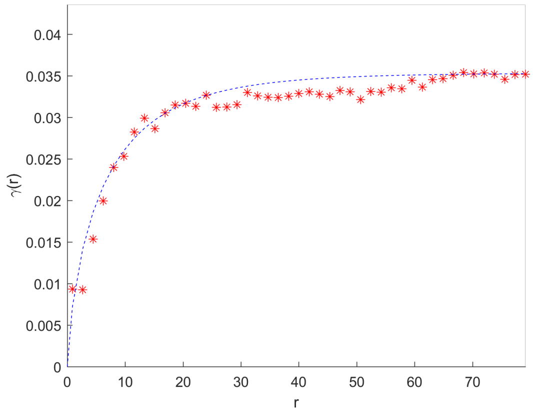

(b) 30°

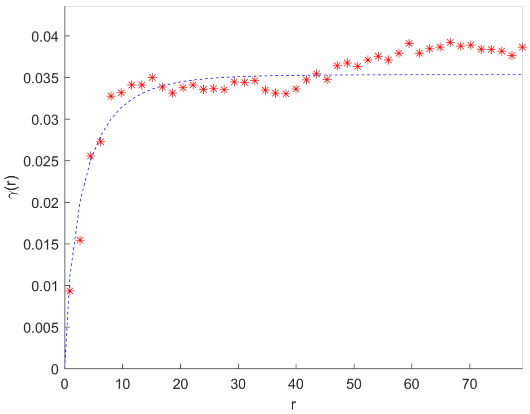

(c) 60°

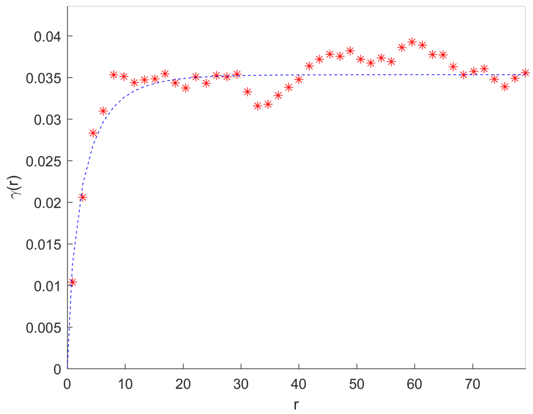

(d) 90°

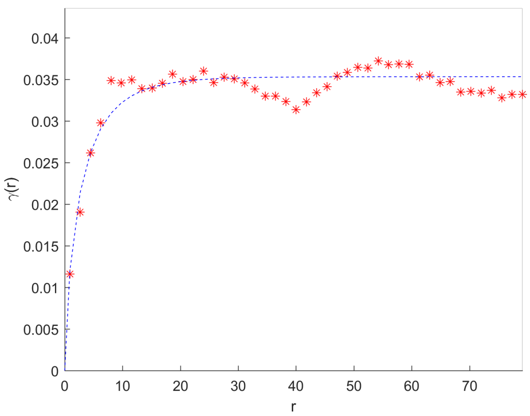

(e) 120°

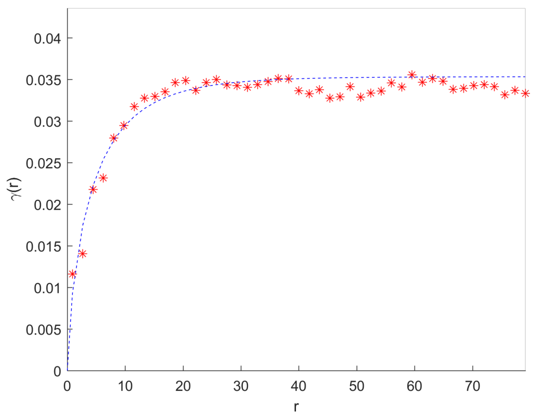

(f) 150°

Figure 6.69 Fitting of the best theoretical model to the directional experimental variograms of the field. The best model is a Gen. Exponential with parameters $\sigma_z^2 = 0.035, \xi_1 = 9.671, R = 0.370, \phi = -83.4°, c_0 = 0.000, \nu = 0.734$. The experimental variogram is calculated with angular tolerance 20°, 45 distance lags and taking into account maximum distance equivalent to about 80.

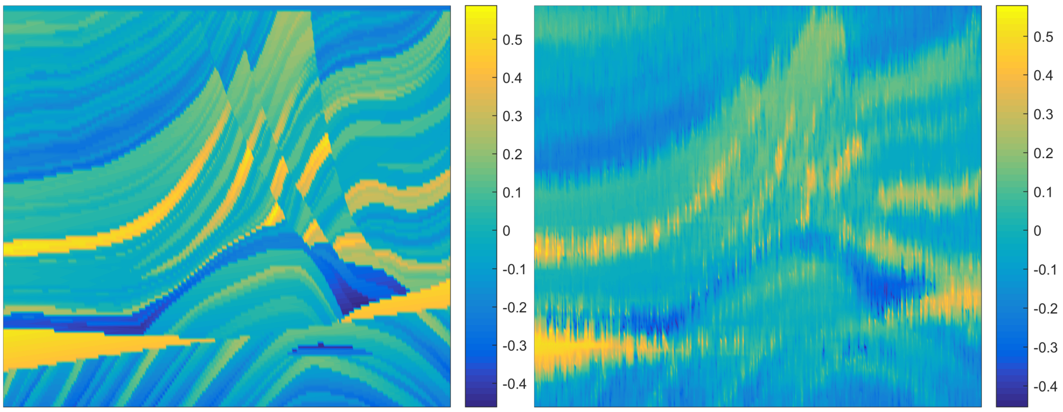

(a) Original Stochastic Component **(b)** Estimated Stochastic Component

Figure 6.70 Original and Estimation of the stochastic component of the field. The model used is a Gen. Exponential with parameters $\sigma_z^2 = 0.035, \xi_1 = 9.671, R = 0.370, \phi = -83.4°, c_0 = 0.000, \nu = 0.734$.

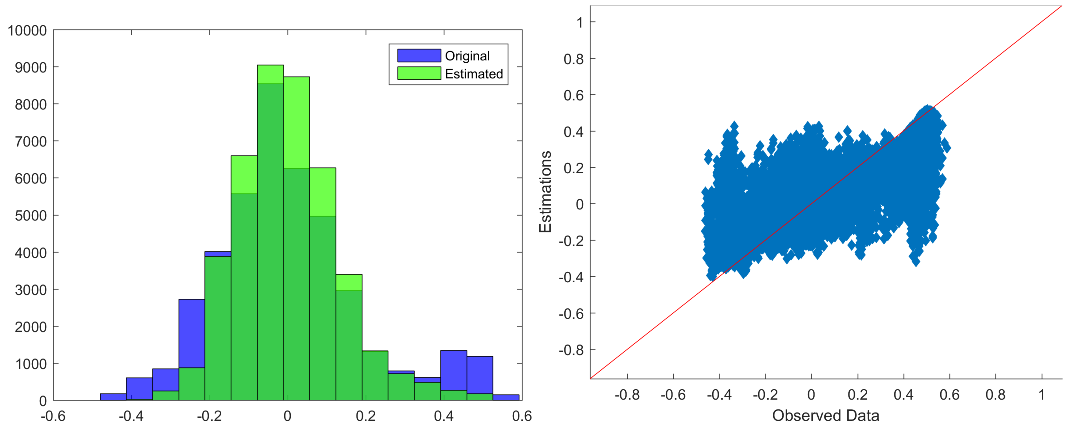

Figure 6.71 Histograms and Scatter plot of original and estimated values of the field's stochastic component. The model used is a Gen. Exponential with parameters $\sigma_z^2 = 0.035, \xi_1 = 9.671, R = 0.370, \phi = -83.4°, c_0 = 0.000, \nu = 0.734$.

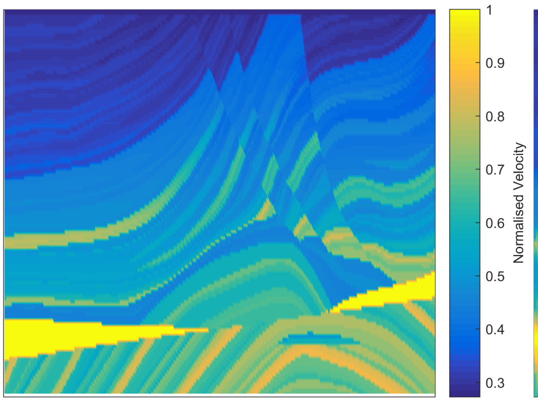

(a) Original Total Field

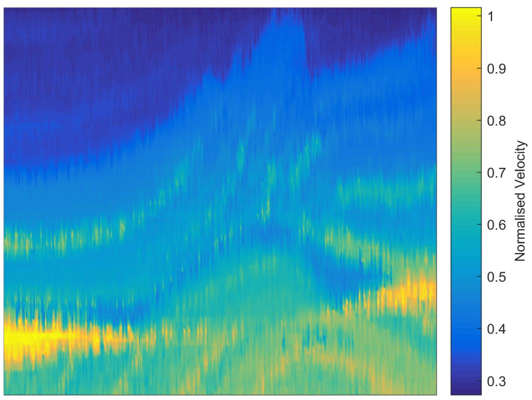

(b) Estimated Total Field

Figure 6.72 Original and estimated total field

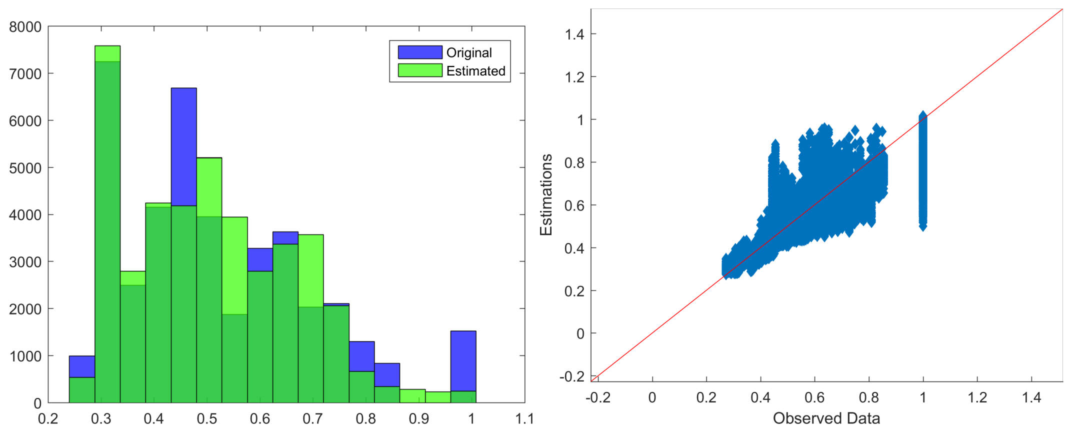

Figure 6.73 Histograms and Scatter plot of original and estimated values (total field)

total distribution. Both the tails of the distribution as the middle of it exhibit significant discrepancies.

In Table 6.55 the measures of the total field (i.e. normalised velocities) estimation performance for the three best models are presented. From these measures it can be observed that the three model's performance is almost identical with the last two performing slightly better than the first. In addition, Fig. 6.74 maps the confidence interval width of the estimations, i.e. it depicts the spatial distribution of the uncertainty. The uncertainty is zero at the known points, while it increases up to 0.37 relatively quickly with the distance of the missing locations from the known points. Also, at the edges of the field of the uncertainty is increased due to the lack of available neighboors.

Table 6.55 Total Field Estimation Scores

Model	MnAE	MxAE	MSE	RMSE	R_p	R_{sp}	r_F
Gen. Exponential	1.331	1.932	1.842	1.357	0.927	0.943	0.872
Spartan	1.329	1.905	1.840	1.357	0.931	0.940	0.875
Spherical	1.329	1.904	1.840	1.357	0.930	0.939	0.874

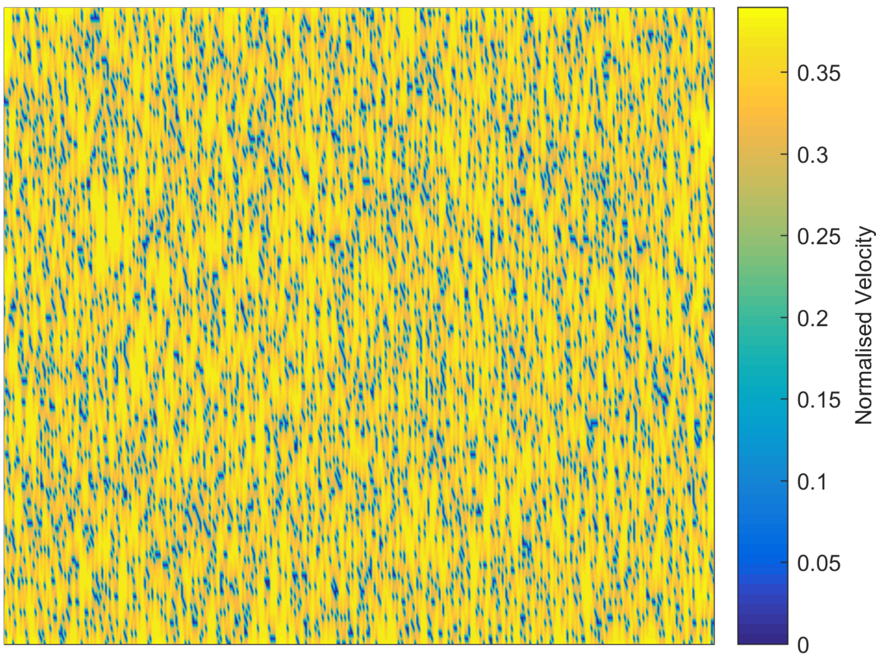

Figure 6.74 Uncertainty of the total field's estimation

Table 6.56 Classification Measures

	4 classes			16 classes		
Model	R_p	R_{sp}	**MCR**	R_p	R_{sp}	**MCR**
Gen. Exponential	0.857	0.876	0.208	0.912	0.938	0.537
Spartan	0.855	0.870	0.219	0.911	0.934	0.579
Spherical	0.855	0.870	0.219	0.911	0.933	0.580

In Table 6.56 are presented the classification measures for the cases of 4 and 16 classes. The increasing of the number of classes leads to the correlation coefficients increasing and to the MCR decreasing. The correlation coefficients' improvement can be attributed to the more realistic model which derives by increasing the N_c. On the contrary, the misclassification rate increases due to the thinning of the binning, which incommodes the interpolation. Also, the first model exhibits the best performance.

DirVar1

The fitting of the ellipses to the pairs of (ϕ, ξ) of each model are depicted in Fig. 6.75, while the estimated anisotropy parameters for all models by means of DVF (see section 5.2.2) are given in Table 6.57. In general, the investigated models' fitting show that the major axis of the anisotropy ellipsis is either on the almost horizontal direction (0°) or on the direction of about $30-40°$. This results agree with the intuitive estimations of the anisotropy angle mentioned at section 6.1.2. The rapid changes of the correlation lengths depending on the direction (due to non-stationarity) may also affect negatively the optimization procedure. On the other hand, the estimated anisotropy ratioscannot be evaluated before the cross validation procedure.

By replacing the estimated anisotropy parameters to the anisotropic variogram models and minimizing the error function of the new models and the experimental directional variograms the rest parameters are estimated, as presented in Table 6.58. The common parameters generally agree for all the investigated models.

After the parameter inference Leave-One-Out Cross Validation (LOOCV) is applied in order to define the best models. The validation measures of the LOOCV, presented in Table 6.59, give as best model the Spartan, followed by the Generalized Mátern and the Generalized Exponential models.

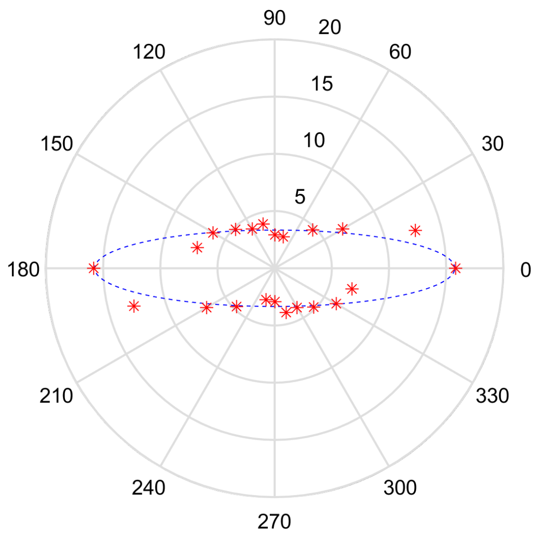

(a) Gen. Exponential

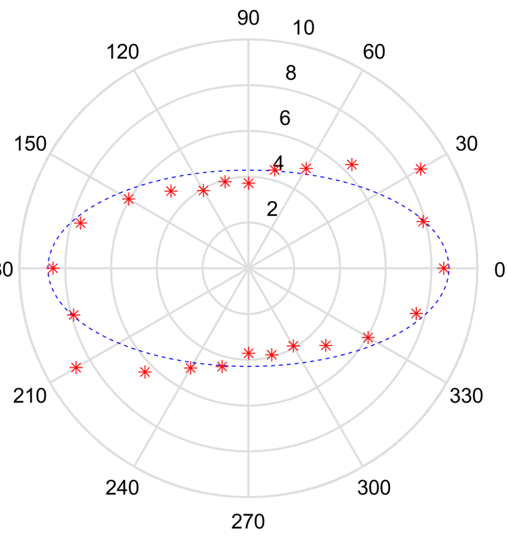

(b) Gaussian

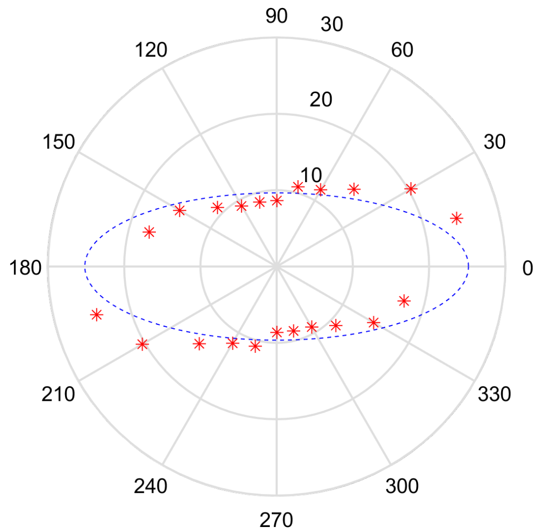

(c) Spherical

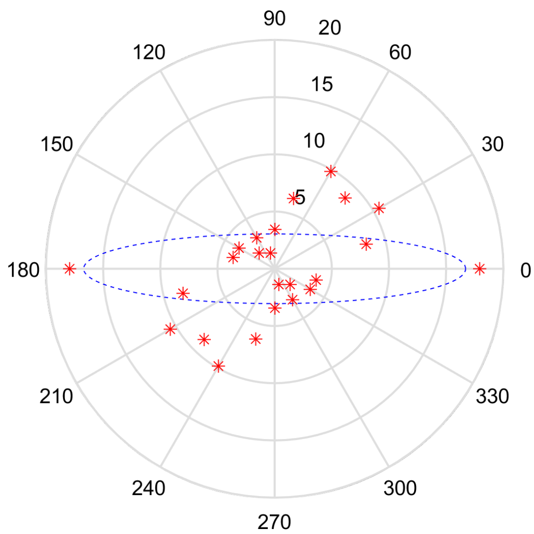

(d) Gen. Matérn

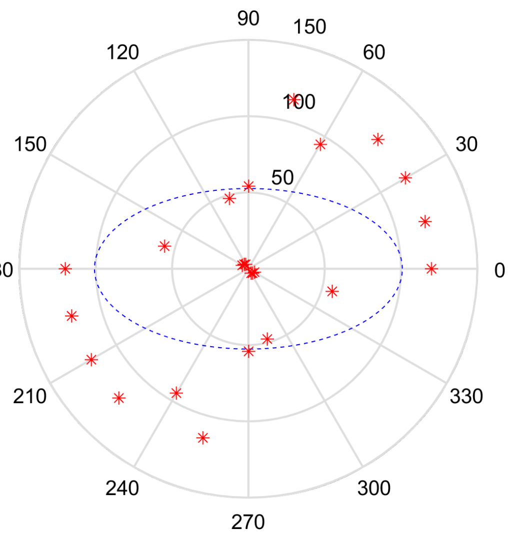

(e) Spartan

Figure 6.75 Fitting of ellipses to the pairs (ϕ, ξ) of the investigated variogram models

Table 6.57 Anisotropy parameters of the investigated variogram models estimated with DVF method

Model	**Anisotropy Parameters**		
	ξ_1	R	ϕ
Gen. Exponential	3.338	0.212	$-90.0°$
Gaussian	4.288	0.489	$-90.0°$
Spherical	9.645	0.383	$-90.0°$
Gen. Matérn	3.043	0.182	$-90.0°$
Spartan	52.606	0.522	$-50.9°$

Table 6.58 Optimum Parameters of the variogram models with the lower degrees of freedom

Model	σ_z^2	c_0	ν
Gen. Exponential	0.030	0.004	1.095
Gaussian	0.026	0.008	–
Spherical	0.026	0.008	–
Gen. Matérn	0.032	0.002	0.499
	η_0	c_0	η_1
Spartan	0.010	0.008	-1.999

Table 6.59 Leave-One-Out Cross Validation Scores (see section 5.3.2

Model	**MnAE**	**MxAE**	**MSE**	**RMSE**	R_p	R_{sp}	r_F
Gen. Exponential	0.046	0.385	0.005	0.072	0.912	0.941	0.816
Gaussian	0.046	0.383	0.005	0.073	0.911	0.940	0.810
Spherical	0.046	0.383	0.005	0.073	0.911	0.940	0.809
Gen. Matérn	0.046	0.385	0.005	0.072	0.912	0.941	0.817
Spartan	0.045	0.403	0.005	0.072	0.914	0.943	0.862

Table 6.60 Ordinary Kriging Scores

Model	MnAE	MxAE	MSE	RMSE	R_p	R_{sp}	r_F
Spartan	0.097	0.829	0.021	0.145	0.639	0.655	0.295
Gen. Matérn	0.092	0.792	0.018	0.133	0.701	0.700	0.491
Gen. Exponential	0.093	0.794	0.018	0.134	0.699	0.699	0.484

The fitting of the best model to the experimental variogram along the directions of $0°, 30°, 60°, 90°, 120°$, and $150°$ is interpretted in Fig. 6.76 (the rest directional variograms can be found in Appendix A). As it can be seen the best theoretical variogram model diverges significantly from the experimental directional variograms. This can be attributed to minimization miscalculations, i.e. inappropiate objective function (very smooth or possible local minima), inappropriate initial values or to the fields complexity. Thus, the analysis is continued without taking any further action.

Implementing OK with the determined best model, the resulting estimation of the stochastic component of the field (i.e the transformed and detrended normalised velocities) is as shown in Fig. 6.77. The scatter diagram and histograms of the original and the estimated values of the stochastic component are illustrated in Fig. 6.78, and the measures of the stochastic component estimation performance for the three best models are presented in Table 6.60.

The resulting estimation of the total field, after the trend addition and Box-Cox transformation inversion, is as shows Fig. 6.79, and the correspomding scatter diagram and histograms are shown in Fig. 6.80. In general, the estimations follow the original values without achieving satisfying proximity of the total distribution. Both the tails of the distribution as the middle of it exhibit significant discrepancies. The measures of the total field (i.e. normalised velocities) estimation performance for the three best models, presented in Table 6.61, show that the three model's performance is almost identical with the last two performing slightly better than the first. Finally, Fig. 6.81 shows the spatial distribution of the ordinary kriging estimations uncertainty. The uncertainty is zero at the known points and increases up to 0.37 gradually with the distance of the investigated points from the data.

Also, in Table 6.62 are presented the classification measures for the cases of 4 and 16 classes. For both $N_c = 4$ and $N_c = 16$ the performance of the two last models is almost identical and slightly better than the first one. Also, in the case of $N_c = 16$ the classification performs better than in the case of $N_c = 4$.

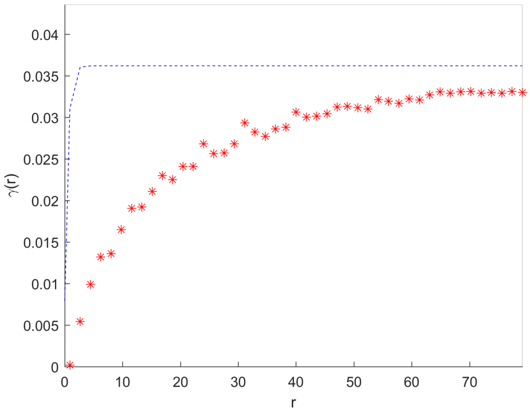

(a) 0°

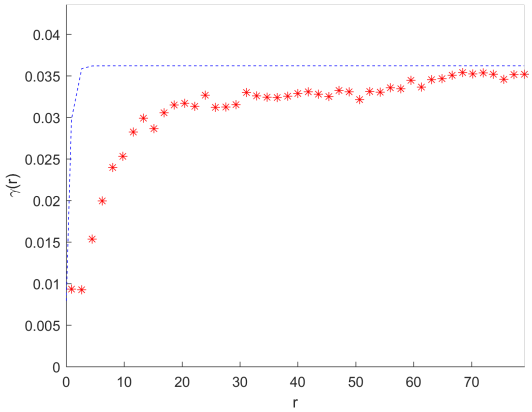

(b) 30°

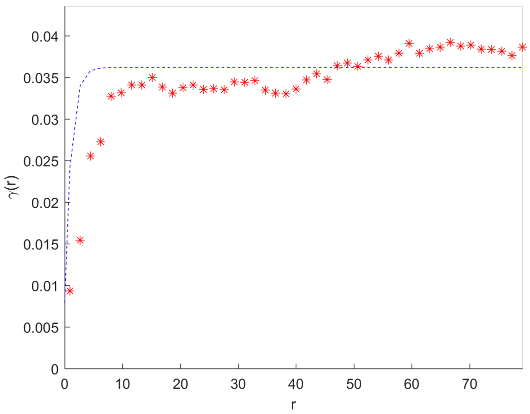

(c) 60°

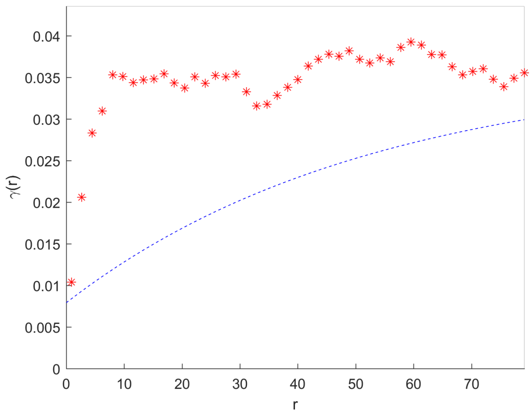

(d) 90°

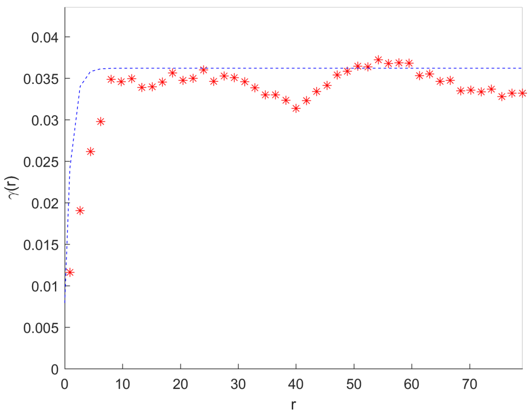

(e) 120°

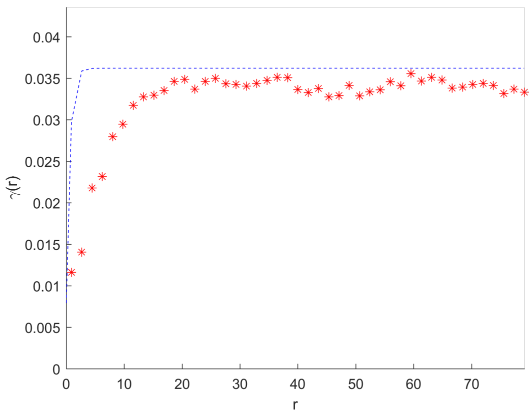

(f) 150°

Figure 6.76 Fitting of the best theoretical model to the experimental directional variograms of the field. The best model is a Spartan with parameters $\eta_0 = 0.010, \xi_1 = 52.606, R = 0.522, \phi = -90.0°, c_0 = 0.008, \eta_1 = -1.999$. The experimental variogram is calculated with angular tolerance 20°, 45 distance lags and taking into account maximum distance equivalent to about 80.

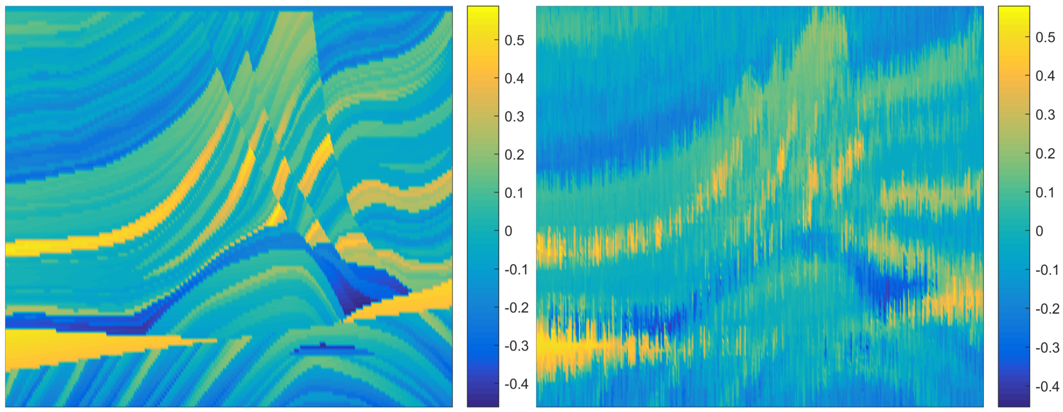

(a) Original Stochastic Component **(b)** Estimated Stochastic Component

Figure 6.77 Original and Estimation of the stochastic component of the field. The model used is a Spartan with parameters $\eta_0 = 0.010, \xi_1 = 52.606, R = 0.522, \phi = -90.0°, c_0 = 0.008, \eta_1 = -1.999$.

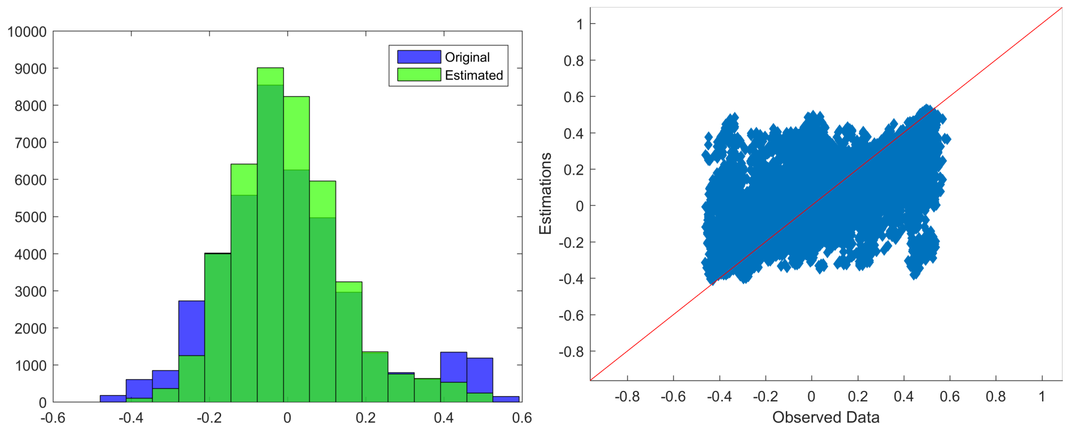

Figure 6.78 Histograms and Scatter plot of original and estimated values of the field's stochastic component. The model used is a Spartan with parameters $\eta_0 = 0.010, \xi_1 = 52.606, R = 0.522, \phi = -90.0°, c_0 = 0.008, \eta_1 = -1.999$.

Table 6.61 Total Field Estimation Scores

Model	MnAE	MxAE	MSE	RMSE	R_p	R_{sp}	r_F
Spartan	1.331	1.945	1.846	1.359	0.904	0.930	0.838
Gen. Matérn	1.331	1.932	1.843	1.357	0.923	0.939	0.867
Gen. Exponential	1.331	1.932	1.843	1.357	0.923	0.939	0.866

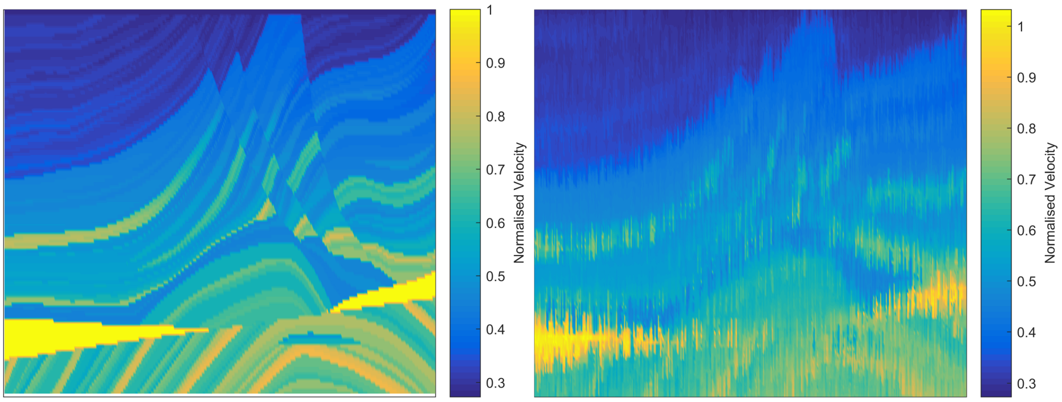

(a) Original Total Field **(b)** Estimated Total Field

Figure 6.79 Original and estimated total field

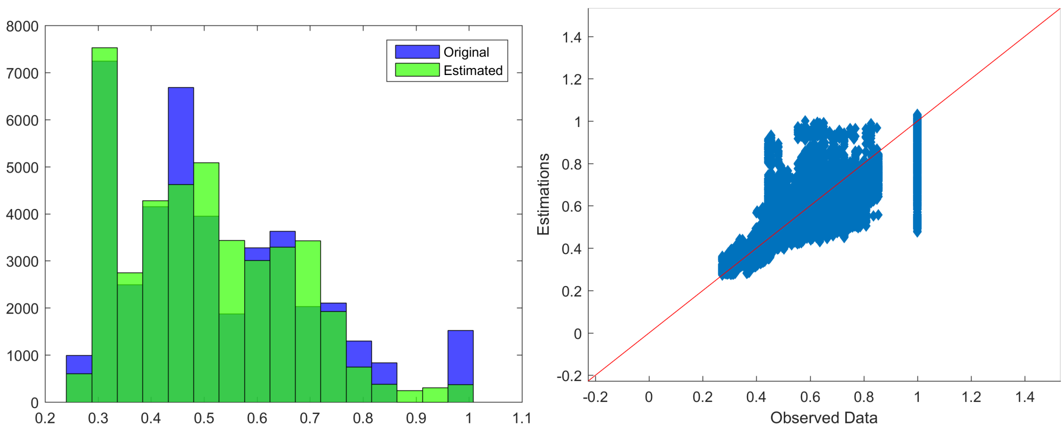

Figure 6.80 Histograms and Scatter plot of original and estimated values (total field)

Table 6.62 Classification Measures

	4 classes			16 classes		
Model	R_p	R_{sp}	**MCR**	R_p	R_{sp}	**MCR**
Spartan	0.838	0.864	0.221	0.888	0.925	0.537
Gen. Matérn	0.854	0.873	0.211	0.907	0.934	0.543
Gen. Exponential	0.853	0.873	0.211	0.907	0.934	0.543

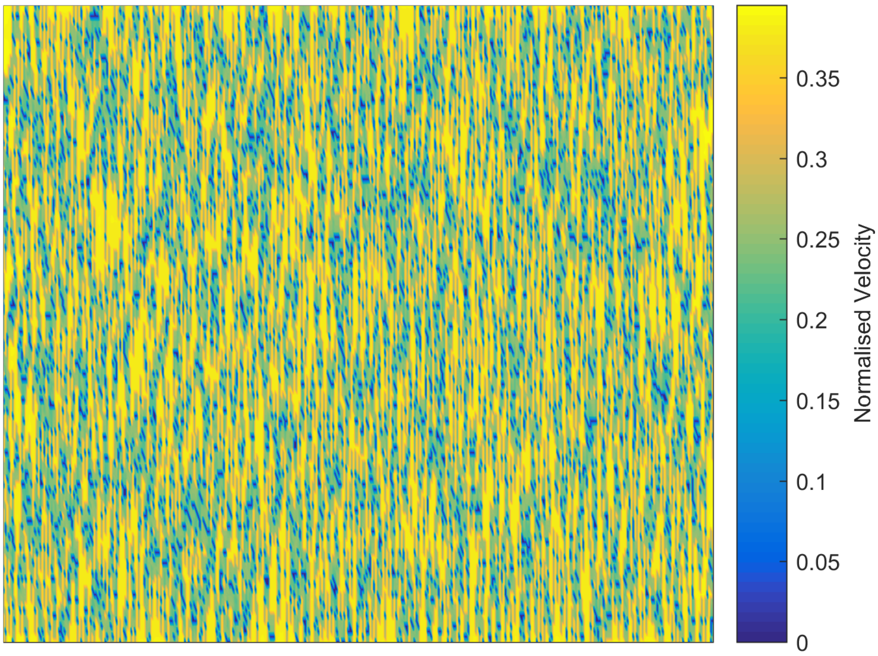

Figure 6.81 Uncertainty of the total field's estimation

DirVar2

The anisotropy parameters of the new coordinations system, estimated by means of DVF, are shown in Table 6.63, while in Fig. 6.82 are displayed the experimental directional variograms of them. The results show that despite small improvement (indicated by the proximity of the new corralation length to 1 and the new anisotropy angle to 0) the anisotropic effect remains at relatively high levels as indicated by the very small increase of the anisotropy ratios. Nevertheless, analysis procedure continues by assuming the new coordinations systems as isotropic.

By minimizing the error function of the isotropic variogram functions of the models and the corresponding experimental omnidirectional (isotropic) variograms of the new coordinations systems (see Fig. 6.83) the parameters of the isotropic models are estimated, as presented in Table 6.64. The parameters of the investigated models generally agree, except from the correlation length given by the Spartan which is significantly smaller than the other models.

The Leave-One-Out Cross Validation (LOOCV) for the estimated models gives the validation measures presented in Table 6.65. As best model derives the Generalized Mátern, followed by Generalized Exponential and Spherical. As it can be seen from Fig. 6.83), though, all the models except Spartan and Gaussian fit fairly well to their corresponding experimental omnidirectional variograms.

Table 6.63 Anisotropy parameters of the new coordinations systems

Model	Anisotropy Parameters		
	ξ_1	R	ϕ
Gen. Exponential	1.055	0.564	$-0.5°$
Gaussian	0.906	0.305	4.3°
Spherical	0.940	0.325	3.4°
Gen. Matérn	1.007	0.293	5.8°
Spartan	1.320	0.269	6.1°

Table 6.64 Optimum Parameters of the isotropic variogram models

Model	σ_z^2	ξ	c_0	ν
Gen. Exponential	0.034	1.128	0.000	1.013
Gaussian	0.033	0.797	0.000	–
Spherical	0.026	1.219	0.006	–
Gen. Matérn	0.033	1.780	0.001	0.509
	η_0	ξ	c_0	η_1
Spartan	0.044	0.089	0.000	-1.989

Table 6.65 Leave-One-Out Cross Validation Scores (see section 5.3.2

Model	MnAE	MxAE	MSE	RMSE	R_p	R_{sp}	r_F
Gen. Exponential	0.032	0.430	0.003	0.057	0.945	0.964	0.883
Gaussian	0.037	0.364	0.003	0.053	0.955	0.980	0.607
Spherical	0.036	0.420	0.004	0.061	0.937	0.960	0.661
Gen. Matérn	0.032	0.371	0.003	0.057	0.946	0.964	0.912
Spartan	0.034	0.437	0.004	0.061	0.937	0.961	0.656

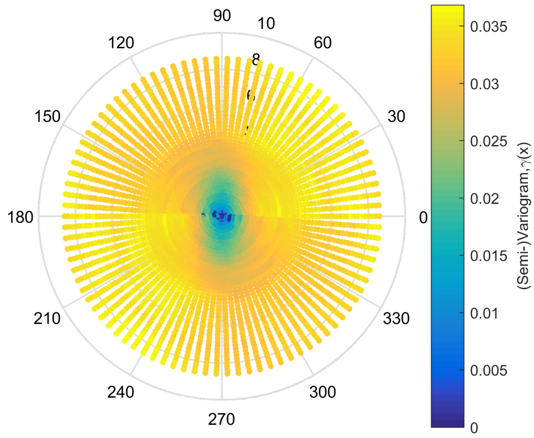

(a) Gen. Exponential

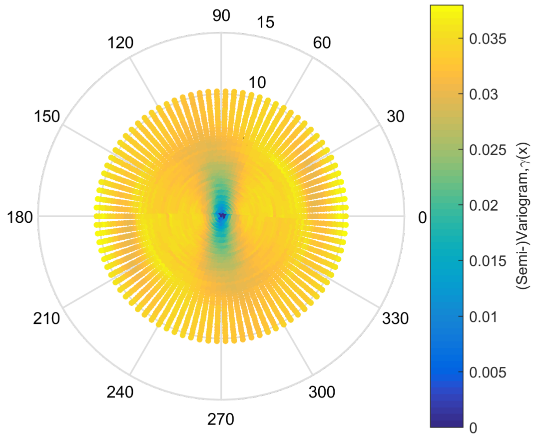

(b) Gaussian

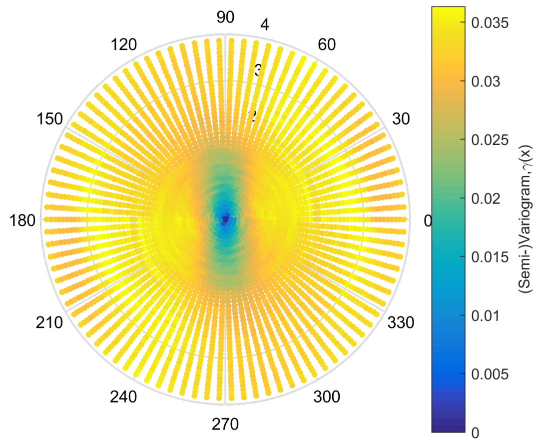

(c) Spherical

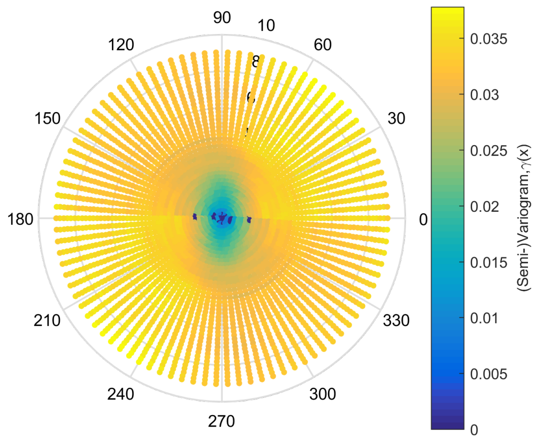

(d) Gen. Matérn

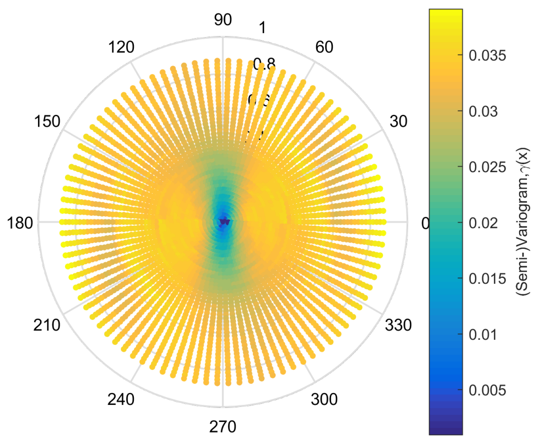

(e) Spartan

Figure 6.82 Experimental directional variograms of the new coordinations systems.

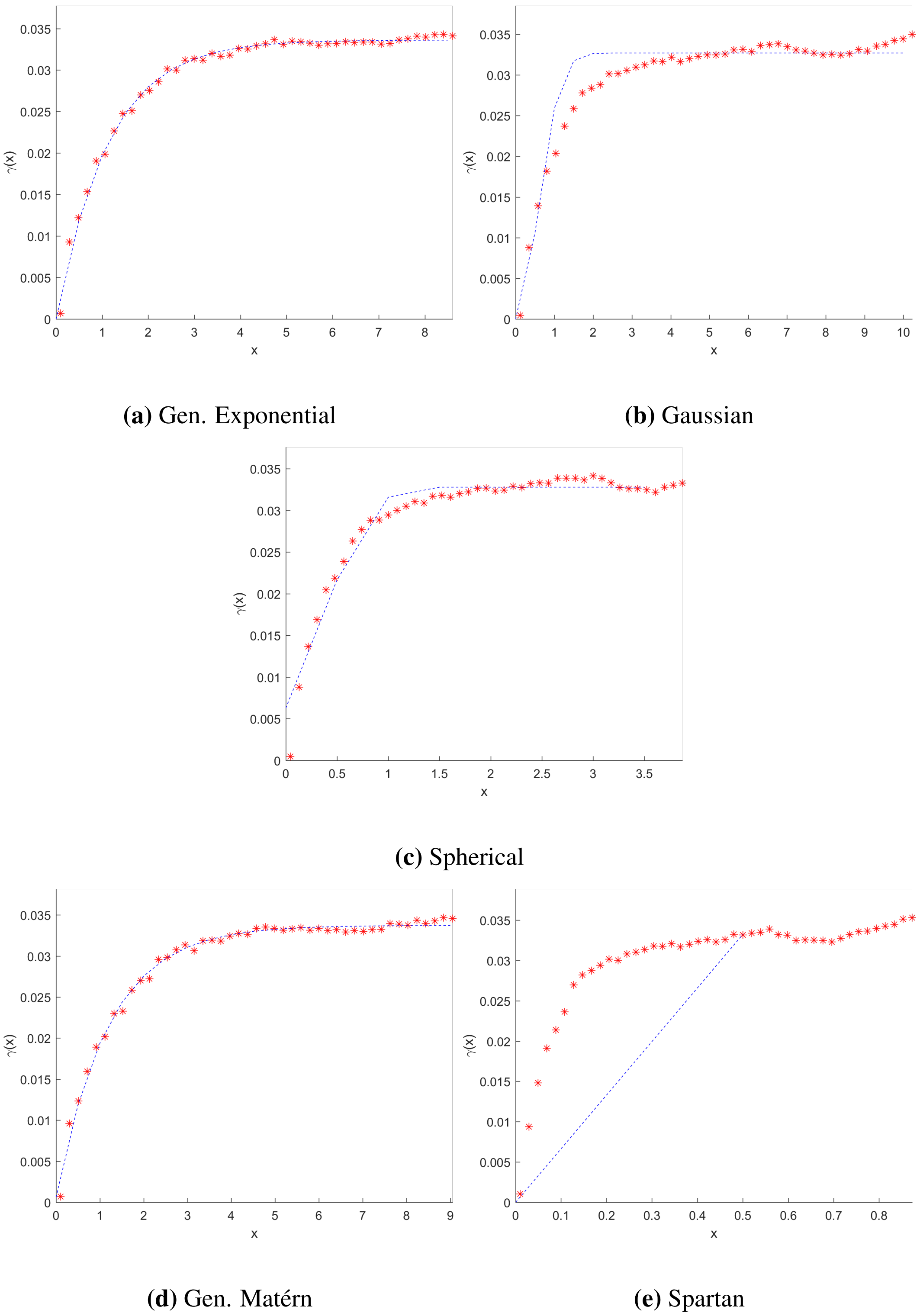

(a) Gen. Exponential

(b) Gaussian

(c) Spherical

(d) Gen. Matérn

(e) Spartan

Figure 6.83 Fitting of the theoretical models to the corresponding experimental omnidirectional variograms of the new coordinations systems.

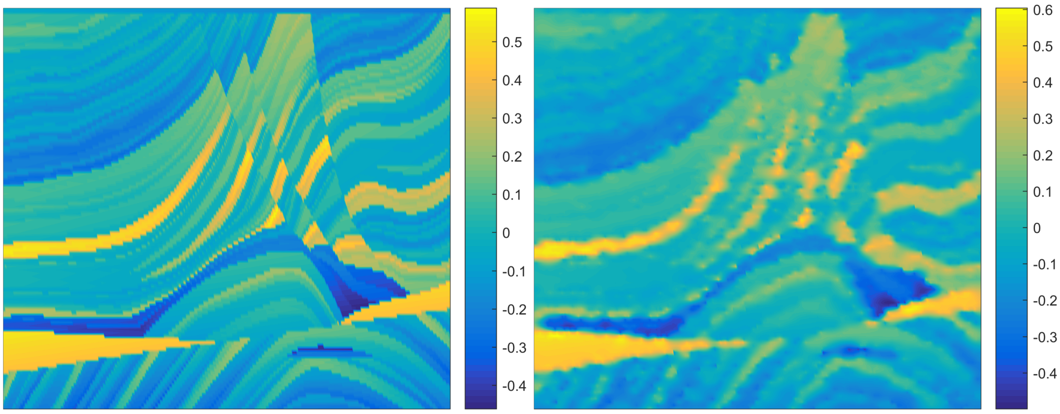

(a) Original Stochastic Component **(b)** Estimated Stochastic Component

Figure 6.84 Original and Estimation of the stochastic component of the field. The model used is a Gen. Mátern with parameters $\sigma_z^2 = 0.033, \xi = 1.780, c_0 = 0.001, \nu = 0.509$.

Table 6.66 Ordinary Kriging Scores

Model	MnAE	MxAE	MSE	RMSE	R_p	R_{sp}	r_F
Gen. Matérn	0.049	0.698	0.006	0.080	0.904	0.891	0.805
Gen. Exponential	0.054	0.763	0.008	0.087	0.885	0.876	0.554
Spherical	0.061	0.727	0.008	0.090	0.877	0.865	0.468

The estimation of the stochastic component of the field (i.e the transformed and detrended normalised velocities) resulting from OK is as shown in Fig. 6.84. The scatter diagram and histograms of the original and the estimated values of the stochastic component are, also, shown in Fig. 6.85, and the measures of the stochastic component estimation performance for the three best models are presented in Table 6.66. The resulting estimation of the total field, after the trend addition and Box-Cox transformation inversion, is as shows Fig. 6.86, and the corresponding scatter diagram and histograms are shown in Fig. 6.87. The estimations follow the original values achieving a very good proximity of the total distribution. The measures of the total field (i.e. normalised velocities) estimation performance for the three best models, presented in Table 6.67, show that their performance is similar with the first model to be slightly better. Also, the spatial distribution of the ordinary kriging estimations uncertainty is shown in Fig. 6.88. The uncertainty (as expected from theory) increases gradually from $\simeq 0.00$ near the known locations to 0.30 at great distances from them.

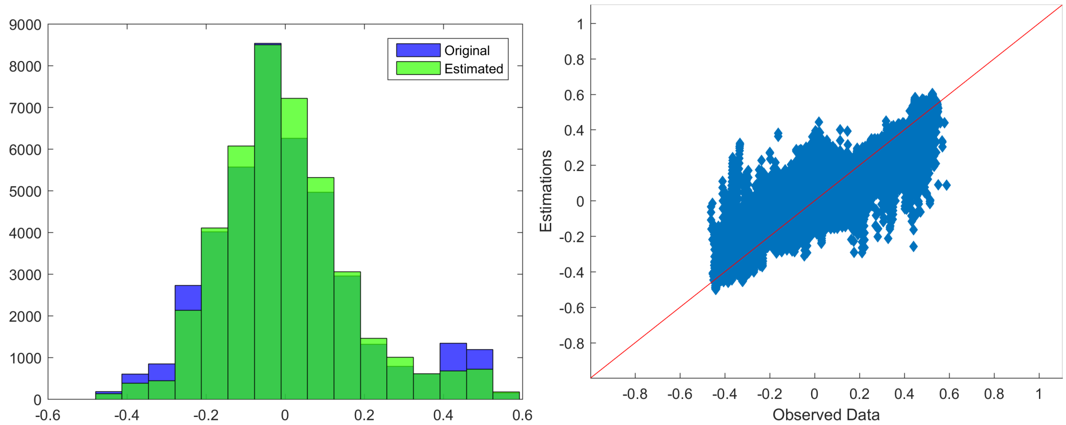

Figure 6.85 Histograms and Scatter plot of original and estimated values of the field's stochastic component. The model used is a Gen. Mátern with parameters $\sigma_z^2 = 0.033, \xi = 1.780, c_0 = 0.001, \nu = 0.509$.

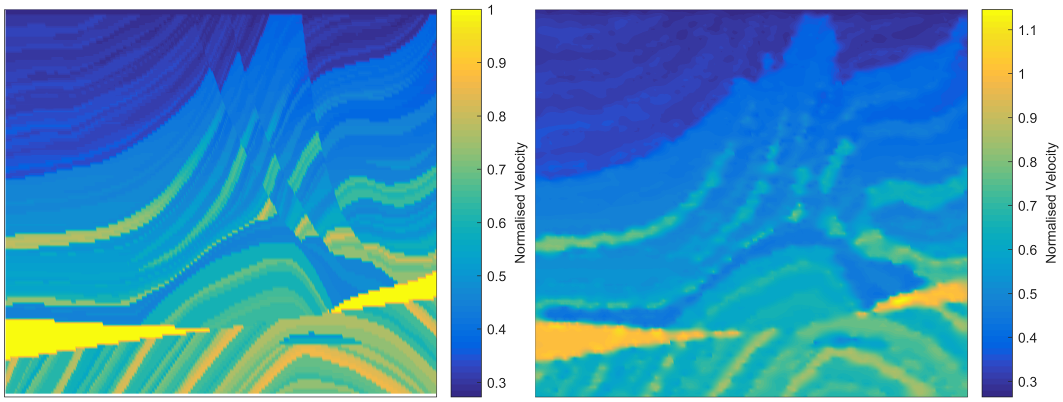

(a) Original Total Field

(b) Estimated Total Field

Figure 6.86 Original and estimated total field

Table 6.67 Total Field Estimation Scores

Model	MnAE	MxAE	MSE	RMSE	R_p	R_{sp}	r_F
Gen. Matérn	1.334	1.888	1.842	1.357	0.955	0.977	0.932
Gen. Exponential	1.334	1.909	1.842	1.357	0.952	0.974	0.926
Spherical	1.333	1.899	1.842	1.357	0.953	0.971	0.926

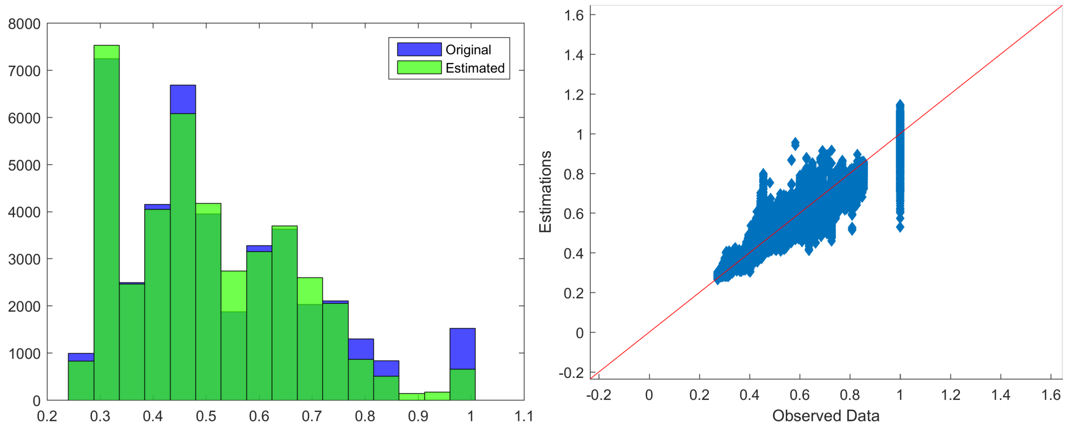

Figure 6.87 Histograms and Scatter plot of original and estimated values (total field)

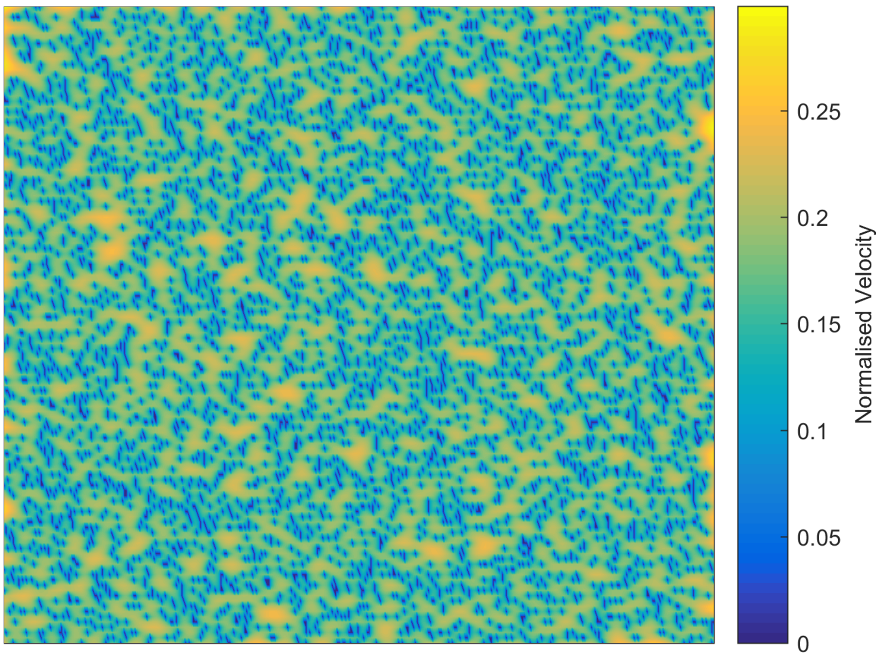

Figure 6.88 Uncertainty of the total field's estimation

Table 6.68 Classification Measures

	4 classes			16 classes		
Model	R_p	R_{sp}	**MCR**	R_p	R_{sp}	**MCR**
Gen. Matérn	0.921	0.923	0.127	0.969	0.972	0.347
Gen. Exponential	0.914	0.919	0.135	0.961	0.969	0.370
Spherical	0.904	0.911	0.153	0.958	0.966	0.420

Finally, in Table 6.68 are presented the classification measures for the cases of 4 and 16 classes. The results show that for all models the measures increase as the number of classes increase, while the first model has the best performance for any number of classes.

CHI1

The estimated anisotropy parameters are given in Table 6.69. The parameters captured by the CHI estimator indicates that the major axis of the anisotropy ellipsis is almost horizontal and is also significantly greater ($\simeq 5$ times) than the minor axis.

By replacing the estimated anisotropy parameters to the anisotropic variogram models and minimizing the error function of the new models and the experimental directional variograms the rest parameters for each model are estimated, as presented in Table 6.70. The estimated values of the variance and the nugget effect are very close but the correlation lengths differ depending on the model. The Spherical model is the one that exhibits a relatively bigger correlation length from the other models, the correlation length of which are close.

The Leave-One-Out Cross Validation (LOOCV) gives as best model the Generalized Exponential, followed by Generalized Mátern and Spartan.

The fitting of the best model to the experimental variogram along the directions of $0°, 30°, 60°, 90°, 120°$, and $150°$ is interpretted in Fig. 6.89 (the rest directional variograms can be found in Appendix A). As it can be seen the best theoretical variogram model diverges significantly from the experimental directional variograms. This can be attributed to minimization miscalculations, i.e. inappropiate objective function (very smooth or possible

Table 6.69 Anisotropy parameters of the investigated variogram models estimated with CHI method

R	ϕ
0.280	$-89.1°$

Table 6.70 Optimum Parameters of the variogram models with the lower degrees of freedom

Model	σ_z^2	ξ	c_0	ν
Gen. Exponential	0.038	0.021	0.000	0.115
Gaussian	0.026	3.533	0.008	–
Spherical	0.028	8.532	0.006	–
Gen. Matérn	0.028	1.057	0.006	3.500
	η_0	ξ	c_0	η_1
Spartan	0.857	2.618	0.000	2.000

Table 6.71 Leave-One-Out Cross Validation Scores (see section 5.3.2

Model	MnAE	MxAE	MSE	RMSE	R_p	R_{sp}	r_F
Gen. Exponential	0.040	0.391	0.004	0.062	0.937	0.955	0.895
Gaussian	0.047	0.384	0.005	0.073	0.911	0.940	0.448
Spherical	0.047	0.383	0.005	0.073	0.911	0.940	0.449
Gen. Matérn	0.043	0.438	0.005	0.069	0.919	0.947	0.546
Spartan	0.046	0.390	0.005	0.072	0.912	0.941	0.464

Table 6.72 Ordinary Kriging Scores

Model	MnAE	MxAE	MSE	RMSE	R_p	R_{sp}	r_F
Gen. Exponential	0.083	0.562	0.013	0.114	0.804	0.788	0.634
Gen. Mátern	0.086	0.788	0.016	0.127	0.736	0.734	0.355
Spartan	0.092	0.784	0.017	0.132	0.710	0.708	0.280

Table 6.73 Total Field Estimation Scores

Model	MnAE	MxAE	MSE	RMSE	R_p	R_{sp}	r_F
Gen. Exponential	1.330	1.888	1.839	1.356	0.945	0.954	0.902
Gen. Mátern	1.331	1.939	1.843	1.357	0.928	0.946	0.874
Spartan	1.331	1.933	1.842	1.357	0.925	0.941	0.867

local minima), inappropriate initial values or to the fields complexity. Thus, the analysis is continued without taking any further action.

Implementing OK with the determined best model, the resulting estimation of the stochastic component of the field (i.e the transformed and detrended normalised velocities) is as shown in Fig. 6.90. The scatter diagram and histograms of the original and the estimated values of the stochastic component are illustrated in Fig. 6.91, and the measures of the stochastic component estimation performance for the three best models are presented in Table 6.72.

The resulting estimation of the total field, after the trend addition and Box-Cox transformation inversion, is as shows Fig. 6.92, and the correspomding scatter diagram and histograms are shown in Fig. 6.93. In general, the estimations follow the original values without achieving satisfying proximity of the total distribution. Both the tails of the distribution as the middle of it exhibit significant discrepancies. The measures of the total field (i.e. normalised velocities) estimation performance for the three best models, presented in Table 6.73, show that the first model has significantly better performance than the other two which have almost the same scores. Finally, Fig. 6.94 shows the spatial distribution of the ordinary kriging estimations uncertainty. The uncertainty is zero at the known points, while at the missing points it is equal to 0.37 with slightly smaller values at the edges.

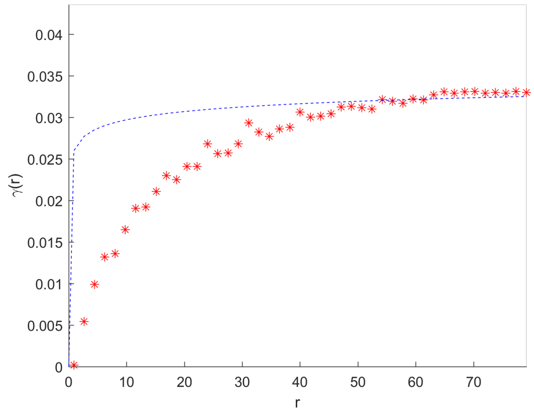

(a) 0°

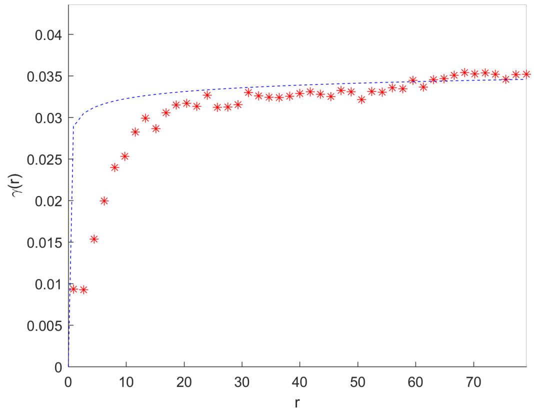

(b) 30°

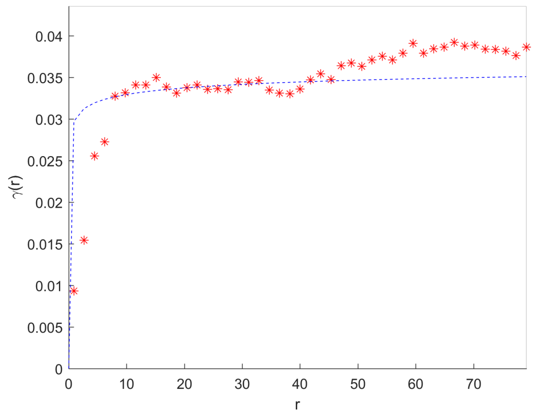

(c) 60°

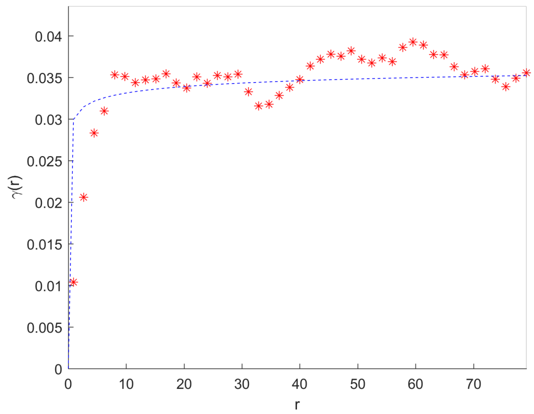

(d) 90°

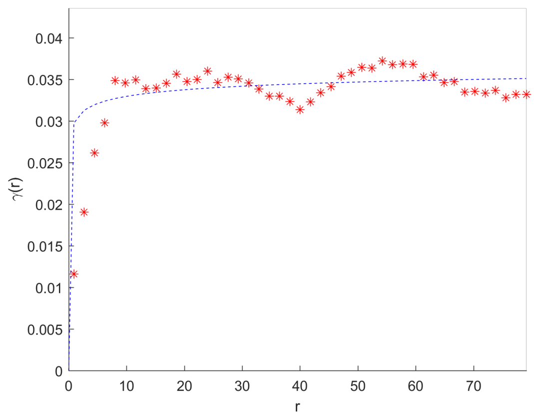

(e) 120°

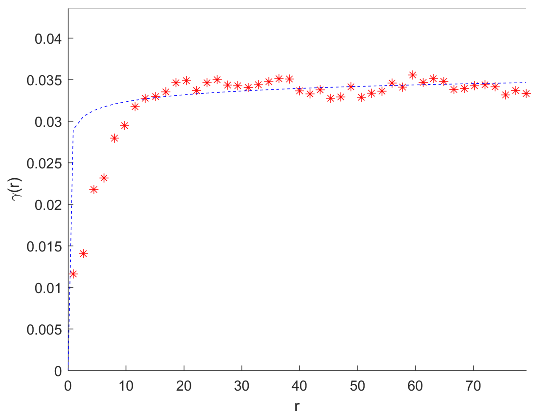

(f) 150°

Figure 6.89 Fitting of the best theoretical model to the experimental directional variograms of the field. The best model is a Gen. Exponential with parameters $\sigma_z^2 = 0.038, \xi_1 = 0.021.338, R = 0.208, \phi = -89.1^\circ, c_0 = 0.000, \nu = 0.115$. The experimental variogram is calculated with angular tolerance 20°, 45 distance lags and taking into account maximum distance equivalent to about 80.

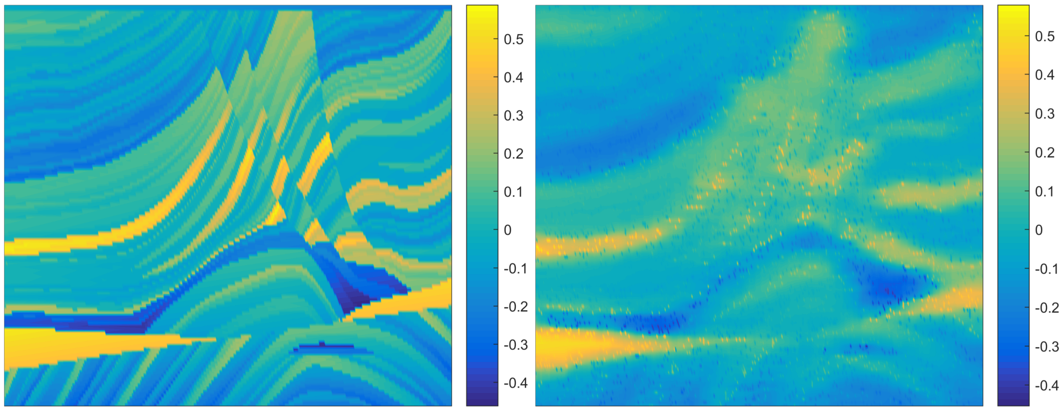

(a) Original Stochastic Component **(b)** Estimated Stochastic Component

Figure 6.90 Original and Estimation of the stochastic component of the field. The model used is a Gen. Exponential with parameters $\sigma_z^2 = 0.038, \xi_1 = 0.021.338, R = 0.208, \phi = -89.1°, c_0 = 0.000, \nu = 0.115$.

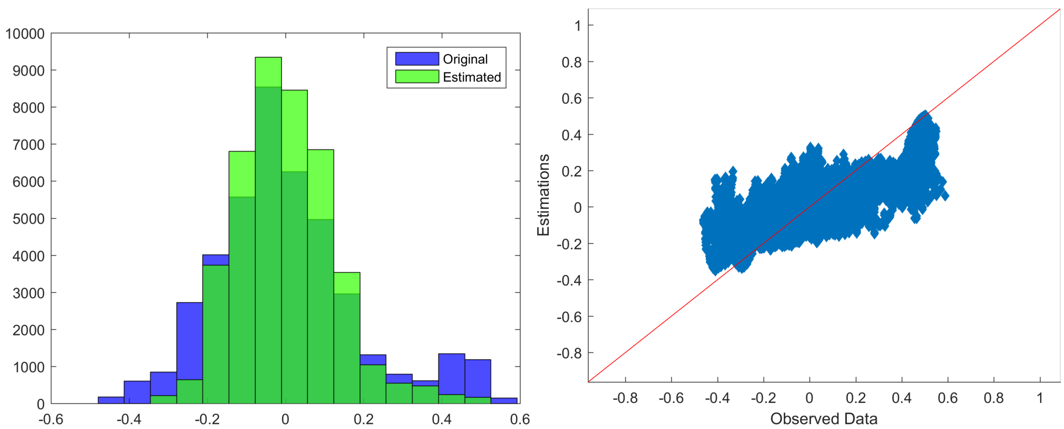

Figure 6.91 Histograms and Scatter plot of original and estimated values of the field's stochastic component. The model used is a Gen. Exponential with parameters $\sigma_z^2 = 0.038, \xi_1 = 0.021.338, R = 0.208, \phi = -89.1°, c_0 = 0.000, \nu = 0.115$.

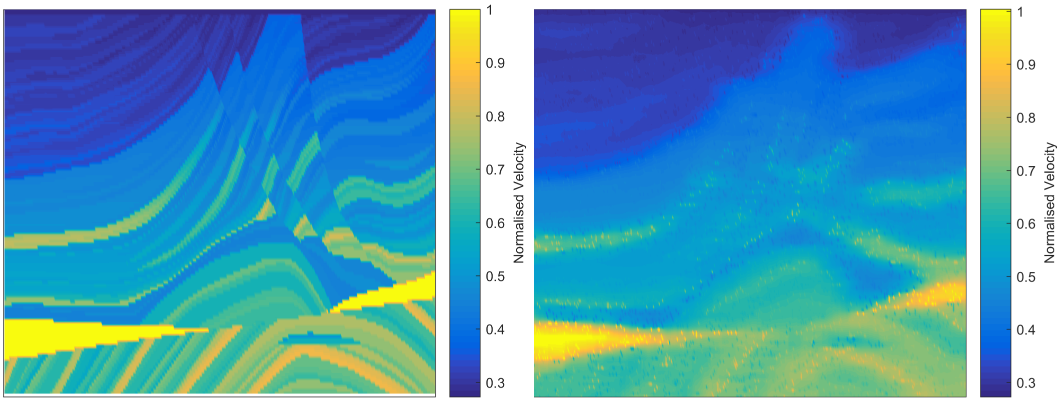

(a) Original Total Field **(b)** Estimated Total Field

Figure 6.92 Original and estimated total field

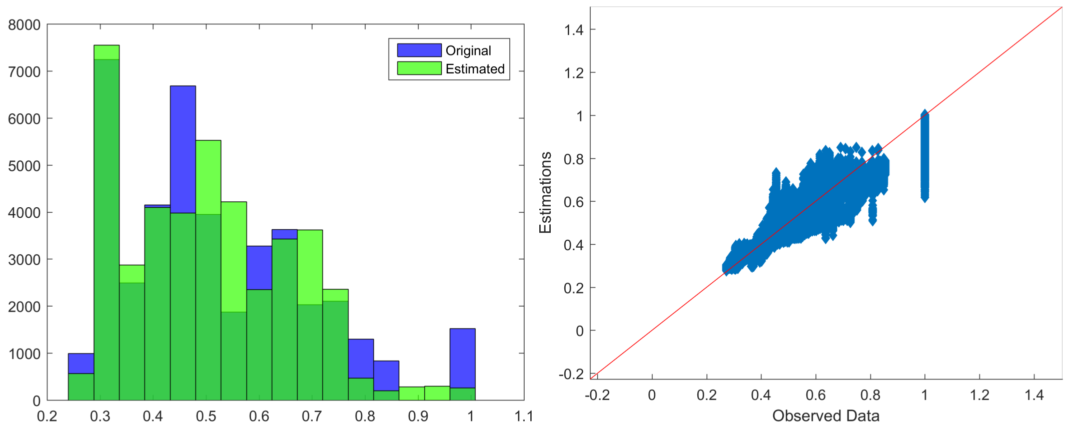

Figure 6.93 Histograms and Scatter plot of original and estimated values (total field)

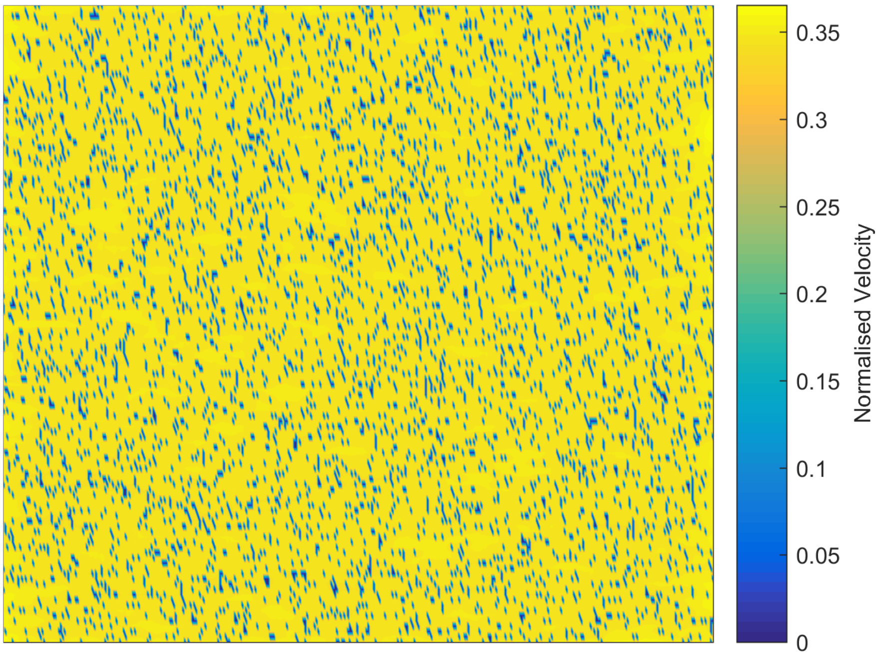

Figure 6.94 Uncertainty of the total field's estimation

Table 6.74 Classification Measures

	4 classes			16 classes		
Model	R_p	R_{sp}	**MCR**	R_p	R_{sp}	**MCR**
Gen. Exponential	0.876	0.886	0.197	0.936	0.948	0.538
Gen. Mátern	0.862	0.880	0.201	0.916	0.941	0.514
Spartan	0.856	0.874	0.209	0.909	0.935	0.541

Also, in Table 6.74 are presented the classification measures for the cases of 4 and 16 classes.

CHI2

The new anisotropy parameters, estimated by means of DVF using the 5 variogram models, are shown in Table 6.75, while in Fig. 6.95 are interpretted the experimental directional variograms of the new coordinations system. All the models give increased anisotropy ratio relatively to the original one, but they still indicate strong anisotropic characteristics. Nevertheless, analysis procedure continues by assuming the new coordinations system as isotropic.

Table 6.75 Anisotropy parameters of the new coordinations systems

Model	**Anisotropy Parameters**		
	ξ_1	R	ϕ
Gen. Exponential	12.432	0.340	5.6°
Gaussian	13.228	0.386	3.8°
Spherical	32.732	0.381	4.9°
Gen. Matérn	16.851	0.290	20.7°
Spartan	37.306	0.404	41.6°

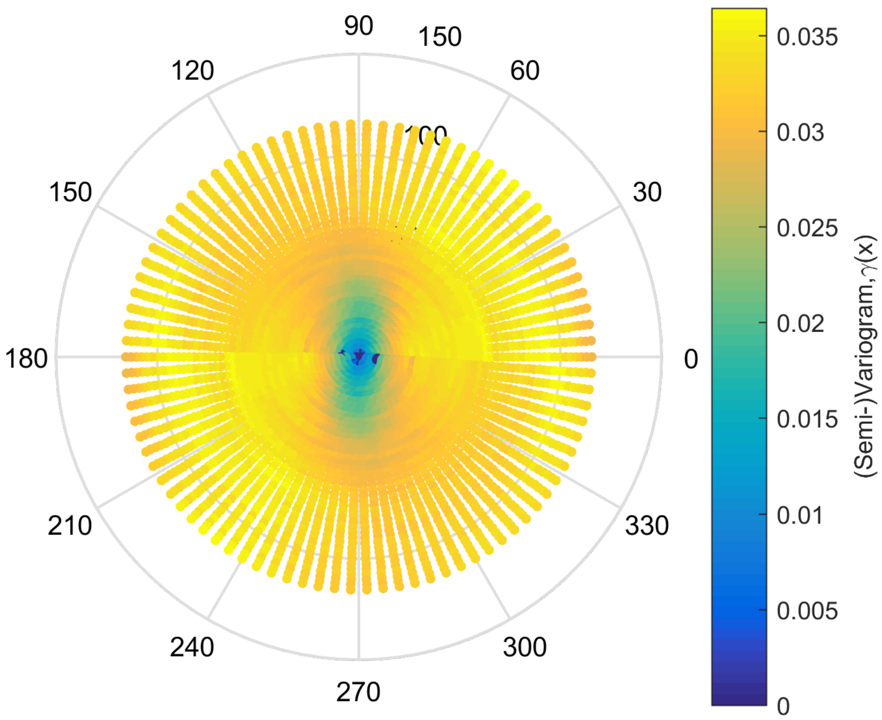

Figure 6.95 Experimental directional variograms of the new coordinations system

Table 6.76 Optimum Parameters of the isotropic variogram models

Model	σ_z^2	ξ	c_0	ν
Gen. Exponential	0.033	14.426	0.000	1.006
Gaussian	0.033	9.201	0.000	–
Spherical	0.026	41.402	0.007	–
Gen. Matérn	0.033	13.192	0.000	0.554
	η_0	ξ	c_0	η_1
Spartan	0.945	15.553	0.000	3.005

By minimizing the error function of the isotropic variogram functions of the models and the corresponding experimental omnidirectional (isotropic) variogram of the new co-ordinations system (see Fig. 6.96) the parameters of the isotropic models are estimated, as presented in Table 6.76. All the models fit well to the experimental omnidirectional variogram. Also, the estimated parameters are very close, except from the correlation lengths which differ significantly depending on the model; the Spherical model is attributed by the large value of about 42, while the rest models' correlation length range from 9 to 15.

The Leave-One-Out Cross Validation (LOOCV) for the estimated models gives the validation measures presented in Table 6.77. As best model derives the Generalized Mátern, followed by Generalized Exponential and Spartan. As it can be seen from Fig. 6.96), the above mentioned models are those that fit better to the experimental omnidirectional variogram.

The estimation of the stochastic component of the field (i.e the transformed and detrended normalised velocities) resulting from OK is as shown in Fig. 6.97. The scatter diagram and histograms of the original and the estimated values of the stochastic component are, also, shown in Fig. 6.98, and the measures of the stochastic component estimation performance for the three best models are presented in Table 6.78. The resulting estimation of the total field, after the trend addition and Box-Cox transformation inversion, is as shows Fig. 6.99, and the correspomding scatter diagram and histograms are shown in Fig. 6.100. In general, the estimations follow the original values achieving a very good proximity of the total distribution. The measures of the total field (i.e. normalised velocities) estimation performance for the three best models, presented in Table 6.79, show that their performance is identical. Also, the spatial distribution of the ordinary kriging estimations uncertainty is

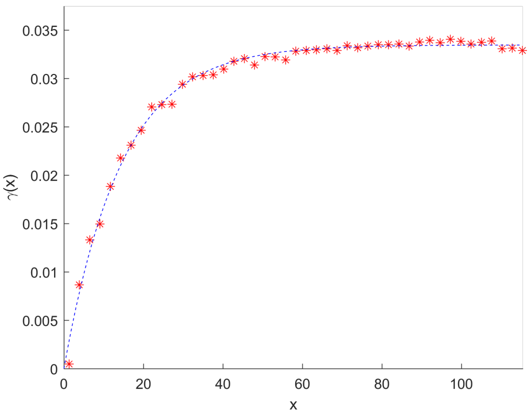

(a) Gen. Exponential

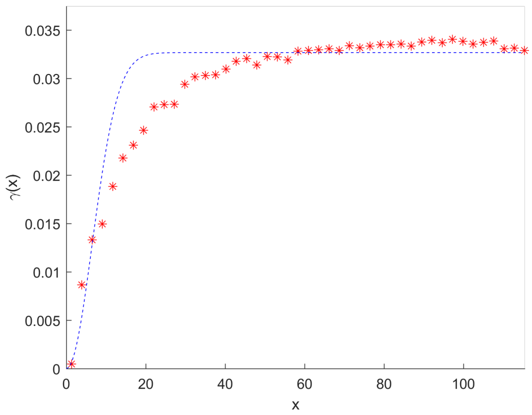

(b) Gaussian

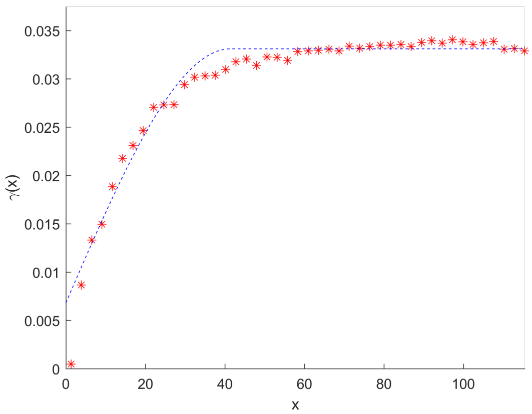

(c) Spherical

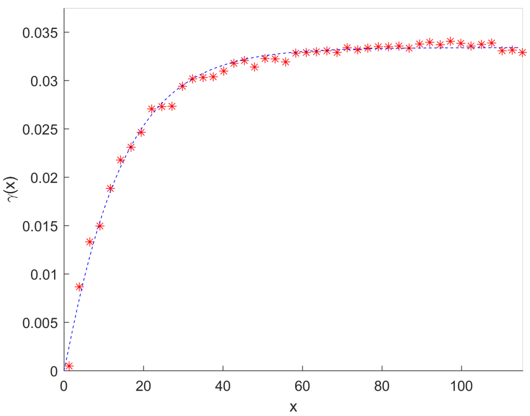

(d) Gen. Matérn

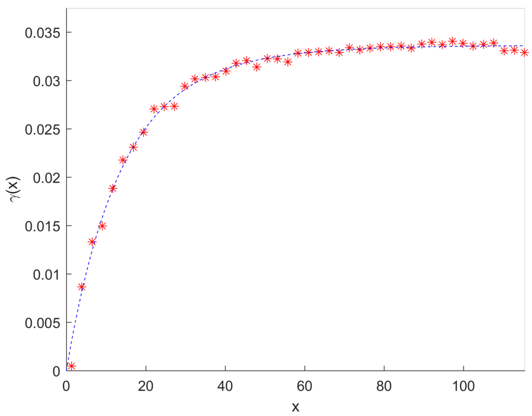

(e) Spartan

Figure 6.96 Fitting of the theoretical models to the corresponding experimental omnidirectional variograms of the new coordinations systems.

Table 6.77 Leave-One-Out Cross Validation Scores (see section 5.3.2

Model	MnAE	MxAE	MSE	RMSE	R_p	R_{sp}	r_F
Gen. Exponential	0.023	0.398	0.002	0.044	0.967	0.976	0.932
Gaussian	12.844	28071.759	254337.941	504.319	0.002	0.813	0.000
Spherical	0.029	0.365	0.002	0.049	0.960	0.972	0.602
Gen. Matérn	0.023	0.403	0.002	0.044	0.967	0.976	0.945
Spartan	0.023	0.397	0.002	0.045	0.967	0.976	0.927

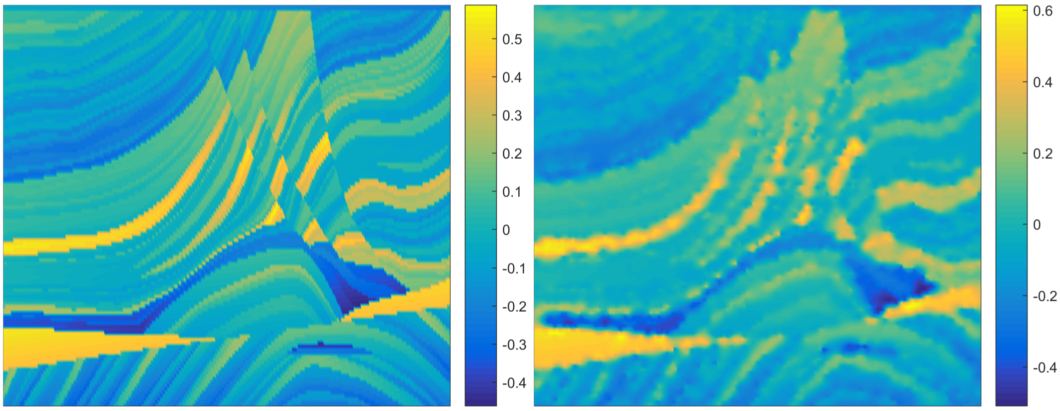

(a) Original Stochastic Component **(b)** Estimated Stochastic Component

Figure 6.97 Original and Estimation of the stochastic component of the field. The model used is a Gen. Mátern with parameters $\sigma_z^2 = 0.033, \xi = 13.192, c_0 = 0.000, \nu = 0.554$.

shown in Fig. 6.88. The uncertainty (as expected from theory) increases gradually from $\simeq 0.00$ near the known locations to 0.30 at great distance from them.

Finally, in Table 6.80 are presented the classification measures for the cases of 4 and 16 classes. The results show that for all models have almost identical performance, while the measures increase as the number of classes increase.

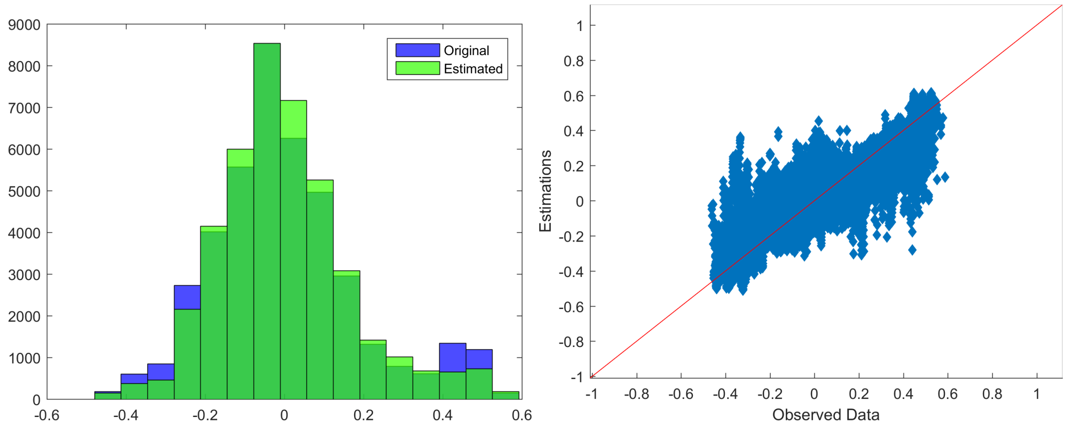

Figure 6.98 Histograms and Scatter plot of original and estimated values of the field's stochastic component. The model used is a Gen. Mátern with parameters $\sigma_z^2 = 0.033, \xi = 13.192, c_0 = 0.000, \nu = 0.554$.

Table 6.78 Ordinary Kriging Scores

Model	MnAE	MxAE	MSE	RMSE	R_p	R_{sp}	r_F
Gen. Matérn	0.048	0.721	0.006	0.080	0.903	0.892	0.806
Gen. Exponential	0.049	0.715	0.006	0.080	0.903	0.892	0.801
Spartan	0.049	0.714	0.006	0.080	0.903	0.892	0.799

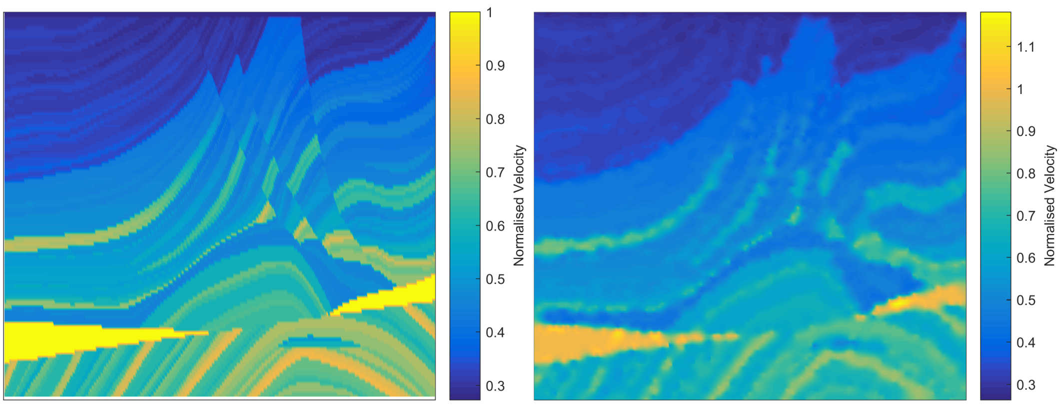

(a) Original Total Field **(b)** Estimated Total Field

Figure 6.99 Original and estimated total field

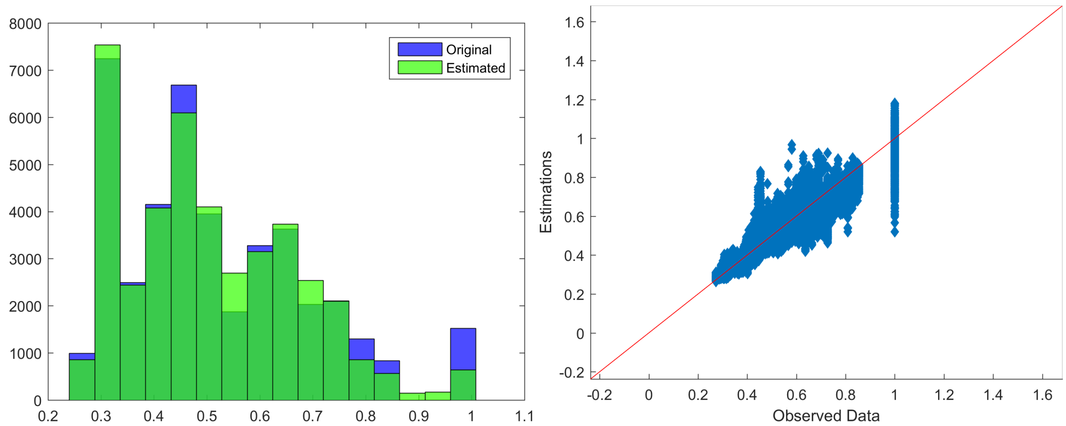

Figure 6.100 Histograms and Scatter plot of original and estimated values (total field)

Table 6.79 Total Field Estimation Scores

Model	MnAE	MxAE	MSE	RMSE	R_p	R_{sp}	r_F
Gen. Matérn	1.334	1.895	1.842	1.357	0.954	0.977	0.932
Gen. Exponential	1.334	1.895	1.842	1.357	0.955	0.977	0.933
Spartan	1.334	1.894	1.842	1.357	0.955	0.977	0.933

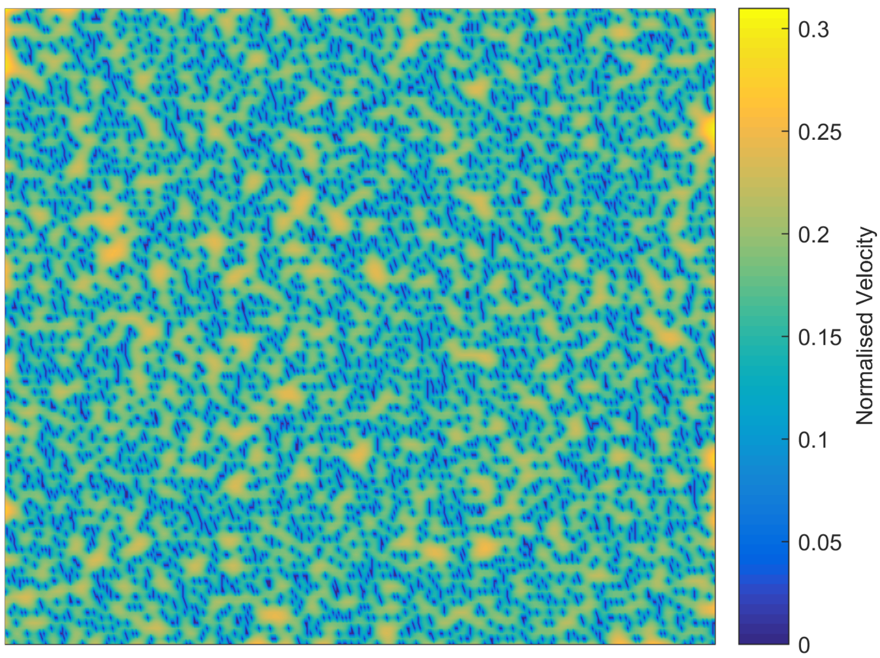

Figure 6.101 Uncertainty of the total field's estimation

Table 6.80 Classification Measures

	4 classes			16 classes		
Model	R_p	R_{sp}	**MCR**	R_p	R_{sp}	**MCR**
Gen. Matérn	0.923	0.925	0.124	0.968	0.973	0.342
Gen. Exponential	0.923	0.925	0.125	0.968	0.973	0.345
Spartan	0.922	0.925	0.125	0.968	0.972	0.346

6.5.2 DGC Simulation

The DGC simulation method is applied to the original dataset (i.e normalised velocities) in one step. The simulation is calculated using 4, 16 and 100 classes. The final results are interpretted in Figs. 6.102, 6.103, and 6.104 along with the histograms of the original and the estimated data and the distribution of the uncertainty of the estimations. The neighboorhood used for the DGC simulation procedure is the same as the one used in OK, i.e 22x4. Finally, some measures of the DGC simulation performance are summarized in Table 6.81. The classification results show that the increasing of the number of classes from 4 to 16 leads to lower errors and higher correlation coefficient. This can be explained by the fact that the field is described better by a more complex model. The misclassification rate, on the contrary, increases with the increasing of the N_c due to the thinning of the bins which affects negatively the accuracy of the estimations. On the other hand, the results obtained by increasing the number of classes to 100 show that the interpolation performance is relatively close to the classification with $N_c = 16$, with slightly higher errors and smaller correlation but significantly higher MCR than the later.

Table 6.81 DGC Validation Measures

Classes	MnAE	RMSE	R_p	MCR
4	0.070	0.080	0.860	0.178
16	0.042	0.077	0.901	0.364
100	0.048	0.085	0.880	0.912

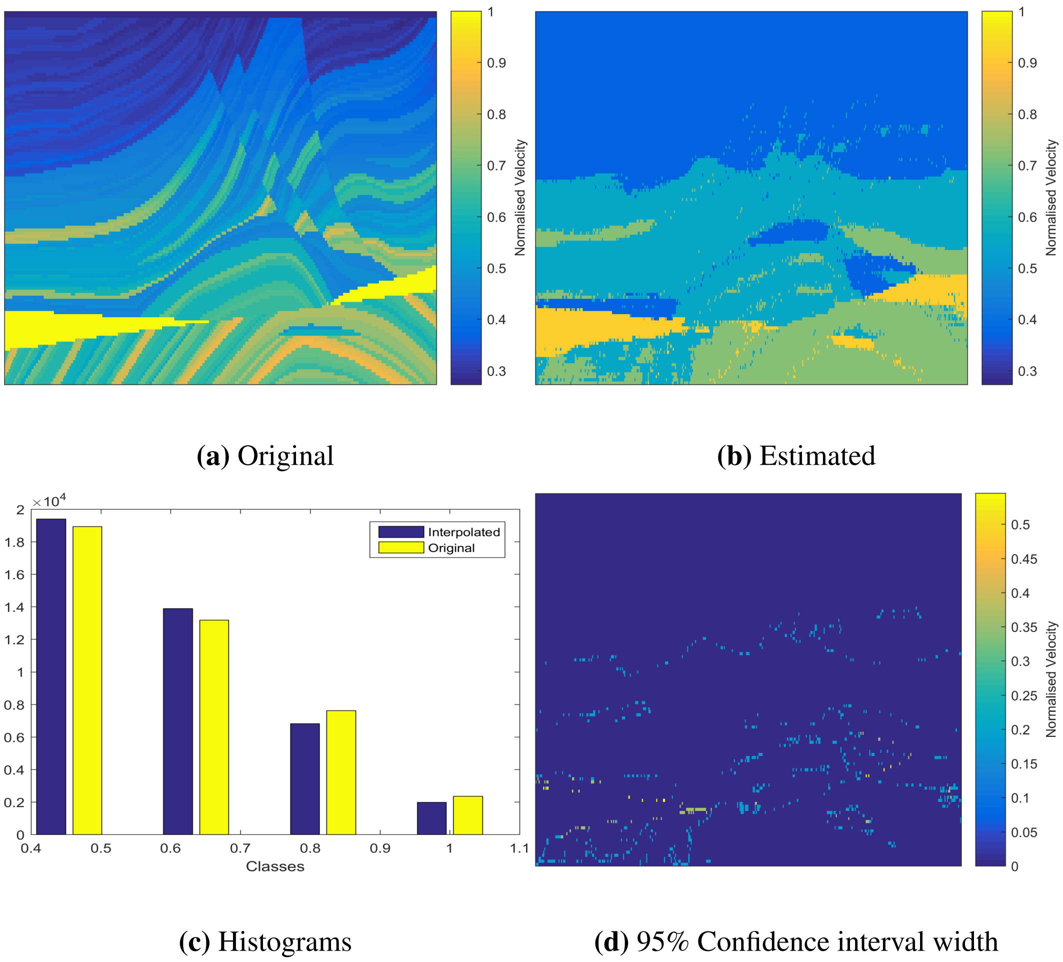

Figure 6.102 Results of DGC simulation with 4 classes

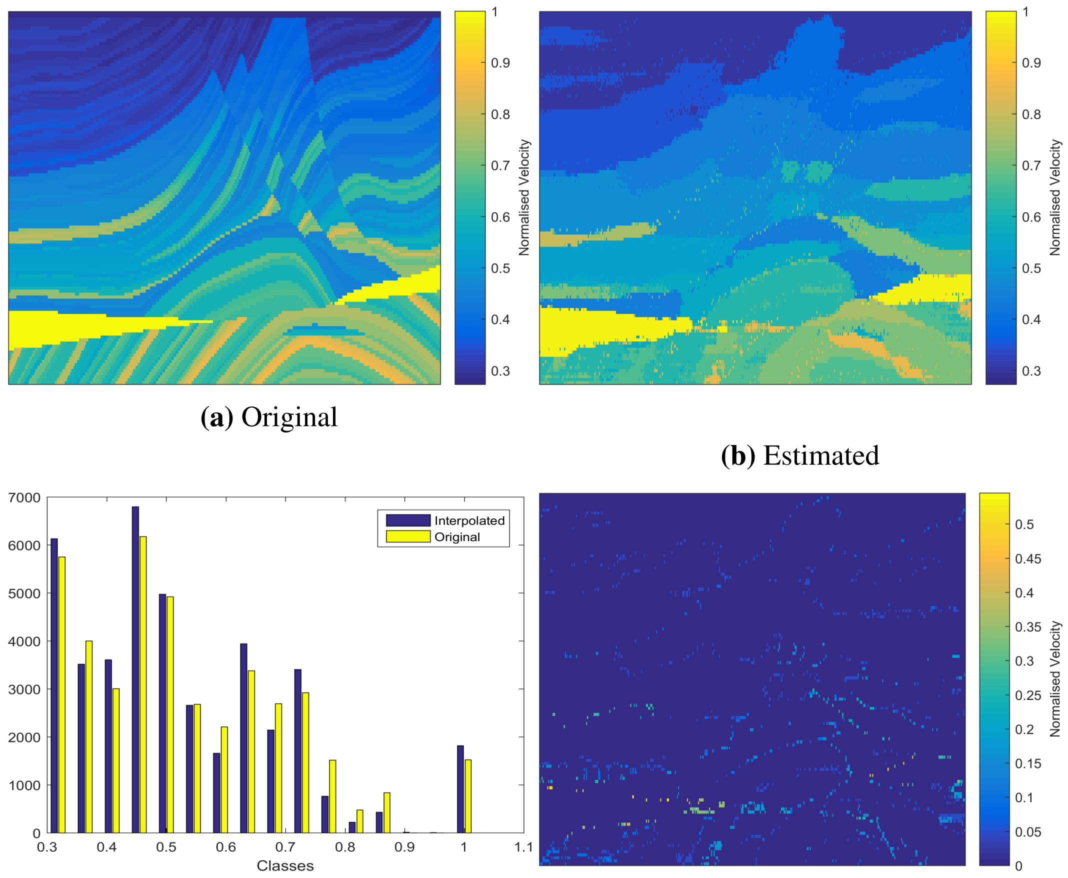

(a) Original

(b) Estimated

(c) Histograms

(d) 95% Confidence interval width

Figure 6.103 Results of DGC simulation with 16 classes

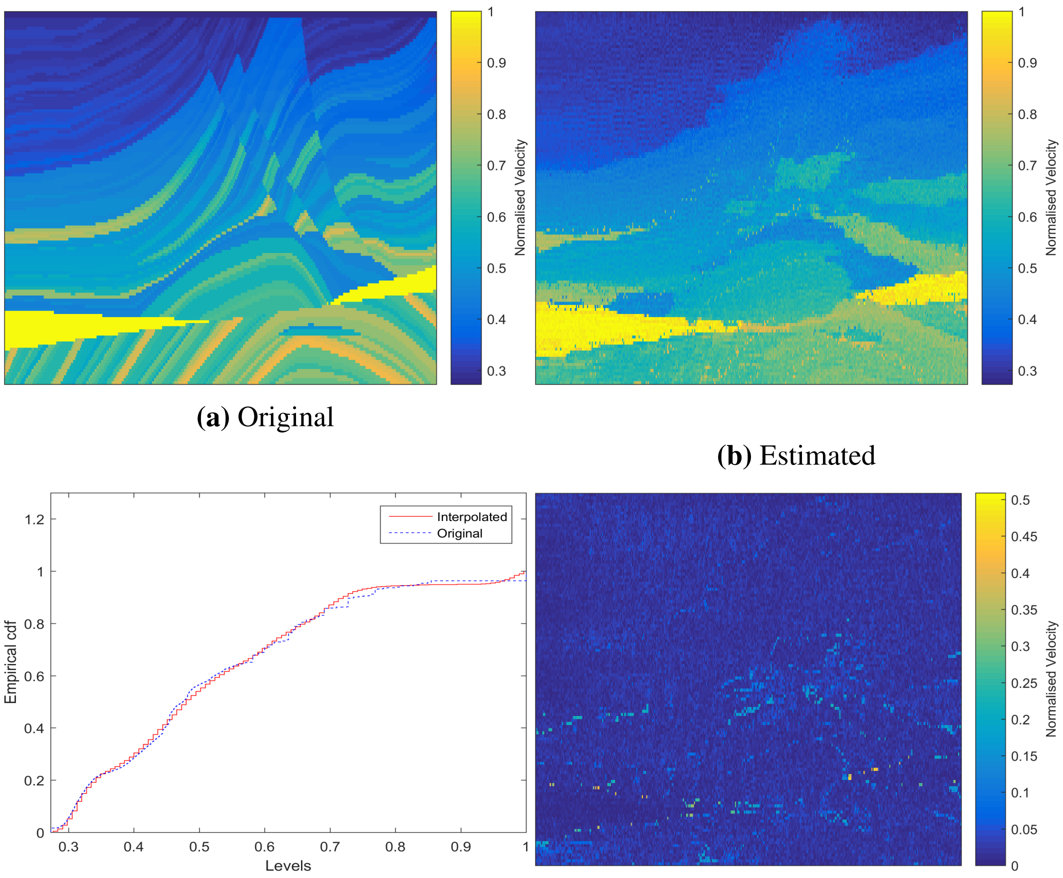

(a) Original

(b) Estimated

(c) Empirical cdf

(d) 95% Confidence interval width

Figure 6.104 Results of DGC simulation with 100 classes

6.5.3 Synopsis

The results of the methods applied to the analysis of the investigated field's random sample are summarized in Table 6.82. These results show that the best methods for the reconstruction of the Marmousi model are the variations *DirVar2* and *CHI2*, which exhibit equal performance. As regards the investigated models, no one shows significantly better performance. However, the Generalized Exponential model is always amongst the three best models. The DGC simulation method has shown comparative performance rates to those of OK estimation, but slightly lower from the later. Notable is also the fact that in all methods the increase of the number of classes results to the improvement of the estimations as indicated by the increase of the correlation coefficients. However, in the DGC method the increase of the classes leads also to the worsening of the misclassification rate, as the complexity of the procedure increases.

Table 6.82 Summarized results for the random sample

		Interpolation			4 Classes		16 Classes	
Method	**Model**	**MnAE**	**RMSE**	R_p	R_p	**MCR**	R_p	**MCR**
DirVar0	**Gen. Expon.**	1.331	1.357	0.927	0.857	0.208	0.912	0.537
	Spartan	1.329	1.357	0.931	0.855	0.219	0.911	0.579
	Spherical	1.329	1.357	0.930	0.855	0.219	0.911	0.580
DirVar1	**Spartan**	1.331	1.359	0.904	0.838	0.221	0.888	0.537
	Gen. Matérn	1.331	1.357	0.923	0.854	0.211	0.907	0.543
	Gen. Expon.	1.331	1.357	0.923	0.853	0.211	0.907	0.543
DirVar2	**Gen. Matérn**	1.334	1.357	0.955	0.921	0.127	0.969	0.347
	Gen. Expon.	1.334	1.357	0.952	0.914	0.135	0.961	0.370
	Spherical	1.333	1.357	0.953	0.904	0.153	0.958	0.420
CHI1	**Gen. Expon.**	1.330	1.356	0.945	0.876	0.197	0.936	0.538
	Gen. Mátern	1.331	1.357	0.928	0.862	0.201	0.916	0.514
	Spartan	1.331	1.357	0.925	0.856	0.209	0.909	0.541
CHI2	**Gen. Matérn**	1.334	1.357	0.954	0.923	0.124	0.968	0.342
	Gen. Expon.	1.334	1.357	0.955	0.923	0.125	0.968	0.345
	Spartan	1.334	1.357	0.955	0.922	0.125	0.968	0.346
DGC	–	0.048	0.085	0.880	0.860	0.178	0.901	0.364

6.6 Problems Encountered

During the above work two major problems were encountered: a) the common entrapement of optimization algorithms in local minima, and b) the non positive-definiteness of some covariance matrices used in the application of OK estimations.

The first problem is crucial for the accuracy and the reliability of the inferred parameters and thus influences significantly the steps following. This problem is strongly related to user defined parameters, such as the maximum distance taken into account in the calculation of the experimental variograms and the number of bins of this distance, to the selection of objective function that is minimized, and to the algorithm employed for the minimization. This issue, for simplicity was addressed by assuming that the selected user defined parameters, objective function (Eq. (5.8)) and optimization algorithm give reliable results. This assumption is not necessarily adequate in all cases. As described in chapter 6, in a few cases the inferred variogram model does not fit well to the corresponding experimental variograms.

Regarding the non positive definiteness of the calculated covariance matrices (despite mathematical proof (see *Bochner's theorem* in section 2.5) that every permissible covariance function as positive definite) it can be attributed to the fast convergence of the majority of permissible covariance function to zero in long distances. This leads to sparse matrices (matrices with many zero elements) that do not have positive eigenvalues. The solution adopted to this problem was the restriction of the neighboorhood size used for OK, which was arbitrarily chosen as described in the previous sections.

Chapter 7

Conclusions

7.1 Conclusions

The main goal of this thesis was to investigate whether geostatistical tools can be used for the simulation geophysical properties based on partial information (i.e., data sets with missing data), and more specifically for the simulation of a synthetic geological media stratigraphic data set. For this purpose two geostatistical methods were applied, Ordinary Kriging and Directional Gradient-Curvature simulation, to reconstruct the Marmousi dataset, a synthetic 2D acoustic model (workshop of 52nd EAEG meeting in 1990), using as data a random and a regular (drill-holes) sample of the entire model. In the case of OK, five methods of parameter inference were used. These methods differed regarding anisotropy estimation (i.e. parametric versus non parametric) and data transformation (transform data to isotropic or not). The results of these methods are summarized in Tables 7.1 and 7.2 for the regular and the random sampling, respectively.

As regards the adequacy of geostatistical tools in geological media simulation, this thesis showed that they can be very helpful if the available data can provide enough information about the investigated property. Then, the geostatistical tools can be used to supplement existing geophysical methods.

Performance measures for both types of sampling (see Tables 7.1 and 7.2) show that all the methods can give relatively good estimates of the missing values, as the achieved correlations between the reconstructed dataset and the real data are high. Moreover, the evaluation and comparison of the methods shows that the OK methods with the best performance are those including separate estimation of anisotropy and data transformation to isotropy, i.e *DirVar2* and *CHI2*. Finally, the DGC simulation method has shown comparable but slightly inferior performance measures to OK estimation. We believe that this is due to the local nature of the latter in contrast with kriging, which accounts for correlations with longer range.

Table 7.1 Summarized scores for the regular sample

		Interpolation			4 Classes		16 Classes	
Method	**Model**	**MnAE**	**RMSE**	R_p	R_p	**MCR**	R_p	**MCR**
DirVar0	**Spherical**	1.317	1.343	0.935	0.860	0.220	0.916	0.584
DirVar1	**Spartan**	1.317	1.343	0.932	0.856	0.219	0.912	0.578
DirVar2	**Gen. Expon.**	1.321	1.343	0.960	0.929	0.116	0.972	0.317
CHI1	**Spherical**	1.317	1.343	0.929	0.848	0.228	0.904	0.591
CHI2	**Spartan**	1.321	1.343	0.959	0.930	0.114	0.974	0.295
DGC	–	0.045	0.079	0.894	0.858	0.193	0.915	0.465

Table 7.2 Summarized scores for the random sample

		Interpolation			4 Classes		16 Classes	
Method	**Model**	**MnAE**	**RMSE**	R_p	R_p	**MCR**	R_p	**MCR**
DirVar0	**Gen. Expon.**	1.331	1.357	0.927	0.857	0.208	0.912	0.537
DirVar1	**Spartan**	1.331	1.359	0.904	0.838	0.221	0.888	0.537
DirVar2	**Gen. Matérn**	1.334	1.357	0.955	0.921	0.127	0.969	0.347
CHI1	**Gen. Expon.**	1.330	1.356	0.945	0.876	0.197	0.936	0.538
CHI2	**Gen. Matérn**	1.334	1.357	0.954	0.923	0.124	0.968	0.342
DGC	–	0.048	0.085	0.880	0.860	0.178	0.901	0.364

Notable is also the fact that in all methods the increase of the number of classes improves the correlation coefficients, but leads to higher misclassification rates.

7.2 Future Studies

In future research, the improvement of the developed geostatistical codes should be the first goal. Improving the optimization step could be essential. A sensitivity analysis that explores the effect of the user defined parameters (i.e. maximum distance taken into account in the calculation of the experimental variograms, number of bins of this distance, objective function that is minimized, algorithm employed for the minimization) could provide useful information. Moreover, different parameter inference methods, such as method of moments and maximum likelihood estimation, could be used. Enhancement of the currently used methods by calculating the derivatives of objective function can also be investigated.

Another point of interest could be the tackling of the non positive-definite matrices that appear in the ordinary kriging step. Also, a comparison of these codes with other existing algorithms could be crucial for the assessment of their performance.

Finally, the implementation of different estimation and simulation methods, such as indicator kriging or plurigaussian simulation method, should be explored. A challenging but promising alternative could also be the analysis of the data with non stationary statistics, in order to tackle the high complexity of the observed patterns.

Bibliography

Adler, R. J. and Taylor, J. E. (2007). *Random Fields and Geometry*. Springer Monographs in Mathematics. Springer. 6

Agou, V. (2016). Geostatistical analysis of precipitation on the island of crete. Master's thesis, Technical University of Crete. 1

Akaike, H. (1974). A new look at the statistical model identification. *IEEE Transactions on Automatic Control*, 19(6):716–723. 40

Bargaoui, Z. K. and Chebbi, A. (2009). Comparison of two kriging interpolation methods applied to spatiotemporal rainfall. *Journal of Hydrology*, 365(1):56–73. 1

Barnett, V. (1981). *Interpreting Multivariate Data*. Wiley series in probability and mathematical statistics: Applied probability and statistics. Wiley. 3

Bochner, S., Tenenbaum, M., and Pollard, H. (1959). *Lectures on Fourier Integrals. Annals of Mathematics Studies*. Princeton University Press. 18

Bourgeois, A., Bourget, M., Lailly, P., Poulet, M., Ricarte, P., and Versteeg, R. (1990). Marmousi, model and data. In *EAEG Workshop-Practical Aspects of Seismic Data Inversion*. 1, 51

Bowman, K. O. and Shenton, L. R. (2004). Estimation: Method of moments. *Encyclopedia of statistical sciences*. 43

Box, G. E. P. and Cox, D. R. (1964). An analysis of transformations. *Journal of the Royal Statistical Society. Series B*, 26(2):211–252. 38

Brognon, G. P. and Verrier, G. R. (1966). Oil and geology in cuanza basin of angola. *AAPG Bulletin*, 50(1):108–158. 51

Burrough, P., McDonnell, R., and Lloyd, C. D. (2013). *Principles of Geographical Information Systems:3rd Revised*. Oxford University Press, 1st edition. 3

Casella, G. and Berger, R. L. (2001). *Statistical Inference*. Duxbury Press, 2nd edition. 8

Chentsov, N. N. (1957). Lévy brownian motion for several parameters and generalized white noise. *Theory of Probability and Its Applications*, 2(2):265–266. 33

Chilès, J.-P. and Delfiner, P. (2012). *Geostatistics: Modeling Spatial Uncertainty*. Wiley Series in Probability and Statistics. Wiley, 2nd edition. 4, 5, 12, 13, 19, 28

Chorti, A. and Hristopulos, D. T. (2008). Nonparametric identification of anisotropic (elliptic) correlations in spatially distributed data sets. *IEEE Transactions on signal processing*, 56(10):4738–4751. 43, 44

Christakos, G. (1992). *Random Field Models in Earth Sciences*. Academic Press, 2nd edition edition. 1

Cressie, N. (1990). The origins of kriging. *Mathematical geology*, 22(3):239–252. 1, 27

Deutsch, C. V. (2002). *Geostatistical Reservoir Modeling*. Oxford university press, 1st edition. 1

Fisher, R. A. (1997). On an absolute criterion for fitting frequency curves. *Statistical Science*, 12(1):39–41. 42

Galetakis, M. (1998). Evaluation of multiple seam lignite deposits of ptolemaes area, using statistical methods. *Mineral Wealth*, 107:55–64. 1

Geisser, S. (1975). The predictive sample reuse method with applications. *Journal of the American Statistical Association*, 70(350):320–328. 45

Geisser, S. (1993). *Predictive Inference*, volume 55. CRC press. 45

Goovaerts, P. (1997). *Geostatistics for Natural Resources Evaluation*. Oxford University Press. 1, 28, 30, 37

Greene, H. J. (1992). *Evaluation of corrosion protection methods for aluminum metal matrix composites*. PhD thesis, University of Southern California. 1

Guttorp, P. and Gneiting, T. (2006). Studies in the history of probability and statistics xlix on the matérn correlation family. *Biometrika*, 93(4):989–995. 19

Hristopulos, D. T. (2002). New anisotropic covariance models and estimation of anisotropic parameters based on the covariance tensor identity. *Stochastic Environmental Research and Risk Assessment*, 16(1):43–62. 43

Hristopulos, D. T. and Elogne, S. N. (2007). Analytic properties and covariance functions for a new class of generalized gibbs random fields. *IEEE Transactions on Information Theory*, 53(12):4667–4679. 19, 36

Irons, T. (2008). Marmousi model. http://reproducibility.org/RSF/book/data/marmousi/paper.pdf, *Accesed on 10 March 2017*. 51

Kelkar, M. and Perez, G. (2002). *Applied Geostatistics for Reservoir Characterization*. Richardson, Tex.: Society of Petroleum Engineers. 1

Khoshnevisan, D. (2002). *Multiparameter Processes: An Introduction to Random Fields*. Springer Monographs in Mathematics. Springer. 6

Kindermann, R. (1980). *Markov Random Fields And Their Applications*. Contemporary mathematics 1. American Mathematical Society. 6

Kitanidis, P. K. (1997). *Introduction to Geostatistics: Applications in Hydrogeology*. Cambridge University Press. 8

Kolmogorov, A. N. (1960). *Foundations of the Theory of Probability*. Chelsea Pub Co, 2nd edition. 6

Krige, D. G. (1951). A statistical approach to some basic mine valuation problems on the witwatersrand. *Journal of the Southern African Institute of Mining and Metallurgy*, 52(6):119–139. 1, 27

Lantuéjoul, C. (2013). *Geostatistical Simulation: Models and Algorithms*. Springer Science & Business Media. 4

Liu, H., Shi, J., and Erdem, E. (2010). Prediction of wind speed time series using modified taylor kriging method. *Energy*, 35(12):4870–4879. 1

Mantoglou, A. and Wilson, J. L. (1982). The turning bands method for simulation of random fields using line generation by a spectral method. *Water Resources Research*, 18(5):1379–1394. 33

Mariethoz, G. and Renard, P. (2010). Reconstruction of incomplete data sets or images using direct sampling. *Mathematical Geosciences*, 42(3):245–268. 1

Matheron, G. (1971). *The Theory of Regionalized Variables and Its Applications*. Centre de Morphologie Mathématique Fontainebleau: Les cahiers du Centre de Morphologie Mathématique de Fontainebleau. École national supérieure des mines. 1

Olea, R. A. (2006). A six-step practical approach to semivariogram modeling. *Stochastic Environmental Research and Risk Assessment*, 20(5):307–318. 42

Oliver, M. A. and Webster, R. (2015). *Basic Steps in Geostatistics: The Variogram and Kriging*. SpringerBriefs in Agriculture. Springer. 28

Papadimitriou, C. H. and Steiglitz, K. (1982). *Combinatorial Optimization: Algorithms and Complexity*. Prentice Hall. 36

Papadopoulou, M., Varouchakis, E., and Karatzas, G. (2009). Simulation of complex aquifer behavior using numerical and geostatistical methodologies. *Desalination*, 237(1-3):42–53. 1

Papoulis, A. and Pillai, S. U. (2002). *Probability, Random Variables and Stochastic Processes*. McGraw-Hill Europe, 4th edition. 8

Pardo-Igúzquiza, E. (1998). Maximum likelihood estimation of spatial covariance parameters. *Mathematical Geology*, 30(1):95–108. 42

Pavlides, A., Hristopulos, D. T., Roumpos, C., and Agioutantis, Z. (2015). Spatial modeling of lignite energy reserves for exploitation planning and quality control. *Energy*, 93(P2):1906–1917. 1

Petrakis, M. P. (2012). Elliptical anisotropy statistics on spatial data and geostatistical applications. Master's thesis, Technical University of Crete. 43

Petrakis, M. P. and Hristopulos, D. T. (2012). Elliptical anisotropy statistics of two-dimensional differentiable gaussian random fields: Joint probability density function and confidence regions. *arXiv preprint arXiv:1203.5010*. 43

Rozanov, Y. A. (1982). *Markov Random Fields*. Springer-Verlag New York. 6

Schwarz, G. (1978). Estimating the dimension of a model. *The Annals of Statistics*, 6(2):461–464. 40

Seni, G. and Elder, J. F. (2010). Ensemble methods in data mining: Improving accuracy through combining predictions. *Synthesis Lectures on Data Mining and Knowledge Discovery*, 2(1):1–126. 45

Shumway, R. H. and Stoffer, D. S. (2011). *Time Series Analysis and Its Applications: With R Examples*. Springer Texts in Statistics. Springer-Verlag New York, 3rd edition. 12

Spathopoulos, F. (1996). An insight on salt tectonics in the angola basin, south atlantic. *Geological Society, London, Special Publications*, 100(1):153–174. 51

Swerling, P. (1962). Statistical properties of the contours of random surfaces. *IRE Transactions on Information Theory*, 8(4):315–321. 44

Thijssen, J. (2016). *A Concise Introduction to Statistical Inference*. Chapman and Hall/CRC. 8

Tobler, W. R. (1970). A computer movie simulating urban growth in the detroit region. *Economic geography*, 46(sup1):234–240. 3

Varouchakis, E., Giannakis, G., Lilli, M., Ioannidou, E., Nikolaidis, N., and Karatzas, G. (2015). Development of a statistical tool for the estimation of riverbank erosion probability. *SOIL Discussions*, 2:647–674. 1

Varouchakis, E. and Hristopulos, D. (2013). Comparison of stochastic and deterministic methods for mapping groundwater level spatial variability in sparsely monitored basins. *Environmental monitoring and assessment*, 185(1):1–19. 1

Verrier, G. and Branco, F. C. (1972). Quenguela-north tertiary trough and oilfield. In *Revue de L Institut Francais du Petrole et Annales des Combustibles Liquides*, volume 27, page 51. xvii, 50

Versteeg, R. and Grau, G. (1990). Practical aspects of seismic data inversion, the marmousi experience eaeg workshop. In *52nd EAEG Meeting, Eur. Assoc. Expl. Geophys., Proceedings of 1990 EAEG Workshop, 52nd EAEG Meeting*, pages 1–194. 1, 51

Webster, R. and Oliver, M. A. (2007). *Geostatistics for Environmental Scientists*. Statistics in Practice. Wiley, 2nd edition. 33

Yaglom, A. M. (1987). *Correlation Theory of Stationary and Related Random Functions: Volume I: Basic Results*. Springer, 1st edition. 13

Žukovič, M. and Hristopulos, D. T. (2013a). A directional gradient-curvature method for gap filling of gridded environmental spatial data with potentially anisotropic correlations. *Atmospheric Environment*, 77:901–909. 1, 34, 36

Žukovič, M. and Hristopulos, D. T. (2013b). Reconstruction of missing data in remote sensing images using conditional stochastic optimization with global geometric constraints. *Stochastic Environmental Research and Risk Assessment*, 27(4):785–806. 1, 34

Appendix A

Figures

In this Appendix are presented the figures illustrating the fitting of the best estimated anisotropic model to the experimental directional variograms implemented to the *DirVar0*, *DirVar1* and *CHI1* methods for the synthetic dataset and the regular and random sample of Marmousi model.

A.1 Synthetic Dataset

A.1.1 DirVar0

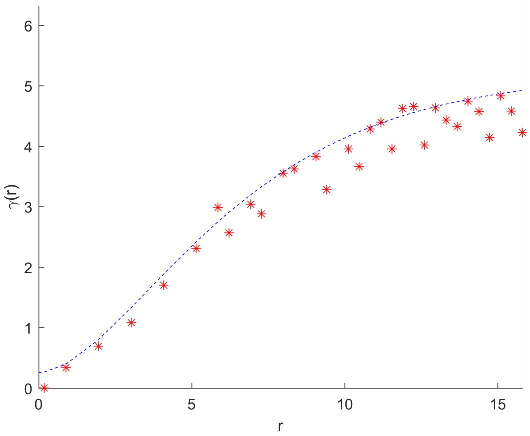

(a) 0°

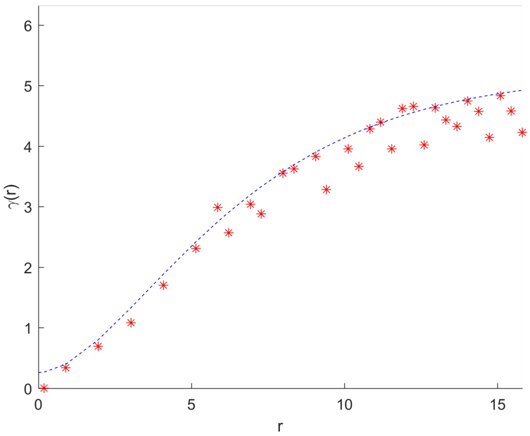

(b) 15°

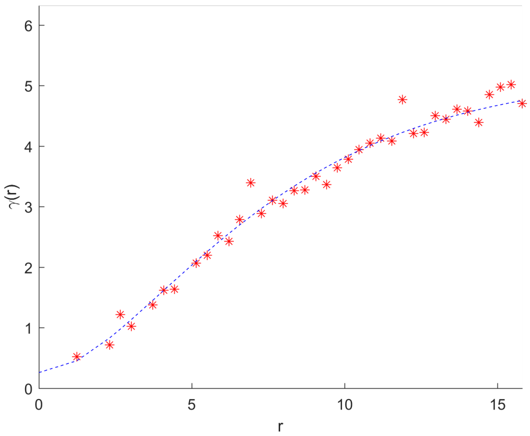

(c) 30°

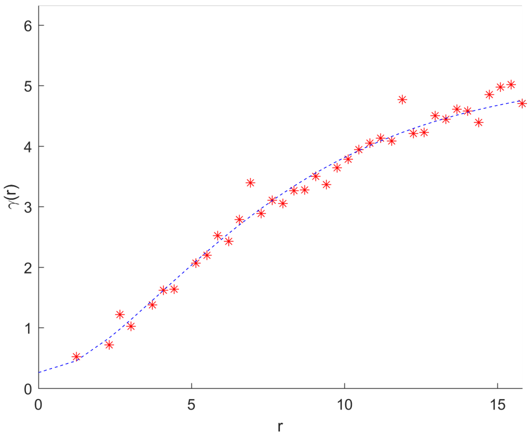

(d) 45°

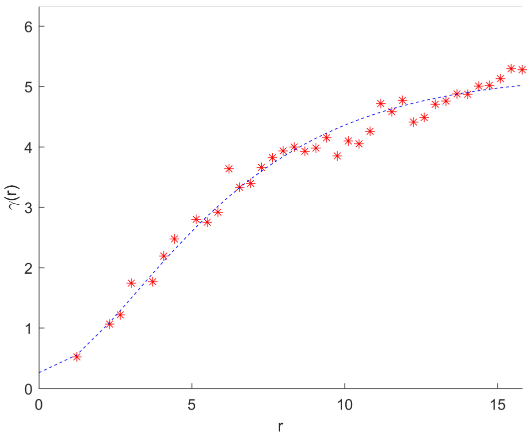

(e) 60°

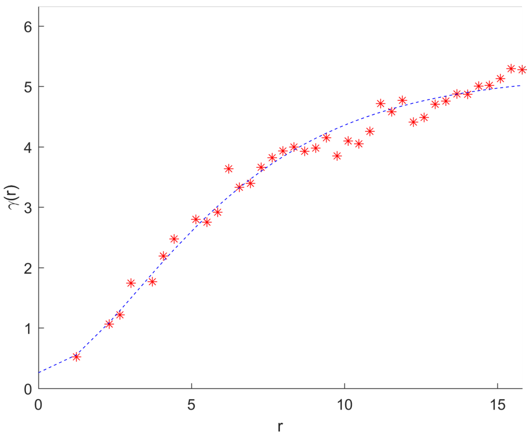

(f) 75°

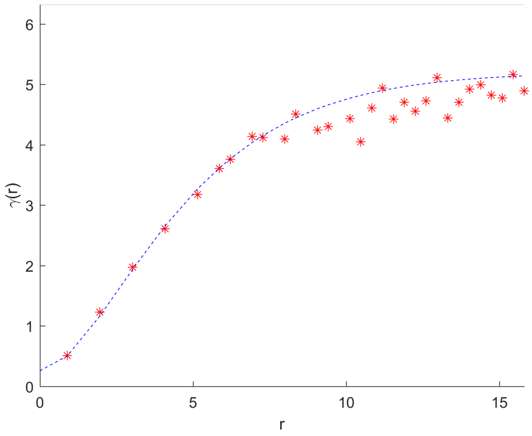

(g) 90°

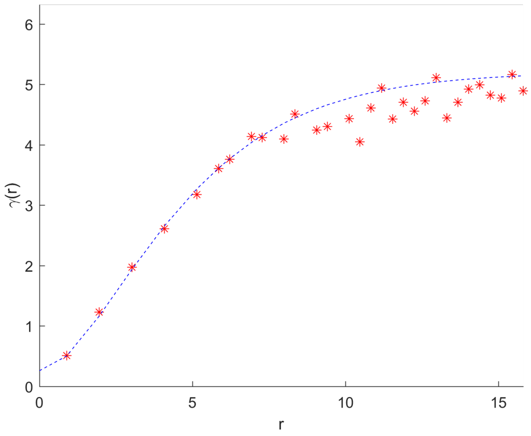

(h) 105°

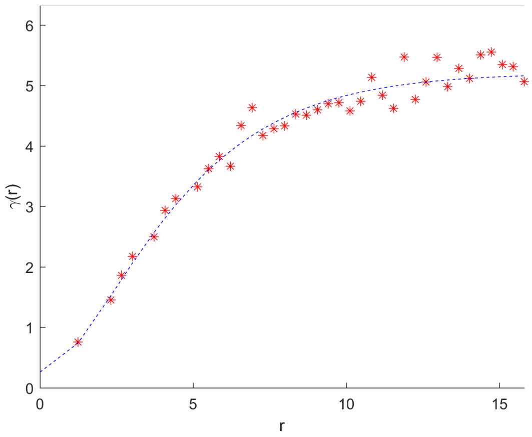

(i) 120°

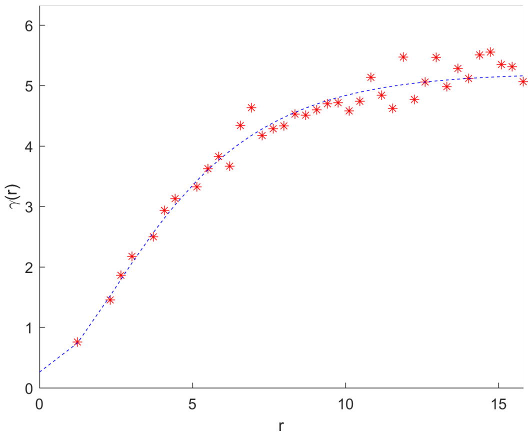

(j) 135°

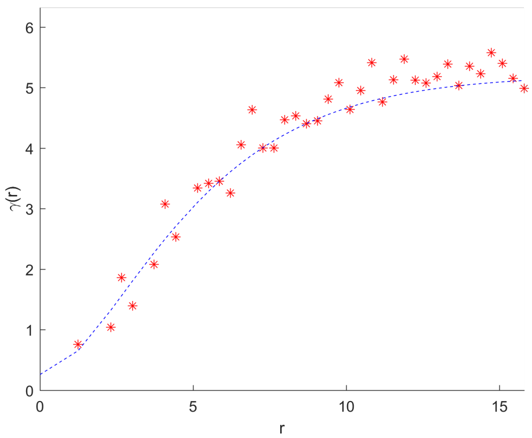

(k) 150°

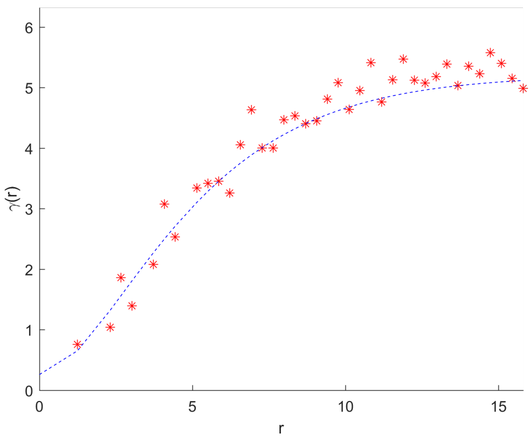

(l) 165°

Figure A.1 Fitting of the best theoretical model to the directional experimental variograms of the field. The best model is a Gen. Mátern with parameters $\sigma_z^2 = 4.945, \xi_1 = 1.694, R = 0.429, \phi = -65.2°, c_0 = 0.260, \nu = 1.525$. The experimental variogram is calculated with angular tolerance 20°, 45 distance lags and taking into account maximum distance equivalent to about 16.

A.1.2 DirVar1

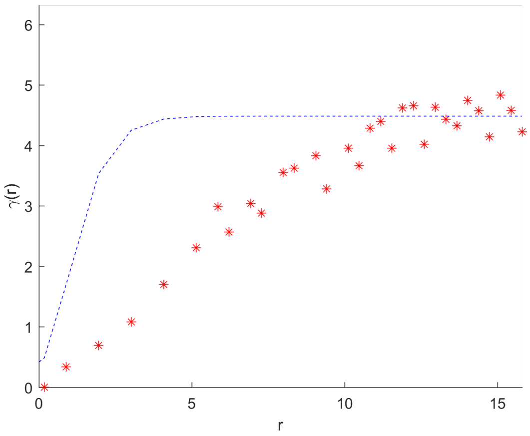

(a) 0°

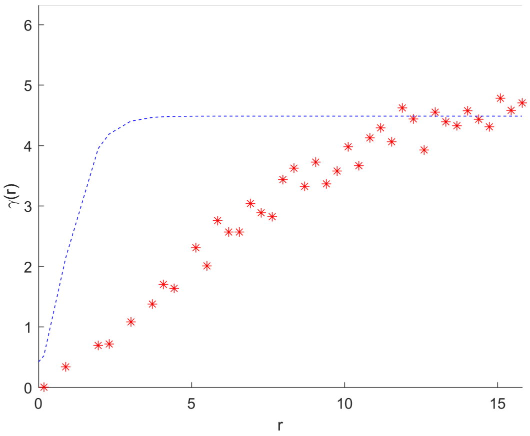

(b) 15°

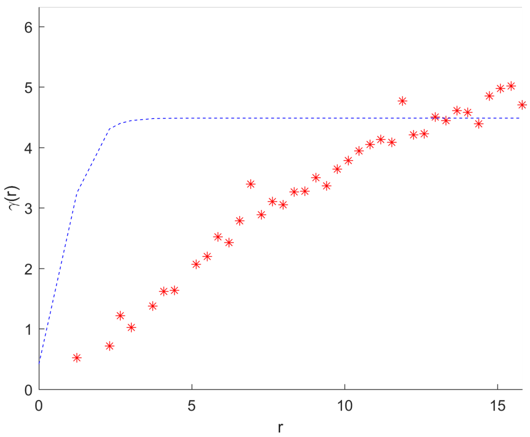

(c) 30°

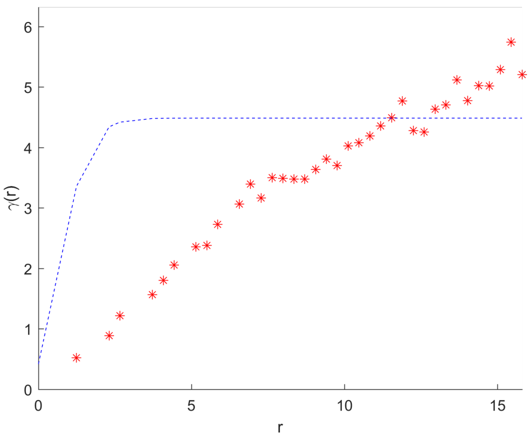

(d) 45°

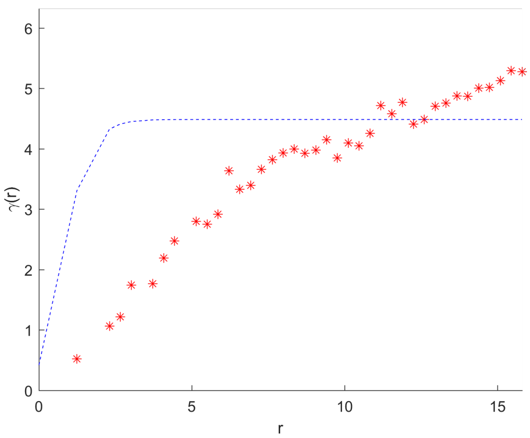

(e) 60°

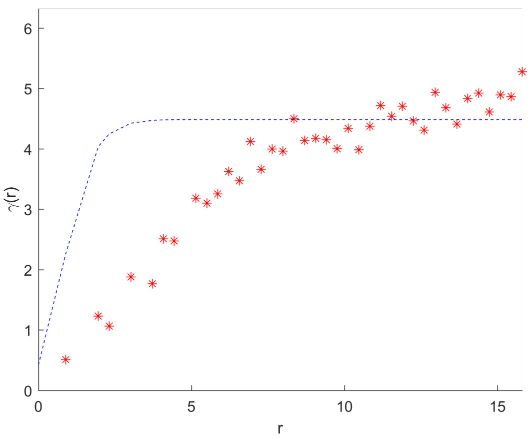

(f) 75°

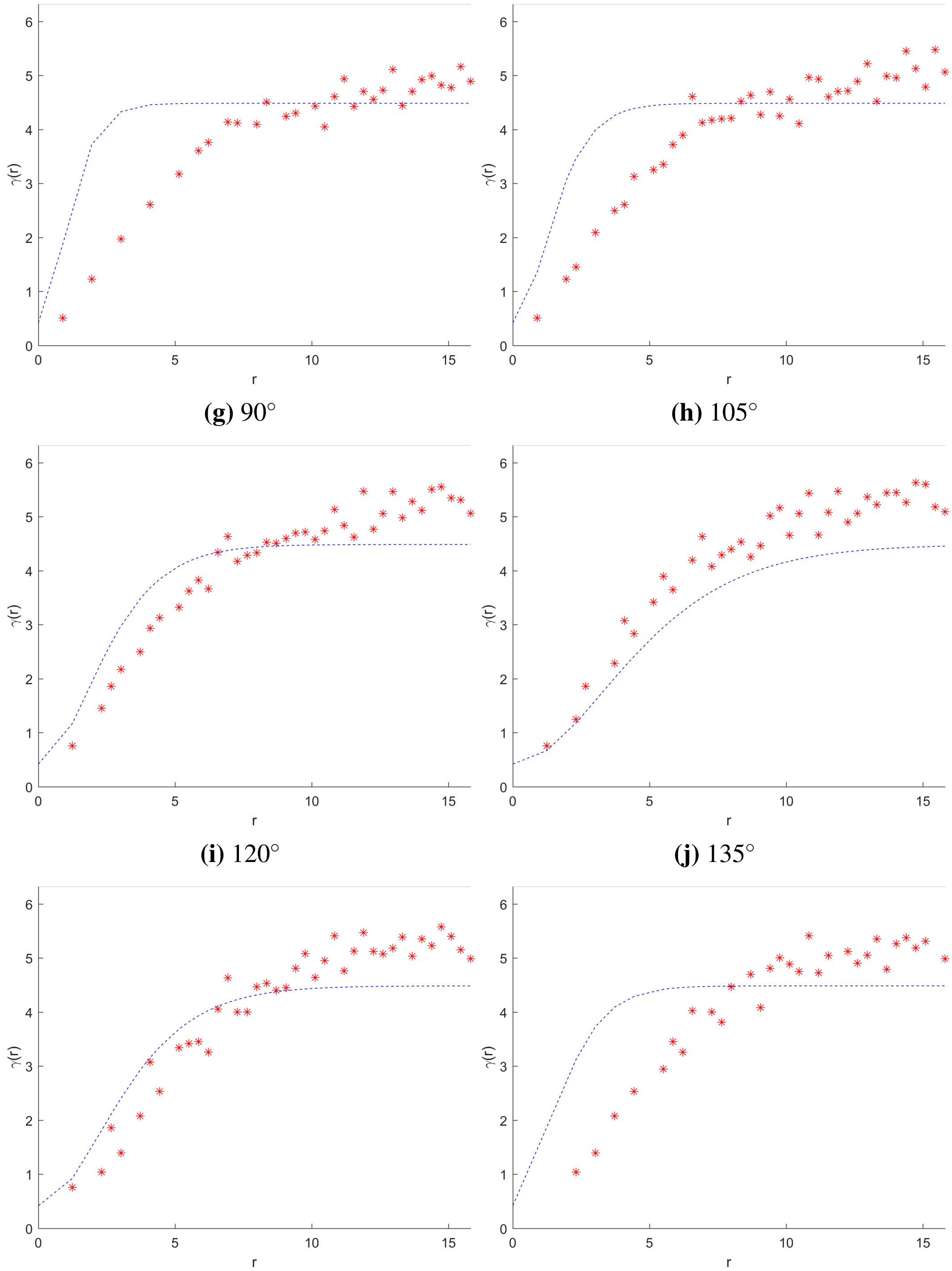

(g) 90°

(h) 105°

(i) 120°

(j) 135°

(k) 150°

(l) 165°

Figure A.2 Fitting of the best theoretical model to the experimental directional variograms of the field. The best model is a Gen. Mátern with parameters $sigma_z^2 = 4.066, \xi_1 = 1.846, R = 0.432, \phi = -42.3°, c_0 = 0.418, \nu = 2.832$. The experimental variogram is calculated with angular tolerance 20°, 45 distance lags and taking into account maximum distance equivalent to about 80.

A.2 Regular Sample

A.2.1 DirVar0

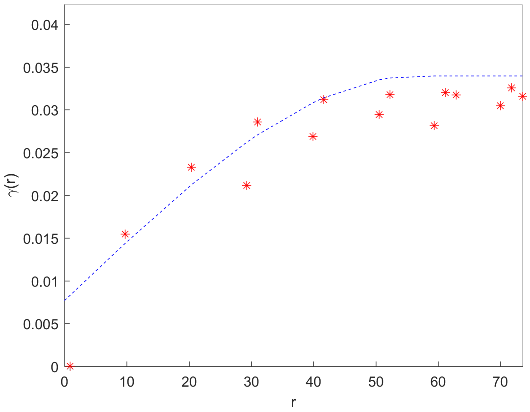

(a) 0°

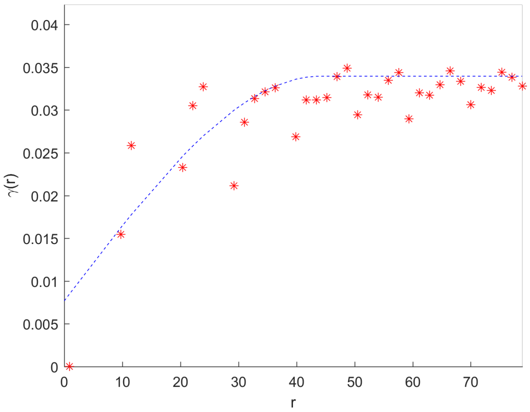

(b) 15°

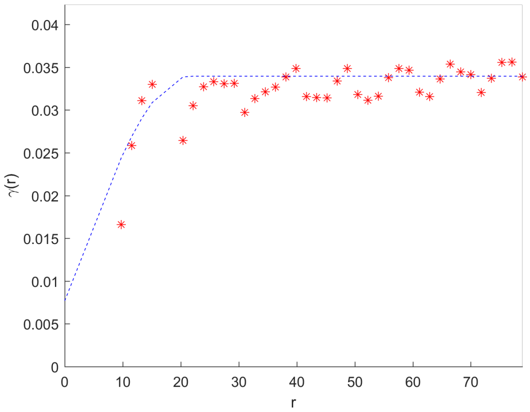

(c) 30°

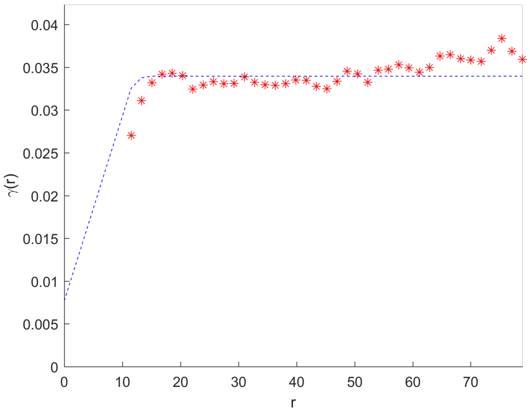

(d) 45°

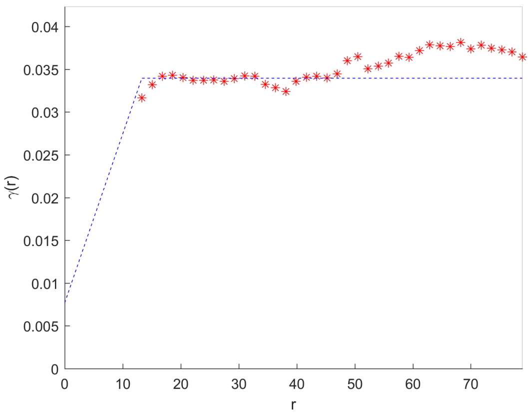

(e) 60°

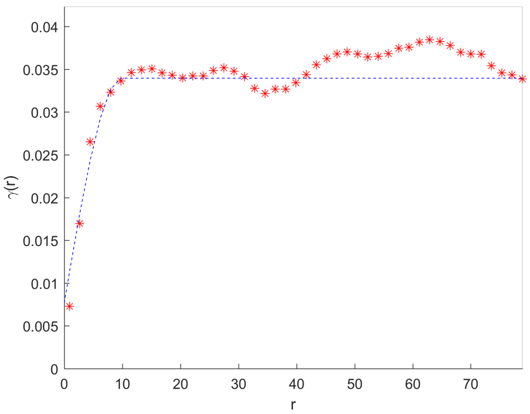

(f) 75°

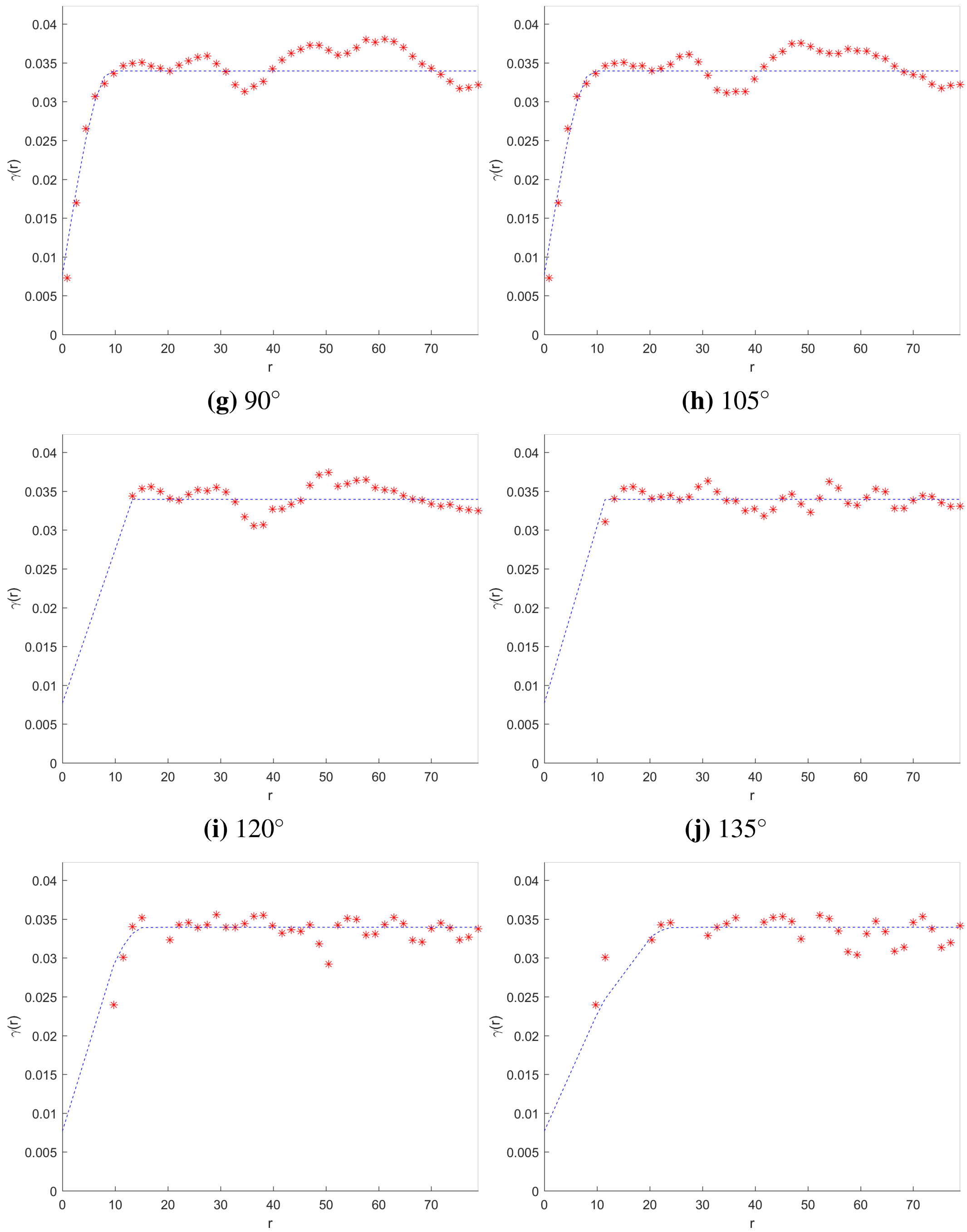

(g) 90° **(h)** 105°

(i) 120° **(j)** 135°

(k) 150° **(l)** 165°

Figure A.3 Fitting of the best theoretical model to the directional experimental (semi-) variograms of the field. The best model is a Spherical with parameters $\sigma_z^2 = 0.026, \xi_1 = 7.657, R = 0.109, \phi = -84.4°, c_0 = 0.008$. The experimental variogram is calculated with angular tolerance 20°, 45 distance lags and taking into account maximum distance equivalent to about 80.

A.2.2 DirVar1

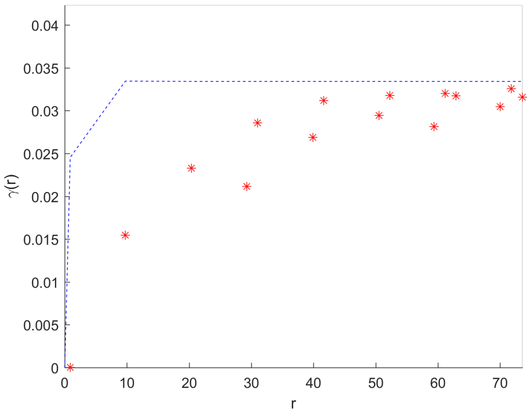

(a) 0°

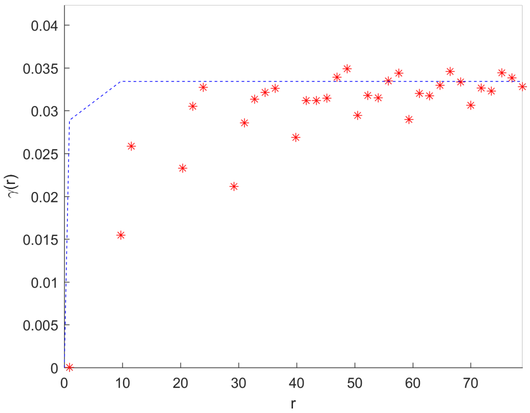

(b) 15°

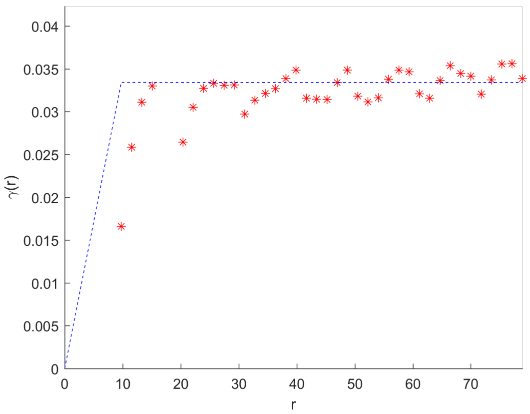

(c) 30°

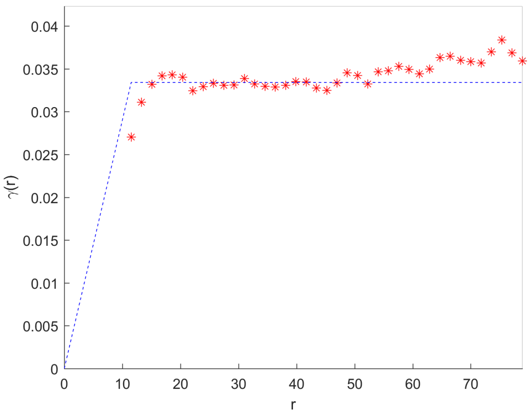

(d) 45°

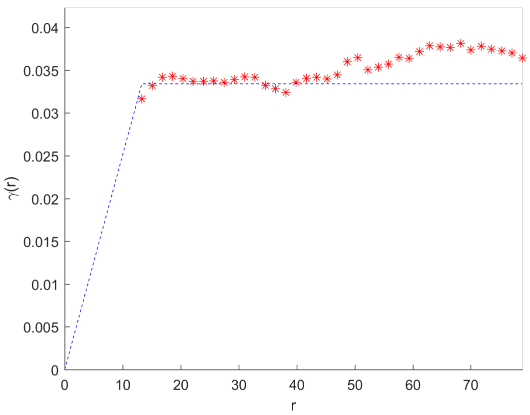

(e) 60°

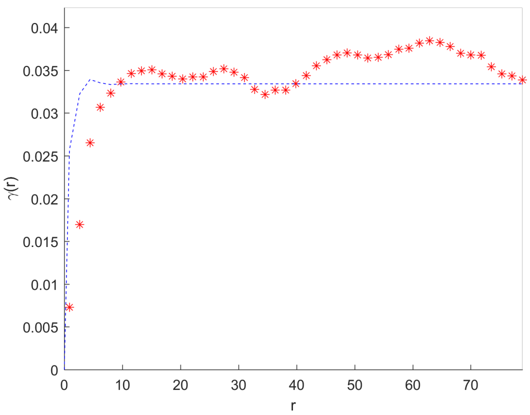

(f) 75°

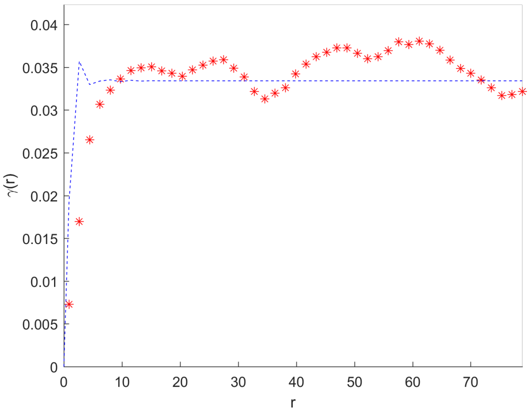

(g) 90°

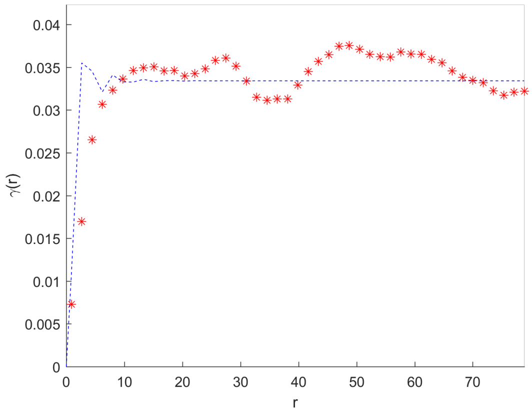

(h) 105°

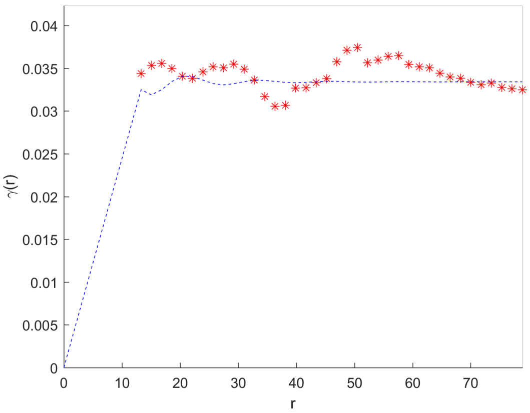

(i) 120°

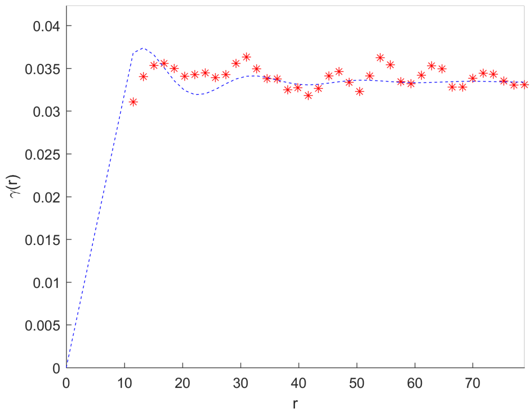

(j) 135°

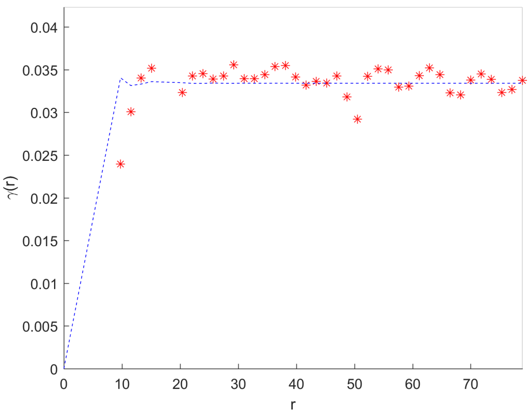

(k) 150°

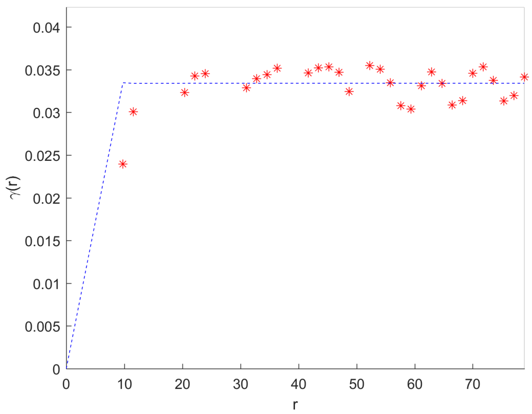

(l) 165°

Figure A.4 Fitting of the best theoretical model to the experimental directional (semi-) variograms of the field. The best model is a Spartan with parameters $\eta_0 = 0.832, \xi_1 = 40.338, R = 0.307, \phi = -50.9^\circ, c_0 = 0.000, \eta_1 = 1.928$. The experimental variogram is calculated with angular tolerance 20°, 45 distance lags and taking into account maximum distance equivalent to about 80.

A.2.3 CHI1

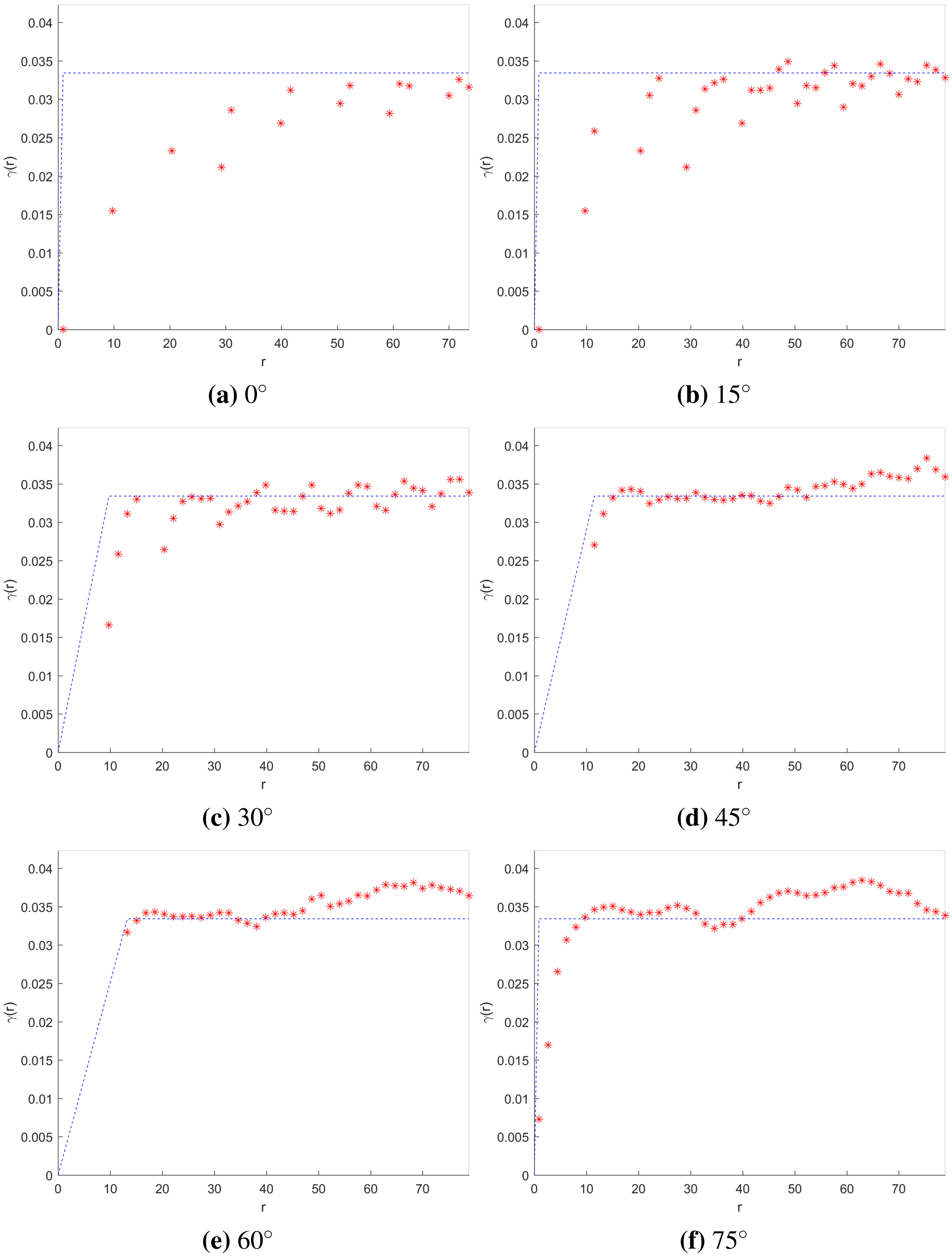

(a) 0°

(b) 15°

(c) 30°

(d) 45°

(e) 60°

(f) 75°

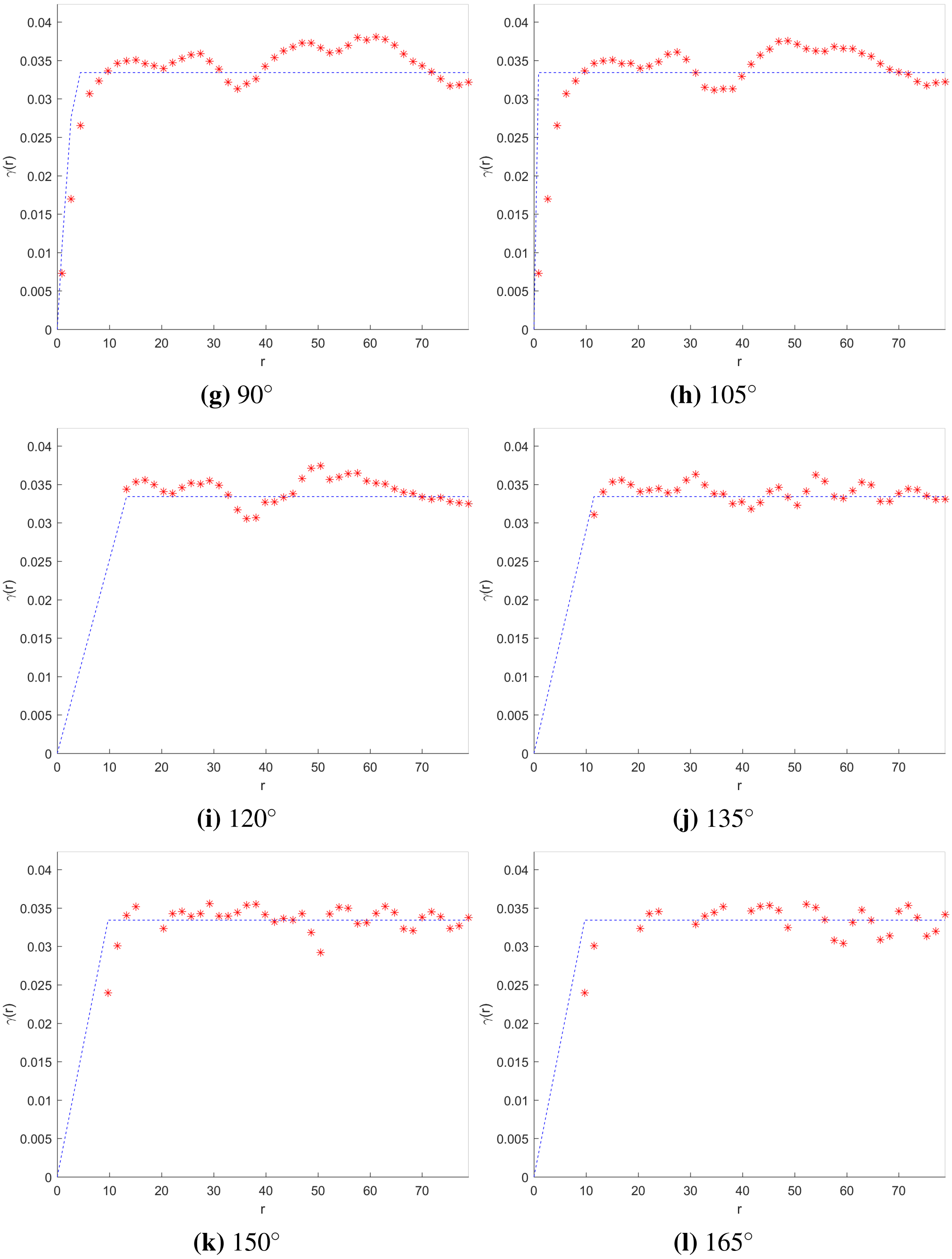

Figure A.5 Fitting of the best theoretical model to the experimental directional (semi-) variograms of the field. The best model is a Spherical with parameters $\sigma_z^2 = 0.033, \xi_1 = 79.760.338, R = 0.108, \phi = -88.5°, c_0 = 0.000$. The experimental variogram is calculated with angular tolerance 20°, 45 distance lags and taking into account maximum distance equivalent to about 80.

A.3 Random Sample

A.3.1 DirVar0

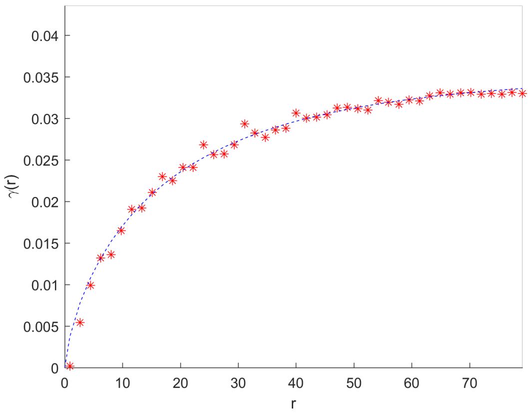

(a) 0°

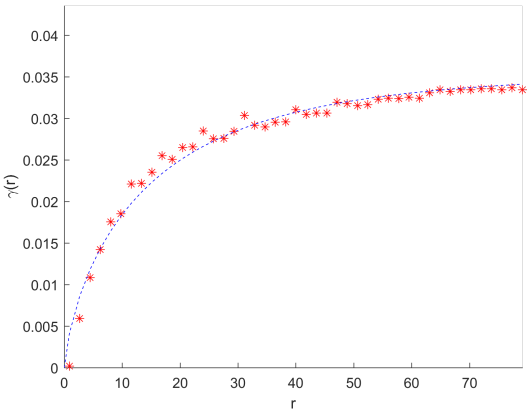

(b) 15°

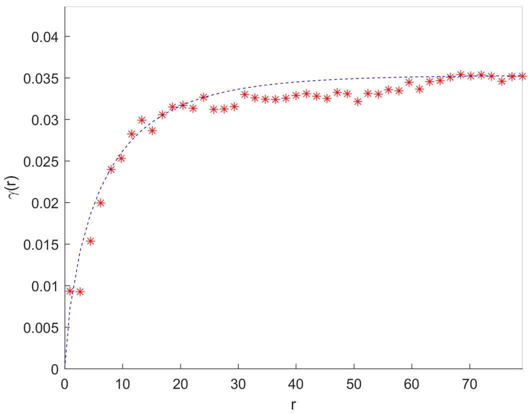

(c) 30°

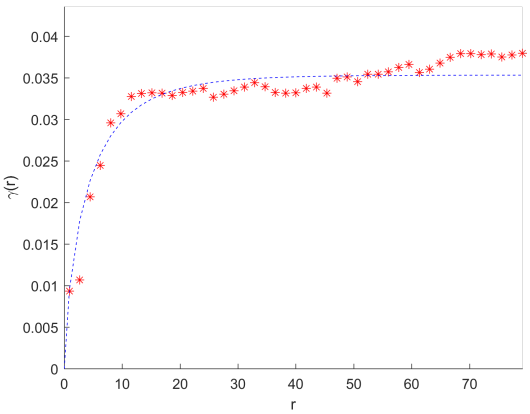

(d) 45°

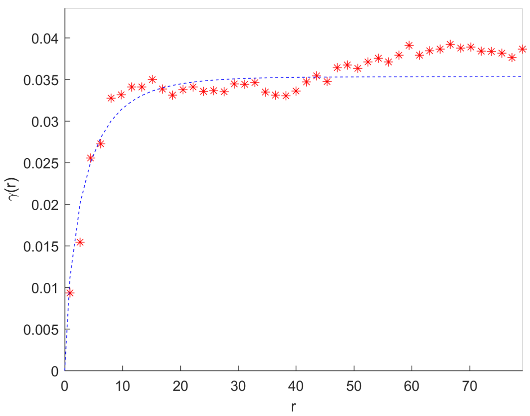

(e) 60°

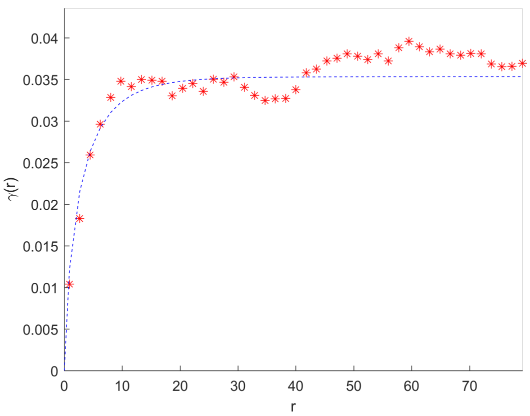

(f) 75°

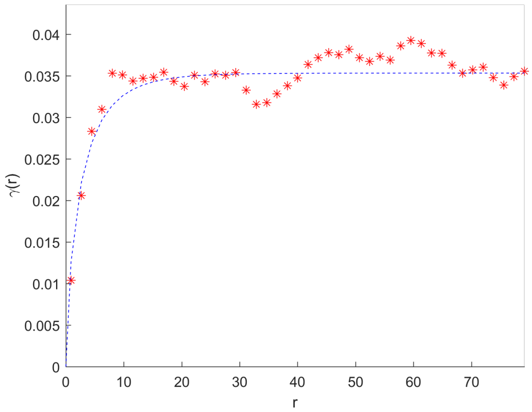

(g) 90°

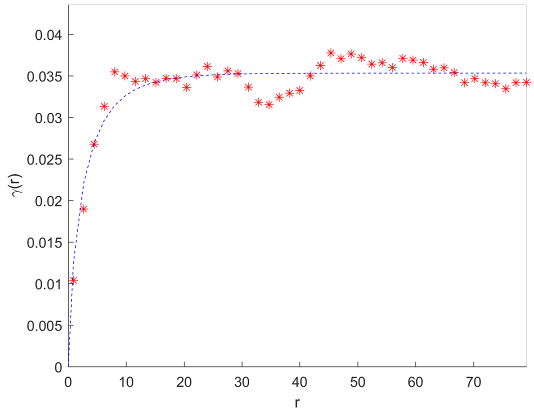

(h) 105°

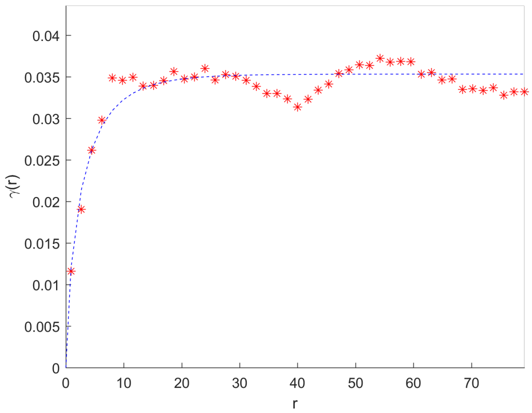

(i) 120°

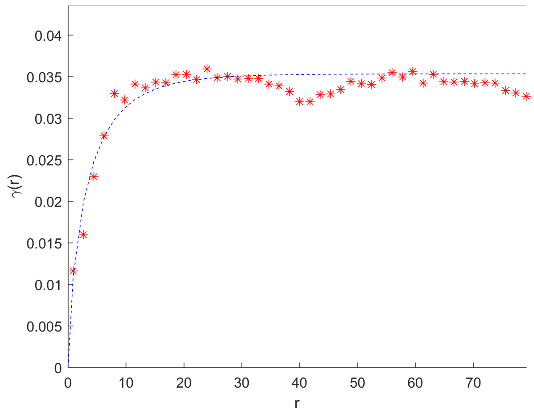

(j) 135°

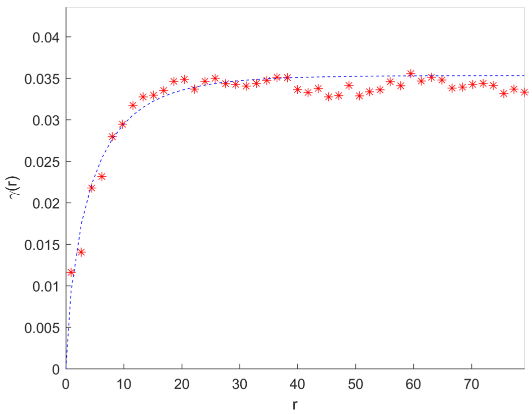

(k) 150°

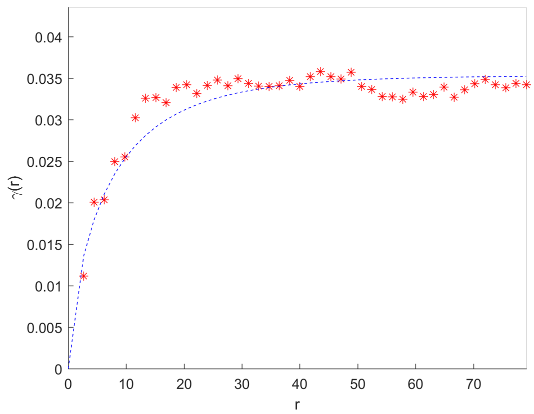

(l) 165°

Figure A.6 Fitting of the best theoretical model to the directional experimental (semi-) variograms of the field. The best model is a Gen. Exponential with parameters $\sigma_z^2 = 0.035, \xi_1 = 9.671, R = 0.370, \phi = -83.4°, c_0 = 0.000, \nu = 0.734$. The experimental variogram is calculated with angular tolerance 20°, 45 distance lags and taking into account maximum distance equivalent to about 80.

A.3.2 DirVar1

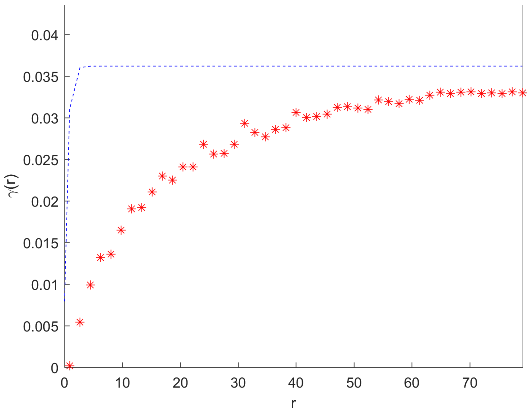

(a) 0°

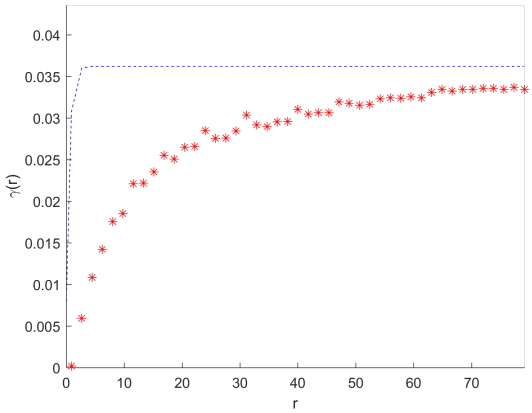

(b) 15°

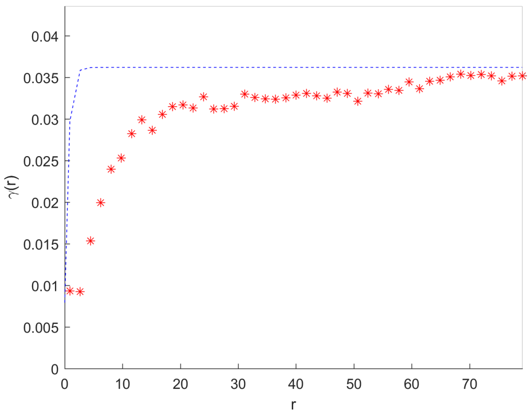

(c) 30°

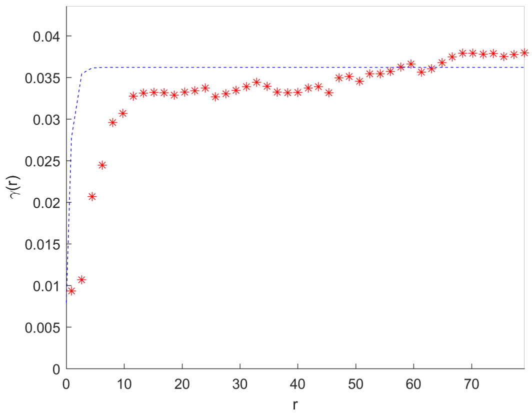

(d) 45°

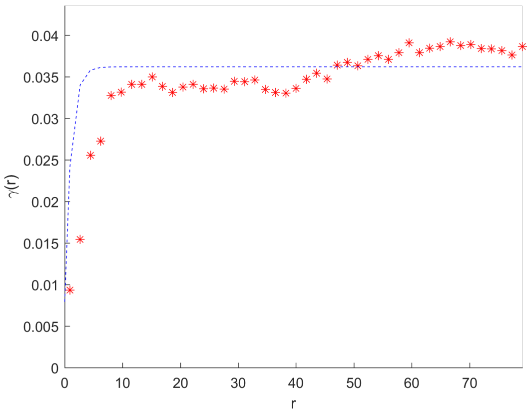

(e) 60°

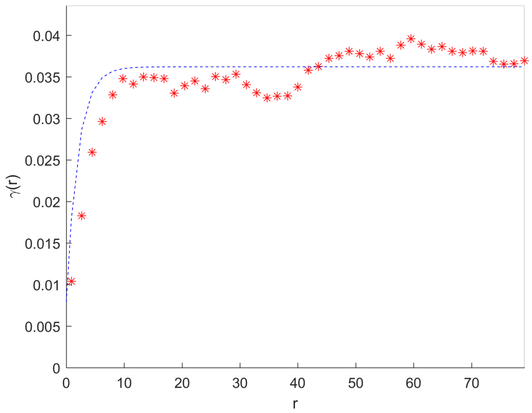

(f) 75°

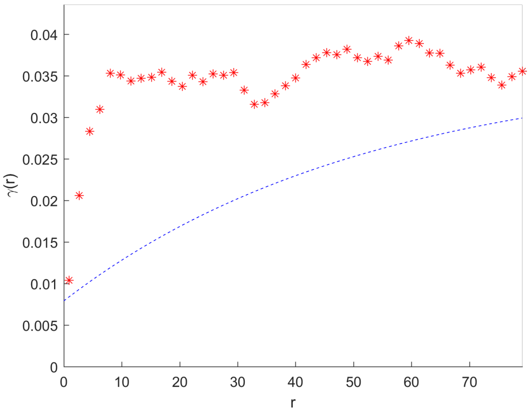

(g) 90°

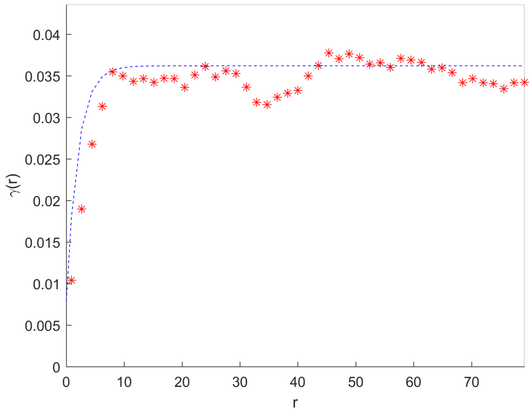

(h) 105°

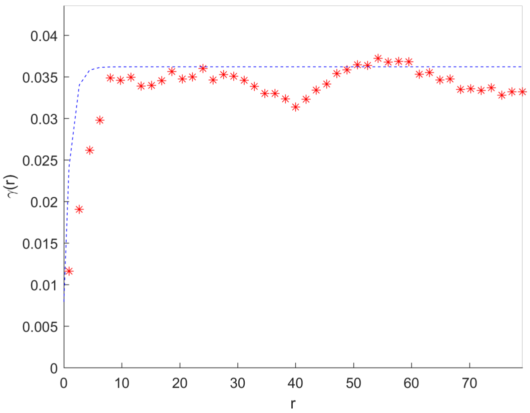

(i) 120°

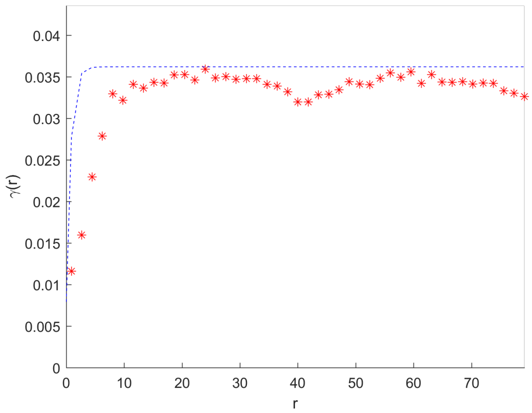

(j) 135°

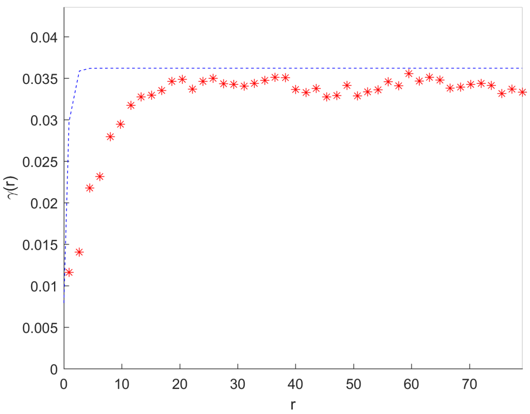

(k) 150°

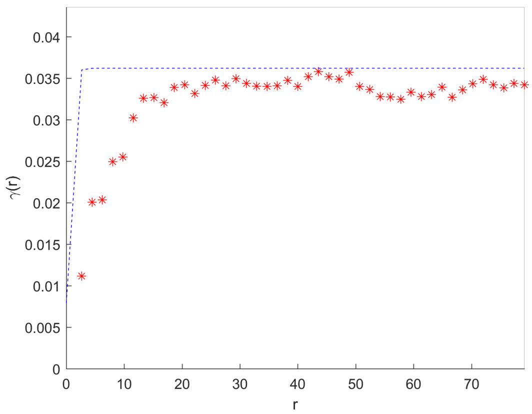

(l) 165°

Figure A.7 Fitting of the best theoretical model to the experimental directional (semi-) variograms of the field. The best model is a Spartan with parameters $\eta_0 = 0.010, \xi_1 = 52.606, R = 0.522, \phi = -90.0^\circ, c_0 = 0.008, \eta_1 = -1.999$. The experimental variogram is calculated with angular tolerance 20°, 45 distance lags and taking into account maximum distance equivalent to about 80.

A.3.3 CHI1

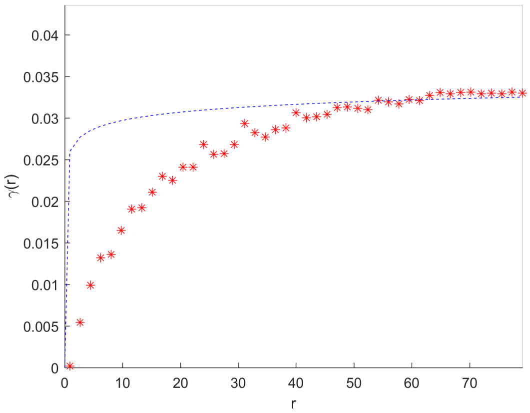

(a) 0°

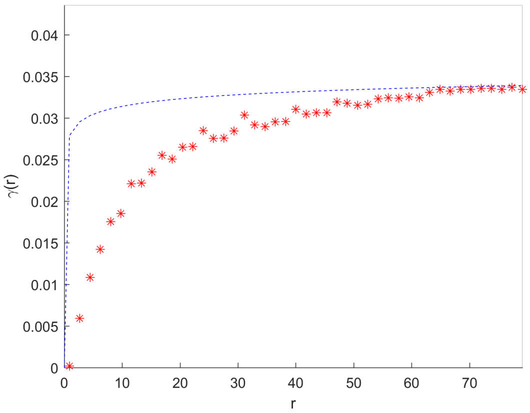

(b) 15°

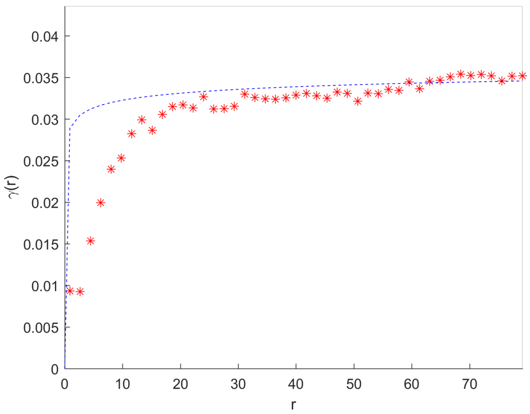

(c) 30°

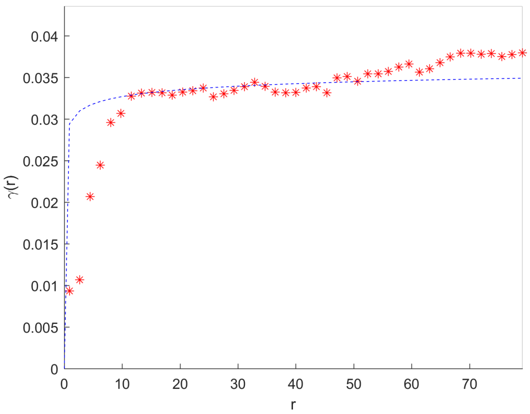

(d) 45°

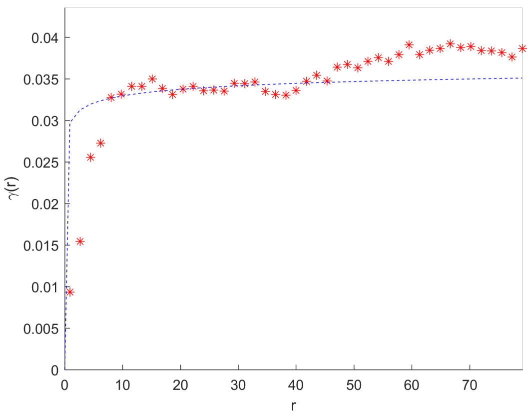

(e) 60°

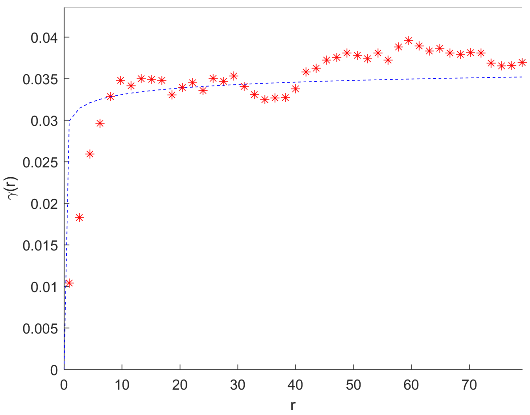

(f) 75°

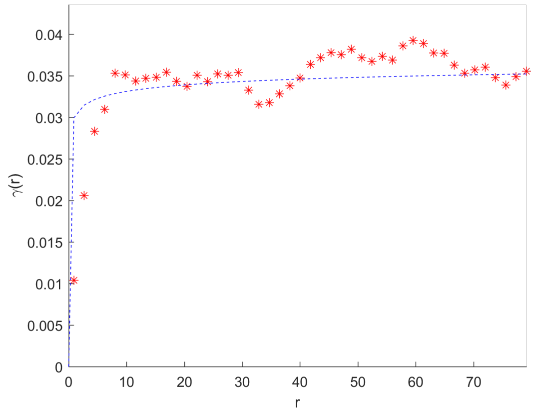

(g) 90°

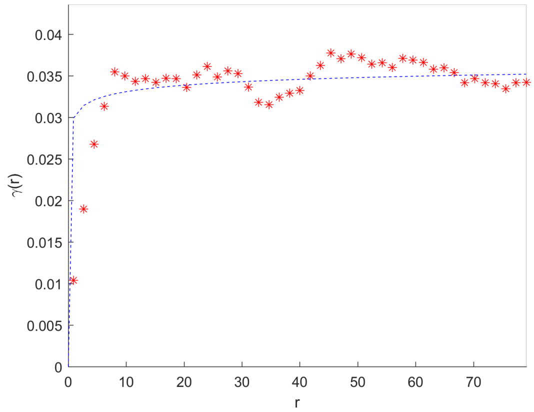

(h) 105°

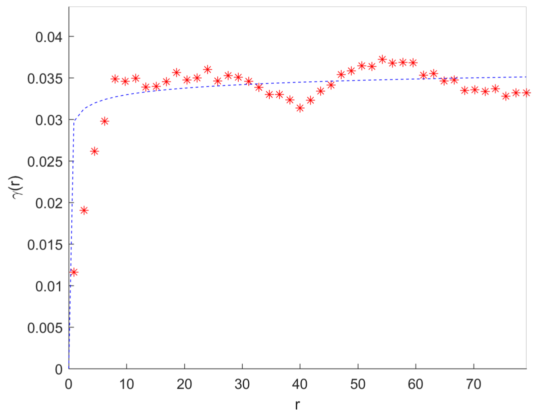

(i) 120°

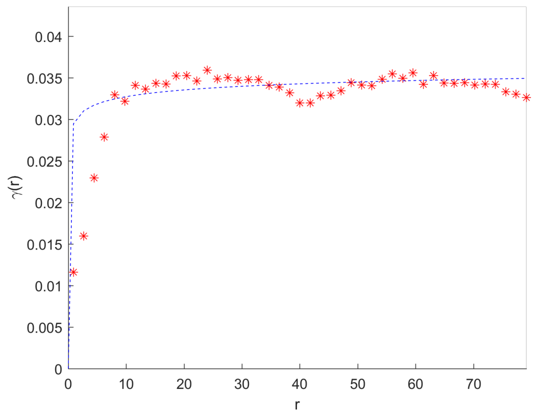

(j) 135°

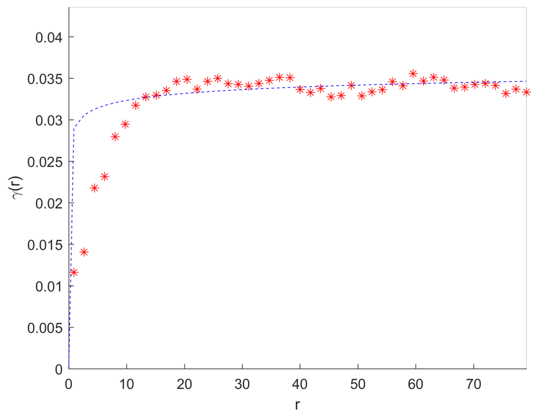

(k) 150°

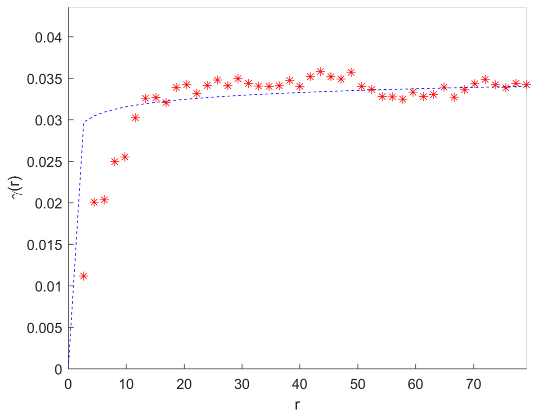

(l) 165°

Figure A.8 Fitting of the best theoretical model to the experimental directional (semi-) variograms of the field. The best model is a Gen. Exponential with parameters $\sigma_z^2 = 0.038, \xi_1 = 0.021.338, R = 0.208, \phi = -89.1^\circ, c_0 = 0.000, \nu = 0.115$. The experimental variogram is calculated with angular tolerance 20°, 45 distance lags and taking into account maximum distance equivalent to about 80.

Appendix B

Codes in MATLAB environment

B.1 Synthetic Dataset

```
                          % Synthetic Data - Test

clc;clear variables;close all;

%################## Preliminary Analysis ##############################
%======================================================================
% Construct Synthetic Data
[x,y,rf] = randomfield('Mate',[4,3,1.8,20,0.2,2],60,60,0); %random field
%Mx = 1.2 + 0.1*x + 0.01*y; %trend
data = rf; %synthetic data
nx = 60; ny = 60;

[row_all, col_all, v_all1] = find(data);

% >>>Original Data Plots<<<

figure; %Simple plot plus colorbar
pcolor(data); shading interp %flat
%title('Synthetic data')
colorbar
set(gca,'XTick',[],'YTick',[])

data_tot_vec = data(:); %total image data in vector form


% Random Sampling (33% of original data)
spoints = 0.33*numel(data); %number of sample points
```

```
[~,idx] = datasample(data_tot_vec,spoints,'Replace',false); %sampling
qpoints = data_tot_vec; qpoints(idx) = 0;
qpoints = reshape(qpoints,ny,nx); %"matrix form" of unknown points
sample = data - qpoints; %"matrix form" of known data
[qrow,qcol,qv1] = find(qpoints); %unknown points coordinations and
    values - VALIDATION SET
[row,col,v1] = find(sample); %known points coordinations and values -
    TRAINING SET
N = length(v1); %number of known points

% Plot Sample
figure; %Simple plot plus colorbar
pcolor(sample); shading interp %flat
%title('Random Sample')
colorbar
set(gca,'XTick',[],'YTick',[])

%>>>Data Histograms & Statistical Moments<<<

numbins = 15;
% Total image histogram
figure;
%subplot(1,2,1)
histfit(data_tot_vec,numbins)
alpha(0.5)
%title('Total image histogram')
% Sample data histogram
figure;%subplot(1,2,2)
histfit(v1,numbins)
alpha(0.5)
%title('Sample data histogram')

% Total image data moments
totim_stats = [min(data(:)) max(data(:)) mean(data(:)) median(data(:))
    var(data(:)) skewness(data(:)) kurtosis(data(:))];
% "Drill-holes" data moments
sample_stats = [min(v1) max(v1) mean(v1) median(v1) var(v1) skewness(v1)
     kurtosis(v1)];


%>>>Normality of data checking and Transformation<<<

% Histogram and Normal Probability Plot
figure; %same as the previous figure plus NPP
```

```
%subplot(1,2,1)
histfit(v1,numbins)
alpha(0.5)
%title('Sample data histogram')
figure;%subplot(1,2,2)
nnp = normplot(v1);
h_ch=get(gcf,'Children');h_str=get(h_ch(1),'Title');set(h_str,'String','
    '); % remove normplot title
[h_orig,kst_p_orig,ksstat_orig,cv_orig] = kstest(v1(:));

v = v1;
qv = qv1;
v_all = v_all1;

fluc = v(:); Mx = zeros(size(fluc)); qMx = zeros(size(qcol));
qfluc = qv-qMx;
fluc_all = v_all-zeros(size(v_all));


%>>> Statistical Analysis of Residuals <<<

% Residuals/Fluctuations moments
fluc_stats = [min(fluc) max(fluc) mean(fluc) median(fluc) var(fluc)
    skewness(fluc) kurtosis(fluc)];


%Maximum distance
c = [col,row];
[k,l] = find(triu(true(N)));
d = hypot(c(k,1)-c(l,1),c(k,2)-c(l,2));
% d = triu(pdist2(c,c));
ncpc = 0.2;
maxdist = max(max(d))*ncpc;
clear k l d
%==============================================================



%% ################## Experimantal Variogram
    ###############################
%==============================================================

% >>> Initialize Basic Parameters <<<
load('statanal.mat')
```

```
c = {col,row}; %known points' coordinations
qc = {qcol,qrow}; %"unknown" points' coordinations
%ncpc = 0.2;
N = size(col,1);
Nu = size(qcol,1);
%maxdist = hypot(col(1,1)-col(N,1),row(1,1)-row(N,1))*ncpc;
nrbins = 45;
phistep = 15;
phitol = 20;
N_kr_mod = 3;

% >>> Experimental (Semi-)Variogram (anisotropic) <<<
x = col; y = row; rf = fluc; iso = 0; flag = 1;
[~,~,~] = expvar(x,y,rf,iso,ncpc,nrbins,4,phitol,2); %exper. variogr. of
    high analysis
[gexp, nr_pairs, c_centers] = expvar(x,y,rf,iso,ncpc,nrbins,phistep,
    phitol,flag);
gexpmax = max(max(gexp));
%===============================================================


%% ################# DirVar0 ############################
%===============================================================

% >>> Fitting I and Parameters of Anisotropic Correlation Estimation (s2
    ,xi1,xi2,phi,c0,v or eta1) <<<

% Desired Models
models = {'Gexp';'Gaus';'Sphe';'Mate';'Spar'};
n_models = length(models);

% Initial Values and Limits for optimization
b = [gexpmax,maxdist*1/3,0.5,10,gexpmax/100]; % s2,xi1,R,phi & c0
b_lb = [eps,eps,eps,-90,eps]; b_ub = [gexpmax*1.5,maxdist,30,90,gexpmax
    /5]; %lower and upper limits
bsp = [1000,maxdist*1/3,0.5,10,gexpmax/100]; % eta0, xi1,R,phi & c0
bsp_lb = [eps,eps,eps,-90,eps]; bsp_ub = [inf,maxdist,30,90,gexpmax/5];
    %lower and upper limits

% Summary cells
model_par0 = {[b,1.5];b;b;[b,1.5];[bsp,1]}; %initial parameters values
model_par_lb = {[b_lb,eps];b_lb;b_lb;[b_lb,0.3];[bsp_lb,-2+eps]}; %lower
    bounds
```

```
model_par_ub = {[b_ub,2-eps];b_ub;b_ub;[b_ub,3.5];[bsp_ub,inf]}; %upper
    bounds

clear b b_lb b_ub bsp bsp_lb bsp_ub

% Estimation of Parameters (s2,xi1,xi2,phi,c0,v or eta1)
bmodel{n_models,1}=[]; fval(n_models,1)=0; tit{n_models,1}=[];
iso = 00;objmod = 'NWEr_m';flag = 1;
for i=1:n_models
    model.function = models{i,1};
    model.params0 = model_par0{i,1};
    model.paramslb = model_par_lb{i,1};
    model.paramsub = model_par_ub{i,1};

   [bmodel{i,1},fval(i,1),tit{i,1}] =...
       variogramfit(gexp,nr_pairs,c_centers,iso,model,objmod,flag);
end

% Anisotropy Estimation (#Not Necessary#)
R0(n_models,1) = 0;phi0(n_models,1) = 0;xi10(n_models,1) = 0;xi20(
    n_models,1) = 0;
for i=1:n_models
    R0(i,1) = bmodel{i,1}(1,3);
    phi0(i,1) = bmodel{i,1}(1,4);
    xi10(i,1) = bmodel{i,1}(1,2);
    xi20(i,1) = bmodel{i,1}(1,2)/R0(i,1);
    if R0(i,1)>1
        R0(i,1) = 1/R0(i,1);bmodel{i,1}(1,3) = R0(i,1);
        xi101 = xi10(i,1);
        xi10(i,1) = xi20(i,1); bmodel{i,1}(1,2) = xi10(i,1);
        xi20(i,1) = xi101;
        if phi0(i,1)>0
            phi0(i,1) = phi0(i,1)-90;
        else
            phi0(i,1) = phi0(i,1)+90;
        end
        bmodel{i,1}(1,4) = phi0(i,1);
    end
end

R = mean(R0); phi = mean(phi0);xi1 = mean(xi10);xi2 = mean(xi20);


% >>> Cross Validation <<<
```

```
% Matrices and Cells preallocation
cv_scores{n_models,1}=[]; cv_checks{n_models,1}=[];
cv_matr{n_models,1}=[]; cv_Ss(n_models,6)= 0;

% Inputs definition
iso = 00; d_col = 1;

% Cross Validation
for i=1:n_models
    model.function = models{i,1};
    model.params = bmodel{i,1};
    model.r_ok = [6,6];

    [cv_scores{i,1}, cv_checks{i,1}, cv_matr{i,1}] =...
        crossval(x,y,rf,iso,d_col,model);
    cv_Ss(i,:) = table2array(cv_scores{i,1}(:,2:end));
end

% Cross Validation Scores
table_h = {'MeanAbsErr','MaxAbsErr','MSE','RMSE','rpearson','rspearman',
    'finalscore'};
% % table_r = {'Gexp';'Gaus';'Sphe';'Mate1/3';'Mate1.0';'Mate1.5';'Mate2
    .0';'Mate2.5';
% %      'Mate3.0';'Mate3.5';'Spar'};
table_r = {'Gexp';'Gaus';'Sphe';'Mate';'Spar'};

relMSE = cv_Ss(:,3)/min(cv_Ss(:,3)); %relative MSE
FinalScore = ((1./relMSE).^2).*cv_Ss(:,5).*cv_Ss(:,6); %finalscore
cv_Ss = [cv_Ss, FinalScore];
cv_Ssf = array2table(cv_Ss,'VariableNames',table_h,'RowNames',table_r);
clear relMSE FinalScore

%Trend addition and Boxcox Inversion
cv_St(n_models,6)= 0;
for i=1:n_models

    cv_matr{i,1}.Z_tr = cv_matr{i,1}.Z;

    cv_matr{i,1}.Z_ibt1 = cv_matr{i,1}.Z_tr;

    cv_matr{i,1}.Z_ibt = real(cv_matr{i,1}.Z_ibt1);
    cv_realZ(i,1) = isreal(cv_matr{i,1}.Z_ibt1); %#ok<SAGROW>

```

```
    cv_St(i,:) = correlstats(v1,cv_matr{i,1}.Z_ibt);%total cv scores

end

% Total Cross Validation Scores
relMSE = cv_St(:,3)/min(cv_St(:,3)); %relative MSE
FinalScore = ((1./relMSE).^2).*cv_St(:,5).*cv_St(:,6); %finalscore
cv_St = [cv_St, FinalScore];
cv_Stf = array2table(cv_St,'VariableNames',table_h,'RowNames',table_r);
clear relMSE FinalScore

%Plots
for i=1:n_models

    % Stochastic Component's figures
    cc1 = [col,row,rf(:);qcol,qrow,zeros(Nu,1)];
    cc2 = [col,row,cv_matr{i,1}.Z(:);qcol,qrow,zeros(Nu,1)];
    Z1(max(cc1(:,2)),max(cc1(:,1)))=0; %#ok<SAGROW>
    Z2=Z1;
    for j = 1:size(cc1,1)
        Z1(cc1(j,2),cc1(j,1)) = cc1(j,3);
        Z2(cc2(j,2),cc2(j,1)) = cc2(j,3);
    end

    figure;pcolor(Z1);%title('Sample Stochastic Component');
    view(2);shading interp; colorbar;set(gca,'XTick',[],'YTick',[]);
    figure;pcolor(Z2);%title(sprintf('Estimation of Sample Stochastic
   Component \n%s',tit{i,1}));
    view(2);shading interp;colorbar;set(gca,'XTick',[],'YTick',[]);
    figure;scatter(rf(:),cv_matr{i,1}.Z(:),'filled','d');hold on;
    dvec1 = [rf(:);cv_matr{i,1}.Z(:)];
    plot([min(dvec1)-0.5,max(dvec1)+0.5],[min(dvec1)-0.5,max(dvec1)
   +0.5],'r');
    axis([min(dvec1)-0.5,max(dvec1)+0.5,min(dvec1)-0.5,max(dvec1)+0.5])
    %title('Scatter Plot')
    xlabel ('Observed Data'); ylabel ('Estimations');
    figure; h = histogram(rf(:),16,'EdgeColor',[0 0 1],'FaceAlpha',0.7);
    hold on
    histogram(cv_matr{i,1}.Z(:),'BinEdges',h.BinEdges,'EdgeColor',[0.2 1
    0]','FaceAlpha',0.7)
    %title('Histograms of Sample Stochastic Component')
    legend({'Original', 'Estimated'});
    clear h
```

```
    % Total Data figures
    cc3 = [col,row,v1(:);qcol,qrow,zeros(Nu,1)];
    cc4 = [col,row,cv_matr{i,1}.Z_ibt(:);qcol,qrow,zeros(Nu,1)];
    Z3(max(cc3(:,2)),max(cc3(:,1)))=0; %#ok<SAGROW>
    Z4=Z3;
    for j = 1:size(cc3,1)
        Z3(cc3(j,2),cc3(j,1)) = cc3(j,3);
        Z4(cc4(j,2),cc4(j,1)) = cc4(j,3);
    end
%   figure;pcolor(Z3);view(2);shading interp; %title('Original Sample
    ');
%   colorbar;set(gca,'XTick',[],'YTick',[]);
    figure;pcolor(Z4);view(2);shading interp; %title(sprintf('Estimation
     of Original Sample \n%s',tit{i,1}));
    colorbar;set(gca,'XTick',[],'YTick',[]);
    figure;scatter(v1(:),cv_matr{i,1}.Z_ibt(:),'filled','d');hold on;
    dvec2 = [v1(:);cv_matr{i,1}.Z_ibt(:)];
    plot([min(dvec2)-0.5,max(dvec2)+0.5],[min(dvec2)-0.5,max(dvec2)
    +0.5],'r');
    axis([min(dvec2)-0.5,max(dvec2)+0.5,min(dvec2)-0.5,max(dvec2)+0.5])
    %title('Scatter Plot')
    xlabel ('Observed Data')
    ylabel ('Estimations')
    figure;h = histogram(v1(:),16,'EdgeColor',[0 0 1],'FaceAlpha',0.7);
    hold on
    histogram(cv_matr{i,1}.Z_ibt(:),'BinEdges',h.BinEdges,'EdgeColor'
    ,[0.2 1 0],'FaceAlpha',0.7)
    %title('Histograms of Sample Data')
    legend({'Original', 'Estimated'});
    clear h

    clear Z1 Z2 Z3 Z4 dvec1 dvec2

end


% >>> Ordinary Kriging <<<

% Sort models based on cross validation scores
[~,ind] = sort(table2array(cv_Stf(:,7)),'descend');

% Matrices and Cells preallocation
Z{N_kr_mod,1}=[]; Z_error{N_kr_mod,1}=[];kr_checks{N_kr_mod,1}=[];
```

```
kr_matr{N_kr_mod,1}=[];
kr_Ss(N_kr_mod,6)= 0; table_r2{N_kr_mod,1} = [];
CI1{N_kr_mod,1}=[];UNC{N_kr_mod,1}=[];

% Inputs definition
xu = qcol; yu = qrow; iso = 00;

% Ordinary Kriging
for i=1:N_kr_mod
    model.function = models{ind(i),1};
    model.params = bmodel{ind(i),1};
    model.r_ok = [6,6];

    [Z{i,1},Z_error{i,1},kr_checks{i,1}, kr_matr{i,1}] =...
        ordkrig(x,y,rf,xu,yu,iso,model);
    kr_Ss(i,:) = correlstats(Z{i,1},qfluc);
    table_r2{i,1} = table_r{ind(i),1};

    %Confidence Intervals (95%)
    CI1{i,1}.low = Z{i,1} - 1.96*sqrt(Z_error{i,1});
    CI1{i,1}.up = Z{i,1} + 1.96*sqrt(Z_error{i,1});
    CI1{i,1}.uncer = 1.96*sqrt(Z_error{i,1});
    UNC{i,1} = real(CI1{i,1}.uncer);
    realCI(i,1) = isreal(CI1{i,1}.uncer); %#ok<SAGROW>
end

% Kriging Scores
relMSE = kr_Ss(:,3)/min(kr_Ss(:,3)); %relative MSE
FinalScore = ((1./relMSE).^2).*kr_Ss(:,5).*kr_Ss(:,6); %finalscore
kr_Ss = [kr_Ss, FinalScore];
kr_Ssf = array2table(kr_Ss,'VariableNames',table_h,'RowNames',table_r2);
clear relMSE FinalScore

%Trend addition and Boxcox Inversion
kr_St(N_kr_mod,6)= 0; Z_tr{N_kr_mod,1} = 0;
Z_ibt1{N_kr_mod,1} = 0;Z_ibt{N_kr_mod,1} = 0;
for i=1:N_kr_mod

    Z_tr{i,1} = Z{i,1};

    Z_ibt1{i,1} = Z_tr{i,1};

    Z_ibt{i,1} = real(Z_ibt1{i,1});
    kr_realZ(i,1) = isreal(Z_ibt1{i,1}); %#ok<SAGROW>
```

```
    kr_St(i,:) = correlstats(qv,Z_ibt{i,1});%total kriging scores

end

% Total Kriging Scores
relMSE = kr_St(:,3)/min(kr_St(:,3)); %relative MSE
FinalScore = ((1./relMSE).^2).*kr_St(:,5).*kr_St(:,6); %finalscore
kr_St = [kr_St, FinalScore];
kr_Stf = array2table(kr_St,'VariableNames',table_h,'RowNames',table_r2);
clear relMSE FinalScore

%Plots
for i=1:N_kr_mod

    % Stochastic Component's figures
    cc1 = [col,row,rf(:);qcol,qrow,qfluc(:)];
    cc2 = [col,row,rf(:);qcol,qrow,Z{i,1}];
    Z1(max(cc1(:,2)),max(cc1(:,1)))=0; %#ok<SAGROW>
    Z2=Z1;
    for j = 1:size(cc1,1)
        Z1(cc1(j,2),cc1(j,1)) = cc1(j,3);
        Z2(cc2(j,2),cc2(j,1)) = cc2(j,3);
    end
    figure;pcolor(Z1);%title('Original Stochastic Component');
    view(2);shading interp; colorbar;set(gca,'XTick',[],'YTick',[]);
    figure;pcolor(Z2); %title(sprintf('Estimation of Stochastic
   Component \n%s',tit{ind(i),1}));
    view(2);shading interp; colorbar;set(gca,'XTick',[],'YTick',[]);
    figure;scatter(qfluc(:),Z{i,1}(:),'filled','d');hold on;
    dvec1 = [qfluc(:);Z{i,1}(:)];
    plot([min(dvec1)-0.5,max(dvec1)+0.5],[min(dvec1)-0.5,max(dvec1)
   +0.5],'r');
    axis([min(dvec1)-0.5,max(dvec1)+0.5,min(dvec1)-0.5,max(dvec1)+0.5])
    %title('Scatter Plot')
    xlabel ('Observed Data')
    ylabel ('Estimations')
    figure;h = histogram(qfluc(:),16,'FaceColor',[0 0 1],'FaceAlpha'
   ,0.7);
    hold on
    histogram(Z{i,1}(:),'BinEdges',h.BinEdges,'FaceColor',[0.2 1 0],'
   FaceAlpha',0.7)
    %title('Histograms of Stochastic Component')
    legend({'Original', 'Estimated'});
```

```
    clear h

    % Total Data figures
    cc3 = [col,row,v1(:);qcol,qrow,Z_ibt{i,1}];
    cc4 = [col,row,zeros(size(col,1),1); qcol,qrow,UNC{i,1}];
    Z3(max(cc3(:,2)),max(cc3(:,1)))=0; %#ok<SAGROW>
    Z4=Z3;
    for j = 1:size(cc3,1)
        Z3(cc3(j,2),cc3(j,1)) = cc3(j,3);
        Z4(cc4(j,2),cc4(j,1)) = cc4(j,3);
    end
    figure;pcolor(Z3); view(2);shading interp; %title(sprintf('Estimation of Original Data \n%s',tit{ind(i),1}));
    colorbar;set(gca,'XTick',[],'YTick',[]);
    figure;scatter(qv1(:),Z_ibt{i,1}(:),'filled','d');hold on;
    dvec2 = [qv1(:);Z_ibt{i,1}(:)];
    plot([min(dvec2)-0.5,max(dvec2)+0.5],[min(dvec2)-0.5,max(dvec2)+0.5],'r');
    axis([min(dvec2)-0.5,max(dvec2)+0.5,min(dvec2)-0.5,max(dvec2)+0.5])
    %title('Scatter Plot')
    xlabel ('Observed Data')
    ylabel ('Estimations')
    figure;h = histogram(qv1(:),16,'FaceColor',[0 0 1],'FaceAlpha',0.7);
    hold on
    histogram(Z_ibt{i,1}(:),'BinEdges',h.BinEdges,'FaceColor',[0.2 1 0],'FaceAlpha',0.7)
    %title('Histograms of Data')
    legend({'Original', 'Estimated'});
    figure;pcolor(Z4); view(2);shading interp; %title('95% Confidence Interval');
    colorbar;set(gca,'XTick',[],'YTick',[]);
    clear h

    clear cc1 cc2 cc3 cc4 Z1 Z2 Z3 Z4 dvec1 dvec2

end


%% ################# DirVar1 ##############################
%==========================================================

% >>> Fitting I and Anisotropy Estimation <<<

% Desired Models
```

```
models = {'Gexp';'Gaus';'Sphe';'Mate';'Spar'};
n_models = length(models);

% Initial Values and Limits for optimization
b = [gexpmax,maxdist*1/3,gexpmax/100]; % s2,xi & c0
b_lb = [eps,eps,eps]; b_ub = [gexpmax*1.5,maxdist,gexpmax/5]; %lower and
    upper limits
bsp = [1000,maxdist*1/3,gexpmax/100]; % eta0, xi, c0
bsp_lb = [eps,eps,eps]; bsp_ub = [inf,maxdist,gexpmax/5]; %lower and
    upper limits

% Summary cells
model_par0 = {[b,1.5];b;b;[b,1.5];[bsp,1]}; %initial parameters values
model_par_lb = {[b_lb,eps];b_lb;b_lb;[b_lb,0.3];[bsp_lb,-2+eps]}; %lower
    bounds
model_par_ub = {[b_ub,2-eps];b_ub;b_ub;[b_ub,3.5];[bsp_ub,inf]}; %upper
    bounds

clear b b_lb b_ub bsp bsp_lb bsp_ub

% Estimation of Anisotropy
R(n_models,1)=0;phi(n_models,1)=0;xi1(n_models,1)=0;xi2(n_models,1)=0;%
    matrices preallocation
er1(n_models,1)=0;er2(n_models,1)=0; %matrices preallocation
objmod = 'NWEr_m';flag = 1;
% nrsampl = 10; samplpc = 50;
for i=1:n_models
    model.function = models{i,1};
    model.params0 = model_par0{i,1};
    model.paramslb = model_par_lb{i,1};
    model.paramsub = model_par_ub{i,1};

     [R(i,1),phi(i,1),xi1(i,1),xi2(i,1),er1(i,1),er2(i,1)] =...
         aniso_dvf(x,y,rf,model,objmod,ncpc,nrbins,phistep,phitol,flag);
%     [R(i,1),phi(i,1),xi1(i,1),xi2(i,1),er1(i,1),er2(i,1)] =...
%         dirvar_ccv_s(x,y,rf,model,objmod,N_ms,ncpc,nrsampl,samplpc,
    nrbins,phistep,phitol,flag);

end

%% >>> Fitting II and Parameters of Correlation Estimation (s2,c0,v or
    eta1) <<<

% Initial Values and Limits for optimization
```

```
b{n_models,1}=[];b_lb{n_models,1}=[];b_ub{n_models,1}=[];
for i = 1:n_models
    b{i,1} = [gexpmax,xi1(i,1),R(i,1),phi(i,1),gexpmax/100];
    b_lb{i,1} = [eps,xi1(i,1),R(i,1),phi(i,1),eps];
    b_ub{i,1} = [inf,xi1(i,1),R(i,1),phi(i,1),gexpmax/5];
end

% Summary cells
model_par0 = {[b{1,1},1.1];b{2,1};b{3,1};[b{4,1},1.5];[b{5,1},1]}; % initial parameters values
model_par_lb = {[b_lb{1,1},eps];b_lb{2,1};b_lb{3,1};[b_lb{4,1},0.3];[b_lb{5,1},-2+eps]};%lower bounds
model_par_ub = {[b_ub{1,1},2];b_ub{2,1};b_ub{3,1};[b_ub{4,1},3.5];[b_ub{5,1},inf]}; %upper bounds

% Estimation of Parameters (s2,c0,v or eta1)
bmodel{n_models,1}=[]; fval(n_models,1)=0;tit{n_models,1}=[];
iso = 00;objmod = 'NWEr_m';flag = 1;
for i=1:n_models
    model.function = models{i,1};
    model.params0 = model_par0{i,1};
    model.paramslb = model_par_lb{i,1};
    model.paramsub = model_par_ub{i,1};

   [bmodel{i,1},fval(i,1),tit{i,1}] =...
        variogramfit(gexp,nr_pairs,c_centers,iso,model,objmod,flag);
end


% >>> Cross Validation <<<

% Matrices and Cells preallocation
cv_scores{n_models,1}=[]; cv_checks{n_models,1}=[];
cv_matr{n_models,1}=[]; cv_Ss(n_models,6)= 0;

% Inputs definition
 iso = 00; d_col = 1;

% Cross Validation
for i=1:n_models
    model.function = models{i,1};
    model.params = bmodel{i,1};
    model.r_ok = [6,6];
```

```
    [cv_scores{i,1}, cv_checks{i,1}, cv_matr{i,1}] =...
        crossval(x,y,rf,iso,d_col,model);
    cv_Ss(i,:) = table2array(cv_scores{i,1}(:,2:end));
end

% Cross Validation Scores
table_h = {'MeanAbsErr','MaxAbsErr','MSE','RMSE','rpearson','rspearman',
    'finalscore'};
table_r = {'Gexp';'Gaus';'Sphe';'Mate';'Spar'};

relMSE = cv_Ss(:,3)/min(cv_Ss(:,3)); %relative MSE
FinalScore = ((1./relMSE).^2).*cv_Ss(:,5).*cv_Ss(:,6); %finalscore
cv_Ss = [cv_Ss, FinalScore];
cv_Ssf = array2table(cv_Ss,'VariableNames',table_h,'RowNames',table_r);
clear relMSE FinalScore

%Trend addition and Boxcox Inversion
cv_St(n_models,6)= 0;
for i=1:n_models

    cv_matr{i,1}.Z_tr = cv_matr{i,1}.Z;

    cv_matr{i,1}.Z_ibt1 = cv_matr{i,1}.Z_tr;

    cv_matr{i,1}.Z_ibt = real(cv_matr{i,1}.Z_ibt1);
    cv_realZ(i,1) = isreal(cv_matr{i,1}.Z_ibt1);

    cv_St(i,:) = correlstats(v1,cv_matr{i,1}.Z_ibt);%total cv scores

end

% Total Cross Validation Scores
relMSE = cv_St(:,3)/min(cv_St(:,3)); %relative MSE
FinalScore = ((1./relMSE).^2).*cv_St(:,5).*cv_St(:,6); %finalscore
cv_St = [cv_St, FinalScore];
cv_Stf = array2table(cv_St,'VariableNames',table_h,'RowNames',table_r);
clear relMSE FinalScore

%Plots
for i=1:n_models

    % Stochastic Component's figures
    cc1 = [col,row,rf(:);qcol,qrow,zeros(Nu,1)];
    cc2 = [col,row,cv_matr{i,1}.Z(:);qcol,qrow,zeros(Nu,1)];
```

```
    Z1(max(cc1(:,2)),max(cc1(:,1)))=0; %#ok<SAGROW>
    Z2=Z1;
    for j = 1:size(cc1,1)
        Z1(cc1(j,2),cc1(j,1)) = cc1(j,3);
        Z2(cc2(j,2),cc2(j,1)) = cc2(j,3);
    end

    figure;pcolor(Z1);%title('Sample Stochastic Component');
    view(2);shading interp; colorbar;set(gca,'XTick',[],'YTick',[]);
    figure;pcolor(Z2);%title(sprintf('Estimation of Sample Stochastic
   Component \n%s',tit{i,1}));
    view(2);shading interp;colorbar;set(gca,'XTick',[],'YTick',[]);
    figure;scatter(rf(:),cv_matr{i,1}.Z(:),'filled','d');hold on;
    dvec1 = [rf(:);cv_matr{i,1}.Z(:)];
    plot([min(dvec1)-0.5,max(dvec1)+0.5],[min(dvec1)-0.5,max(dvec1)
   +0.5],'r');
    axis([min(dvec1)-0.5,max(dvec1)+0.5,min(dvec1)-0.5,max(dvec1)+0.5])
    %title('Scatter Plot')
    xlabel ('Observed Data'); ylabel ('Estimations');
    figure; h = histogram(rf(:),16,'EdgeColor',[0 0 1],'FaceAlpha',0.7);
    hold on
    histogram(cv_matr{i,1}.Z(:),'BinEdges',h.BinEdges,'EdgeColor',[0.2 1
    0]','FaceAlpha',0.7)
    %title('Histograms of Sample Stochastic Component')
    legend({'Original', 'Estimated'});
    clear h


    % Total Data figures
    cc3 = [col,row,v1(:);qcol,qrow,zeros(Nu,1)];
    cc4 = [col,row,cv_matr{i,1}.Z_ibt(:);qcol,qrow,zeros(Nu,1)];
    Z3(max(cc3(:,2)),max(cc3(:,1)))=0; %#ok<SAGROW>
    Z4=Z3;
    for j = 1:size(cc3,1)
        Z3(cc3(j,2),cc3(j,1)) = cc3(j,3);
        Z4(cc4(j,2),cc4(j,1)) = cc4(j,3);
    end
%      figure;pcolor(Z3);view(2);shading interp; %title('Original Sample
   ');
%      colorbar;set(gca,'XTick',[],'YTick',[]);
    figure;pcolor(Z4);view(2);shading interp; %title(sprintf('Estimation
    of Original Sample \n%s',tit{i,1}));
    colorbar;set(gca,'XTick',[],'YTick',[]);
    figure;scatter(v1(:),cv_matr{i,1}.Z_ibt(:),'filled','d');hold on;
```

```
    dvec2 = [v1(:);cv_matr{i,1}.Z_ibt(:)];
    plot([min(dvec2)-0.5,max(dvec2)+0.5],[min(dvec2)-0.5,max(dvec2)
   +0.5],'r');
    axis([min(dvec2)-0.5,max(dvec2)+0.5,min(dvec2)-0.5,max(dvec2)+0.5])
    %title('Scatter Plot')
    xlabel ('Observed Data')
    ylabel ('Estimations')
    figure;h = histogram(v1(:),16,'EdgeColor',[0 0 1],'FaceAlpha',0.7);
    hold on
    histogram(cv_matr{i,1}.Z_ibt(:),'BinEdges',h.BinEdges,'EdgeColor'
   ,[0.2 1 0],'FaceAlpha',0.7)
    %title('Histograms of Sample Data')
    legend({'Original', 'Estimated'});
    clear h

    clear Z1 Z2 Z3 Z4 dvec1 dvec2

end


% >>> Ordinary Kriging <<<

% Sort models based on cross validation scores
[~,ind] = sort(table2array(cv_Stf(:,7)),'descend');

% Matrices and Cells preallocation
Z{N_kr_mod,1}=[]; Z_error{N_kr_mod,1}=[];kr_checks{N_kr_mod,1}=[];
kr_matr{N_kr_mod,1}=[];
kr_Ss(N_kr_mod,6)= 0; table_r2{N_kr_mod,1} = [];
CI1{N_kr_mod,1}=[];UNC{N_kr_mod,1}=[];

% Inputs definition
xu = qcol; yu = qrow; iso = 00;

% Ordinary Kriging
for i=1:N_kr_mod
    model.function = models{ind(i),1};
    model.params = bmodel{ind(i),1};
    model.r_ok = [6,6];

    [Z{i,1},Z_error{i,1},kr_checks{i,1}, kr_matr{i,1}] =...
        ordkrig(x,y,rf,xu,yu,iso,model);
    kr_Ss(i,:) = correlstats(Z{i,1},qfluc);
    table_r2{i,1} = table_r{ind(i),1};
```

```

    %Confidence Intervals (95%)
    CI1{i,1}.low = Z{i,1} - 1.96*sqrt(Z_error{i,1});
    CI1{i,1}.up = Z{i,1} + 1.96*sqrt(Z_error{i,1});
    CI1{i,1}.uncer = 1.96*sqrt(Z_error{i,1});
    UNC{i,1} = real(CI1{i,1}.uncer);
    realCI(i,1) = isreal(CI1{i,1}.uncer);
end

% Kriging Scores
relMSE = kr_Ss(:,3)/min(kr_Ss(:,3)); %relative MSE
FinalScore = ((1./relMSE).^2).*kr_Ss(:,5).*kr_Ss(:,6); %finalscore
kr_Ss = [kr_Ss, FinalScore];
kr_Ssf = array2table(kr_Ss,'VariableNames',table_h,'RowNames',table_r2);
clear relMSE FinalScore

%Trend addition and Boxcox Inversion
kr_St(N_kr_mod,6)= 0; Z_tr{N_kr_mod,1} = 0;
Z_ibt1{N_kr_mod,1} = 0;Z_ibt{N_kr_mod,1} = 0;
for i=1:N_kr_mod

    Z_tr{i,1} = Z{i,1};

    Z_ibt1{i,1} = Z_tr{i,1};

    Z_ibt{i,1} = real(Z_ibt1{i,1});
    kr_realZ(i,1) = isreal(Z_ibt1{i,1});

    kr_St(i,:) = correlstats(qv,Z_ibt{i,1});%total kriging scores

end

% Total Kriging Scores
relMSE = kr_St(:,3)/min(kr_St(:,3)); %relative MSE
FinalScore = ((1./relMSE).^2).*kr_St(:,5).*kr_St(:,6); %finalscore
kr_St = [kr_St, FinalScore];
kr_Stf = array2table(kr_St,'VariableNames',table_h,'RowNames',table_r2);
clear relMSE FinalScore

%Plots
for i=1:N_kr_mod

    % Stochastic Component's figures
    cc1 = [col,row,rf(:);qcol,qrow,qfluc(:)];
```

```
cc2 = [col,row,rf(:);qcol,qrow,Z{i,1}];
Z1(max(cc1(:,2)),max(cc1(:,1)))=0; %#ok<SAGROW>
Z2=Z1;
for j = 1:size(cc1,1)
    Z1(cc1(j,2),cc1(j,1)) = cc1(j,3);
    Z2(cc2(j,2),cc2(j,1)) = cc2(j,3);
end
figure;pcolor(Z1);%title('Original Stochastic Component');
view(2);shading interp; colorbar;set(gca,'XTick',[],'YTick',[]);
figure;pcolor(Z2); %title(sprintf('Estimation of Stochastic
Component \n%s',tit{ind(i),1}));
view(2);shading interp; colorbar;set(gca,'XTick',[],'YTick',[]);
figure;scatter(qfluc(:),Z{i,1}(:),'filled','d');hold on;
dvec1 = [qfluc(:);Z{i,1}(:)];
plot([min(dvec1)-0.5,max(dvec1)+0.5],[min(dvec1)-0.5,max(dvec1)
+0.5],'r');
axis([min(dvec1)-0.5,max(dvec1)+0.5,min(dvec1)-0.5,max(dvec1)+0.5])
%title('Scatter Plot')
xlabel ('Observed Data')
ylabel ('Estimations')
figure;h = histogram(qfluc(:),16,'FaceColor',[0 0 1],'FaceAlpha'
,0.7);
hold on
histogram(Z{i,1}(:),'BinEdges',h.BinEdges,'FaceColor',[0.2 1 0],'
FaceAlpha',0.7)
%title('Histograms of Stochastic Component')
legend({'Original', 'Estimated'});
clear h

% Total Data figures
cc3 = [col,row,v1(:);qcol,qrow,Z_ibt{i,1}];
cc4 = [col,row,zeros(size(col,1),1); qcol,qrow,UNC{i,1}];
Z3(max(cc3(:,2)),max(cc3(:,1)))=0; %#ok<SAGROW>
Z4=Z3;
for j = 1:size(cc3,1)
    Z3(cc3(j,2),cc3(j,1)) = cc3(j,3);
    Z4(cc4(j,2),cc4(j,1)) = cc4(j,3);
end
figure;pcolor(Z3); view(2);shading interp; %title(sprintf('
Estimation of Original Data \n%s',tit{ind(i),1}));
colorbar;set(gca,'XTick',[],'YTick',[]);
figure;scatter(qv1(:),Z_ibt{i,1}(:),'filled','d');hold on;
dvec2 = [qv1(:);Z_ibt{i,1}(:)];
```

```
    plot([min(dvec2)-0.5,max(dvec2)+0.5],[min(dvec2)-0.5,max(dvec2)
   +0.5],'r');
    axis([min(dvec2)-0.5,max(dvec2)+0.5,min(dvec2)-0.5,max(dvec2)+0.5])
   %title('Scatter Plot')
    xlabel ('Observed Data')
    ylabel ('Estimations')
    figure;h = histogram(qv1(:),16,'FaceColor',[0 0 1],'FaceAlpha',0.7);
    hold on
    histogram(Z_ibt{i,1}(:),'BinEdges',h.BinEdges,'FaceColor',[0.2 1 0],
   'FaceAlpha',0.7)
   %title('Histograms of Data')
    legend({'Original', 'Estimated'});
    figure;pcolor(Z4); view(2);shading interp; %title('95% Confidence
   Interval');
    colorbar;set(gca,'XTick',[],'YTick',[]);
    clear h

    clear cc1 cc2 cc3 cc4 Z1 Z2 Z3 Z4 dvec1 dvec2

end
%
   ============================================================================
```

C:/Users/Vasilis/Desktop/AB/Dissertation/DiplomaThesis/MyThesis/Appendix2/Test4Appendix.m

B.2 Regular Sample

```
                        % Dissertation
                       % Regular Sample

clc;clear variables;close all;

%################# Preliminary Analysis ############################
%====================================================================

% Basic parameters
n_data = 2; %if 2 normalised velocities are used,else if 1 are used
               %velocities in km/s,else if 0 the original velocities are
   used
n_dr = 10; %distance between drills
```

```matlab

% Load Data
load marm.in
ny = 122; nx = 384; %>>a priori known size of the image<<
marm_rf = reshape(marm,ny,nx);
marm_rf = flipud(marm_rf);

idata0 = marm_rf; %original velocities (m/s)
idata1 = marm_rf/1000;%velocities in km/s
idata2 = marm_rf/max(max(marm_rf)); %normalised velocities

color = 'white';fsize = 18.0; font = 'Cambria'; fweig = 'bold';

if n_data==0
    data = idata0;
    colbtitle = 'Velocity (m/s)';
elseif n_data==1
    data = idata1;
    colbtitle = 'Velocity (km/s)';
elseif n_data==2
    data = idata2;
    colbtitle = 'Normalised Velocity';
else
    error('Error: Not valid value for n_data input. It must be 0,1 or 2.')
end

[row_all, col_all, v_all1] = find(data);

% >>>Original Data Plots<<<

figure;%Simple plot
pcolor(data); shading interp %flat
%title('Geological Section (Velocity Model)')
set(gca,'XLim',[0 nx],'YLim',[0 ny],'XTick',[],'YTick',[])

figure; %Simple plot plus colorbar
pcolor(data); shading interp %flat
%title('Geological Section (Velocity Model)')
c = colorbar;
c.Label.String = colbtitle;
set(gca,'XLim',[0 nx],'YLim',[0 ny],'XTick',[],'YTick',[])

figure; %Plot with actual distances and colorbar
```

```
pcolor(flipud(data)); shading interp %flat
%title('Geological Section (Velocity Model)')
c = colorbar;
c.Label.String = colbtitle;
xlabel('Distance (km)');
ylabel('Depth (km)');
ax = gca;
ax.XAxisLocation = 'top';
ax.XLim = [0 nx]; ax.YLim = [0 ny];
ax.XTick = (0:9.2)*nx/9.2;
ax.XTickLabel = (ax.XTick)*9.2/nx;
ax.YTick = (0:0.5:3)*ny/3;
ax.YTickLabel = (ax.YTick)*3/ny;
ax.YDir = 'reverse';

data_tot_vec = data(:); %total image data in vector form

% >>>Define "drill-holes"<<<
data2 = data;
dr1 = floor((nx - floor(nx/n_dr)*n_dr)/2)+1; %location of first "drilling" on x axis
data2(:,dr1:n_dr:nx)= 0;
[qrow,qcol,qv1] = find(data2); %unknown points coordinations and values
drills = data - data2; %square form of "drill-holes"
[row,col,v1] = find(drills); %known points coordinations and values - TRAINING SET
N = length(v1); %number of known points

% >>>Sample ("drill-holes") Plot<<<

figure; %Simple plot
pcolor(drills); shading interp %flat
%title('"Drill-holes": part of geological section taken as data')
set(gca,'XLim',[0 nx],'YLim',[0 ny],'XTick',[],'YTick',[])

figure; %Simple plot plus colorbar
pcolor(drills); shading interp %flat
%title('"Drill-holes": part of geological section taken as data')
c1 = colorbar;
c1.Label.String = colbtitle;
set(gca,'XLim',[0 nx],'YLim',[0 ny],'XTick',[],'YTick',[])

figure; %Plot with actual distances and colorbar
pcolor(flipud(drills)); shading interp %flat
```

```
%title('Geological Section (Velocity Model)')
c1 = colorbar;
c1.Label.String = colbtitle;
xlabel('Distance (km)');
ylabel('Depth (km)');
ax = gca;
ax.XAxisLocation = 'top';
ax.XLim = [0 nx]; ax.YLim = [0 ny];
ax.XTick = (0:9.2)*nx/9.2;
ax.XTickLabel = (ax.XTick)*9.2/nx;
ax.YTick = (0:0.5:3)*ny/3;
ax.YTickLabel = (ax.YTick)*3/ny;
ax.YDir = 'reverse';

%>>>Data Histograms & Statistical Moments<<<

numbins = 15;
% Total image histogram
figure;
%subplot(1,2,1)
histfit(data_tot_vec,numbins)
alpha(0.5)
%title('Total image histogram')
% "Drills-holes" data histogram
figure;%subplot(1,2,2)
histfit(v1,numbins)
alpha(0.5)
%title('Drill-holes data histogram')

% Total image data moments
totim_stats = [min(data_tot_vec) max(data_tot_vec) mean(data_tot_vec)
    median(data_tot_vec) var(data_tot_vec) skewness(data_tot_vec)
    kurtosis(data_tot_vec)];
% "Drill-holes" data moments
drills_stats = [min(v1) max(v1) mean(v1) median(v1) var(v1) skewness(v1)
     kurtosis(v1)];


%>>>Normality of data checking and Transformation<<<

% Histogram and Normal Probability Plot
figure; %same as the previous figure plus NPP
%subplot(1,2,1)
histfit(v1,numbins)
```

```
alpha(0.5)
%title('Drill-holes data histogram')
figure; %subplot(1,2,2)
nnp = normplot(v1);
h_ch=get(gcf,'Children');h_str=get(h_ch(1),'Title');set(h_str,'String','
    '); % remove normplot title
[h_orig,kst_p_orig,ksstat_orig,cv_orig] = kstest(v1(:));

% BoxCox Transformation
[v, lambda] = boxcox(v1); %known points boxcox transformation
qv = (qv1.^lambda -1)/lambda; %unknown points boxcox transformation
v_all = (v_all1.^lambda -1)/lambda; %all points boxcox transformation
figure;
%subplot(1,2,1)
histfit(v,numbins)
alpha(0.5)
%title('Transformed data histogram')
figure; %subplot(1,2,2)
normplot(v)
h_ch=get(gcf,'Children');h_str=get(h_ch(1),'Title');set(h_str,'String','
    '); % remove normplot title
[h_bxtr,p_bxtr,ksstat_bxtr,cv_bxtr] = kstest(v(:));

%>>> Data Trend Estimation <<<
nfr = 2;
trmodel = 'linear';
v_trend = reshape(v,ny,N/ny);
[fluc,Mx,Mx_func,a,trend_scores,dfreq,a_trends] = detrendv(col,row,
    v_trend,nfr,trmodel,0);
qMx = Mx_func(qcol,qrow,a); %trend on the unknown points
qfluc = qv-qMx; %fluctuations/residuals on the unknown points

%Plot data & trend
X = col(:); Y = row(:); rf1 = v_trend(:);
figure;
scatter3(X,flipud(Y),rf1,'r','filled')
hold on
Xfit = min(X):1:max(X); nxfit = length(Xfit);
Yfit = min(Y):1:max(Y); nyfit = length(Yfit);
[XFIT,YFIT] = meshgrid(Xfit,Yfit);
VFIT = Mx_func(XFIT(:),YFIT(:),a);
VFIT = flipud(reshape(VFIT,nyfit,nxfit));
mesh(XFIT,YFIT,VFIT)
colorbar
```

```
%xlabel('x')
%ylabel('y')
xlabel('Alongside Section')
ylabel('Depth')
zlabel('Transformed Normalised Velocity')
%set(gca,'YTick',flipud(get(gca,'YTick')));
%set(gca,'YDir','reverse');
%title('Data & Trend Model')
view(-52,6)
shading interp
c = colorbar; c.Label.String = 'Transformed Normalised Velocity';

%Detrend whole dataset
Mx_all = Mx_func(col_all,row_all,a); %trend on the unknown points
fluc_all = v_all-Mx_all; %fluctuations/residuals on the unknown points
fluc_all = reshape(fluc_all,ny,nx);

figure; %Plot with actual distances and colorbar
pcolor(flipud(fluc_all)); shading interp %flat
%title('Detrended Geological Section')
c1 = colorbar;
% c1.Label.String = colbtitle;
xlabel('Distance (km)');
ylabel('Depth (km)');
ax = gca;
ax.XAxisLocation = 'top';
ax.XLim = [0 nx]; ax.YLim = [0 ny];
ax.XTick = (0:9.2)*nx/9.2;
ax.XTickLabel = (ax.XTick)*9.2/nx;
ax.YTick = (0:0.5:3)*ny/3;
ax.YTickLabel = (ax.YTick)*3/ny;
ax.YDir = 'reverse';

%>>> Statistical Analysis of Residuals <<<

% Residuals/Fluctuations moments
fluc_stats = [min(fluc) max(fluc) mean(fluc) median(fluc) var(fluc)
    skewness(fluc) kurtosis(fluc)];

% Histogram and Normal Probablity Plot
figure;
%subplot(1,2,1)
histfit(fluc,numbins)
alpha(0.5)
```

```
%title('Histogram of detrended data')
figure; %subplot(1,2,2)
normplot(fluc)
h_ch=get(gcf,'Children');h_str=get(h_ch(1),'Title');set(h_str,'String','
    '); % remove normplot title
[h_fluc,p_fluc,ksstat_fluc,cv_fluc] = kstest(fluc(:));
%===========================================================================



%% ################## Experimantal Variogram
    ##############################
%===========================================================================

% >>> Initialize Basic Parameters <<<
c = {col,row}; %known points' coordinations
qc = {qcol,qrow}; %"unknown" points' coordinations
ncpc = 0.2;
N = size(col,1);
Nu = size(qcol,1);
maxdist = hypot(col(1,1)-col(N,1),row(1,1)-row(N,1))*ncpc;
nrbins = 45;
phistep = 15;
phitol = 20;
N_kr_mod = 3;

% >>> Experimental (Semi-)Variogram (anisotropic) <<<
x = col; y = row; rf = fluc; iso = 0; flag = 1;
[~,~,~] = expvar(x,y,rf,iso,ncpc,nrbins,4,phitol,2); %exper. variogr. of
     high analysis
[gexp, nr_pairs, c_centers] = expvar(x,y,rf,iso,ncpc,nrbins,phistep,
    phitol,flag);
gexpmax = max(max(gexp));
%===========================================================================


%% ################## DirVar0 ##############################
%===========================================================================

% >>> Fitting I and Parameters of Anisotropic Correlation Estimation (s2
    ,xi1,xi2,phi,c0,v or eta1) <<<

% Desired Models
models = {'Gexp';'Gaus';'Sphe';'Mate';'Spar'};
```

```
n_models = length(models);

% Initial Values and Limits for optimization
b = [gexpmax,maxdist*2/3,0.5,10,gexpmax/100]; % s2,xi1,R,phi & c0
b_lb = [eps,eps,eps,-90,eps]; b_ub = [gexpmax*1.5,maxdist*1.5,30,90,
    gexpmax/5]; %lower and upper limits
bsp = [1000,maxdist*2/3,0.5,10,gexpmax/100]; % eta0, xi1,R,phi & c0
bsp_lb = [eps,eps,eps,-90,eps]; bsp_ub = [inf,maxdist*1.5,30,90,gexpmax
    /5]; %lower and upper limits

% Summary cells
model_par0 = {[b,1.5];b;b;[b,1.5];[bsp,1]}; %initial parameters values
model_par_lb = {[b_lb,eps];b_lb;b_lb;[b_lb,0.3];[bsp_lb,-2+eps]}; %lower
     bounds
model_par_ub = {[b_ub,2-eps];b_ub;b_ub;[b_ub,3.5];[bsp_ub,inf]}; %upper
    bounds

clear b b_lb b_ub bsp bsp_lb bsp_ub

% Estimation of Parameters (s2,xi1,xi2,phi,c0,v or eta1)
bmodel{n_models,1}=[]; fval(n_models,1)=0; tit{n_models,1}=[];
iso = 00;objmod = 'NWEr_m';flag = 1;
for i=1:n_models
    model.function = models{i,1};
    model.params0 = model_par0{i,1};
    model.paramslb = model_par_lb{i,1};
    model.paramsub = model_par_ub{i,1};

   [bmodel{i,1},fval(i,1),tit{i,1}] =...
        variogramfit(gexp,nr_pairs,c_centers,iso,model,objmod,flag);
end

% Anisotropy Estimation (#Not Necessary#)
R0(n_models,1) = 0;phi0(n_models,1) = 0;xi10(n_models,1) = 0;xi20(
    n_models,1) = 0;
for i=1:n_models
    R0(i,1) = bmodel{i,1}(1,3);
    phi0(i,1) = bmodel{i,1}(1,4);
    xi10(i,1) = bmodel{i,1}(1,2);
    xi20(i,1) = bmodel{i,1}(1,2)/R0(i,1);
    if R0(i,1)>1
        R0(i,1) = 1/R0(i,1);bmodel{i,1}(1,3) = R0(i,1);
        xi101 = xi10(i,1);
        xi10(i,1) = xi20(i,1); bmodel{i,1}(1,2) = xi20(i,1);
```

```
        xi20(i,1) = xi101;
        if phi0(i,1)>0
            phi0(i,1) = phi0(i,1)-90;
        else
            phi0(i,1) = phi0(i,1)+90;
        end
        bmodel{i,1}(1,4) = phi0(i,1);
    end
end

R = mean(R0); phi = mean(phi0);xi1 = mean(xi10);xi2 = mean(xi20);


% >>> Cross Validation <<<

% Matrices and Cells preallocation
cv_scores{n_models,1}=[]; cv_checks{n_models,1}=[];
cv_matr{n_models,1}=[]; cv_Ss(n_models,6)= 0;

% Inputs definition
x = reshape(x,ny,N/ny); y = reshape(y,ny,N/ny);
rf = reshape(rf,ny,N/ny); iso = 00; d_col = 1;

% Cross Validation
for i=1:n_models
    model.function = models{i,1};
    model.params = bmodel{i,1};
    model.r_ok = [22,4];

    [cv_scores{i,1}, cv_checks{i,1}, cv_matr{i,1}] =...
        crossval(x,y,rf,iso,d_col,model);
    cv_Ss(i,:) = table2array(cv_scores{i,1}(:,2:end));
end

% Cross Validation Scores
table_h = {'MeanAbsErr','MaxAbsErr','MSE','RMSE','rpearson','rspearman',
    'finalscore'};
table_r = {'Gexp';'Gaus';'Sphe';'Mate';'Spar'};

relMSE = cv_Ss(:,3)/min(cv_Ss(:,3)); %relative MSE
FinalScore = ((1./relMSE).^2).*cv_Ss(:,5).*cv_Ss(:,6); %finalscore
cv_Ss = [cv_Ss, FinalScore];
cv_Ssf = array2table(cv_Ss,'VariableNames',table_h,'RowNames',table_r);
clear relMSE FinalScore
```

```
%Trend addition and Boxcox Inversion
cv_St(n_models,6)= 0;
for i=1:n_models

    cv_matr{i,1}.Z_tr = Mx + cv_matr{i,1}.Z;

    if lambda==00
        cv_matr{i,1}.Z_ibt1 = cv_matr{i,1}.Z_tr;
    elseif lambda==0
        cv_matr{i,1}.Z_ibt1 = exp(cv_matr{i,1}.Z_tr);
    else
        cv_matr{i,1}.Z_ibt1 = (lambda*cv_matr{i,1}.Z_tr + 1).^(1/lambda)
    ;
    end
    cv_matr{i,1}.Z_ibt = real(cv_matr{i,1}.Z_ibt1);
    cv_realZ(i,1) = isreal(cv_matr{i,1}.Z_ibt1); %#ok<SAGROW>

    cv_St(i,:) = correlstats(v1,cv_matr{i,1}.Z_ibt);%total cv scores

end

% Total Cross Validation Scores
relMSE = cv_St(:,3)/min(cv_St(:,3)); %relative MSE
FinalScore = ((1./relMSE).^2).*cv_St(:,5).*cv_St(:,6); %finalscore
cv_St = [cv_St, FinalScore];
cv_Stf = array2table(cv_St,'VariableNames',table_h,'RowNames',table_r);
clear relMSE FinalScore

%Plots
for i=1:n_models

    % Stochastic Component's figures
    Z1 = reshape(rf,ny,N/ny);
    Z2 = reshape(cv_matr{i,1}.Z,ny,N/ny);

    figure;pcolor(Z1);%title('Sample Stochastic Component');
    view(2);shading interp; colorbar;set(gca,'XTick',[],'YTick',[]);
    figure;pcolor(Z2);%title(sprintf('Estimation of Sample Stochastic
    Component \n%s',tit{i,1}));
    view(2);shading interp;colorbar;set(gca,'XTick',[],'YTick',[]);
    figure;scatter(Z1(:),Z2(:),'filled','d');hold on;
    dvec1 = [Z1(:);Z2(:)];
```

```
plot([min(dvec1)-0.5,max(dvec1)+0.5],[min(dvec1)-0.5,max(dvec1)
+0.5],'r');
axis([min(dvec1)-0.5,max(dvec1)+0.5,min(dvec1)-0.5,max(dvec1)+0.5])
%title('Scatter Plot')
xlabel ('Observed Data'); ylabel ('Estimations');
figure; h = histogram(Z1(:),16,'EdgeColor',[0 0 1],'FaceAlpha',0.7);
hold on
histogram(Z2(:),'BinEdges',h.BinEdges,'EdgeColor',[0.2 1 0]','
FaceAlpha',0.7)
%title('Histograms of Sample Stochastic Component')
legend({'Original', 'Estimated'});
clear h


% Total Data figures
Z3 = reshape(v1,ny,N/ny);
Z4 = reshape(cv_matr{i,1}.Z_ibt,ny,N/ny);
%    figure;pcolor(Z3);view(2);shading interp; %title('Original Sample
');
%    c = colorbar; c.Label.String = 'Normalised Velocity';set(gca,'
XTick',[],'YTick',[]);
figure;pcolor(Z4);view(2);shading interp; %title(sprintf('Estimation
of Original Sample \n%s',tit{i,1}));
c = colorbar; c.Label.String = 'Normalised Velocity';set(gca,'XTick'
,[],'YTick',[]);
figure;scatter(Z3(:),Z4(:),'filled','d');hold on;
dvec2 = [Z3(:);Z4(:)];
plot([min(dvec2)-0.5,max(dvec2)+0.5],[min(dvec2)-0.5,max(dvec2)
+0.5],'r');
axis([min(dvec2)-0.5,max(dvec2)+0.5,min(dvec2)-0.5,max(dvec2)+0.5])
%title('Scatter Plot')
xlabel ('Observed Data')
ylabel ('Estimations')
figure;h = histogram(Z3(:),16,'EdgeColor',[0 0 1],'FaceAlpha',0.7);
hold on
histogram(Z4(:),'BinEdges',h.BinEdges,'EdgeColor',[0.2 1 0],'
FaceAlpha',0.7)
%title('Histograms of Sample Data')
legend({'Original', 'Estimated'});
clear h

clear Z1 Z2 Z3 Z4 dvec1 dvec2

end
```

```
% >>> Ordinary Kriging <<<

% Sort models based on cross validation scores
[~,ind] = sort(table2array(cv_Stf(:,7)),'descend');

% Matrices and Cells preallocation
Z{N_kr_mod,1}=[]; Z_error{N_kr_mod,1}=[];kr_checks{N_kr_mod,1}=[];
kr_matr{N_kr_mod,1}=[];
kr_Ss(N_kr_mod,6)= 0; table_r2{N_kr_mod,1} = [];
CI1{N_kr_mod,1}=[];UNC{N_kr_mod,1}=[];

% Inputs definition
x = reshape(x,ny,N/ny); y = reshape(y,ny,N/ny); rf = reshape(rf,ny,N/ny)
    ;
xu = reshape(qcol,ny,Nu/ny); yu = reshape(qrow,ny,Nu/ny); iso = 00;

% Ordinary Kriging
for i=1:N_kr_mod
    model.function = models{ind(i),1};
    model.params = bmodel{ind(i),1};
    model.r_ok = [22,4];

    [Z{i,1},Z_error{i,1},kr_checks{i,1}, kr_matr{i,1}] =...
        ordkrig(x,y,rf,xu,yu,iso,model);
    kr_Ss(i,:) = correlstats(Z{i,1},qfluc);
    table_r2{i,1} = table_r{ind(i),1};

    %Confidence Intervals (95%)
    CI1{i,1}.low = Z{i,1} - 1.96*sqrt(Z_error{i,1});
    CI1{i,1}.up = Z{i,1} + 1.96*sqrt(Z_error{i,1});
    CI1{i,1}.uncer = 1.96*sqrt(Z_error{i,1});
    UNC{i,1} = real(CI1{i,1}.uncer);
    realCI(i,1) = isreal(CI1{i,1}.uncer); %#ok<SAGROW>
end

% Kriging Scores
relMSE = kr_Ss(:,3)/min(kr_Ss(:,3)); %relative MSE
FinalScore = ((1./relMSE).^2).*kr_Ss(:,5).*kr_Ss(:,6); %finalscore
kr_Ss = [kr_Ss, FinalScore];
kr_Ssf = array2table(kr_Ss,'VariableNames',table_h,'RowNames',table_r2);
clear relMSE FinalScore
```

```
%Trend addition and Boxcox Inversion
kr_St(N_kr_mod,6)= 0; Z_tr{N_kr_mod,1} = 0;
Z_ibt1{N_kr_mod,1} = 0;Z_ibt{N_kr_mod,1} = 0;
for i=1:N_kr_mod

    Z_tr{i,1} = qMx + Z{i,1};

    if lambda==00
        Z_ibt1{i,1} = Z_tr{i,1};
    elseif lambda==0
        Z_ibt1{i,1} = exp(Z_tr{i,1});
    else
        Z_ibt1{i,1} = (lambda*Z_tr{i,1} + 1).^(1/lambda);
    end
    Z_ibt{i,1} = real(Z_ibt1{i,1});
    kr_realZ(i,1) = isreal(Z_ibt1{i,1});  %#ok<SAGROW>

    kr_St(i,:) = correlstats(qv,Z_ibt{i,1});%total kriging scores

end

% Total Kriging Scores
relMSE = kr_St(:,3)/min(kr_St(:,3)); %relative MSE
FinalScore = ((1./relMSE).^2).*kr_St(:,5).*kr_St(:,6); %finalscore
kr_St = [kr_St, FinalScore];
kr_Stf = array2table(kr_St,'VariableNames',table_h,'RowNames',table_r2);
clear relMSE FinalScore

%Plots
for i=1:N_kr_mod

    % Stochastic Component's figures
    cc1 = [col,row,rf(:);qcol,qrow,qfluc(:)];
    cc2 = [col,row,rf(:);qcol,qrow,Z{i,1}];
    Z1(max(cc1(:,2)),max(cc1(:,1)))=0; %#ok<SAGROW>
    Z2=Z1;
    for j = 1:size(cc1,1)
        Z1(cc1(j,2),cc1(j,1)) = cc1(j,3);
        Z2(cc2(j,2),cc2(j,1)) = cc2(j,3);
    end
    figure;pcolor(Z1);%title('Original Stochastic Component');
    view(2);shading interp; colorbar;set(gca,'XTick',[],'YTick',[]);
    figure;pcolor(Z2); %title(sprintf('Estimation of Stochastic
   Component \n%s',tit{ind(i),1}));
```

```
view(2);shading interp; colorbar;set(gca,'XTick',[],'YTick',[]);
figure;scatter(qfluc(:),Z{i,1}(:),'filled','d');hold on;
dvec1 = [qfluc(:);Z{i,1}(:)];
plot([min(dvec1)-0.5,max(dvec1)+0.5],[min(dvec1)-0.5,max(dvec1)
+0.5],'r');
axis([min(dvec1)-0.5,max(dvec1)+0.5,min(dvec1)-0.5,max(dvec1)+0.5])
%title('Scatter Plot')
xlabel ('Observed Data')
ylabel ('Estimations')
figure;h = histogram(qfluc(:),16,'FaceColor',[0 0 1],'FaceAlpha'
,0.7);
hold on
histogram(Z{i,1}(:),'BinEdges',h.BinEdges,'FaceColor',[0.2 1 0],'
FaceAlpha',0.7)
%title('Histograms of Stochastic Component')
legend({'Original', 'Estimated'});
clear h

% Total Data figures
cc3 = [col,row,v1(:);qcol,qrow,Z_ibt{i,1}];
cc4 = [col,row,zeros(size(col,1),1); qcol,qrow,UNC{i,1}];
Z3(max(cc3(:,2)),max(cc3(:,1)))=0; %#ok<SAGROW>
Z4=Z3;
for j = 1:size(cc3,1)
    Z3(cc3(j,2),cc3(j,1)) = cc3(j,3);
    Z4(cc4(j,2),cc4(j,1)) = cc4(j,3);
end
figure;pcolor(Z3); view(2);shading interp; %title(sprintf('
Estimation of Original Data \n%s',tit{ind(i),1}));
c = colorbar; c.Label.String = 'Normalised Velocity';set(gca,'XTick'
,[],'YTick',[]);
figure;scatter(qv1(:),Z_ibt{i,1},'filled','d');hold on;
dvec2 = [qv1(:);Z_ibt{i,1}(:)];
plot([min(dvec2)-0.5,max(dvec2)+0.5],[min(dvec2)-0.5,max(dvec2)
+0.5],'r');
axis([min(dvec2)-0.5,max(dvec2)+0.5,min(dvec2)-0.5,max(dvec2)+0.5])
%title('Scatter Plot')
xlabel ('Observed Data')
ylabel ('Estimations')
figure;h = histogram(qv1(:),16,'FaceColor',[0 0 1],'FaceAlpha',0.7);
hold on
histogram(Z_ibt{i,1}(:),'BinEdges',h.BinEdges,'FaceColor',[0.2 1 0],
'FaceAlpha',0.7)
%title('Histograms of Data')
```

```
    legend({'Original', 'Estimated'});
    figure;pcolor(Z4); view(2);shading interp; %title('95% Confidence
   Interval');
    c1 = colorbar; c1.Label.String = 'Normalised Velocity'; set(gca,'
   XTick',[],'YTick',[]);
    clear h

    clear cc1 cc2 cc3 cc4 Z1 Z2 Z3 Z4 dvec1 dvec2

end

% >>>Correlation Coefficient of Indicators<<<
edges4 = (1500:4000/4:5500)/5500;
[~,~,ind_data4] = histcounts(qv1,edges4);
ind4_est{N_kr_mod,1}=[];Rpearson4(N_kr_mod,1)=0;Rspearman4(N_kr_mod,1)
   =0;
MCR4(N_kr_mod,1)=0;

edges16 = (1500:4000/16:5500)/5500;
[~,~,ind_data16] = histcounts(qv1,edges16);
ind16_est{N_kr_mod,1}=[];Rpearson16(N_kr_mod,1)=0;Rspearman16(N_kr_mod
   ,1)=0;
MCR16(N_kr_mod,1)=0;

for i=1:N_kr_mod
    [~,~,ind4_est{i,1}] = histcounts(Z_ibt{i,1},edges4);
    ind4_est{i,1}(Z_ibt{i,1}<=edges4(1)) = 1;
    ind4_est{i,1}(Z_ibt{i,1}>=edges4(end)) = length(edges4)-1;
    Rpearson4(i,1) = corr(ind4_est{i,1},ind_data4);
    Rspearman4(i,1) = corr(ind4_est{i,1},ind_data4,'type','Spearman');
    MCR4(i,1) = sum(ind4_est{i,1}~=ind_data4)/Nu;

    [~,~,ind16_est{i,1}] = histcounts(Z_ibt{i,1},edges16);
    ind16_est{i,1}(Z_ibt{i,1}<=edges16(1)) = 1;
    ind16_est{i,1}(Z_ibt{i,1}>=edges16(end)) = length(edges16)-1;
    Rpearson16(i,1) = corr(ind16_est{i,1},ind_data16);
    Rspearman16(i,1) = corr(ind16_est{i,1},ind_data16,'type','Spearman')
   ;
    MCR16(i,1) = sum(ind16_est{i,1}~=ind_data16)/Nu;

end

% Kriging Indicators Scores Table
```

```
table_h = {'MeanAbsErr','MaxAbsErr','MSE','RMSE','Rpearson','Rspearman'
    };
table_h2 = {'MeanAbsErr','MaxAbsErr','MSE','RMSE','Rpearson','Rspearman'
    ,'Rpearson4','Rspearman4','MCR4','Rpearson16','Rspearman16','MCR16'};
kr_iSsf = array2table(kr_Ss(:,1:end-1),'VariableNames',table_h,'RowNames
    ',table_r2);
kr_iStf = array2table([kr_St(:,1:end-1),Rpearson4,Rspearman4,MCR4,
    Rpearson16,Rspearman16,MCR16],'VariableNames',table_h2,'RowNames',
    table_r2);
%=============================================================


%% ################## DirVar1 ##############################
%=============================================================

% >>> Fitting I and Anisotropy Estimation <<<

% Desired Models
models = {'Gexp';'Gaus';'Sphe';'Mate';'Spar'};
n_models = length(models);

% Initial Values and Limits for optimization
b = [gexpmax,maxdist*2/3,gexpmax/100]; % s2,xi & c0
b_lb = [eps,eps,eps]; b_ub = [gexpmax*1.5,maxdist*1.5,gexpmax/5]; %lower
     and upper limits
bsp = [1000,maxdist*2/3,gexpmax/100]; % eta0, xi, c0
bsp_lb = [eps,eps,eps]; bsp_ub = [inf,maxdist*1.5,gexpmax/5]; %lower and
     upper limits

% Summary cells
model_par0 = {[b,1.5];b;b;[b,1.5];[bsp,1]}; %initial parameters values
model_par_lb = {[b_lb,eps];b_lb;b_lb;[b_lb,0.3];[bsp_lb,-2+eps]}; %lower
     bounds
model_par_ub = {[b_ub,2-eps];b_ub;b_ub;[b_ub,3.5];[bsp_ub,inf]}; %upper
    bounds

clear b b_lb b_ub bsp bsp_lb bsp_ub

% Estimation of Anisotropy
R(n_models,1)=0;phi(n_models,1)=0;xi1(n_models,1)=0;xi2(n_models,1)=0;%
    matrices preallocation
er1(n_models,1)=0;er2(n_models,1)=0; %matrices preallocation
objmod = 'NWEr_m';flag = 1;
% nrsampl = 10; samplpc = 50;
```

```
for i=1:n_models
    model.function = models{i,1};
    model.params0 = model_par0{i,1};
    model.paramslb = model_par_lb{i,1};
    model.paramsub = model_par_ub{i,1};

     [R(i,1),phi(i,1),xi1(i,1),xi2(i,1),er1(i,1),er2(i,1)] =...
         aniso_dvf(x,y,rf,model,objmod,ncpc,nrbins,phistep,phitol,flag);
%     [R(i,1),phi(i,1),xi1(i,1),xi2(i,1),er1(i,1),er2(i,1)] =...
%         dirvar_ccv_s(x,y,rf,model,objmod,N_ms,ncpc,nrsampl,samplpc,nrbins,phistep,phitol,flag);

end

save('dirvar1_iso.mat')

% >>> Fitting II and Parameters of Correlation Estimation (s2,c0,v or eta1) <<<

% Initial Values and Limits for optimization
b{n_models,1}=[];b_lb{n_models,1}=[];b_ub{n_models,1}=[];
for i = 1:n_models
    b{i,1} = [gexpmax,xi1(i,1),R(i,1),phi(i,1),gexpmax/100];
    b_lb{i,1} = [eps,xi1(i,1),R(i,1),phi(i,1),eps];
    b_ub{i,1} = [inf,xi1(i,1),R(i,1),phi(i,1),gexpmax/5];
end

% Summary cells
model_par0 = {[b{1,1},1.1];b{2,1};b{3,1};[b{4,1},1.5];[b{5,1},1]}; % initial parameters values
model_par_lb = {[b_lb{1,1},eps];b_lb{2,1};b_lb{3,1};[b_lb{4,1},0.3];[b_lb{5,1},-2+eps]};%lower bounds
model_par_ub = {[b_ub{1,1},2];b_ub{2,1};b_ub{3,1};[b_ub{4,1},3.5];[b_ub{5,1},inf]}; %upper bounds

% Estimation of Parameters (s2,c0,v or eta1)
bmodel{n_models,1}=[]; fval(n_models,1)=0;tit{n_models,1}=[];
iso = 00;objmod = 'NWEr_m';flag = 1;
for i=1:n_models
    model.function = models{i,1};
    model.params0 = model_par0{i,1};
    model.paramslb = model_par_lb{i,1};
    model.paramsub = model_par_ub{i,1};
```

```
    [bmodel{i,1},fval(i,1),tit{i,1}] =...
        variogramfit(gexp,nr_pairs,c_centers,iso,model,objmod,flag);
end


% >>> Cross Validation <<<

% Matrices and Cells preallocation
cv_scores{n_models,1}=[]; cv_checks{n_models,1}=[];
cv_matr{n_models,1}=[]; cv_Ss(n_models,6)= 0;

% Inputs definition
x = reshape(x,ny,N/ny); y = reshape(y,ny,N/ny);
rf = reshape(rf,ny,N/ny); iso = 00; d_col = 1;

% Cross Validation
for i=1:n_models
    model.function = models{i,1};
    model.params = bmodel{i,1};
    model.r_ok = [22,4];

    [cv_scores{i,1}, cv_checks{i,1}, cv_matr{i,1}] =...
        crossval(x,y,rf,iso,d_col,model);
    cv_Ss(i,:) = table2array(cv_scores{i,1}(:,2:end));
end

% Cross Validation Scores
table_h = {'MeanAbsErr','MaxAbsErr','MSE','RMSE','rpearson','rspearman',
    'finalscore'};
table_r = {'Gexp';'Gaus';'Sphe';'Mate';'Spar'};

relMSE = cv_Ss(:,3)/min(cv_Ss(:,3)); %relative MSE
FinalScore = ((1./relMSE).^2).*cv_Ss(:,5).*cv_Ss(:,6); %finalscore
cv_Ss = [cv_Ss, FinalScore];
cv_Ssf = array2table(cv_Ss,'VariableNames',table_h,'RowNames',table_r);
clear relMSE FinalScore

%Trend addition and Boxcox Inversion
cv_St(n_models,6)= 0;
for i=1:n_models

    cv_matr{i,1}.Z_tr = Mx + cv_matr{i,1}.Z;

    if lambda==00
```

```
            cv_matr{i,1}.Z_ibt1 = cv_matr{i,1}.Z_tr;
        elseif lambda==0
            cv_matr{i,1}.Z_ibt1 = exp(cv_matr{i,1}.Z_tr);
        else
            cv_matr{i,1}.Z_ibt1 = (lambda*cv_matr{i,1}.Z_tr + 1).^(1/lambda);
        end
        cv_matr{i,1}.Z_ibt = real(cv_matr{i,1}.Z_ibt1);
        cv_realZ(i,1) = isreal(cv_matr{i,1}.Z_ibt1); %#ok<SAGROW>

        cv_St(i,:) = correlstats(v1,cv_matr{i,1}.Z_ibt);%total cv scores

end

% Total Cross Validation Scores
relMSE = cv_St(:,3)/min(cv_St(:,3)); %relative MSE
FinalScore = ((1./relMSE).^2).*cv_St(:,5).*cv_St(:,6); %finalscore
cv_St = [cv_St, FinalScore];
cv_Stf = array2table(cv_St,'VariableNames',table_h,'RowNames',table_r);
clear relMSE FinalScore

%Plots
for i=1:n_models

    % Stochastic Component's figures
    Z1 = reshape(rf,ny,N/ny);
    Z2 = reshape(cv_matr{i,1}.Z,ny,N/ny);

    figure;pcolor(Z1);%title('Sample Stochastic Component');
    view(2);shading interp; colorbar;set(gca,'XTick',[],'YTick',[]);
    figure;pcolor(Z2);%title(sprintf('Estimation of Sample Stochastic Component \n%s',tit{i,1}));
    view(2);shading interp;colorbar;set(gca,'XTick',[],'YTick',[]);
    figure;scatter(Z1(:),Z2(:),'filled','d');hold on;
    dvec1 = [Z1(:);Z2(:)];
    plot([min(dvec1)-0.5,max(dvec1)+0.5],[min(dvec1)-0.5,max(dvec1)+0.5],'r');
    axis([min(dvec1)-0.5,max(dvec1)+0.5,min(dvec1)-0.5,max(dvec1)+0.5])
    %title('Scatter Plot')
    xlabel ('Observed Data'); ylabel ('Estimations');
    figure; h = histogram(Z1(:),16,'EdgeColor',[0 0 1],'FaceAlpha',0.7);
    hold on
    histogram(Z2(:),'BinEdges',h.BinEdges,'EdgeColor',[0.2 1 0]','FaceAlpha',0.7)
```

```
    %title('Histograms of Sample Stochastic Component')
    legend({'Original', 'Estimated'});
    clear h


    % Total Data figures
    Z3 = reshape(v1,ny,N/ny);
    Z4 = reshape(cv_matr{i,1}.Z_ibt,ny,N/ny);
%     figure;pcolor(Z3);view(2);shading interp; %title('Original Sample
    ');
%     c = colorbar; c.Label.String = 'Normalised Velocity';set(gca,'
    XTick',[],'YTick',[]);
    figure;pcolor(Z4);view(2);shading interp; %title(sprintf('Estimation
     of Original Sample \n%s',tit{i,1}));
    c = colorbar; c.Label.String = 'Normalised Velocity';set(gca,'XTick'
    ,[],'YTick',[]);
    figure;scatter(Z3(:),Z4(:),'filled','d');hold on;
    dvec2 = [Z3(:);Z4(:)];
    plot([min(dvec2)-0.5,max(dvec2)+0.5],[min(dvec2)-0.5,max(dvec2)
    +0.5],'r');
    axis([min(dvec2)-0.5,max(dvec2)+0.5,min(dvec2)-0.5,max(dvec2)+0.5])
    %title('Scatter Plot')
    xlabel ('Observed Data')
    ylabel ('Estimations')
    figure;h = histogram(Z3(:),16,'EdgeColor',[0 0 1],'FaceAlpha',0.7);
    hold on
    histogram(Z4(:),'BinEdges',h.BinEdges,'EdgeColor',[0.2 1 0],'
    FaceAlpha',0.7)
    %title('Histograms of Sample Data')
    legend({'Original', 'Estimated'});
    clear h

    clear Z1 Z2 Z3 Z4 dvec1 dvec2

end



% >>> Ordinary Kriging <<<

% Sort models based on cross validation scores
[~,ind] = sort(table2array(cv_Stf(:,7)),'descend');

% Matrices and Cells preallocation
```

```
Z{N_kr_mod,1}=[];  Z_error{N_kr_mod,1}=[];kr_checks{N_kr_mod,1}=[];
kr_matr{N_kr_mod,1}=[];
kr_Ss(N_kr_mod,6)= 0; table_r2{N_kr_mod,1} = [];
CI1{N_kr_mod,1}=[];UNC{N_kr_mod,1}=[];

% Inputs definition
x = reshape(x,ny,N/ny); y = reshape(y,ny,N/ny); rf = reshape(rf,ny,N/ny)
    ;
xu = reshape(qcol,ny,Nu/ny); yu = reshape(qrow,ny,Nu/ny); iso = 00;

% Ordinary Kriging
for i=1:N_kr_mod
    model.function = models{ind(i),1};
    model.params = bmodel{ind(i),1};
    model.r_ok = [22,4];

    [Z{i,1},Z_error{i,1},kr_checks{i,1}, kr_matr{i,1}] =...
        ordkrig(x,y,rf,xu,yu,iso,model);
    kr_Ss(i,:) = correlstats(Z{i,1},qfluc);
    table_r2{i,1} = table_r{ind(i),1};

    %Confidence Intervals (95%)
    CI1{i,1}.low = Z{i,1} - 1.96*sqrt(Z_error{i,1});
    CI1{i,1}.up = Z{i,1} + 1.96*sqrt(Z_error{i,1});
    CI1{i,1}.uncer = 1.96*sqrt(Z_error{i,1});
    UNC{i,1} = real(CI1{i,1}.uncer);
    realCI(i,1) = isreal(CI1{i,1}.uncer); %#ok<SAGROW>
end

% Kriging Scores
relMSE = kr_Ss(:,3)/min(kr_Ss(:,3)); %relative MSE
FinalScore = ((1./relMSE).^2).*kr_Ss(:,5).*kr_Ss(:,6); %finalscore
kr_Ss = [kr_Ss, FinalScore];
kr_Ssf = array2table(kr_Ss,'VariableNames',table_h,'RowNames',table_r2);
clear relMSE FinalScore

%Trend addition and Boxcox Inversion
kr_St(N_kr_mod,6)= 0; Z_tr{N_kr_mod,1} = 0;
Z_ibt1{N_kr_mod,1} = 0;Z_ibt{N_kr_mod,1} = 0;
for i=1:N_kr_mod

    Z_tr{i,1} = qMx + Z{i,1};

    if lambda==00
```

```
            Z_ibt1{i,1} = Z_tr{i,1};
        elseif lambda==0
            Z_ibt1{i,1} = exp(Z_tr{i,1});
        else
            Z_ibt1{i,1} = (lambda*Z_tr{i,1} + 1).^(1/lambda);
        end
        Z_ibt{i,1} = real(Z_ibt1{i,1});
        kr_realZ(i,1) = isreal(Z_ibt1{i,1});  %#ok<SAGROW>

        kr_St(i,:) = correlstats(qv,Z_ibt{i,1});%total kriging scores

end

% Total Kriging Scores
relMSE = kr_St(:,3)/min(kr_St(:,3)); %relative MSE
FinalScore = ((1./relMSE).^2).*kr_St(:,5).*kr_St(:,6); %finalscore
kr_St = [kr_St, FinalScore];
kr_Stf = array2table(kr_St,'VariableNames',table_h,'RowNames',table_r2);
clear relMSE FinalScore

%Plots
for i=1:N_kr_mod

    % Stochastic Component's figures
    cc1 = [col,row,rf(:);qcol,qrow,qfluc(:)];
    cc2 = [col,row,rf(:);qcol,qrow,Z{i,1}];
    Z1(max(cc1(:,2)),max(cc1(:,1)))=0; %#ok<SAGROW>
    Z2=Z1;
    for j = 1:size(cc1,1)
        Z1(cc1(j,2),cc1(j,1)) = cc1(j,3);
        Z2(cc2(j,2),cc2(j,1)) = cc2(j,3);
    end
    figure;pcolor(Z1);%title('Original Stochastic Component');
    view(2);shading interp; colorbar;set(gca,'XTick',[],'YTick',[]);
    figure;pcolor(Z2); %title(sprintf('Estimation of Stochastic
   Component \n%s',tit{ind(i),1}));
    view(2);shading interp; colorbar;set(gca,'XTick',[],'YTick',[]);
    figure;scatter(qfluc(:),Z{i,1}(:),'filled','d');hold on;
    dvec1 = [qfluc(:);Z{i,1}(:)];
    plot([min(dvec1)-0.5,max(dvec1)+0.5],[min(dvec1)-0.5,max(dvec1)
   +0.5],'r');
    axis([min(dvec1)-0.5,max(dvec1)+0.5,min(dvec1)-0.5,max(dvec1)+0.5])
    %title('Scatter Plot')
    xlabel ('Observed Data')
```

```
ylabel ('Estimations')
figure;h = histogram(qfluc(:),16,'FaceColor',[0 0 1],'FaceAlpha',0.7);
hold on
histogram(Z{i,1}(:),'BinEdges',h.BinEdges,'FaceColor',[0.2 1 0],'FaceAlpha',0.7)
%title('Histograms of Stochastic Component')
legend({'Original', 'Estimated'});
clear h

% Total Data figures
cc3 = [col,row,v1(:);qcol,qrow,Z_ibt{i,1}];
cc4 = [col,row,zeros(size(col,1),1); qcol,qrow,UNC{i,1}];
Z3(max(cc3(:,2)),max(cc3(:,1)))=0; %#ok<SAGROW>
Z4=Z3;
for j = 1:size(cc3,1)
    Z3(cc3(j,2),cc3(j,1)) = cc3(j,3);
    Z4(cc4(j,2),cc4(j,1)) = cc4(j,3);
end
figure;pcolor(Z3); view(2);shading interp; %title(sprintf('Estimation of Original Data \n%s',tit{ind(i),1}));
c = colorbar; c.Label.String = 'Normalised Velocity';set(gca,'XTick',[],'YTick',[]);
figure;scatter(qv1(:),Z_ibt{i,1},'filled','d');hold on;
dvec2 = [qv1(:);Z_ibt{i,1}(:)];
plot([min(dvec2)-0.5,max(dvec2)+0.5],[min(dvec2)-0.5,max(dvec2)+0.5],'r');
axis([min(dvec2)-0.5,max(dvec2)+0.5,min(dvec2)-0.5,max(dvec2)+0.5])
%title('Scatter Plot')
xlabel ('Observed Data')
ylabel ('Estimations')
figure;h = histogram(qv1(:),16,'FaceColor',[0 0 1],'FaceAlpha',0.7);
hold on
histogram(Z_ibt{i,1}(:),'BinEdges',h.BinEdges,'FaceColor',[0.2 1 0],'FaceAlpha',0.7)
%title('Histograms of Data')
legend({'Original', 'Estimated'});
figure;pcolor(Z4); view(2);shading interp; %title('95% Confidence Interval');
c1 = colorbar; c1.Label.String = 'Normalised Velocity'; set(gca,'XTick',[],'YTick',[]);
clear h

clear cc1 cc2 cc3 cc4 Z1 Z2 Z3 Z4 dvec1 dvec2
```

```
end

%% >>>Correlation Coefficient of Indicators<<<
edges4 = (1500:4000/4:5500)/5500;
[~,~,ind_data4] = histcounts(qv1,edges4);
ind4_est{N_kr_mod,1}=[];Rpearson4(N_kr_mod,1)=0;Rspearman4(N_kr_mod,1)
    =0;
MCR4(N_kr_mod,1)=0;

edges16 = (1500:4000/16:5500)/5500;
[~,~,ind_data16] = histcounts(qv1,edges16);
ind16_est{N_kr_mod,1}=[];Rpearson16(N_kr_mod,1)=0;Rspearman16(N_kr_mod
    ,1)=0;
MCR16(N_kr_mod,1)=0;

for i=1:N_kr_mod
    [~,~,ind4_est{i,1}] = histcounts(Z_ibt{i,1},edges4);
    ind4_est{i,1}(Z_ibt{i,1}<=edges4(1)) = 1;
    ind4_est{i,1}(Z_ibt{i,1}>=edges4(end)) = length(edges4)-1;
    Rpearson4(i,1) = corr(ind4_est{i,1},ind_data4);
    Rspearman4(i,1) = corr(ind4_est{i,1},ind_data4,'type','Spearman');
    MCR4(i,1) = sum(ind4_est{i,1}~=ind_data4)/Nu;

    [~,~,ind16_est{i,1}] = histcounts(Z_ibt{i,1},edges16);
    ind16_est{i,1}(Z_ibt{i,1}<=edges16(1)) = 1;
    ind16_est{i,1}(Z_ibt{i,1}>=edges16(end)) = length(edges16)-1;
    Rpearson16(i,1) = corr(ind16_est{i,1},ind_data16);
    Rspearman16(i,1) = corr(ind16_est{i,1},ind_data16,'type','Spearman')
    ;
    MCR16(i,1) = sum(ind16_est{i,1}~=ind_data16)/Nu;
end

% Kriging Indicators Scores Table
table_h = {'MeanAbsErr','MaxAbsErr','MSE','RMSE','Rpearson','Rspearman'
    };
table_h2 = {'MeanAbsErr','MaxAbsErr','MSE','RMSE','Rpearson','Rspearman'
    ,'Rpearson4','Rspearman4','MCR4','Rpearson16','Rspearman16','MCR16'
    ,};
kr_iSsf = array2table(kr_Ss(:,1:end-1),'VariableNames',table_h,'RowNames
    ',table_r2);
kr_iStf = array2table([kr_St(:,1:end-1),Rpearson4,Rspearman4,MCR4,
    Rpearson16,Rspearman16,MCR16],'VariableNames',table_h2,'RowNames',
    table_r2);
```

```
%==========================================================================

%% ################## DirVar2 ###############################
%==========================================================================

load('dirvar1_iso.mat')

% >>> Rescaling and Rotation of the random field

% (Inverse) Transformation Matrix
A{n_models,1} = []; c_tr{n_models,1} = []; x_tr{n_models,1} = []; y_tr{
    n_models,1} = [];
qc_tr{n_models,1} = []; qx_tr{n_models,1} = []; qy_tr{n_models,1} = [];
R_tr(n_models,1)=0; phi_tr(n_models,1)=0; xi1_tr(n_models,1)=0; xi2_tr(
    n_models,1)=0;

gexp_tr{n_models,1}=[]; nr_pairs_tr{n_models,1}=[]; c_centers_tr{
    n_models,1}=[];

for i=1:n_models
A{i,1} = [cos(phi(i,1)*pi/180)/xi1(i,1), sin(phi(i,1)*pi/180)/xi1(i,1);
-sin(phi(i,1)*pi/180)/xi2(i,1), cos(phi(i,1)*pi/180)/xi2(i,1)];

% Rescale and Rotate Coordinations
c_tr{i,1} = A{i,1}*[c{1,1}';c{1,2}']; %transformed coordinations of
    known points
x_tr{i,1} = reshape(c_tr{i,1}(1,:)',ny,N/ny);
y_tr{i,1} = reshape(c_tr{i,1}(2,:)',ny,N/ny);
qc_tr{i,1} = A{i,1}*[qc{1,1}';qc{1,2}']; %transformed coordinations of
    unknown points
qx_tr{i,1} = reshape(qc_tr{i,1}(1,:)',ny,Nu/ny);
qy_tr{i,1} = reshape(qc_tr{i,1}(2,:)',ny,Nu/ny);

% >>> Check isotropy <<<

% Experimental Variogram (anisotropic)
x = x_tr{i,1}; y = y_tr{i,1}; rf = fluc; iso = 0;
[~,~,~] = expvar(x,y,rf,iso,ncpc,nrbins,4,phitol,2); %exper. variogr. of
     high analysis
%[gexp_tr{i,1}, nr_pairs_tr{i,1}, c_centers_tr{i,1}] = expvar(x,y,rf,iso
    ,ncpc,nrbins,phistep,phitol,2);

% Estimation of New Anisotropy
```

```
model.function = models{i,1};
model.params0 = model_par0{i,1};
model.paramslb = model_par_lb{i,1};
model.paramsub = model_par_ub{i,1};
[R_tr(i,1),phi_tr(i,1),xi1_tr(i,1),xi2_tr(i,1),~,~] = ...
    aniso_dvf(c_tr{i,1}(1,:),c_tr{i,1}(2,:),rf,model,'NWEr_m',1.5*ncpc,
    nrbins,phistep,phitol,0);

end


% >>> Fitting II and Parameters of Correlation Estimation (s2,c0,v or
    eta1) <<<

% Experimental (Semi-)Variogram (isotropic)
gexp2{n_models,1}=[];nr_pairs2{n_models,1}=[]; c_centers2{n_models
    ,1}=[];
gexpmax2(n_models,1)=0;maxdist2(n_models,1)=0;
for i=1:n_models
x = x_tr{i,1}; y = y_tr{i,1}; rf = fluc; iso = 1; flag = 1;
[~,~,~] = expvar(x,y,rf,iso,ncpc,nrbins,4,phitol,2); %exper. variogr. of
     high analysis
[gexp2{i,1}, nr_pairs2{i,1}, c_centers2{i,1}] = expvar(x,y,rf,iso,ncpc,
    nrbins,phistep,phitol,flag);
gexpmax2(i,1) = max(max(gexp2{i,1}));
maxdist2(i,1) = hypot(c_tr{i,1}(1,1)-c_tr{i,1}(1,N),c_tr{i,1}(2,1)-c_tr{
    i,1}(2,N))*ncpc;
end

% Initial Values and Limits for optimization
b{n_models,1}=[];b_lb{n_models,1}=[];b_ub{n_models,1}=[];
for i = 1:n_models
     b{i,1} = [gexpmax2(i,1),maxdist2(i,1)*2/3,gexpmax2(i,1)/100];
     b_lb{i,1} = [eps,eps,eps];
     b_ub{i,1} = [inf,maxdist2(i,1)*1.5,gexpmax2(i,1)/5];
end

% Summary cells
model_par0 = {[b{1,1},1.1];b{2,1};b{3,1};[b{4,1},1.5];[b{5,1},1]}; %
    initial parameters values
model_par_lb = {[b_lb{1,1},eps];b_lb{2,1};b_lb{3,1};[b_lb{4,1},0.3];[
    b_lb{5,1},-2+eps]};%lower bounds
model_par_ub = {[b_ub{1,1},2];b_ub{2,1};b_ub{3,1};[b_ub{4,1},3.5];[b_ub
    {5,1},inf]}; %upper bounds
```

```
% Estimation of Parameters (s2,c0,v or eta1)
bmodel{n_models,1}=[]; fval(n_models,1)=0; tit{n_models,1}=[];
iso = 1;objmod = 'NWEr_m';flag = 1;
for i=1:n_models
    model.function = models{i,1};
    model.params0 = model_par0{i,1};
    model.paramslb = model_par_lb{i,1};
    model.paramsub = model_par_ub{i,1};

   [bmodel{i,1},fval(i,1),tit{i,1}] =...
       variogramfit(gexp2{i,1},nr_pairs2{i,1},c_centers2{i,1},iso,model,
   objmod,flag);
end


% >>> Cross Validation <<<

% Matrices and Cells preallocation
cv_scores{n_models,1}=[]; cv_checks{n_models,1}=[];
cv_matr{n_models,1}=[]; cv_Ss(n_models,6)= 0;

% Inputs definition
x = reshape(x,ny,N/ny); y = reshape(y,ny,N/ny);
rf = reshape(rf,ny,N/ny); iso = 1; d_col = 1;

% Cross Validation
for i=1:n_models
    x = reshape(x_tr{i,1},ny,N/ny); y = reshape(y_tr{i,1},ny,N/ny);
    model.function = models{i,1};
    model.params = bmodel{i,1};
    r_ok1 = pdist2([x(1,1),y(1,1)],[x(1,2),y(1,2)])*2.0;
    r_ok2 = pdist2([x(1,1),y(1,1)],[x(2,1),y(2,1)])*4.0;
    model.r_ok = [r_ok1, r_ok2];

    [cv_scores{i,1}, cv_checks{i,1}, cv_matr{i,1}] =...
        crossval(x,y,rf,iso,d_col,model);
    cv_Ss(i,:) = table2array(cv_scores{i,1}(:,2:end));
end

% Cross Validation Scores
table_h = {'MeanAbsErr','MaxAbsErr','MSE','RMSE','rpearson','rspearman',
    'finalscore'};
table_r = {'Gexp';'Gaus';'Sphe';'Mate';'Spar'};
```

```
relMSE = cv_Ss(:,3)/min(cv_Ss(:,3)); %relative MSE
FinalScore = ((1./relMSE).^2).*cv_Ss(:,5).*cv_Ss(:,6); %finalscore
cv_Ss = [cv_Ss, FinalScore];
cv_Ssf = array2table(cv_Ss,'VariableNames',table_h,'RowNames',table_r);
clear relMSE FinalScore

%Trend addition and Boxcox Inversion
cv_St(n_models,6)= 0;
for i=1:n_models

    cv_matr{i,1}.Z_tr = Mx + cv_matr{i,1}.Z;

    if lambda==00
        cv_matr{i,1}.Z_ibt1 = cv_matr{i,1}.Z_tr;
    elseif lambda==0
        cv_matr{i,1}.Z_ibt1 = exp(cv_matr{i,1}.Z_tr);
    else
        cv_matr{i,1}.Z_ibt1 = (lambda*cv_matr{i,1}.Z_tr + 1).^(1/lambda)
    ;
    end
    cv_matr{i,1}.Z_ibt = real(cv_matr{i,1}.Z_ibt1);
    cv_realZ(i,1) = isreal(cv_matr{i,1}.Z_ibt1); %#ok<SAGROW>

    cv_St(i,:) = correlstats(v1,cv_matr{i,1}.Z_ibt);%total cv scores

end

% Total Cross Validation Scores
relMSE = cv_St(:,3)/min(cv_St(:,3)); %relative MSE
FinalScore = ((1./relMSE).^2).*cv_St(:,5).*cv_St(:,6); %finalscore
cv_St = [cv_St, FinalScore];
cv_Stf = array2table(cv_St,'VariableNames',table_h,'RowNames',table_r);
clear relMSE FinalScore

%Plots
for i=1:n_models

    % Stochastic Component's figures
    Z1 = reshape(rf,ny,N/ny);
    Z2 = reshape(cv_matr{i,1}.Z,ny,N/ny);

    figure;pcolor(Z1);%title('Sample Stochastic Component');
    view(2);shading interp; colorbar;set(gca,'XTick',[],'YTick',[]);
```

```
 figure;pcolor(Z2);%title(sprintf('Estimation of Sample Stochastic Component \n%s',tit{i,1}));
 view(2);shading interp;colorbar;set(gca,'XTick',[],'YTick',[]);
 figure;scatter(Z1(:),Z2(:),'filled','d');hold on;
 dvec1 = [Z1(:);Z2(:)];
 plot([min(dvec1)-0.5,max(dvec1)+0.5],[min(dvec1)-0.5,max(dvec1)+0.5],'r');
 axis([min(dvec1)-0.5,max(dvec1)+0.5,min(dvec1)-0.5,max(dvec1)+0.5])
 %title('Scatter Plot')
 xlabel ('Observed Data'); ylabel ('Estimations');
 figure; h = histogram(Z1(:),16,'EdgeColor',[0 0 1],'FaceAlpha',0.7);
 hold on
 histogram(Z2(:),'BinEdges',h.BinEdges,'EdgeColor',[0.2 1 0]','FaceAlpha',0.7)
 %title('Histograms of Sample Stochastic Component')
 legend({'Original', 'Estimated'});
 clear h


 % Total Data figures
 Z3 = reshape(v1,ny,N/ny);
 Z4 = reshape(cv_matr{i,1}.Z_ibt,ny,N/ny);
%    figure;pcolor(Z3);view(2);shading interp; %title('Original Sample');
%    c = colorbar; c.Label.String = 'Normalised Velocity';set(gca,'XTick',[],'YTick',[]);
 figure;pcolor(Z4);view(2);shading interp; %title(sprintf('Estimation of Original Sample \n%s',tit{i,1}));
 c = colorbar; c.Label.String = 'Normalised Velocity';set(gca,'XTick',[],'YTick',[]);
 figure;scatter(Z3(:),Z4(:),'filled','d');hold on;
 dvec2 = [Z3(:);Z4(:)];
 plot([min(dvec2)-0.5,max(dvec2)+0.5],[min(dvec2)-0.5,max(dvec2)+0.5],'r');
 axis([min(dvec2)-0.5,max(dvec2)+0.5,min(dvec2)-0.5,max(dvec2)+0.5])
 %title('Scatter Plot')
 xlabel ('Observed Data')
 ylabel ('Estimations')
 figure;h = histogram(Z3(:),16,'EdgeColor',[0 0 1],'FaceAlpha',0.7);
 hold on
 histogram(Z4(:),'BinEdges',h.BinEdges,'EdgeColor',[0.2 1 0],'FaceAlpha',0.7)
 %title('Histograms of Sample Data')
 legend({'Original', 'Estimated'});
```

```
    clear h

    clear Z1 Z2 Z3 Z4 dvec1 dvec2

end


% >>> Ordinary Kriging <<<

% Sort models based on cross validation scores
[~,ind] = sort(table2array(cv_Stf(:,7)),'descend');

% Matrices and Cells preallocation
Z{N_kr_mod,1}=[];  Z_error{N_kr_mod,1}=[];kr_checks{N_kr_mod,1}=[];
kr_matr{N_kr_mod,1}=[];
kr_Ss(N_kr_mod,6)= 0;  table_r2{N_kr_mod,1} = [];
CI1{N_kr_mod,1}=[];UNC{N_kr_mod,1}=[];

% Inputs definition
rf = reshape(rf,ny,N/ny);  iso = 1;

% Ordinary Kriging
for i=1:N_kr_mod
    x = reshape(x_tr{i,1},ny,N/ny);  y = reshape(y_tr{i,1},ny,N/ny);
    xu = qx_tr{i,1};  yu = qy_tr{i,1};
    model.function = models{ind(i),1};
    model.params = bmodel{ind(i),1};
    r_ok1 = pdist2([x(1,1),y(1,1)],[x(1,2),y(1,2)])*2.0;
    r_ok2 = pdist2([x(1,1),y(1,1)],[x(2,1),y(2,1)])*4.0;
    model.r_ok = [r_ok1, r_ok2];

    [Z{i,1},Z_error{i,1},kr_checks{i,1}, kr_matr{i,1}] =...
        ordkrig(x,y,rf,xu,yu,iso,model);
    kr_Ss(i,:) = correlstats(Z{i,1},qfluc);
    table_r2{i,1} = table_r{ind(i),1};

    %Confidence Intervals (95%)
    CI1{i,1}.low = Z{i,1} - 1.96*sqrt(Z_error{i,1});
    CI1{i,1}.up = Z{i,1} + 1.96*sqrt(Z_error{i,1});
    CI1{i,1}.uncer = 1.96*sqrt(Z_error{i,1});
    UNC{i,1} = real(CI1{i,1}.uncer);
    realCI(i,1) = isreal(CI1{i,1}.uncer); %#ok<SAGROW>
end
```

```
% Kriging Scores
relMSE = kr_Ss(:,3)/min(kr_Ss(:,3)); %relative MSE
FinalScore = ((1./relMSE).^2).*kr_Ss(:,5).*kr_Ss(:,6); %finalscore
kr_Ss = [kr_Ss, FinalScore];
kr_Ssf = array2table(kr_Ss,'VariableNames',table_h,'RowNames',table_r2);
clear relMSE FinalScore

%Trend addition and Boxcox Inversion
kr_St(N_kr_mod,6)= 0; Z_tr{N_kr_mod,1} = 0;
Z_ibt1{N_kr_mod,1} = 0;Z_ibt{N_kr_mod,1} = 0;
for i=1:N_kr_mod

    Z_tr{i,1} = qMx + Z{i,1};

    if lambda==00
        Z_ibt1{i,1} = Z_tr{i,1};
    elseif lambda==0
        Z_ibt1{i,1} = exp(Z_tr{i,1});
    else
        Z_ibt1{i,1} = (lambda*Z_tr{i,1} + 1).^(1/lambda);
    end
    Z_ibt{i,1} = real(Z_ibt1{i,1});
    kr_realZ(i,1) = isreal(Z_ibt1{i,1});  %#ok<SAGROW>

    kr_St(i,:) = correlstats(qv,Z_ibt{i,1});%total kriging scores

end

% Total Kriging Scores
relMSE = kr_St(:,3)/min(kr_St(:,3)); %relative MSE
FinalScore = ((1./relMSE).^2).*kr_St(:,5).*kr_St(:,6); %finalscore
kr_St = [kr_St, FinalScore];
kr_Stf = array2table(kr_St,'VariableNames',table_h,'RowNames',table_r2);
clear relMSE FinalScore

%Plots
for i=1:N_kr_mod

   % Stochastic Component's figures
    cc1 = [col,row,rf(:);qcol,qrow,qfluc(:)];
    cc2 = [col,row,rf(:);qcol,qrow,Z{i,1}];
    Z1(max(cc1(:,2)),max(cc1(:,1)))=0; %#ok<SAGROW>
    Z2=Z1;
    for j = 1:size(cc1,1)
```

```
        Z1(cc1(j,2),cc1(j,1)) = cc1(j,3);
        Z2(cc2(j,2),cc2(j,1)) = cc2(j,3);
    end
    figure;pcolor(Z1);%title('Original Stochastic Component');
    view(2);shading interp; colorbar;set(gca,'XTick',[],'YTick',[]);
    figure;pcolor(Z2); %title(sprintf('Estimation of Stochastic Component \n%s',tit{ind(i),1}));
    view(2);shading interp; colorbar;set(gca,'XTick',[],'YTick',[]);
    figure;scatter(qfluc(:),Z{i,1}(:),'filled','d');hold on;
    dvec1 = [qfluc(:);Z{i,1}(:)];
    plot([min(dvec1)-0.5,max(dvec1)+0.5],[min(dvec1)-0.5,max(dvec1)+0.5],'r');
    axis([min(dvec1)-0.5,max(dvec1)+0.5,min(dvec1)-0.5,max(dvec1)+0.5])
    %title('Scatter Plot')
    xlabel ('Observed Data')
    ylabel ('Estimations')
    figure;h = histogram(qfluc(:),16,'FaceColor',[0 0 1],'FaceAlpha',0.7);
    hold on
    histogram(Z{i,1}(:),'BinEdges',h.BinEdges,'FaceColor',[0.2 1 0],'FaceAlpha',0.7)
    %title('Histograms of Stochastic Component')
    legend({'Original', 'Estimated'});
    clear h

    % Total Data figures
    cc3 = [col,row,v1(:);qcol,qrow,Z_ibt{i,1}];
    cc4 = [col,row,zeros(size(col,1),1); qcol,qrow,UNC{i,1}];
    Z3(max(cc3(:,2)),max(cc3(:,1)))=0; %#ok<SAGROW>
    Z4=Z3;
    for j = 1:size(cc3,1)
        Z3(cc3(j,2),cc3(j,1)) = cc3(j,3);
        Z4(cc4(j,2),cc4(j,1)) = cc4(j,3);
    end
    figure;pcolor(Z3); view(2);shading interp; %title(sprintf('Estimation of Original Data \n%s',tit{ind(i),1}));
    c = colorbar; c.Label.String = 'Normalised Velocity';set(gca,'XTick',[],'YTick',[]);
    figure;scatter(qv1(:),Z_ibt{i,1},'filled','d');hold on;
    dvec2 = [qv1(:);Z_ibt{i,1}(:)];
    plot([min(dvec2)-0.5,max(dvec2)+0.5],[min(dvec2)-0.5,max(dvec2)+0.5],'r');
    axis([min(dvec2)-0.5,max(dvec2)+0.5,min(dvec2)-0.5,max(dvec2)+0.5])
    %title('Scatter Plot')
```

```
    xlabel ('Observed Data')
    ylabel ('Estimations')
    figure;h = histogram(qv1(:),16,'FaceColor',[0 0 1],'FaceAlpha',0.7);
    hold on
    histogram(Z_ibt{i,1}(:),'BinEdges',h.BinEdges,'FaceColor',[0.2 1 0],
    'FaceAlpha',0.7)
    %title('Histograms of Data')
    legend({'Original', 'Estimated'});
    figure;pcolor(Z4); view(2);shading interp; %title('95% Confidence
    Interval');
    c1 = colorbar; c1.Label.String = 'Normalised Velocity'; set(gca,'
    XTick',[],'YTick',[]);
    clear h

    clear cc1 cc2 cc3 cc4 Z1 Z2 Z3 Z4 dvec1 dvec2

end

% >>>Correlation Coefficient of Indicators<<<
edges4 = (1500:4000/4:5500)/5500;
[~,~,ind_data4] = histcounts(qv1,edges4);
ind4_est{N_kr_mod,1}=[];Rpearson4(N_kr_mod,1)=0;Rspearman4(N_kr_mod,1)
    =0;
MCR4(N_kr_mod,1)=0;

edges16 = (1500:4000/16:5500)/5500;
[~,~,ind_data16] = histcounts(qv1,edges16);
ind16_est{N_kr_mod,1}=[];Rpearson16(N_kr_mod,1)=0;Rspearman16(N_kr_mod
    ,1)=0;
MCR16(N_kr_mod,1)=0;

for i=1:N_kr_mod
    [~,~,ind4_est{i,1}] = histcounts(Z_ibt{i,1},edges4);
    ind4_est{i,1}(Z_ibt{i,1}<=edges4(1)) = 1;
    ind4_est{i,1}(Z_ibt{i,1}>=edges4(end)) = length(edges4)-1;
    Rpearson4(i,1) = corr(ind4_est{i,1},ind_data4);
    Rspearman4(i,1) = corr(ind4_est{i,1},ind_data4,'type','Spearman');
    MCR4(i,1) = sum(ind4_est{i,1}~=ind_data4)/Nu;


    [~,~,ind16_est{i,1}] = histcounts(Z_ibt{i,1},edges16);
    ind16_est{i,1}(Z_ibt{i,1}<=edges16(1)) = 1;
    ind16_est{i,1}(Z_ibt{i,1}>=edges16(end)) = length(edges16)-1;
    Rpearson16(i,1) = corr(ind16_est{i,1},ind_data16);
```

```
    Rspearman16(i,1) = corr(ind16_est{i,1},ind_data16,'type','Spearman')
        ;
    MCR16(i,1) = sum(ind16_est{i,1}~=ind_data16)/Nu;

end

% Kriging Indicators Scores Table
table_h = {'MeanAbsErr','MaxAbsErr','MSE','RMSE','Rpearson','Rspearman'
    };
table_h2 = {'MeanAbsErr','MaxAbsErr','MSE','RMSE','Rpearson','Rspearman'
    ,'Rpearson4','Rspearman4','MCR4','Rpearson16','Rspearman16','MCR16'
    ,};
kr_iSsf = array2table(kr_Ss(:,1:end-1),'VariableNames',table_h,'RowNames
    ',table_r2);
kr_iStf = array2table([kr_St(:,1:end-1),Rpearson4,Rspearman4,MCR4,
    Rpearson16,Rspearman16,MCR16],'VariableNames',table_h2,'RowNames',
    table_r2);
%=============================================================



%% ################## CHI1 ##############################
%=============================================================

% >>> Anisotropy estimation with CHI <<<

x1 = reshape(x,ny,N/ny);y1 = reshape(y,ny,N/ny);rf1 = reshape(rf,ny,N/ny
    );
[R,phi] = aniso_cc_grid(x1,y1,rf1);
if R>1
    R = 1/R;
    if phi>0
        phi = phi-90;
    elseif phi<0
        phi = phi+90;
    end
end

save('chi1_iso.mat')



% >>> Fitting II and Parameters of Correlation Estimation (s2,c0,v or
    eta1) <<<

% Desired Models
```

```
models = {'Gexp';'Gaus';'Sphe';'Mate';'Spar'};
n_models = length(models);

% Initial Values and Limits for optimization
b = [gexpmax,maxdist*1/3,R,phi,gexpmax/100]; % s2,xi & c0
b_lb = [eps,eps,R,phi,eps]; b_ub = [gexpmax*1.5,maxdist,R,phi,gexpmax
    /5]; %lower and upper limits
bsp = [1000,maxdist*1/3,R,phi,gexpmax/100]; % eta0, xi, c0
bsp_lb = [eps,eps,R,phi,eps]; bsp_ub = [inf,maxdist,R,phi,gexpmax/5]; %
    lower and upper limits

% Summary cells
model_par0 = {[b,1.5];b;b;[b,1.5];[bsp,1]}; %initial parameters values
model_par_lb = {[b_lb,eps];b_lb;b_lb;[b_lb,0.3];[bsp_lb,-2+eps]}; %lower
     bounds
model_par_ub = {[b_ub,2-eps];b_ub;b_ub;[b_ub,3.5];[bsp_ub,inf]}; %upper
    bounds

clear b b_lb b_ub bsp bsp_lb bsp_ub

% Estimation of Parameters (s2,xi1,c0,v or eta1)
bmodel{n_models,1}=[]; fval(n_models,1)=0;tit{n_models,1}=[];
iso = 00;objmod = 'NWEr_m';flag = 1;
for i=1:n_models
    model.function = models{i,1};
    model.params0 = model_par0{i,1};
    model.paramslb = model_par_lb{i,1};
    model.paramsub = model_par_ub{i,1};

   [bmodel{i,1},fval(i,1),tit{i,1}] =...
        variogramfit(gexp,nr_pairs,c_centers,iso,model,objmod,flag);
end


% >>> Cross Validation <<<

% Matrices and Cells preallocation
cv_scores{n_models,1}=[]; cv_checks{n_models,1}=[];
cv_matr{n_models,1}=[]; cv_Ss(n_models,6)= 0;

% Inputs definition
x = reshape(x,ny,N/ny); y = reshape(y,ny,N/ny);
rf = reshape(rf,ny,N/ny); iso = 00; d_col = 1;
```

```
% Cross Validation
for i=1:n_models
    model.function = models{i,1};
    model.params = bmodel{i,1};
    model.r_ok = [22,4];

    [cv_scores{i,1}, cv_checks{i,1}, cv_matr{i,1}] =...
        crossval(x,y,rf,iso,d_col,model);
    cv_Ss(i,:) = table2array(cv_scores{i,1}(:,2:end));
end

% Cross Validation Scores
table_h = {'MeanAbsErr','MaxAbsErr','MSE','RMSE','rpearson','rspearman',
    'finalscore'};
table_r = {'Gexp';'Gaus';'Sphe';'Mate';'Spar'};

relMSE = cv_Ss(:,3)/min(cv_Ss(:,3)); %relative MSE
FinalScore = ((1./relMSE).^2).*cv_Ss(:,5).*cv_Ss(:,6); %finalscore
cv_Ss = [cv_Ss, FinalScore];
cv_Ssf = array2table(cv_Ss,'VariableNames',table_h,'RowNames',table_r);
clear relMSE FinalScore

%Trend addition and Boxcox Inversion
cv_St(n_models,6)= 0;
for i=1:n_models

    cv_matr{i,1}.Z_tr = Mx + cv_matr{i,1}.Z;

    if lambda==00
        cv_matr{i,1}.Z_ibt1 = cv_matr{i,1}.Z_tr;
    elseif lambda==0
        cv_matr{i,1}.Z_ibt1 = exp(cv_matr{i,1}.Z_tr);
    else
        cv_matr{i,1}.Z_ibt1 = (lambda*cv_matr{i,1}.Z_tr + 1).^(1/lambda)
    ;
    end
    cv_matr{i,1}.Z_ibt = real(cv_matr{i,1}.Z_ibt1);
    cv_realZ(i,1) = isreal(cv_matr{i,1}.Z_ibt1); %#ok<SAGROW>

    cv_St(i,:) = correlstats(v1,cv_matr{i,1}.Z_ibt);%total cv scores

end

% Total Cross Validation Scores
```

```
relMSE = cv_St(:,3)/min(cv_St(:,3)); %relative MSE
FinalScore = ((1./relMSE).^2).*cv_St(:,5).*cv_St(:,6); %finalscore
cv_St = [cv_St, FinalScore];
cv_Stf = array2table(cv_St,'VariableNames',table_h,'RowNames',table_r);
clear relMSE FinalScore

%Plots
for i=1:n_models

    % Stochastic Component's figures
    Z1 = reshape(rf,ny,N/ny);
    Z2 = reshape(cv_matr{i,1}.Z,ny,N/ny);

    figure;pcolor(Z1);%title('Sample Stochastic Component');
    view(2);shading interp; colorbar;set(gca,'XTick',[],'YTick',[]);
    figure;pcolor(Z2);%title(sprintf('Estimation of Sample Stochastic
    Component \n%s',tit{i,1}));
    view(2);shading interp;colorbar;set(gca,'XTick',[],'YTick',[]);
    figure;scatter(Z1(:),Z2(:),'filled','d');hold on;
    dvec1 = [Z1(:);Z2(:)];
    plot([min(dvec1)-0.5,max(dvec1)+0.5],[min(dvec1)-0.5,max(dvec1)
    +0.5],'r');
    axis([min(dvec1)-0.5,max(dvec1)+0.5,min(dvec1)-0.5,max(dvec1)+0.5])
    %title('Scatter Plot')
    xlabel ('Observed Data'); ylabel ('Estimations');
    figure; h = histogram(Z1(:),16,'EdgeColor',[0 0 1],'FaceAlpha',0.7);
    hold on
    histogram(Z2(:),'BinEdges',h.BinEdges,'EdgeColor',[0.2 1 0]','
    FaceAlpha',0.7)
    %title('Histograms of Sample Stochastic Component')
    legend({'Original', 'Estimated'});
    clear h


    % Total Data figures
    Z3 = reshape(v1,ny,N/ny);
    Z4 = reshape(cv_matr{i,1}.Z_ibt,ny,N/ny);
%     figure;pcolor(Z3);view(2);shading interp; %title('Original Sample
    ');
%     c = colorbar; c.Label.String = 'Normalised Velocity';set(gca,'
    XTick',[],'YTick',[]);
    figure;pcolor(Z4);view(2);shading interp; %title(sprintf('Estimation
     of Original Sample \n%s',tit{i,1}));
```

```
    c = colorbar; c.Label.String = 'Normalised Velocity';set(gca,'XTick'
    ,[],'YTick',[]);
    figure;scatter(Z3(:),Z4(:),'filled','d');hold on;
    dvec2 = [Z3(:);Z4(:)];
    plot([min(dvec2)-0.5,max(dvec2)+0.5],[min(dvec2)-0.5,max(dvec2)
    +0.5],'r');
    axis([min(dvec2)-0.5,max(dvec2)+0.5,min(dvec2)-0.5,max(dvec2)+0.5])
    %title('Scatter Plot')
    xlabel ('Observed Data')
    ylabel ('Estimations')
    figure;h = histogram(Z3(:),16,'EdgeColor',[0 0 1],'FaceAlpha',0.7);
    hold on
    histogram(Z4(:),'BinEdges',h.BinEdges,'EdgeColor',[0.2 1 0],'
    FaceAlpha',0.7)
    %title('Histograms of Sample Data')
    legend({'Original', 'Estimated'});
    clear h

    clear Z1 Z2 Z3 Z4 dvec1 dvec2

end


% >>> Ordinary Kriging <<<

% Sort models based on cross validation scores
[~,ind] = sort(table2array(cv_Stf(:,7)),'descend');

% Matrices and Cells preallocation
Z{N_kr_mod,1}=[]; Z_error{N_kr_mod,1}=[];kr_checks{N_kr_mod,1}=[];
kr_matr{N_kr_mod,1}=[];
kr_Ss(N_kr_mod,6)= 0; table_r2{N_kr_mod,1} = [];
CI1{N_kr_mod,1}=[];UNC{N_kr_mod,1}=[];

% Inputs definition
x = reshape(x,ny,N/ny); y = reshape(y,ny,N/ny); rf = reshape(rf,ny,N/ny)
    ;
xu = reshape(qcol,ny,Nu/ny); yu = reshape(qrow,ny,Nu/ny); iso = 00;

% Ordinary Kriging
for i=1:N_kr_mod
    model.function = models{ind(i),1};
    model.params = bmodel{ind(i),1};
```

```
    model.r_ok = [22,4];

    [Z{i,1},Z_error{i,1},kr_checks{i,1}, kr_matr{i,1}] =...
        ordkrig(x,y,rf,xu,yu,iso,model);
    kr_Ss(i,:) = correlstats(Z{i,1},qfluc);
    table_r2{i,1} = table_r{ind(i),1};

    %Confidence Intervals (95%)
    CI1{i,1}.low = Z{i,1} - 1.96*sqrt(Z_error{i,1});
    CI1{i,1}.up = Z{i,1} + 1.96*sqrt(Z_error{i,1});
    CI1{i,1}.uncer = 1.96*sqrt(Z_error{i,1});
    UNC{i,1} = real(CI1{i,1}.uncer);
    realCI(i,1) = isreal(CI1{i,1}.uncer); %#ok<SAGROW>
end

% Kriging Scores
relMSE = kr_Ss(:,3)/min(kr_Ss(:,3)); %relative MSE
FinalScore = ((1./relMSE).^2).*kr_Ss(:,5).*kr_Ss(:,6); %finalscore
kr_Ss = [kr_Ss, FinalScore];
kr_Ssf = array2table(kr_Ss,'VariableNames',table_h,'RowNames',table_r2);
clear relMSE FinalScore

%Trend addition and Boxcox Inversion
kr_St(N_kr_mod,6)= 0; Z_tr{N_kr_mod,1} = 0;
Z_ibt1{N_kr_mod,1} = 0;Z_ibt{N_kr_mod,1} = 0;
for i=1:N_kr_mod

    Z_tr{i,1} = qMx + Z{i,1};

    if lambda==00
        Z_ibt1{i,1} = Z_tr{i,1};
    elseif lambda==0
        Z_ibt1{i,1} = exp(Z_tr{i,1});
    else
        Z_ibt1{i,1} = (lambda*Z_tr{i,1} + 1).^(1/lambda);
    end
    Z_ibt{i,1} = real(Z_ibt1{i,1});
    kr_realZ(i,1) = isreal(Z_ibt1{i,1});  %#ok<SAGROW>

    kr_St(i,:) = correlstats(qv,Z_ibt{i,1});%total kriging scores

end

% Total Kriging Scores
```

```
relMSE = kr_St(:,3)/min(kr_St(:,3)); %relative MSE
FinalScore = ((1./relMSE).^2).*kr_St(:,5).*kr_St(:,6); %finalscore
kr_St = [kr_St, FinalScore];
kr_Stf = array2table(kr_St,'VariableNames',table_h,'RowNames',table_r2);
clear relMSE FinalScore

%Plots
for i=1:N_kr_mod

    % Stochastic Component's figures
    cc1 = [col,row,rf(:);qcol,qrow,qfluc(:)];
    cc2 = [col,row,rf(:);qcol,qrow,Z{i,1}];
    Z1(max(cc1(:,2)),max(cc1(:,1)))=0; %#ok<SAGROW>
    Z2=Z1;
    for j = 1:size(cc1,1)
        Z1(cc1(j,2),cc1(j,1)) = cc1(j,3);
        Z2(cc2(j,2),cc2(j,1)) = cc2(j,3);
    end
    figure;pcolor(Z1);%title('Original Stochastic Component');
    view(2);shading interp; colorbar;set(gca,'XTick',[],'YTick',[]);
    figure;pcolor(Z2); %title(sprintf('Estimation of Stochastic
   Component \n%s',tit{ind(i),1}));
    view(2);shading interp; colorbar;set(gca,'XTick',[],'YTick',[]);
    figure;scatter(qfluc(:),Z{i,1}(:),'filled','d');hold on;
    dvec1 = [qfluc(:);Z{i,1}(:)];
    plot([min(dvec1)-0.5,max(dvec1)+0.5],[min(dvec1)-0.5,max(dvec1)
   +0.5],'r');
    axis([min(dvec1)-0.5,max(dvec1)+0.5,min(dvec1)-0.5,max(dvec1)+0.5])
    %title('Scatter Plot')
    xlabel ('Observed Data')
    ylabel ('Estimations')
    figure;h = histogram(qfluc(:),16,'FaceColor',[0 0 1],'FaceAlpha'
   ,0.7);
    hold on
    histogram(Z{i,1}(:),'BinEdges',h.BinEdges,'FaceColor',[0.2 1 0],'
   FaceAlpha',0.7)
    %title('Histograms of Stochastic Component')
    legend({'Original', 'Estimated'});
    clear h

    % Total Data figures
    cc3 = [col,row,v1(:);qcol,qrow,Z_ibt{i,1}];
    cc4 = [col,row,zeros(size(col,1),1); qcol,qrow,UNC{i,1}];
    Z3(max(cc3(:,2)),max(cc3(:,1)))=0; %#ok<SAGROW>
```

```
    Z4=Z3;
    for j = 1:size(cc3,1)
        Z3(cc3(j,2),cc3(j,1)) = cc3(j,3);
        Z4(cc4(j,2),cc4(j,1)) = cc4(j,3);
    end
    figure;pcolor(Z3); view(2);shading interp; %title(sprintf('Estimation of Original Data \n%s',tit{ind(i),1}));
    c = colorbar; c.Label.String = 'Normalised Velocity';set(gca,'XTick',[],'YTick',[]);
    figure;scatter(qv1(:),Z_ibt{i,1},'filled','d');hold on;
    dvec2 = [qv1(:);Z_ibt{i,1}(:)];
    plot([min(dvec2)-0.5,max(dvec2)+0.5],[min(dvec2)-0.5,max(dvec2)+0.5],'r');
    axis([min(dvec2)-0.5,max(dvec2)+0.5,min(dvec2)-0.5,max(dvec2)+0.5])
    %title('Scatter Plot')
    xlabel ('Observed Data')
    ylabel ('Estimations')
    figure;h = histogram(qv1(:),16,'FaceColor',[0 0 1],'FaceAlpha',0.7);
    hold on
    histogram(Z_ibt{i,1}(:),'BinEdges',h.BinEdges,'FaceColor',[0.2 1 0],'FaceAlpha',0.7)
    %title('Histograms of Data')
    legend({'Original', 'Estimated'});
    figure;pcolor(Z4); view(2);shading interp; %title('95% Confidence Interval');
    c1 = colorbar; c1.Label.String = 'Normalised Velocity'; set(gca,'XTick',[],'YTick',[]);
    clear h

    clear cc1 cc2 cc3 cc4 Z1 Z2 Z3 Z4 dvec1 dvec2

end

% >>>Correlation Coefficient of Indicators<<<
edges4 = (1500:4000/4:5500)/5500;
[~,~,ind_data4] = histcounts(qv1,edges4);
ind4_est{N_kr_mod,1}=[];Rpearson4(N_kr_mod,1)=0;Rspearman4(N_kr_mod,1)=0;
MCR4(N_kr_mod,1)=0;

edges16 = (1500:4000/16:5500)/5500;
[~,~,ind_data16] = histcounts(qv1,edges16);
ind16_est{N_kr_mod,1}=[];Rpearson16(N_kr_mod,1)=0;Rspearman16(N_kr_mod,1)=0;
```

```
MCR16(N_kr_mod,1)=0;

for i=1:N_kr_mod
    [~,~,ind4_est{i,1}] = histcounts(Z_ibt{i,1},edges4);
    ind4_est{i,1}(Z_ibt{i,1}<=edges4(1)) = 1;
    ind4_est{i,1}(Z_ibt{i,1}>=edges4(end)) = length(edges4)-1;
    Rpearson4(i,1) = corr(ind4_est{i,1},ind_data4);
    Rspearman4(i,1) = corr(ind4_est{i,1},ind_data4,'type','Spearman');
    MCR4(i,1) = sum(ind4_est{i,1}~=ind_data4)/Nu;


    [~,~,ind16_est{i,1}] = histcounts(Z_ibt{i,1},edges16);
    ind16_est{i,1}(Z_ibt{i,1}<=edges16(1)) = 1;
    ind16_est{i,1}(Z_ibt{i,1}>=edges16(end)) = length(edges16)-1;
    Rpearson16(i,1) = corr(ind16_est{i,1},ind_data16);
    Rspearman16(i,1) = corr(ind16_est{i,1},ind_data16,'type','Spearman')
    ;
    MCR16(i,1) = sum(ind16_est{i,1}~=ind_data16)/Nu;

end

% Kriging Indicators Scores Table
table_h = {'MeanAbsErr','MaxAbsErr','MSE','RMSE','Rpearson','Rspearman'
    };
table_h2 = {'MeanAbsErr','MaxAbsErr','MSE','RMSE','Rpearson','Rspearman'
    ,'Rpearson4','Rspearman4','MCR4','Rpearson16','Rspearman16','MCR16'
    ,};
kr_iSsf = array2table(kr_Ss(:,1:end-1),'VariableNames',table_h,'RowNames
    ',table_r2);
kr_iStf = array2table([kr_St(:,1:end-1),Rpearson4,Rspearman4,MCR4,
    Rpearson16,Rspearman16,MCR16],'VariableNames',table_h2,'RowNames',
    table_r2);
%=============================================================================


%% ################## CHI2 ################################
%=============================================================================

load('chi1_iso.mat')

% >>> Fitting II and Estimation of xi1 & xi2 <<<

xi1 = R;xi2 = 1;
```

```
% Desired Models
models = {'Gexp';'Gaus';'Sphe';'Mate';'Spar'};
n_models = length(models);

% >>> Rescaling and Rotation of the random field

% (Inverse) Transformation Matrix
A = [cos(phi*pi/180)/xi1, sin(phi*pi/180)/xi1;
-sin(phi*pi/180)/xi2, cos(phi*pi/180)/xi2];

% Rescale and Rotate Coordinations
c_tr = A*[c{1,1}';c{1,2}']; %transformed coordinations
x_tr = reshape(c_tr(1,:)',ny,N/ny);
y_tr = reshape(c_tr(2,:)',ny,N/ny);
qc_tr = A*[qc{1,1}';qc{1,2}']; %transformed coordinations of unknown
    points
qx_tr = reshape(qc_tr(1,:)',ny,Nu/ny);
qy_tr = reshape(qc_tr(2,:)',ny,Nu/ny);

% >>> Check isotropy <<<

% Experimental Variogram (anisotropic)
x = x_tr; y = y_tr; rf = fluc; iso = 0;
[~,~,~] = expvar(x,y,rf,iso,ncpc,nrbins,4,phitol,2); %exper. variogr. of
     high analysis
%[gexp_tr, nr_pairs_tr, c_centers_tr] = expvar(x,y,rf,iso,ncpc,nrbins,
    phistep,phitol,2);

%Initial Values and Limits for optimization
b = [gexpmax,maxdist*1/3,gexpmax/100]; % s2,xi & c0
b_lb = [eps,eps,eps]; b_ub = [gexpmax*1.5,maxdist,gexpmax/5]; %lower and
     upper limits
bsp = [1000,maxdist*1/3,gexpmax/100]; % eta0, xi, c0
bsp_lb = [eps,eps,eps]; bsp_ub = [inf,maxdist,gexpmax/5]; %lower and
    upper limits

%Summary cells
model_par0 = {[b,1.5];b;b;[b,1.5];[bsp,1]}; %initial parameters values
model_par_lb = {[b_lb,eps];b_lb;b_lb;[b_lb,0.3];[bsp_lb,-2+eps]}; %lower
     bounds
model_par_ub = {[b_ub,2-eps];b_ub;b_ub;[b_ub,3.5];[bsp_ub,inf]}; %upper
    bounds

clear b b_lb b_ub bsp bsp_lb bsp_ub
```

```
% Estimation of New Anisotropy
R_tr(n_models,1)=0; phi_tr(n_models,1)=0; xi1_tr(n_models,1)=0; xi2_tr(
    n_models,1)=0;
for i=1:n_models
     model.function = models{i,1};
     model.params0 = model_par0{i,1};
     model.paramslb = model_par_lb{i,1};
     model.paramsub = model_par_ub{i,1};
     [R_tr(i,1),phi_tr(i,1),xi1_tr(i,1),xi2_tr(i,1),~,~] = ...
         aniso_dvf(c_tr(1,:),c_tr(2,:),rf,model,'NWEr_m',20,0.4,nrbins,
    phistep,phitol,0);
end



% >>> Fitting III and Parameters of Correlation Estimation (s2,c0,v or
    eta1) <<<

% Experimental (Semi-)Variogram (isotropic)
x = x_tr; y = y_tr; rf = fluc; iso = 1; flag = 1;
[~,~,~] = expvar(x,y,rf,iso,ncpc,nrbins,4,phitol,flag); %exper. variogr.
     of high analysis
[gexp2, nr_pairs2, c_centers2] = expvar(x,y,rf,iso,ncpc,nrbins,phistep,
    phitol,flag);
gexpmax2 = max(max(gexp2));

% Initial Values and Limits for optimization
maxdist2 = hypot(c_tr(1,1)-c_tr(1,N),c_tr(2,1)-c_tr(2,N))*ncpc;

b = [gexpmax2,maxdist2*2/3,gexpmax2/100]; % s2,xi & c0
b_lb = [eps,eps,eps]; b_ub = [gexpmax2*1.5,maxdist2*1.5,gexpmax2/5]; %
    lower and upper limits
bsp = [1000,maxdist2*2/3,gexpmax2/100]; % eta0, xi, c0
bsp_lb = [eps,eps,eps]; bsp_ub = [inf,maxdist2*1.5,gexpmax2/5]; %lower
    and upper limits

% Summary cells
model_par0 = {[b,1.5];b;b;[b,1.5];[bsp,1]}; %initial parameters values
model_par_lb = {[b_lb,eps];b_lb;b_lb;[b_lb,0.3];[bsp_lb,-2+eps]}; %lower
     bounds
model_par_ub = {[b_ub,2-eps];b_ub;b_ub;[b_ub,3.5];[bsp_ub,inf]}; %upper
    bounds
```

```
clear b b_lb b_ub bsp bsp_lb bsp_ub

% Estimation of Parameters (s2,c0,v or eta1)
bmodel2{n_models,1}=[]; fval2(n_models,1)=0;tit2{n_models,1}=[];
iso = 1;objmod = 'NWEr_m';flag = 1;
for i=1:n_models
    model.function = models{i,1};
    model.params0 = model_par0{i,1};
    model.paramslb = model_par_lb{i,1};
    model.paramsub = model_par_ub{i,1};

   [bmodel2{i,1},fval2(i,1),tit2{i,1}] =...
        variogramfit(gexp2,nr_pairs2,c_centers2,iso,model,objmod,flag);
end



% >>> Cross Validation <<<

% Matrices and Cells preallocation
cv_scores{n_models,1}=[]; cv_checks{n_models,1}=[];
cv_matr{n_models,1}=[]; cv_Ss(n_models,6)= 0;

% Inputs definition
x = reshape(x_tr,ny,N/ny); y = reshape(y_tr,ny,N/ny);
rf = reshape(rf,ny,N/ny); iso = 1;d_col = 1;

% Cross Validation
for i=1:n_models
    model.function = models{i,1};
    model.params = bmodel2{i,1};
    r_ok1 = pdist2([x(1,1),y(1,1)],[x(1,2),y(1,2)])*2.0;
    r_ok2 = pdist2([x(1,1),y(1,1)],[x(2,1),y(2,1)])*4.0;
    model.r_ok = [r_ok1, r_ok2];

    [cv_scores{i,1}, cv_checks{i,1}, cv_matr{i,1}] =...
        crossval(x,y,rf,iso,d_col,model);
    cv_Ss(i,:) = table2array(cv_scores{i,1}(:,2:end));
end

% Cross Validation Scores
table_h = {'MeanAbsErr','MaxAbsErr','MSE','RMSE','rpearson','rspearman',
    'finalscore'};
table_r = {'Gexp';'Gaus';'Sphe';'Mate';'Spar'};
```

```
relMSE = cv_Ss(:,3)/min(cv_Ss(:,3)); %relative MSE
FinalScore = ((1./relMSE).^2).*cv_Ss(:,5).*cv_Ss(:,6); %finalscore
cv_Ss = [cv_Ss, FinalScore];
cv_Ssf = array2table(cv_Ss,'VariableNames',table_h,'RowNames',table_r);
clear relMSE FinalScore

%Trend addition and Boxcox Inversion
cv_St(n_models,6)= 0;
for i=1:n_models

    cv_matr{i,1}.Z_tr = Mx + cv_matr{i,1}.Z;

    if lambda==00
        cv_matr{i,1}.Z_ibt1 = cv_matr{i,1}.Z_tr;
    elseif lambda==0
        cv_matr{i,1}.Z_ibt1 = exp(cv_matr{i,1}.Z_tr);
    else
        cv_matr{i,1}.Z_ibt1 = (lambda*cv_matr{i,1}.Z_tr + 1).^(1/lambda)
    ;
    end
    cv_matr{i,1}.Z_ibt = real(cv_matr{i,1}.Z_ibt1);
    cv_realZ(i,1) = isreal(cv_matr{i,1}.Z_ibt1); %#ok<SAGROW>

    cv_St(i,:) = correlstats(v1,cv_matr{i,1}.Z_ibt);%total cv scores

end

% Total Cross Validation Scores
relMSE = cv_St(:,3)/min(cv_St(:,3)); %relative MSE
FinalScore = ((1./relMSE).^2).*cv_St(:,5).*cv_St(:,6); %finalscore
cv_St = [cv_St, FinalScore];
cv_Stf = array2table(cv_St,'VariableNames',table_h,'RowNames',table_r);
clear relMSE FinalScore

%Plots
for i=1:n_models

    % Stochastic Component's figures
    Z1 = reshape(rf,ny,N/ny);
    Z2 = reshape(cv_matr{i,1}.Z,ny,N/ny);

    figure;pcolor(Z1);%title('Sample Stochastic Component');
    view(2);shading interp; colorbar;set(gca,'XTick',[],'YTick',[]);
```

```
 figure;pcolor(Z2);%title(sprintf('Estimation of Sample Stochastic Component \n%s',tit{i,1}));
 view(2);shading interp;colorbar;set(gca,'XTick',[],'YTick',[]);
 figure;scatter(Z1(:),Z2(:),'filled','d');hold on;
 dvec1 = [Z1(:);Z2(:)];
 plot([min(dvec1)-0.5,max(dvec1)+0.5],[min(dvec1)-0.5,max(dvec1)+0.5],'r');
 axis([min(dvec1)-0.5,max(dvec1)+0.5,min(dvec1)-0.5,max(dvec1)+0.5])
 %title('Scatter Plot')
 xlabel ('Observed Data'); ylabel ('Estimations');
 figure; h = histogram(Z1(:),16,'EdgeColor',[0 0 1],'FaceAlpha',0.7);
 hold on
 histogram(Z2(:),'BinEdges',h.BinEdges,'EdgeColor',[0.2 1 0]',' FaceAlpha',0.7)
 %title('Histograms of Sample Stochastic Component')
 legend({'Original', 'Estimated'});
 clear h


 % Total Data figures
 Z3 = reshape(v1,ny,N/ny);
 Z4 = reshape(cv_matr{i,1}.Z_ibt,ny,N/ny);
%    figure;pcolor(Z3);view(2);shading interp; %title('Original Sample');
%    c = colorbar; c.Label.String = 'Normalised Velocity';set(gca,' XTick',[],'YTick',[]);
 figure;pcolor(Z4);view(2);shading interp; %title(sprintf('Estimation of Original Sample \n%s',tit{i,1}));
 c = colorbar; c.Label.String = 'Normalised Velocity';set(gca,'XTick',[],'YTick',[]);
 figure;scatter(Z3(:),Z4(:),'filled','d');hold on;
 dvec2 = [Z3(:);Z4(:)];
 plot([min(dvec2)-0.5,max(dvec2)+0.5],[min(dvec2)-0.5,max(dvec2)+0.5],'r');
 axis([min(dvec2)-0.5,max(dvec2)+0.5,min(dvec2)-0.5,max(dvec2)+0.5])
 %title('Scatter Plot')
 xlabel ('Observed Data')
 ylabel ('Estimations')
 figure;h = histogram(Z3(:),16,'EdgeColor',[0 0 1],'FaceAlpha',0.7);
 hold on
 histogram(Z4(:),'BinEdges',h.BinEdges,'EdgeColor',[0.2 1 0],' FaceAlpha',0.7)
 %title('Histograms of Sample Data')
 legend({'Original', 'Estimated'});
```

```
    clear h

    clear Z1 Z2 Z3 Z4 dvec1 dvec2

end


% >>> Ordinary Kriging <<<

% Sort models based on cross validation scores
[~,ind] = sort(table2array(cv_Stf(:,7)),'descend');

% Matrices and Cells preallocation
Z{N_kr_mod,1}=[];  Z_error{N_kr_mod,1}=[];kr_checks{N_kr_mod,1}=[];
kr_matr{N_kr_mod,1}=[];
kr_Ss(N_kr_mod,6)= 0; table_r2{N_kr_mod,1} = [];
CI1{N_kr_mod,1}=[];UNC{N_kr_mod,1}=[];

% Inputs definition
x = reshape(x_tr,ny,N/ny); y = reshape(y_tr,ny,N/ny);
rf = reshape(rf,ny,N/ny); xu = qx_tr; yu = qy_tr; iso=1;

% Ordinary Kriging
for i=1:N_kr_mod
    model.function = models{ind(i),1};
    model.params = bmodel2{ind(i),1};
    r_ok1 = pdist2([x(1,1),y(1,1)],[x(1,2),y(1,2)])*2.0;
    r_ok2 = pdist2([x(1,1),y(1,1)],[x(2,1),y(2,1)])*4.0;
    model.r_ok = [r_ok1, r_ok2];

    [Z{i,1},Z_error{i,1},kr_checks{i,1}, kr_matr{i,1}] =...
        ordkrig(x,y,rf,xu,yu,iso,model);
    kr_Ss(i,:) = correlstats(Z{i,1},qfluc);
    table_r2{i,1} = table_r{ind(i),1};

    %Confidence Intervals (95%)
    CI1{i,1}.low = Z{i,1} - 1.96*sqrt(Z_error{i,1});
    CI1{i,1}.up = Z{i,1} + 1.96*sqrt(Z_error{i,1});
    CI1{i,1}.uncer = 1.96*sqrt(Z_error{i,1});
    UNC{i,1} = real(CI1{i,1}.uncer);
    realCI(i,1) = isreal(CI1{i,1}.uncer); %#ok<SAGROW>
end

% Kriging Scores
```

```
relMSE = kr_Ss(:,3)/min(kr_Ss(:,3)); %relative MSE
FinalScore = ((1./relMSE).^2).*kr_Ss(:,5).*kr_Ss(:,6); %finalscore
kr_Ss = [kr_Ss, FinalScore];
kr_Ssf = array2table(kr_Ss,'VariableNames',table_h,'RowNames',table_r2);
clear relMSE FinalScore

%Trend addition and Boxcox Inversion
kr_St(N_kr_mod,6)= 0; Z_tr{N_kr_mod,1} = 0;
Z_ibt1{N_kr_mod,1} = 0;Z_ibt{N_kr_mod,1} = 0;
for i=1:N_kr_mod

    Z_tr{i,1} = qMx + Z{i,1};

    if lambda==00
        Z_ibt1{i,1} = Z_tr{i,1};
    elseif lambda==0
        Z_ibt1{i,1} = exp(Z_tr{i,1});
    else
        Z_ibt1{i,1} = (lambda*Z_tr{i,1} + 1).^(1/lambda);
    end
    Z_ibt{i,1} = real(Z_ibt1{i,1});
    kr_realZ(i,1) = isreal(Z_ibt1{i,1});  %#ok<SAGROW>

    kr_St(i,:) = correlstats(qv,Z_ibt{i,1});%total kriging scores

end

% Total Kriging Scores
relMSE = kr_St(:,3)/min(kr_St(:,3)); %relative MSE
FinalScore = ((1./relMSE).^2).*kr_St(:,5).*kr_St(:,6); %finalscore
kr_St = [kr_St, FinalScore];
kr_Stf = array2table(kr_St,'VariableNames',table_h,'RowNames',table_r2);
clear relMSE FinalScore

%Plots
for i=1:N_kr_mod

    % Stochastic Component's figures
    cc1 = [col,row,rf(:);qcol,qrow,qfluc(:)];
    cc2 = [col,row,rf(:);qcol,qrow,Z{i,1}];
    Z1(max(cc1(:,2)),max(cc1(:,1)))=0; %#ok<SAGROW>
    Z2=Z1;
    for j = 1:size(cc1,1)
        Z1(cc1(j,2),cc1(j,1)) = cc1(j,3);
```

```
        Z2(cc2(j,2),cc2(j,1)) = cc2(j,3);
    end
    figure;pcolor(Z1);%title('Original Stochastic Component');
    view(2);shading interp; colorbar;set(gca,'XTick',[],'YTick',[]);
    figure;pcolor(Z2); %title(sprintf('Estimation of Stochastic
Component \n%s',tit{ind(i),1}));
    view(2);shading interp; colorbar;set(gca,'XTick',[],'YTick',[]);
    figure;scatter(qfluc(:),Z{i,1}(:),'filled','d');hold on;
    dvec1 = [qfluc(:);Z{i,1}(:)];
    plot([min(dvec1)-0.5,max(dvec1)+0.5],[min(dvec1)-0.5,max(dvec1)
+0.5],'r');
    axis([min(dvec1)-0.5,max(dvec1)+0.5,min(dvec1)-0.5,max(dvec1)+0.5])
    %title('Scatter Plot')
    xlabel ('Observed Data')
    ylabel ('Estimations')
    figure;h = histogram(qfluc(:),16,'FaceColor',[0 0 1],'FaceAlpha'
,0.7);
    hold on
    histogram(Z{i,1}(:),'BinEdges',h.BinEdges,'FaceColor',[0.2 1 0],'
FaceAlpha',0.7)
    %title('Histograms of Stochastic Component')
    legend({'Original', 'Estimated'});
    clear h

    % Total Data figures
    cc3 = [col,row,v1(:);qcol,qrow,Z_ibt{i,1}];
    cc4 = [col,row,zeros(size(col,1),1); qcol,qrow,UNC{i,1}];
    Z3(max(cc3(:,2)),max(cc3(:,1)))=0; %#ok<SAGROW>
    Z4=Z3;
    for j = 1:size(cc3,1)
        Z3(cc3(j,2),cc3(j,1)) = cc3(j,3);
        Z4(cc4(j,2),cc4(j,1)) = cc4(j,3);
    end
    figure;pcolor(Z3); view(2);shading interp; %title(sprintf('
Estimation of Original Data \n%s',tit{ind(i),1}));
    c = colorbar; c.Label.String = 'Normalised Velocity';set(gca,'XTick'
,[],'YTick',[]);
    figure;scatter(qv1(:),Z_ibt{i,1},'filled','d');hold on;
    dvec2 = [qv1(:);Z_ibt{i,1}(:)];
    plot([min(dvec2)-0.5,max(dvec2)+0.5],[min(dvec2)-0.5,max(dvec2)
+0.5],'r');
    axis([min(dvec2)-0.5,max(dvec2)+0.5,min(dvec2)-0.5,max(dvec2)+0.5])
    %title('Scatter Plot')
    xlabel ('Observed Data')
```

```
    ylabel ('Estimations')
    figure;h = histogram(qv1(:),16,'FaceColor',[0 0 1],'FaceAlpha',0.7);
    hold on
    histogram(Z_ibt{i,1}(:),'BinEdges',h.BinEdges,'FaceColor',[0.2 1 0],'FaceAlpha',0.7)
    %title('Histograms of Data')
    legend({'Original', 'Estimated'});
    figure;pcolor(Z4); view(2);shading interp; %title('95% Confidence Interval');
    c1 = colorbar; c1.Label.String = 'Normalised Velocity'; set(gca,'XTick',[],'YTick',[]);
    clear h

    clear cc1 cc2 cc3 cc4 Z1 Z2 Z3 Z4 dvec1 dvec2

end

% >>>Correlation Coefficient of Indicators<<<
edges4 = (1500:4000/4:5500)/5500;
[~,~,ind_data4] = histcounts(qv1,edges4);
ind4_est{N_kr_mod,1}=[];Rpearson4(N_kr_mod,1)=0;Rspearman4(N_kr_mod,1)=0;
MCR4(N_kr_mod,1)=0;

edges16 = (1500:4000/16:5500)/5500;
[~,~,ind_data16] = histcounts(qv1,edges16);
ind16_est{N_kr_mod,1}=[];Rpearson16(N_kr_mod,1)=0;Rspearman16(N_kr_mod,1)=0;
MCR16(N_kr_mod,1)=0;

for i=1:N_kr_mod
    [~,~,ind4_est{i,1}] = histcounts(Z_ibt{i,1},edges4);
    ind4_est{i,1}(Z_ibt{i,1}<=edges4(1)) = 1;
    ind4_est{i,1}(Z_ibt{i,1}>=edges4(end)) = length(edges4)-1;
    Rpearson4(i,1) = corr(ind4_est{i,1},ind_data4);
    Rspearman4(i,1) = corr(ind4_est{i,1},ind_data4,'type','Spearman');
    MCR4(i,1) = sum(ind4_est{i,1}~=ind_data4)/Nu;

    [~,~,ind16_est{i,1}] = histcounts(Z_ibt{i,1},edges16);
    ind16_est{i,1}(Z_ibt{i,1}<=edges16(1)) = 1;
    ind16_est{i,1}(Z_ibt{i,1}>=edges16(end)) = length(edges16)-1;
    Rpearson16(i,1) = corr(ind16_est{i,1},ind_data16);
    Rspearman16(i,1) = corr(ind16_est{i,1},ind_data16,'type','Spearman');
```

```
    MCR16(i,1) = sum(ind16_est{i,1}~=ind_data16)/Nu;

end

% Kriging Indicators Scores Table
table_h = {'MeanAbsErr','MaxAbsErr','MSE','RMSE','Rpearson','Rspearman'
    };
table_h2 = {'MeanAbsErr','MaxAbsErr','MSE','RMSE','Rpearson','Rspearman'
    ,'Rpearson4','Rspearman4','MCR4','Rpearson16','Rspearman16','MCR16'
    ,};
kr_iSsf = array2table(kr_Ss(:,1:end-1),'VariableNames',table_h,'RowNames
    ',table_r2);
kr_iStf = array2table([kr_St(:,1:end-1),Rpearson4,Rspearman4,MCR4,
    Rpearson16,Rspearman16,MCR16],'VariableNames',table_h2,'RowNames',
    table_r2);
%
    ==========================================================================
```

C:/Users/Vasilis/Desktop/AB/Dissertation/DiplomaThesis/MyThesis/Appendix2/AllRG4Appendix.m

B.3 Random Sample

```
                    % Dissertation
                   % Random Sample

clc;clear variables;close all;

%################## Preliminary Analysis #############################
%===================================================================

% Basic parameters
n_data = 2; %if 2 normalised velocities are used (values from 0 to 1),
    else
            %if 1 are used velocities in km/s,else if 0 the original
            %velocities are used (m/s)

% Load Data
load marm.in
ny = 122; nx = 384; %>>a priori known size of the image<<
marm_rf = reshape(marm,ny,nx);
marm_rf = flipud(marm_rf);
```

```
idata0 = marm_rf; %original velocities (m/s)
idata1 = marm_rf/1000;%velocities in km/s
idata2 = marm_rf/max(max(marm_rf)); %normalised velocities

color = 'white';fsize = 18.0; font = 'Cambria'; fweig = 'bold';%figure
    appearance parameters

if n_data==0
    data = idata0;
    colbtitle = 'Velocity (m/s)';
elseif n_data==1
    data = idata1;
    colbtitle = 'Velocity (km/s)';
elseif n_data==2
    data = idata2;
    colbtitle = 'Normalised Velocity';
else
    error('Error: Not valid value for n_data input. It must be 0,1 or 2.
    ')
end

[row_all, col_all, v_all1] = find(data);

% >>>Original Data Plots<<<

figure;%Simple plot
pcolor(data); shading interp %flat
%title('Geological Section (Velocity Model)')
set(gca,'XLim',[0 nx],'YLim',[0 ny],'XTick',[],'YTick',[])

figure; %Simple plot plus colorbar
pcolor(data); shading interp %flat
%title('Geological Section (Velocity Model)')
c = colorbar;
c.Label.String = colbtitle;
set(gca,'XLim',[0 nx],'YLim',[0 ny],'XTick',[],'YTick',[])

figure; %Plot with actual distances and colorbar
pcolor(flipud(data)); shading interp %flat
%title('Geological Section (Velocity Model)')
c = colorbar;
c.Label.String = colbtitle;
xlabel('Distance (km)');
```

```
ylabel('Depth (km)');
ax = gca;
ax.XAxisLocation = 'top';
ax.XLim = [0 nx]; ax.YLim = [0 ny];
ax.XTick = (0:9.2)*nx/9.2;
ax.XTickLabel = (ax.XTick)*9.2/nx;
ax.YTick = (0:0.5:3)*ny/3;
ax.YTickLabel = (ax.YTick)*3/ny;
ax.YDir = 'reverse';

data_tot_vec = data(:); %total image data in vector form


% Random Sampling (122*39=4758 points)
spoints = 122*39; %number of sample points
[~,idx] = datasample(data_tot_vec,spoints,'Replace',false); %sampling
qpoints = data_tot_vec; qpoints(idx) = 0;
qpoints = reshape(qpoints,ny,nx); %"matrix form" of unknown points
sample = data - qpoints; %"matrix form" of known data
[qrow,qcol,qv1] = find(qpoints); %unknown points coordinations and
    values - VALIDATION SET
[row,col,v1] = find(sample); %known points coordinations and values -
    TRAINING SET
N = length(v1); %number of known points

% Plot Sample
figure; %Simple plot
pcolor(sample); shading interp %flat
%title('Random Sample')
set(gca,'XLim',[0 nx],'YLim',[0 ny],'XTick',[],'YTick',[])

figure; %Simple plot plus colorbar
pcolor(sample); shading interp %flat
%title('Random Sample')
c1 = colorbar;
c1.Label.String = colbtitle;
set(gca,'XLim',[0 nx],'YLim',[0 ny],'XTick',[],'YTick',[])

figure; %Plot with actual distances and colorbar
pcolor(flipud(sample)); shading interp %flat
%title('Geological Section (Velocity Model)')
c1 = colorbar;
c1.Label.String = colbtitle;
xlabel('Distance (km)');
```

```
ylabel('Depth (km)');
ax = gca;
ax.XAxisLocation = 'top';
ax.XLim = [0 nx]; ax.YLim = [0 ny];
ax.XTick = (0:9.2)*nx/9.2;
ax.XTickLabel = (ax.XTick)*9.2/nx;
ax.YTick = (0:0.5:3)*ny/3;
ax.YTickLabel = (ax.YTick)*3/ny;
ax.YDir = 'reverse';

%>>>Data Histograms & Statistical Moments<<<

numbins = 15;
% Total image histogram
figure;
%subplot(1,2,1)
 histfit(data_tot_vec,numbins)
 alpha(0.5)
%title('Total image histogram')
% Sample data histogram
figure;%subplot(1,2,2)
 histfit(v1,numbins)
 alpha(0.5)
%title('Sample data histogram')

% Total image data moments
totim_stats = [min(data(:)) max(data(:)) mean(data(:)) median(data(:))
    var(data(:)) skewness(data(:)) kurtosis(data(:))];
% "Drill-holes" data moments
sample_stats = [min(v1) max(v1) mean(v1) median(v1) var(v1) skewness(v1)
     kurtosis(v1)];


%>>>Normality of data checking and Transformation<<<

% Histogram and Normal Probability Plot
figure; %same as the previous figure plus NPP
%subplot(1,2,1)
 histfit(v1,numbins)
 alpha(0.5)
%title('Sample data histogram')
figure;%subplot(1,2,2)
nnp = normplot(v1);
```

```
h_ch=get(gcf,'Children');h_str=get(h_ch(1),'Title');set(h_str,'String','
    '); % remove normplot title
[h_orig,kst_p_orig,ksstat_orig,cv_orig] = kstest(v1(:));

% BoxCox Transformation
[v, lambda] = boxcox(v1);%known points boxcox transformation
qv = (qv1.^lambda -1)/lambda; %unknown points boxcox transformation
v_all = (v_all1.^lambda -1)/lambda; %all points boxcox transformation
figure;
%subplot(1,2,1)
histfit(v,numbins)
alpha(0.5)
%title('Transformed data histogram')
figure;%subplot(1,2,2)
normplot(v)
h_ch=get(gcf,'Children');h_str=get(h_ch(1),'Title');set(h_str,'String','
    '); % remove normplot title
[h_bxtr,p_bxtr,ksstat_bxtr,cv_bxtr] = kstest(v(:));

%>>> Data Trend Estimation <<<

nfr = 2;
trmodel = 'linear';
v_trend = reshape(v,ny,N/ny);
[fluc,Mx,Mx_func,a,trend_scores,dfreq,a_trends] = detrendv(col,row,
    v_trend,nfr,trmodel,0);
qMx = Mx_func(qcol,qrow,a); %trend on the unknown points
qfluc = qv-qMx; %fluctuations/residuals on the unknown points

%Plot data & trend
X = col(:); Y = row(:); rf1 = v_trend(:);
figure;
scatter3(X,flipud(Y),rf1,'r','filled')
hold on
Xfit = min(X):1:max(X); nxfit = length(Xfit);
Yfit = min(Y):1:max(Y); nyfit = length(Yfit);
[XFIT,YFIT] = meshgrid(Xfit,Yfit);
VFIT = Mx_func(XFIT(:),YFIT(:),a);
VFIT = flipud(reshape(VFIT,nyfit,nxfit));
mesh(XFIT,YFIT,VFIT)
colorbar
%xlabel('x')
%ylabel('y')
xlabel('Alongside Section')
```

```
ylabel('Depth')
zlabel('Transformed Normalised Velocity')
%set(gca,'YTick',flipud(get(gca,'YTick')));
%set(gca,'YDir','reverse');
%title('Data & Trend Model')
view(-52,6)
shading interp
c = colorbar; c.Label.String = 'Transformed Normalised Velocity';

%Detrend whole dataset
Mx_all = Mx_func(col_all,row_all,a); %trend on the unknown points
fluc_all = v_all-Mx_all; %fluctuations/residuals on the unknown points
fluc_all = reshape(fluc_all,ny,nx);

figure; %Plot with actual distances and colorbar
pcolor(flipud(fluc_all)); shading interp %flat
%title('Detrended Geological Section')
c1 = colorbar;
% c1.Label.String = colbtitle;
xlabel('Distance (km)');
ylabel('Depth (km)');
ax = gca;
ax.XAxisLocation = 'top';
ax.XLim = [0 nx]; ax.YLim = [0 ny];
ax.XTick = (0:9.2)*nx/9.2;
ax.XTickLabel = (ax.XTick)*9.2/nx;
ax.YTick = (0:0.5:3)*ny/3;
ax.YTickLabel = (ax.YTick)*3/ny;
ax.YDir = 'reverse';

%>>> Statistical Analysis of Residuals <<<

% Residuals/Fluctuations moments
fluc_stats = [min(fluc) max(fluc) mean(fluc) median(fluc) var(fluc)
    skewness(fluc) kurtosis(fluc)];


% Histogram and Normal Probablity Plot
figure;
%subplot(1,2,1)
histfit(fluc,numbins)
alpha(0.5)
%title('Histogram of detrended data')
figure;%subplot(1,2,2)
```

```
normplot(fluc)
h_ch=get(gcf,'Children');h_str=get(h_ch(1),'Title');set(h_str,'String','
    '); % remove normplot title
[h_fluc,p_fluc,ksstat_fluc,cv_fluc] = kstest(fluc(:));

%Maximum distance
c = [col,row];
[k,l] = find(triu(true(N)));
d = hypot(c(k,1)-c(l,1),c(k,2)-c(l,2));
% d = triu(pdist2(c,c));
ncpc = 0.2;
maxdist = max(max(d))*ncpc;
clear k l d
%===============================================================


%% ################# Experimantal Variogram
    ##############################
%===============================================================

% >>> Initialize Basic Parameters <<<
c = {col,row}; %known points' coordinations
qc = {qcol,qrow}; %"unknown" points' coordinations
%ncpc = 0.2;
N = size(col,1);
Nu = size(qcol,1);
%maxdist = hypot(col(1,1)-col(N,1),row(1,1)-row(N,1))*ncpc;
nrbins = 45;
phistep = 15;
phitol = 20;
N_kr_mod = 3;

% >>> Experimental (Semi-)Variogram (anisotropic) <<<
x = col; y = row; rf = fluc; iso = 0; flag = 1;
[~,~,~] = expvar(x,y,rf,iso,ncpc,nrbins,4,phitol,2); %exper. variogr. of
     high analysis
[gexp, nr_pairs, c_centers] = expvar(x,y,rf,iso,ncpc,nrbins,phistep,
    phitol,flag);
gexpmax = max(max(gexp));
%===============================================================

```

```
%% ################## DirVar0 ##############################
%==================================================================

% >>> Fitting I and Parameters of Anisotropic Correlation Estimation (s2
    ,xi1,xi2,phi,c0,v or eta1) <<<

% Desired Models
models = {'Gexp';'Gaus';'Sphe';'Mate';'Spar'};
n_models = length(models);

% Initial Values and Limits for optimization
b = [gexpmax,maxdist*2/3,0.5,10,gexpmax/100]; % s2,xi1,R,phi & c0
b_lb = [eps,eps,eps,-90,eps]; b_ub = [gexpmax*1.5,maxdist*1.5,30,90,
    gexpmax/5]; %lower and upper limits
bsp = [1000,maxdist*2/3,0.5,10,gexpmax/100]; % eta0, xi1,R,phi & c0
bsp_lb = [eps,eps,eps,-90,eps]; bsp_ub = [inf,maxdist*1.5,30,90,gexpmax
    /5]; %lower and upper limits

% Summary cells
model_par0 = {[b,1.5];b;b;[b,1.5];[bsp,1]}; %initial parameters values
model_par_lb = {[b_lb,eps];b_lb;b_lb;[b_lb,0.3];[bsp_lb,-2+eps]}; %lower
     bounds
model_par_ub = {[b_ub,2-eps];b_ub;b_ub;[b_ub,3.5];[bsp_ub,inf]}; %upper
    bounds

clear b b_lb b_ub bsp bsp_lb bsp_ub

% Estimation of Parameters (s2,xi1,xi2,phi,c0,v or eta1)
bmodel{n_models,1}=[]; fval(n_models,1)=0; tit{n_models,1}=[];
iso = 00;objmod = 'NWEr_m';flag = 1;
for i=1:n_models
    model.function = models{i,1};
    model.params0 = model_par0{i,1};
    model.paramslb = model_par_lb{i,1};
    model.paramsub = model_par_ub{i,1};

   [bmodel{i,1},fval(i,1),tit{i,1}] =...
        variogramfit(gexp,nr_pairs,c_centers,iso,model,objmod,flag);
end

% Anisotropy Estimation (#Not Necessary#)
R0(n_models,1) = 0;phi0(n_models,1) = 0;xi10(n_models,1) = 0;xi20(
    n_models,1) = 0;
```

```
for i=1:n_models
    R0(i,1) = bmodel{i,1}(1,3);
    phi0(i,1) = bmodel{i,1}(1,4);
    xi10(i,1) = bmodel{i,1}(1,2);
    xi20(i,1) = bmodel{i,1}(1,2)/R0(i,1);
    if R0(i,1)>1
        R0(i,1) = 1/R0(i,1);bmodel{i,1}(1,3) = R0(i,1);
        xi101 = xi10(i,1);
        xi10(i,1) = xi20(i,1); bmodel{i,1}(1,2) = xi10(i,1);
        xi20(i,1) = xi101;
        if phi0(i,1)>0
            phi0(i,1) = phi0(i,1)-90;
        else
            phi0(i,1) = phi0(i,1)+90;
        end
        bmodel{i,1}(1,4) = phi0(i,1);
    end
end

R = mean(R0); phi = mean(phi0);xi1 = mean(xi10);xi2 = mean(xi20);


% >>> Cross Validation <<<

% Matrices and Cells preallocation
cv_scores{n_models,1}=[]; cv_checks{n_models,1}=[];
cv_matr{n_models,1}=[]; cv_Ss(n_models,6)= 0;

% Inputs definition
iso = 00; d_col = 1;

% Cross Validation
for i=1:n_models
    model.function = models{i,1};
    model.params = bmodel{i,1};
    model.r_ok = [22,4];

    [cv_scores{i,1}, cv_checks{i,1}, cv_matr{i,1}] =...
        crossval(x,y,rf,iso,d_col,model);
    cv_Ss(i,:) = table2array(cv_scores{i,1}(:,2:end));
end

% Cross Validation Scores
```

```
table_h = {'MeanAbsErr','MaxAbsErr','MSE','RMSE','rpearson','rspearman','finalscore'};
table_r = {'Gexp';'Gaus';'Sphe';'Mate';'Spar'};

relMSE = cv_Ss(:,3)/min(cv_Ss(:,3)); %relative MSE
FinalScore = ((1./relMSE).^2).*cv_Ss(:,5).*cv_Ss(:,6); %finalscore
cv_Ss = [cv_Ss, FinalScore];
cv_Ssf = array2table(cv_Ss,'VariableNames',table_h,'RowNames',table_r);
clear relMSE FinalScore

%Trend addition and Boxcox Inversion
cv_St(n_models,6)= 0;
for i=1:n_models

    cv_matr{i,1}.Z_tr = Mx + cv_matr{i,1}.Z;

    if lambda==00
        cv_matr{i,1}.Z_ibt1 = cv_matr{i,1}.Z_tr;
    elseif lambda==0
        cv_matr{i,1}.Z_ibt1 = exp(cv_matr{i,1}.Z_tr);
    else
        cv_matr{i,1}.Z_ibt1 = (lambda*cv_matr{i,1}.Z_tr + 1).^(1/lambda);
    end
    cv_matr{i,1}.Z_ibt = real(cv_matr{i,1}.Z_ibt1);
    cv_realZ(i,1) = isreal(cv_matr{i,1}.Z_ibt1); %#ok<SAGROW>

    cv_St(i,:) = correlstats(v1,cv_matr{i,1}.Z_ibt);%total cv scores

end

% Total Cross Validation Scores
relMSE = cv_St(:,3)/min(cv_St(:,3)); %relative MSE
FinalScore = ((1./relMSE).^2).*cv_St(:,5).*cv_St(:,6); %finalscore
cv_St = [cv_St, FinalScore];
cv_Stf = array2table(cv_St,'VariableNames',table_h,'RowNames',table_r);
clear relMSE FinalScore

%Plots
for i=1:n_models

    % Stochastic Component's figures
    cc1 = [col,row,rf(:);qcol,qrow,zeros(Nu,1)];
    cc2 = [col,row,cv_matr{i,1}.Z(:);qcol,qrow,zeros(Nu,1)];
```

```
    Z1(max(cc1(:,2)),max(cc1(:,1)))=0; %#ok<SAGROW>
    Z2=Z1;
    for j = 1:size(cc1,1)
        Z1(cc1(j,2),cc1(j,1)) = cc1(j,3);
        Z2(cc2(j,2),cc2(j,1)) = cc2(j,3);
    end

    figure;pcolor(Z1);%title('Sample Stochastic Component');
    view(2);shading interp; colorbar;set(gca,'XTick',[],'YTick',[]);
    figure;pcolor(Z2);%title(sprintf('Estimation of Sample Stochastic
   Component \n%s',tit{i,1}));
    view(2);shading interp;colorbar;set(gca,'XTick',[],'YTick',[]);
    figure;scatter(rf(:),cv_matr{i,1}.Z(:),'filled','d');hold on;
    dvec1 = [rf(:);cv_matr{i,1}.Z(:)];
    plot([min(dvec1)-0.5,max(dvec1)+0.5],[min(dvec1)-0.5,max(dvec1)
   +0.5],'r');
    axis([min(dvec1)-0.5,max(dvec1)+0.5,min(dvec1)-0.5,max(dvec1)+0.5])
    %title('Scatter Plot')
    xlabel ('Observed Data'); ylabel ('Estimations');
    figure; h = histogram(rf(:),16,'EdgeColor',[0 0 1],'FaceAlpha',0.7);
    hold on
    histogram(cv_matr{i,1}.Z(:),'BinEdges',h.BinEdges,'EdgeColor',[0.2 1
    0]','FaceAlpha',0.7)
    %title('Histograms of Sample Stochastic Component')
    legend({'Original', 'Estimated'});
    clear h


    % Total Data figures
    cc3 = [col,row,v1(:);qcol,qrow,zeros(Nu,1)];
    cc4 = [col,row,cv_matr{i,1}.Z_ibt(:);qcol,qrow,zeros(Nu,1)];
    Z3(max(cc3(:,2)),max(cc3(:,1)))=0; %#ok<SAGROW>
    Z4=Z3;
    for j = 1:size(cc3,1)
        Z3(cc3(j,2),cc3(j,1)) = cc3(j,3);
        Z4(cc4(j,2),cc4(j,1)) = cc4(j,3);
    end
%     figure;pcolor(Z3);view(2);shading interp; %title('Original Sample
   ');
%     c = colorbar; c.Label.String = 'Normalised Velocity';set(gca,'
   XTick',[],'YTick',[]);
    figure;pcolor(Z4);view(2);shading interp; %title(sprintf('Estimation
    of Original Sample \n%s',tit{i,1}));
```

```
    c = colorbar; c.Label.String = 'Normalised Velocity';set(gca,'XTick'
    ,[],'YTick',[]);
    figure;scatter(v1(:),cv_matr{i,1}.Z_ibt(:),'filled','d');hold on;
    dvec2 = [v1(:);cv_matr{i,1}.Z_ibt(:)];
    plot([min(dvec2)-0.5,max(dvec2)+0.5],[min(dvec2)-0.5,max(dvec2)
   +0.5],'r');
    axis([min(dvec2)-0.5,max(dvec2)+0.5,min(dvec2)-0.5,max(dvec2)+0.5])
    %title('Scatter Plot')
    xlabel ('Observed Data')
    ylabel ('Estimations')
    figure;h = histogram(v1(:),16,'EdgeColor',[0 0 1],'FaceAlpha',0.7);
    hold on
    histogram(cv_matr{i,1}.Z_ibt(:),'BinEdges',h.BinEdges,'EdgeColor'
    ,[0.2 1 0],'FaceAlpha',0.7)
    %title('Histograms of Sample Data')
    legend({'Original', 'Estimated'});
    clear h

    clear Z1 Z2 Z3 Z4 dvec1 dvec2

end

T_4 = toc(t1)/60-T_1-T_2-T_3


% >>> Ordinary Kriging <<<

% Sort models based on cross validation scores
[~,ind] = sort(table2array(cv_Stf(:,7)),'descend');

% Matrices and Cells preallocation
Z{N_kr_mod,1}=[]; Z_error{N_kr_mod,1}=[];kr_checks{N_kr_mod,1}=[];
kr_matr{N_kr_mod,1}=[];
kr_Ss(N_kr_mod,6)= 0; table_r2{N_kr_mod,1} = [];
CI1{N_kr_mod,1}=[];UNC{N_kr_mod,1}=[];

% Inputs definition
xu = qcol; yu = qrow; iso = 00;

% Ordinary Kriging
for i=1:N_kr_mod
    model.function = models{ind(i),1};
    model.params = bmodel{ind(i),1};
    model.r_ok = [22,4];
```

```
    [Z{i,1},Z_error{i,1},kr_checks{i,1}, kr_matr{i,1}] =...
        ordkrig(x,y,rf,xu,yu,iso,model);
    kr_Ss(i,:) = correlstats(Z{i,1},qfluc);
    table_r2{i,1} = table_r{ind(i),1};

    %Confidence Intervals (95%)
    CI1{i,1}.low = Z{i,1} - 1.96*sqrt(Z_error{i,1});
    CI1{i,1}.up = Z{i,1} + 1.96*sqrt(Z_error{i,1});
    CI1{i,1}.uncer = 1.96*sqrt(Z_error{i,1});
    UNC{i,1} = real(CI1{i,1}.uncer);
    realCI(i,1) = isreal(CI1{i,1}.uncer); %#ok<SAGROW>
end

% Kriging Scores
relMSE = kr_Ss(:,3)/min(kr_Ss(:,3)); %relative MSE
FinalScore = ((1./relMSE).^2).*kr_Ss(:,5).*kr_Ss(:,6); %finalscore
kr_Ss = [kr_Ss, FinalScore];
kr_Ssf = array2table(kr_Ss,'VariableNames',table_h,'RowNames',table_r2);
clear relMSE FinalScore

%Trend addition and Boxcox Inversion
kr_St(N_kr_mod,6)= 0; Z_tr{N_kr_mod,1} = 0;
Z_ibt1{N_kr_mod,1} = 0;Z_ibt{N_kr_mod,1} = 0;
for i=1:N_kr_mod

    Z_tr{i,1} = qMx + Z{i,1};

    if lambda==00
        Z_ibt1{i,1} = Z_tr{i,1};
    elseif lambda==0
        Z_ibt1{i,1} = exp(Z_tr{i,1});
    else
        Z_ibt1{i,1} = (lambda*Z_tr{i,1} + 1).^(1/lambda);
    end
    Z_ibt{i,1} = real(Z_ibt1{i,1});
    kr_realZ(i,1) = isreal(Z_ibt1{i,1});  %#ok<SAGROW>

    kr_St(i,:) = correlstats(qv,Z_ibt{i,1});%total kriging scores

end

% Total Kriging Scores
relMSE = kr_St(:,3)/min(kr_St(:,3)); %relative MSE
```

```
FinalScore = ((1./relMSE).^2).*kr_St(:,5).*kr_St(:,6); %finalscore
kr_St = [kr_St, FinalScore];
kr_Stf = array2table(kr_St,'VariableNames',table_h,'RowNames',table_r2);
clear relMSE FinalScore

%Plots
for i=1:N_kr_mod

    % Stochastic Component's figures
    cc1 = [col,row,rf(:);qcol,qrow,qfluc(:)];
    cc2 = [col,row,rf(:);qcol,qrow,Z{i,1}];
    Z1(max(cc1(:,2)),max(cc1(:,1)))=0; %#ok<SAGROW>
    Z2=Z1;
    for j = 1:size(cc1,1)
        Z1(cc1(j,2),cc1(j,1)) = cc1(j,3);
        Z2(cc2(j,2),cc2(j,1)) = cc2(j,3);
    end
    figure;pcolor(Z1);%title('Original Stochastic Component');
    view(2);shading interp; colorbar;set(gca,'XTick',[],'YTick',[]);
    figure;pcolor(Z2); %title(sprintf('Estimation of Stochastic
   Component \n%s',tit{ind(i),1}));
    view(2);shading interp; colorbar;set(gca,'XTick',[],'YTick',[]);
    figure;scatter(qfluc(:),Z{i,1}(:),'filled','d');hold on;
    dvec1 = [qfluc(:);Z{i,1}(:)];
    plot([min(dvec1)-0.5,max(dvec1)+0.5],[min(dvec1)-0.5,max(dvec1)
   +0.5],'r');
    axis([min(dvec1)-0.5,max(dvec1)+0.5,min(dvec1)-0.5,max(dvec1)+0.5])
    %title('Scatter Plot')
    xlabel ('Observed Data')
    ylabel ('Estimations')
    figure;h = histogram(qfluc(:),16,'FaceColor',[0 0 1],'FaceAlpha'
   ,0.7);
    hold on
    histogram(Z{i,1}(:),'BinEdges',h.BinEdges,'FaceColor',[0.2 1 0],'
   FaceAlpha',0.7)
    %title('Histograms of Stochastic Component')
    legend({'Original', 'Estimated'});
    clear h

    % Total Data figures
    cc3 = [col,row,v1(:);qcol,qrow,Z_ibt{i,1}];
    cc4 = [col,row,zeros(size(col,1),1); qcol,qrow,UNC{i,1}];
    Z3(max(cc3(:,2)),max(cc3(:,1)))=0; %#ok<SAGROW>
    Z4=Z3;
```

```
    for j = 1:size(cc3,1)
        Z3(cc3(j,2),cc3(j,1)) = cc3(j,3);
        Z4(cc4(j,2),cc4(j,1)) = cc4(j,3);
    end
    figure;pcolor(Z3); view(2);shading interp; %title(sprintf('Estimation of Original Data \n%s',tit{ind(i),1}));
    c = colorbar; c.Label.String = 'Normalised Velocity';set(gca,'XTick',[],'YTick',[]);
    figure;scatter(qv1(:),Z_ibt{i,1}(:),'filled','d');hold on;
    dvec2 = [qv1(:);Z_ibt{i,1}(:)];
    plot([min(dvec2)-0.5,max(dvec2)+0.5],[min(dvec2)-0.5,max(dvec2)+0.5],'r');
    axis([min(dvec2)-0.5,max(dvec2)+0.5,min(dvec2)-0.5,max(dvec2)+0.5])
    %title('Scatter Plot')
    xlabel ('Observed Data')
    ylabel ('Estimations')
    figure;h = histogram(qv1(:),16,'FaceColor',[0 0 1],'FaceAlpha',0.7);
    hold on
    histogram(Z_ibt{i,1}(:),'BinEdges',h.BinEdges,'FaceColor',[0.2 1 0],'FaceAlpha',0.7)
    %title('Histograms of Data')
    legend({'Original', 'Estimated'});
    figure;pcolor(Z4); view(2);shading interp; %title('95% Confidence Interval');
    c1 = colorbar; c1.Label.String = 'Normalised Velocity'; set(gca,'XTick',[],'YTick',[]);
    clear h

    clear cc1 cc2 cc3 cc4 Z1 Z2 Z3 Z4 dvec1 dvec2

end

% >>>Correlation Coefficient of Indicators<<<
edges4 = (1500:4000/4:5500)/5500;
[~,~,ind_data4] = histcounts(qv1,edges4);
ind4_est{N_kr_mod,1}=[];Rpearson4(N_kr_mod,1)=0;Rspearman4(N_kr_mod,1)=0;
MCR4(N_kr_mod,1)=0;

edges16 = (1500:4000/16:5500)/5500;
[~,~,ind_data16] = histcounts(qv1,edges16);
ind16_est{N_kr_mod,1}=[];Rpearson16(N_kr_mod,1)=0;Rspearman16(N_kr_mod,1)=0;
MCR16(N_kr_mod,1)=0;
```

```

for i=1:N_kr_mod
    [~,~,ind4_est{i,1}] = histcounts(Z_ibt{i,1},edges4);
    ind4_est{i,1}(Z_ibt{i,1}<=edges4(1)) = 1;
    ind4_est{i,1}(Z_ibt{i,1}>=edges4(end)) = length(edges4)-1;
    Rpearson4(i,1) = corr(ind4_est{i,1},ind_data4);
    Rspearman4(i,1) = corr(ind4_est{i,1},ind_data4,'type','Spearman');
    MCR4(i,1) = sum(ind4_est{i,1}~=ind_data4)/Nu;

    [~,~,ind16_est{i,1}] = histcounts(Z_ibt{i,1},edges16);
    ind16_est{i,1}(Z_ibt{i,1}<=edges16(1)) = 1;
    ind16_est{i,1}(Z_ibt{i,1}>=edges16(end)) = length(edges16)-1;
    Rpearson16(i,1) = corr(ind16_est{i,1},ind_data16);
    Rspearman16(i,1) = corr(ind16_est{i,1},ind_data16,'type','Spearman')
    ;
    MCR16(i,1) = sum(ind16_est{i,1}~=ind_data16)/Nu;

end

% Kriging Indicators Scores Table
table_h = {'MeanAbsErr','MaxAbsErr','MSE','RMSE','Rpearson','Rspearman'
    };
table_h2 = {'MeanAbsErr','MaxAbsErr','MSE','RMSE','Rpearson','Rspearman'
    ,'Rpearson4','Rspearman4','MCR4','Rpearson16','Rspearman16','MCR16'
    ,};
kr_iSsf = array2table(kr_Ss(:,1:end-1),'VariableNames',table_h,'RowNames
    ',table_r2);
kr_iStf = array2table([kr_St(:,1:end-1),Rpearson4,Rspearman4,MCR4,
    Rpearson16,Rspearman16,MCR16],'VariableNames',table_h2,'RowNames',
    table_r2);
%==============================================================


%% ################## DirVar1 ##############################
%==============================================================

% >>> Fitting I and Anisotropy Estimation <<<

% Desired Models
models = {'Gexp';'Gaus';'Sphe';'Mate';'Spar'};
n_models = length(models);

% Initial Values and Limits for optimization
b = [gexpmax,maxdist*2/3,gexpmax/100]; % s2,xi & c0
```

```
b_lb = [eps,eps,eps]; b_ub = [gexpmax*1.5,maxdist*1.5,gexpmax/5]; %lower and upper limits
bsp = [1000,maxdist*2/3,gexpmax/100]; % eta0, xi, c0
bsp_lb = [eps,eps,eps]; bsp_ub = [inf,maxdist*1.5,gexpmax/5]; %lower and upper limits

% Summary cells
model_par0 = {[b,1.5];b;b;[b,1.5];[bsp,1]}; %initial parameters values
model_par_lb = {[b_lb,eps];b_lb;b_lb;[b_lb,0.3];[bsp_lb,-2+eps]}; %lower bounds
model_par_ub = {[b_ub,2-eps];b_ub;b_ub;[b_ub,3.5];[bsp_ub,inf]}; %upper bounds

clear b b_lb b_ub bsp bsp_lb bsp_ub

% Estimation of Anisotropy
R(n_models,1)=0;phi(n_models,1)=0;xi1(n_models,1)=0;xi2(n_models,1)=0;% matrices preallocation
er1(n_models,1)=0;er2(n_models,1)=0; %matrices preallocation
objmod = 'NWEr_m';flag = 1;
% nrsampl = 10; samplpc = 50;
for i=1:n_models
    model.function = models{i,1};
    model.params0 = model_par0{i,1};
    model.paramslb = model_par_lb{i,1};
    model.paramsub = model_par_ub{i,1};

     [R(i,1),phi(i,1),xi1(i,1),xi2(i,1),er1(i,1),er2(i,1)] =...
         aniso_dvf(x,y,rf,model,objmod,ncpc,nrbins,phistep,phitol,flag);
%     [R(i,1),phi(i,1),xi1(i,1),xi2(i,1),er1(i,1),er2(i,1)] =...
%         dirvar_ccv_s(x,y,rf,model,objmod,N_ms,ncpc,nrsampl,samplpc,nrbins,phistep,phitol,flag);

end

save('dirvar1_iso.mat')


% >>> Fitting II and Parameters of Correlation Estimation (s2,c0,v or eta1) <<<

% Initial Values and Limits for optimization
b{n_models,1}=[];b_lb{n_models,1}=[];b_ub{n_models,1}=[];
for i = 1:n_models
```

```
    b{i,1} = [gexpmax,xi1(i,1),R(i,1),phi(i,1),gexpmax/100];
    b_lb{i,1} = [eps,xi1(i,1),R(i,1),phi(i,1),eps];
    b_ub{i,1} = [inf,xi1(i,1),R(i,1),phi(i,1),gexpmax/5];
end

% Summary cells
model_par0 = {[b{1,1},1.1];b{2,1};b{3,1};[b{4,1},1.5];[b{5,1},1]}; % initial parameters values
model_par_lb = {[b_lb{1,1},eps];b_lb{2,1};b_lb{3,1};[b_lb{4,1},0.3];[b_lb{5,1},-2+eps]};%lower bounds
model_par_ub = {[b_ub{1,1},2];b_ub{2,1};b_ub{3,1};[b_ub{4,1},3.5];[b_ub{5,1},inf]}; %upper bounds

% Estimation of Parameters (s2,c0,v or eta1)
bmodel{n_models,1}=[]; fval(n_models,1)=0;tit{n_models,1}=[];
iso = 00;objmod = 'NWEr_m';flag = 1;
for i=1:n_models
    model.function = models{i,1};
    model.params0 = model_par0{i,1};
    model.paramslb = model_par_lb{i,1};
    model.paramsub = model_par_ub{i,1};

   [bmodel{i,1},fval(i,1),tit{i,1}] =...
       variogramfit(gexp,nr_pairs,c_centers,iso,model,objmod,flag);
end


% >>> Cross Validation <<<

% Matrices and Cells preallocation
cv_scores{n_models,1}=[]; cv_checks{n_models,1}=[];
cv_matr{n_models,1}=[]; cv_Ss(n_models,6)= 0;

% Inputs definition
 iso = 00; d_col = 1;

% Cross Validation
for i=1:n_models
    model.function = models{i,1};
    model.params = bmodel{i,1};
    model.r_ok = [22,4];

    [cv_scores{i,1}, cv_checks{i,1}, cv_matr{i,1}] =...
        crossval(x,y,rf,iso,d_col,model);
```

```
    cv_Ss(i,:) = table2array(cv_scores{i,1}(:,2:end));
end

% Cross Validation Scores
table_h = {'MeanAbsErr','MaxAbsErr','MSE','RMSE','rpearson','rspearman',
    'finalscore'};
table_r = {'Gexp';'Gaus';'Sphe';'Mate';'Spar'};

relMSE = cv_Ss(:,3)/min(cv_Ss(:,3)); %relative MSE
FinalScore = ((1./relMSE).^2).*cv_Ss(:,5).*cv_Ss(:,6); %finalscore
cv_Ss = [cv_Ss, FinalScore];
cv_Ssf = array2table(cv_Ss,'VariableNames',table_h,'RowNames',table_r);
clear relMSE FinalScore

%Trend addition and Boxcox Inversion
cv_St(n_models,6)= 0;
for i=1:n_models

    cv_matr{i,1}.Z_tr = Mx + cv_matr{i,1}.Z;

    if lambda==00
        cv_matr{i,1}.Z_ibt1 = cv_matr{i,1}.Z_tr;
    elseif lambda==0
        cv_matr{i,1}.Z_ibt1 = exp(cv_matr{i,1}.Z_tr);
    else
        cv_matr{i,1}.Z_ibt1 = (lambda*cv_matr{i,1}.Z_tr + 1).^(1/lambda)
    ;
    end
    cv_matr{i,1}.Z_ibt = real(cv_matr{i,1}.Z_ibt1);
    cv_realZ(i,1) = isreal(cv_matr{i,1}.Z_ibt1); %#ok<SAGROW>

    cv_St(i,:) = correlstats(v1,cv_matr{i,1}.Z_ibt);%total cv scores

end

% Total Cross Validation Scores
relMSE = cv_St(:,3)/min(cv_St(:,3)); %relative MSE
FinalScore = ((1./relMSE).^2).*cv_St(:,5).*cv_St(:,6); %finalscore
cv_St = [cv_St, FinalScore];
cv_Stf = array2table(cv_St,'VariableNames',table_h,'RowNames',table_r);
clear relMSE FinalScore

%Plots
for i=1:n_models
```

```
    % Stochastic Component's figures
    cc1 = [col,row,rf(:);qcol,qrow,zeros(Nu,1)];
    cc2 = [col,row,cv_matr{i,1}.Z(:);qcol,qrow,zeros(Nu,1)];
    Z1(max(cc1(:,2)),max(cc1(:,1)))=0; %#ok<SAGROW>
    Z2=Z1;
    for j = 1:size(cc1,1)
        Z1(cc1(j,2),cc1(j,1)) = cc1(j,3);
        Z2(cc2(j,2),cc2(j,1)) = cc2(j,3);
    end

    figure;pcolor(Z1);%title('Sample Stochastic Component');
    view(2);shading interp; colorbar;set(gca,'XTick',[],'YTick',[]);
    figure;pcolor(Z2);%title(sprintf('Estimation of Sample Stochastic
   Component \n%s',tit{i,1}));
    view(2);shading interp;colorbar;set(gca,'XTick',[],'YTick',[]);
    figure;scatter(rf(:),cv_matr{i,1}.Z(:),'filled','d');hold on;
    dvec1 = [rf(:);cv_matr{i,1}.Z(:)];
    plot([min(dvec1)-0.5,max(dvec1)+0.5],[min(dvec1)-0.5,max(dvec1)
   +0.5],'r');
    axis([min(dvec1)-0.5,max(dvec1)+0.5,min(dvec1)-0.5,max(dvec1)+0.5])
    %title('Scatter Plot')
    xlabel ('Observed Data'); ylabel ('Estimations');
    figure; h = histogram(rf(:),16,'EdgeColor',[0 0 1],'FaceAlpha',0.7);
    hold on
    histogram(cv_matr{i,1}.Z(:),'BinEdges',h.BinEdges,'EdgeColor',[0.2 1
     0]','FaceAlpha',0.7)
    %title('Histograms of Sample Stochastic Component')
    legend({'Original', 'Estimated'});
    clear h


    % Total Data figures
    cc3 = [col,row,v1(:);qcol,qrow,zeros(Nu,1)];
    cc4 = [col,row,cv_matr{i,1}.Z_ibt(:);qcol,qrow,zeros(Nu,1)];
    Z3(max(cc3(:,2)),max(cc3(:,1)))=0; %#ok<SAGROW>
    Z4=Z3;
    for j = 1:size(cc3,1)
        Z3(cc3(j,2),cc3(j,1)) = cc3(j,3);
        Z4(cc4(j,2),cc4(j,1)) = cc4(j,3);
    end
%     figure;pcolor(Z3);view(2);shading interp; %title('Original Sample
   ');
```

```
%     c = colorbar; c.Label.String = 'Normalised Velocity';set(gca,'
    XTick',[],'YTick',[]);
     figure;pcolor(Z4);view(2);shading interp; %title(sprintf('Estimation
     of Original Sample \n%s',tit{i,1}));
     c = colorbar; c.Label.String = 'Normalised Velocity';set(gca,'XTick'
    ,[],'YTick',[]);
     figure;scatter(v1(:),cv_matr{i,1}.Z_ibt(:),'filled','d');hold on;
     dvec2 = [v1(:);cv_matr{i,1}.Z_ibt(:)];
     plot([min(dvec2)-0.5,max(dvec2)+0.5],[min(dvec2)-0.5,max(dvec2)
    +0.5],'r');
     axis([min(dvec2)-0.5,max(dvec2)+0.5,min(dvec2)-0.5,max(dvec2)+0.5])
    %title('Scatter Plot')
     xlabel ('Observed Data')
     ylabel ('Estimations')
     figure;h = histogram(v1(:),16,'EdgeColor',[0 0 1],'FaceAlpha',0.7);
     hold on
     histogram(cv_matr{i,1}.Z_ibt(:),'BinEdges',h.BinEdges,'EdgeColor'
    ,[0.2 1 0],'FaceAlpha',0.7)
    %title('Histograms of Sample Data')
     legend({'Original', 'Estimated'});
     clear h

     clear Z1 Z2 Z3 Z4 dvec1 dvec2

end



% >>> Ordinary Kriging <<<

% Sort models based on cross validation scores
[~,ind] = sort(table2array(cv_Stf(:,7)),'descend');

% Matrices and Cells preallocation
Z{N_kr_mod,1}=[]; Z_error{N_kr_mod,1}=[];kr_checks{N_kr_mod,1}=[];
kr_matr{N_kr_mod,1}=[];
kr_Ss(N_kr_mod,6)= 0; table_r2{N_kr_mod,1} = [];
CI1{N_kr_mod,1}=[];UNC{N_kr_mod,1}=[];

% Inputs definition
xu = qcol; yu = qrow; iso = 00;

% Ordinary Kriging
for i=1:N_kr_mod
```

```
    model.function = models{ind(i),1};
    model.params = bmodel{ind(i),1};
    model.r_ok = [22,4];

    [Z{i,1},Z_error{i,1},kr_checks{i,1}, kr_matr{i,1}] =...
        ordkrig(x,y,rf,xu,yu,iso,model);
    kr_Ss(i,:) = correlstats(Z{i,1},qfluc);
    table_r2{i,1} = table_r{ind(i),1};

    %Confidence Intervals (95%)
    CI1{i,1}.low = Z{i,1} - 1.96*sqrt(Z_error{i,1});
    CI1{i,1}.up = Z{i,1} + 1.96*sqrt(Z_error{i,1});
    CI1{i,1}.uncer = 1.96*sqrt(Z_error{i,1});
    UNC{i,1} = real(CI1{i,1}.uncer);
    realCI(i,1) = isreal(CI1{i,1}.uncer); %#ok<SAGROW>
end

% Kriging Scores
relMSE = kr_Ss(:,3)/min(kr_Ss(:,3)); %relative MSE
FinalScore = ((1./relMSE).^2).*kr_Ss(:,5).*kr_Ss(:,6); %finalscore
kr_Ss = [kr_Ss, FinalScore];
kr_Ssf = array2table(kr_Ss,'VariableNames',table_h,'RowNames',table_r2);
clear relMSE FinalScore

%Trend addition and Boxcox Inversion
kr_St(N_kr_mod,6)= 0; Z_tr{N_kr_mod,1} = 0;
Z_ibt1{N_kr_mod,1} = 0;Z_ibt{N_kr_mod,1} = 0;
for i=1:N_kr_mod

    Z_tr{i,1} = qMx + Z{i,1};

    if lambda==00
        Z_ibt1{i,1} = Z_tr{i,1};
    elseif lambda==0
        Z_ibt1{i,1} = exp(Z_tr{i,1});
    else
        Z_ibt1{i,1} = (lambda*Z_tr{i,1} + 1).^(1/lambda);
    end
    Z_ibt{i,1} = real(Z_ibt1{i,1});
    kr_realZ(i,1) = isreal(Z_ibt1{i,1});  %#ok<SAGROW>

    kr_St(i,:) = correlstats(qv,Z_ibt{i,1});%total kriging scores

end
```

```
% Total Kriging Scores
relMSE = kr_St(:,3)/min(kr_St(:,3)); %relative MSE
FinalScore = ((1./relMSE).^2).*kr_St(:,5).*kr_St(:,6); %finalscore
kr_St = [kr_St, FinalScore];
kr_Stf = array2table(kr_St,'VariableNames',table_h,'RowNames',table_r2);
clear relMSE FinalScore

%Plots
for i=1:N_kr_mod

    % Stochastic Component's figures
    cc1 = [col,row,rf(:);qcol,qrow,qfluc(:)];
    cc2 = [col,row,rf(:);qcol,qrow,Z{i,1}];
    Z1(max(cc1(:,2)),max(cc1(:,1)))=0; %#ok<SAGROW>
    Z2=Z1;
    for j = 1:size(cc1,1)
        Z1(cc1(j,2),cc1(j,1)) = cc1(j,3);
        Z2(cc2(j,2),cc2(j,1)) = cc2(j,3);
    end
    figure;pcolor(Z1);%title('Original Stochastic Component');
    view(2);shading interp; colorbar;set(gca,'XTick',[],'YTick',[]);
    figure;pcolor(Z2); %title(sprintf('Estimation of Stochastic
   Component \n%s',tit{ind(i),1}));
    view(2);shading interp; colorbar;set(gca,'XTick',[],'YTick',[]);
    figure;scatter(qfluc(:),Z{i,1}(:),'filled','d');hold on;
    dvec1 = [qfluc(:);Z{i,1}(:)];
    plot([min(dvec1)-0.5,max(dvec1)+0.5],[min(dvec1)-0.5,max(dvec1)
   +0.5],'r');
    axis([min(dvec1)-0.5,max(dvec1)+0.5,min(dvec1)-0.5,max(dvec1)+0.5])
    %title('Scatter Plot')
    xlabel ('Observed Data')
    ylabel ('Estimations')
    figure;h = histogram(qfluc(:),16,'FaceColor',[0 0 1],'FaceAlpha'
   ,0.7);
    hold on
    histogram(Z{i,1}(:),'BinEdges',h.BinEdges,'FaceColor',[0.2 1 0],'
   FaceAlpha',0.7)
    %title('Histograms of Stochastic Component')
    legend({'Original', 'Estimated'});
    clear h

    % Total Data figures
    cc3 = [col,row,v1(:);qcol,qrow,Z_ibt{i,1}];
```

```
    cc4 = [col,row,zeros(size(col,1),1); qcol,qrow,UNC{i,1}];
    Z3(max(cc3(:,2)),max(cc3(:,1)))=0; %#ok<SAGROW>
    Z4=Z3;
    for j = 1:size(cc3,1)
        Z3(cc3(j,2),cc3(j,1)) = cc3(j,3);
        Z4(cc4(j,2),cc4(j,1)) = cc4(j,3);
    end
    figure;pcolor(Z3); view(2);shading interp; %title(sprintf('Estimation of Original Data \n%s',tit{ind(i),1}));
    c = colorbar; c.Label.String = 'Normalised Velocity';set(gca,'XTick',[],'YTick',[]);
    figure;scatter(qv1(:),Z_ibt{i,1}(:),'filled','d');hold on;
    dvec2 = [qv1(:);Z_ibt{i,1}(:)];
    plot([min(dvec2)-0.5,max(dvec2)+0.5],[min(dvec2)-0.5,max(dvec2)+0.5],'r');
    axis([min(dvec2)-0.5,max(dvec2)+0.5,min(dvec2)-0.5,max(dvec2)+0.5])
    %title('Scatter Plot')
    xlabel ('Observed Data')
    ylabel ('Estimations')
    figure;h = histogram(qv1(:),16,'FaceColor',[0 0 1],'FaceAlpha',0.7);
    hold on
    histogram(Z_ibt{i,1}(:),'BinEdges',h.BinEdges,'FaceColor',[0.2 1 0],'FaceAlpha',0.7)
    %title('Histograms of Data')
    legend({'Original', 'Estimated'});
    figure;pcolor(Z4); view(2);shading interp; %title('95% Confidence Interval');
    c1 = colorbar; c1.Label.String = 'Normalised Velocity'; set(gca,'XTick',[],'YTick',[]);
    clear h

    clear cc1 cc2 cc3 cc4 Z1 Z2 Z3 Z4 dvec1 dvec2

end

% >>>Correlation Coefficient of Indicators<<<
edges4 = (1500:4000/4:5500)/5500;
[~,~,ind_data4] = histcounts(qv1,edges4);
ind4_est{N_kr_mod,1}=[];Rpearson4(N_kr_mod,1)=0;Rspearman4(N_kr_mod,1)=0;
MCR4(N_kr_mod,1)=0;

edges16 = (1500:4000/16:5500)/5500;
[~,~,ind_data16] = histcounts(qv1,edges16);
```

```
ind16_est{N_kr_mod,1}=[];Rpearson16(N_kr_mod,1)=0;Rspearman16(N_kr_mod
    ,1)=0;
MCR16(N_kr_mod,1)=0;

for i=1:N_kr_mod
    [~,~,ind4_est{i,1}] = histcounts(Z_ibt{i,1},edges4);
    ind4_est{i,1}(Z_ibt{i,1}<=edges4(1)) = 1;
    ind4_est{i,1}(Z_ibt{i,1}>=edges4(end)) = length(edges4)-1;
    Rpearson4(i,1) = corr(ind4_est{i,1},ind_data4);
    Rspearman4(i,1) = corr(ind4_est{i,1},ind_data4,'type','Spearman');
    MCR4(i,1) = sum(ind4_est{i,1}~=ind_data4)/Nu;

    [~,~,ind16_est{i,1}] = histcounts(Z_ibt{i,1},edges16);
    ind16_est{i,1}(Z_ibt{i,1}<=edges16(1)) = 1;
    ind16_est{i,1}(Z_ibt{i,1}>=edges16(end)) = length(edges16)-1;
    Rpearson16(i,1) = corr(ind16_est{i,1},ind_data16);
    Rspearman16(i,1) = corr(ind16_est{i,1},ind_data16,'type','Spearman')
    ;
    MCR16(i,1) = sum(ind16_est{i,1}~=ind_data16)/Nu;
end

% Kriging Indicators Scores Table
table_h = {'MeanAbsErr','MaxAbsErr','MSE','RMSE','Rpearson','Rspearman'
    };
table_h2 = {'MeanAbsErr','MaxAbsErr','MSE','RMSE','Rpearson','Rspearman'
    ,'Rpearson4','Rspearman4','MCR4','Rpearson16','Rspearman16','MCR16'
    ,};
kr_iSsf = array2table(kr_Ss(:,1:end-1),'VariableNames',table_h,'RowNames
    ',table_r2);
kr_iStf = array2table([kr_St(:,1:end-1),Rpearson4,Rspearman4,MCR4,
    Rpearson16,Rspearman16,MCR16],'VariableNames',table_h2,'RowNames',
    table_r2);
%=============================================================


%% ################# DirVar2 ##############################
%=============================================================

load('dirvar1_iso.mat')

% >>> Rescaling and Rotation of the random field

% (Inverse) Transformation Matrix
```

```
A{n_models,1} = []; c_tr{n_models,1} = []; x_tr{n_models,1} = []; y_tr{
    n_models,1} = [];
qc_tr{n_models,1} = []; qx_tr{n_models,1} = []; qy_tr{n_models,1} = [];
R_tr(n_models,1)=0; phi_tr(n_models,1)=0; xi1_tr(n_models,1)=0; xi2_tr(
    n_models,1)=0;

gexp_tr{n_models,1}=[]; nr_pairs_tr{n_models,1}=[]; c_centers_tr{
    n_models,1}=[];

for i=1:n_models
A{i,1} = [cos(phi(i,1)*pi/180)/xi1(i,1), sin(phi(i,1)*pi/180)/xi1(i,1);
-sin(phi(i,1)*pi/180)/xi2(i,1), cos(phi(i,1)*pi/180)/xi2(i,1)];

% Rescale and Rotate Coordinations
c_tr{i,1} = A{i,1}*[c{1,1}';c{1,2}']; %transformed coordinations of
    known points
x_tr{i,1} = c_tr{i,1}(1,:)';
y_tr{i,1} = c_tr{i,1}(2,:)';
qc_tr{i,1} = A{i,1}*[qc{1,1}';qc{1,2}']; %transformed coordinations of
    unknown points
qx_tr{i,1} = qc_tr{i,1}(1,:)';
qy_tr{i,1} = qc_tr{i,1}(2,:)';

% >>> Check isotropy <<<

% Experimental Variogram (anisotropic)
x = x_tr{i,1}; y = y_tr{i,1}; rf = fluc; iso = 0;
[~,~,~] = expvar(x,y,rf,iso,ncpc,nrbins,4,phitol,2); %exper. variogr. of
     high analysis
%[gexp_tr{i,1}, nr_pairs_tr{i,1}, c_centers_tr{i,1}] = expvar(x,y,rf,iso
    ,ncpc,nrbins,phistep,phitol,2);

% Estimation of New Anisotropy
model.function = models{i,1};
model.params0 = model_par0{i,1};
model.paramslb = model_par_lb{i,1};
model.paramsub = model_par_ub{i,1};
[R_tr(i,1),phi_tr(i,1),xi1_tr(i,1),xi2_tr(i,1),~,~] = ...
     aniso_dvf(c_tr{i,1}(1,:),c_tr{i,1}(2,:),rf,model,'NWEr_m',ncpc,
    nrbins,phistep,phitol,0);

end
```

```
% >>> Fitting II and Parameters of Correlation Estimation (s2,c0,v or
    etal) <<<

% Experimental (Semi-)Variogram (isotropic)
gexp2{n_models,1}=[];nr_pairs2{n_models,1}=[]; c_centers2{n_models
    ,1}=[];
gexpmax2(n_models,1)=0;maxdist2(n_models,1)=0;
[k,l] = find(triu(true(N)));
for i=1:n_models
x = x_tr{i,1}; y = y_tr{i,1}; rf = fluc; iso = 1; flag = 1;
[~,~,~] = expvar(x,y,rf,iso,ncpc,nrbins,4,phitol,2); %exper. variogr. of
     high analysis
[gexp2{i,1}, nr_pairs2{i,1}, c_centers2{i,1}] = expvar(x,y,rf,iso,ncpc,
    nrbins,phistep,phitol,flag);
gexpmax2(i,1) = max(max(gexp2{i,1}));
d = hypot(c_tr{i,1}(1,k)-c_tr{i,1}(1,l),c_tr{i,1}(2,k)-c_tr{i,1}(2,l));
maxdist2(i,1) = ncpc*max(max(d));
clear d
end

% Initial Values and Limits for optimization
b{n_models,1}=[];b_lb{n_models,1}=[];b_ub{n_models,1}=[];
for i = 1:n_models
    b{i,1} = [gexpmax2(i,1),maxdist2(i,1)*2/3,gexpmax2(i,1)/100];
    b_lb{i,1} = [eps,eps,eps];
    b_ub{i,1} = [inf,maxdist2(i,1)*1.5,gexpmax2(i,1)/5];
end

% Summary cells
model_par0 = {[b{1,1},1.1];b{2,1};b{3,1};[b{4,1},1.5];[b{5,1},1]}; %
    initial parameters values
model_par_lb = {[b_lb{1,1},eps];b_lb{2,1};b_lb{3,1};[b_lb{4,1},0.3];[
    b_lb{5,1},-2+eps]};%lower bounds
model_par_ub = {[b_ub{1,1},2];b_ub{2,1};b_ub{3,1};[b_ub{4,1},3.5];[b_ub
    {5,1},inf]}; %upper bounds

% Estimation of Parameters (s2,c0,v or etal)
bmodel{n_models,1}=[]; fval(n_models,1)=0;tit{n_models,1}=[];
iso = 1;objmod = 'NWEr_m';flag = 1;
for i=1:n_models
    model.function = models{i,1};
    model.params0 = model_par0{i,1};
    model.paramslb = model_par_lb{i,1};
    model.paramsub = model_par_ub{i,1};
```

```
    [bmodel{i,1},fval(i,1),tit{i,1}] =...
        variogramfit(gexp2{i,1},nr_pairs2{i,1},c_centers2{i,1},iso,model,
    objmod,flag);
end


% >>> Cross Validation <<<

% Matrices and Cells preallocation
cv_scores{n_models,1}=[]; cv_checks{n_models,1}=[];
cv_matr{n_models,1}=[]; cv_Ss(n_models,6)= 0;

% Inputs definition
rf = rf(:); iso = 1; d_col = 1;

% Cross Validation
for i=1:n_models
     x = x_tr{i,1}(:); y = y_tr{i,1}(:);
     model.function = models{i,1};
     model.params = bmodel{i,1};
     rx_tr = pdist2(x_tr{i,1}(:),x_tr{i,1}(:));
     ry_tr = pdist2(y_tr{i,1}(:),y_tr{i,1}(:));
     model.r_ok = [mean(rx_tr(:))/5,mean(ry_tr(:))/5];

     [cv_scores{i,1}, cv_checks{i,1}, cv_matr{i,1}] =...
         crossval(x,y,rf,iso,d_col,model);
     cv_Ss(i,:) = table2array(cv_scores{i,1}(:,2:end));
end

% Cross Validation Scores
table_h = {'MeanAbsErr','MaxAbsErr','MSE','RMSE','rpearson','rspearman',
    'finalscore'};
table_r = {'Gexp';'Gaus';'Sphe';'Mate';'Spar'};

relMSE = cv_Ss(:,3)/min(cv_Ss(:,3)); %relative MSE
FinalScore = ((1./relMSE).^2).*cv_Ss(:,5).*cv_Ss(:,6); %finalscore
cv_Ss = [cv_Ss, FinalScore];
cv_Ssf = array2table(cv_Ss,'VariableNames',table_h,'RowNames',table_r);
clear relMSE FinalScore

%Trend addition and Boxcox Inversion
cv_St(n_models,6)= 0;
for i=1:n_models
```

```
    cv_matr{i,1}.Z_tr = Mx + cv_matr{i,1}.Z;

    if lambda==00
        cv_matr{i,1}.Z_ibt1 = cv_matr{i,1}.Z_tr;
    elseif lambda==0
        cv_matr{i,1}.Z_ibt1 = exp(cv_matr{i,1}.Z_tr);
    else
        cv_matr{i,1}.Z_ibt1 = (lambda*cv_matr{i,1}.Z_tr + 1).^(1/lambda)
   ;
    end
    cv_matr{i,1}.Z_ibt = real(cv_matr{i,1}.Z_ibt1);
    cv_realZ(i,1) = isreal(cv_matr{i,1}.Z_ibt1); %#ok<SAGROW>

    cv_St(i,:) = correlstats(v1,cv_matr{i,1}.Z_ibt);%total cv scores

end

% Total Cross Validation Scores
relMSE = cv_St(:,3)/min(cv_St(:,3)); %relative MSE
FinalScore = ((1./relMSE).^2).*cv_St(:,5).*cv_St(:,6); %finalscore
cv_St = [cv_St, FinalScore];
cv_Stf = array2table(cv_St,'VariableNames',table_h,'RowNames',table_r);
clear relMSE FinalScore

%Plots
for i=1:n_models

    % Stochastic Component's figures
    cc1 = [col,row,rf(:);qcol,qrow,zeros(Nu,1)];
    cc2 = [col,row,cv_matr{i,1}.Z(:);qcol,qrow,zeros(Nu,1)];
    Z1(max(cc1(:,2)),max(cc1(:,1)))=0; %#ok<SAGROW>
    Z2=Z1;
    for j = 1:size(cc1,1)
        Z1(cc1(j,2),cc1(j,1)) = cc1(j,3);
        Z2(cc2(j,2),cc2(j,1)) = cc2(j,3);
    end

    figure;pcolor(Z1);%title('Sample Stochastic Component');
    view(2);shading interp; colorbar;set(gca,'XTick',[],'YTick',[]);
    figure;pcolor(Z2);%title(sprintf('Estimation of Sample Stochastic
   Component \n%s',tit{i,1}));
    view(2);shading interp;colorbar;set(gca,'XTick',[],'YTick',[]);
    figure;scatter(rf(:),cv_matr{i,1}.Z(:),'filled','d');hold on;
```

```
    dvec1 = [rf(:);cv_matr{i,1}.Z(:)];
    plot([min(dvec1)-0.5,max(dvec1)+0.5],[min(dvec1)-0.5,max(dvec1)+0.5],'r');
    axis([min(dvec1)-0.5,max(dvec1)+0.5,min(dvec1)-0.5,max(dvec1)+0.5])
    %title('Scatter Plot')
    xlabel ('Observed Data'); ylabel ('Estimations');
    figure; h = histogram(rf(:),16,'EdgeColor',[0 0 1],'FaceAlpha',0.7);
    hold on
    histogram(cv_matr{i,1}.Z(:),'BinEdges',h.BinEdges,'EdgeColor',[0.2 1 0]','FaceAlpha',0.7)
    %title('Histograms of Sample Stochastic Component')
    legend({'Original', 'Estimated'});
    clear h


    % Total Data figures
    cc3 = [col,row,v1(:);qcol,qrow,zeros(Nu,1)];
    cc4 = [col,row,cv_matr{i,1}.Z_ibt(:);qcol,qrow,zeros(Nu,1)];
    Z3(max(cc3(:,2)),max(cc3(:,1)))=0; %#ok<SAGROW>
    Z4=Z3;
    for j = 1:size(cc3,1)
        Z3(cc3(j,2),cc3(j,1)) = cc3(j,3);
        Z4(cc4(j,2),cc4(j,1)) = cc4(j,3);
    end
%     figure;pcolor(Z3);view(2);shading interp; %title('Original Sample');
%     c = colorbar; c.Label.String = 'Normalised Velocity';set(gca,'XTick',[],'YTick',[]);
    figure;pcolor(Z4);view(2);shading interp; %title(sprintf('Estimation of Original Sample \n%s',tit{i,1}));
    c = colorbar; c.Label.String = 'Normalised Velocity';set(gca,'XTick',[],'YTick',[]);
    figure;scatter(v1(:),cv_matr{i,1}.Z_ibt(:),'filled','d');hold on;
    dvec2 = [v1(:);cv_matr{i,1}.Z_ibt(:)];
    plot([min(dvec2)-0.5,max(dvec2)+0.5],[min(dvec2)-0.5,max(dvec2)+0.5],'r');
    axis([min(dvec2)-0.5,max(dvec2)+0.5,min(dvec2)-0.5,max(dvec2)+0.5])
    %title('Scatter Plot')
    xlabel ('Observed Data')
    ylabel ('Estimations')
    figure;h = histogram(v1(:),16,'EdgeColor',[0 0 1],'FaceAlpha',0.7);
    hold on
    histogram(cv_matr{i,1}.Z_ibt(:),'BinEdges',h.BinEdges,'EdgeColor',[0.2 1 0],'FaceAlpha',0.7)
```

```
    %title('Histograms of Sample Data')
    legend({'Original', 'Estimated'});
    clear h

    clear Z1 Z2 Z3 Z4 dvec1 dvec2

end


% >>> Ordinary Kriging <<<

% Sort models based on cross validation scores
[~,ind] = sort(table2array(cv_Stf(:,7)),'descend');

% Matrices and Cells preallocation
Z{N_kr_mod,1}=[]; Z_error{N_kr_mod,1}=[];kr_checks{N_kr_mod,1}=[];
kr_matr{N_kr_mod,1}=[];
kr_Ss(N_kr_mod,6)= 0; table_r2{N_kr_mod,1} = [];
CI1{N_kr_mod,1}=[];UNC{N_kr_mod,1}=[];

% Inputs definition
rf = rf(:); iso = 1;

% Ordinary Kriging
for i=1:N_kr_mod
    x = x_tr{i,1}(:); y = y_tr{i,1}(:);
    xu = qx_tr{i,1}(:); yu = qy_tr{i,1}(:);
    model.function = models{ind(i),1};
    model.params = bmodel{ind(i),1};
    rx_tr = pdist2(x_tr{i,1}(:),x_tr{i,1}(:));
    ry_tr = pdist2(y_tr{i,1}(:),y_tr{i,1}(:));
    model.r_ok = [mean(rx_tr(:))/5,mean(ry_tr(:))/5];

    [Z{i,1},Z_error{i,1},kr_checks{i,1}, kr_matr{i,1}] =...
        ordkrig(x,y,rf,xu,yu,iso,model);
    kr_Ss(i,:) = correlstats(Z{i,1},qfluc);
    table_r2{i,1} = table_r{ind(i),1};

    %Confidence Intervals (95%)
    CI1{i,1}.low = Z{i,1} - 1.96*sqrt(Z_error{i,1});
    CI1{i,1}.up = Z{i,1} + 1.96*sqrt(Z_error{i,1});
    CI1{i,1}.uncer = 1.96*sqrt(Z_error{i,1});
    UNC{i,1} = real(CI1{i,1}.uncer);
    realCI(i,1) = isreal(CI1{i,1}.uncer); %#ok<SAGROW>
```

```
end

% Kriging Scores
relMSE = kr_Ss(:,3)/min(kr_Ss(:,3)); %relative MSE
FinalScore = ((1./relMSE).^2).*kr_Ss(:,5).*kr_Ss(:,6); %finalscore
kr_Ss = [kr_Ss, FinalScore];
kr_Ssf = array2table(kr_Ss,'VariableNames',table_h,'RowNames',table_r2);
clear relMSE FinalScore

%Trend addition and Boxcox Inversion
kr_St(N_kr_mod,6)= 0; Z_tr{N_kr_mod,1} = 0;
Z_ibt1{N_kr_mod,1} = 0;Z_ibt{N_kr_mod,1} = 0;
for i=1:N_kr_mod

    Z_tr{i,1} = qMx + Z{i,1};

    if lambda==00
        Z_ibt1{i,1} = Z_tr{i,1};
    elseif lambda==0
        Z_ibt1{i,1} = exp(Z_tr{i,1});
    else
        Z_ibt1{i,1} = (lambda*Z_tr{i,1} + 1).^(1/lambda);
    end
    Z_ibt{i,1} = real(Z_ibt1{i,1});
    kr_realZ(i,1) = isreal(Z_ibt1{i,1});  %#ok<SAGROW>

    kr_St(i,:) = correlstats(qv,Z_ibt{i,1});%total kriging scores

end

% Total Kriging Scores
relMSE = kr_St(:,3)/min(kr_St(:,3)); %relative MSE
FinalScore = ((1./relMSE).^2).*kr_St(:,5).*kr_St(:,6); %finalscore
kr_St = [kr_St, FinalScore];
kr_Stf = array2table(kr_St,'VariableNames',table_h,'RowNames',table_r2);
clear relMSE FinalScore

%Plots
for i=1:N_kr_mod

    % Stochastic Component's figures
    cc1 = [col,row,rf(:);qcol,qrow,qfluc(:)];
    cc2 = [col,row,rf(:);qcol,qrow,Z{i,1}];
    Z1(max(cc1(:,2)),max(cc1(:,1)))=0; %#ok<SAGROW>
```

```
Z2=Z1;
for j = 1:size(cc1,1)
    Z1(cc1(j,2),cc1(j,1)) = cc1(j,3);
    Z2(cc2(j,2),cc2(j,1)) = cc2(j,3);
end
figure;pcolor(Z1);%title('Original Stochastic Component');
view(2);shading interp; colorbar;set(gca,'XTick',[],'YTick',[]);
figure;pcolor(Z2); %title(sprintf('Estimation of Stochastic
Component \n%s',tit{ind(i),1}));
view(2);shading interp; colorbar;set(gca,'XTick',[],'YTick',[]);
figure;scatter(qfluc(:),Z{i,1}(:),'filled','d');hold on;
dvec1 = [qfluc(:);Z{i,1}(:)];
plot([min(dvec1)-0.5,max(dvec1)+0.5],[min(dvec1)-0.5,max(dvec1)
+0.5],'r');
axis([min(dvec1)-0.5,max(dvec1)+0.5,min(dvec1)-0.5,max(dvec1)+0.5])
%title('Scatter Plot')
xlabel ('Observed Data')
ylabel ('Estimations')
figure;h = histogram(qfluc(:),16,'FaceColor',[0 0 1],'FaceAlpha'
,0.7);
hold on
histogram(Z{i,1}(:),'BinEdges',h.BinEdges,'FaceColor',[0.2 1 0],'
FaceAlpha',0.7)
%title('Histograms of Stochastic Component')
legend({'Original', 'Estimated'});
clear h

% Total Data figures
cc3 = [col,row,v1(:);qcol,qrow,Z_ibt{i,1}];
cc4 = [col,row,zeros(size(col,1),1); qcol,qrow,UNC{i,1}];
Z3(max(cc3(:,2)),max(cc3(:,1)))=0; %#ok<SAGROW>
Z4=Z3;
for j = 1:size(cc3,1)
    Z3(cc3(j,2),cc3(j,1)) = cc3(j,3);
    Z4(cc4(j,2),cc4(j,1)) = cc4(j,3);
end
figure;pcolor(Z3); view(2);shading interp; %title(sprintf('
Estimation of Original Data \n%s',tit{ind(i),1}));
c = colorbar; c.Label.String = 'Normalised Velocity';set(gca,'XTick'
,[],'YTick',[]);
figure;scatter(qv1(:),Z_ibt{i,1}(:),'filled','d');hold on;
dvec2 = [qv1(:);Z_ibt{i,1}(:)];
plot([min(dvec2)-0.5,max(dvec2)+0.5],[min(dvec2)-0.5,max(dvec2)
+0.5],'r');
```

```
    axis([min(dvec2)-0.5,max(dvec2)+0.5,min(dvec2)-0.5,max(dvec2)+0.5])
    %title('Scatter Plot')
    xlabel ('Observed Data')
    ylabel ('Estimations')
    figure;h = histogram(qv1(:),16,'FaceColor',[0 0 1],'FaceAlpha',0.7);
    hold on
    histogram(Z_ibt{i,1}(:),'BinEdges',h.BinEdges,'FaceColor',[0.2 1 0],'FaceAlpha',0.7)
    %title('Histograms of Data')
    legend({'Original', 'Estimated'});
    figure;pcolor(Z4); view(2);shading interp; %title('95% Confidence Interval');
    c1 = colorbar; c1.Label.String = 'Normalised Velocity'; set(gca,'XTick',[],'YTick',[]);
    clear h

    clear cc1 cc2 cc3 cc4 Z1 Z2 Z3 Z4 dvec1 dvec2

end

% >>>Correlation Coefficient of Indicators<<<
edges4 = (1500:4000/4:5500)/5500;
[~,~,ind_data4] = histcounts(qv1,edges4);
ind4_est{N_kr_mod,1}=[];Rpearson4(N_kr_mod,1)=0;Rspearman4(N_kr_mod,1)=0;
MCR4(N_kr_mod,1)=0;

edges16 = (1500:4000/16:5500)/5500;
[~,~,ind_data16] = histcounts(qv1,edges16);
ind16_est{N_kr_mod,1}=[];Rpearson16(N_kr_mod,1)=0;Rspearman16(N_kr_mod,1)=0;
MCR16(N_kr_mod,1)=0;

for i=1:N_kr_mod
    [~,~,ind4_est{i,1}] = histcounts(Z_ibt{i,1},edges4);
    ind4_est{i,1}(Z_ibt{i,1}<=edges4(1)) = 1;
    ind4_est{i,1}(Z_ibt{i,1}>=edges4(end)) = length(edges4)-1;
    Rpearson4(i,1) = corr(ind4_est{i,1},ind_data4);
    Rspearman4(i,1) = corr(ind4_est{i,1},ind_data4,'type','Spearman');
    MCR4(i,1) = sum(ind4_est{i,1}~=ind_data4)/Nu;

    [~,~,ind16_est{i,1}] = histcounts(Z_ibt{i,1},edges16);
    ind16_est{i,1}(Z_ibt{i,1}<=edges16(1)) = 1;
    ind16_est{i,1}(Z_ibt{i,1}>=edges16(end)) = length(edges16)-1;
```

```
    Rpearson16(i,1) = corr(ind16_est{i,1},ind_data16);
    Rspearman16(i,1) = corr(ind16_est{i,1},ind_data16,'type','Spearman');
    MCR16(i,1) = sum(ind16_est{i,1}~=ind_data16)/Nu;

end

% Kriging Indicators Scores Table
table_h = {'MeanAbsErr','MaxAbsErr','MSE','RMSE','Rpearson','Rspearman'};
table_h2 = {'MeanAbsErr','MaxAbsErr','MSE','RMSE','Rpearson','Rspearman','Rpearson4','Rspearman4','MCR4','Rpearson16','Rspearman16','MCR16',};
kr_iSsf = array2table(kr_Ss(:,1:end-1),'VariableNames',table_h,'RowNames',table_r2);
kr_iStf = array2table([kr_St(:,1:end-1),Rpearson4,Rspearman4,MCR4,Rpearson16,Rspearman16,MCR16],'VariableNames',table_h2,'RowNames',table_r2);
%=======================================================================


%% ################# CHI1 #############################
%=======================================================================

% >>> Anisotropy estimation with CHI <<<

[R,phi] = aniso_interp_scatter(x,y,rf,nx,'v4');
if R>1
    R = 1/R;
    if phi>0
        phi = phi-90;
    elseif phi<0
        phi = phi+90;
    end
end

save('chi1_iso.mat')

% >>> Fitting II and Parameters of Correlation Estimation (s2,c0,v or eta1) <<<

% Desired Models
models = {'Gexp';'Gaus';'Sphe';'Mate';'Spar'};
n_models = length(models);
```

```
% Initial Values and Limits for optimization
b = [gexpmax, maxdist*1/3,R, phi, gexpmax/100]; % s2, xi & c0
b_lb = [eps, eps,R, phi, eps]; b_ub = [gexpmax*1.5, maxdist,R, phi, gexpmax
    /5]; %lower and upper limits
bsp = [1000, maxdist*1/3,R, phi, gexpmax/100]; % eta0, xi, c0
bsp_lb = [eps, eps,R, phi, eps]; bsp_ub = [inf, maxdist,R, phi, gexpmax/5]; %
    lower and upper limits

% Summary cells
model_par0 = {[b,1.5];b;b;[b,1.5];[bsp,1]}; %initial parameters values
model_par_lb = {[b_lb, eps];b_lb;b_lb;[b_lb,0.3];[bsp_lb,-2+eps]}; %lower
     bounds
model_par_ub = {[b_ub,2-eps];b_ub;b_ub;[b_ub,3.5];[bsp_ub,inf]}; %upper
    bounds

clear b b_lb b_ub bsp bsp_lb bsp_ub

% Estimation of Parameters (s2,xi1,c0,v or eta1)
bmodel{n_models,1}=[]; fval(n_models,1)=0;tit{n_models,1}=[];
iso = 00;objmod = 'NWEr_m';flag = 1;
for i=1:n_models
     model.function = models{i,1};
     model.params0 = model_par0{i,1};
     model.paramslb = model_par_lb{i,1};
     model.paramsub = model_par_ub{i,1};

    [bmodel{i,1},fval(i,1),tit{i,1}] =...
         variogramfit(gexp, nr_pairs, c_centers, iso, model, objmod, flag);
end


% >>> Cross Validation <<<

% Matrices and Cells preallocation
cv_scores{n_models,1}=[]; cv_checks{n_models,1}=[];
cv_matr{n_models,1}=[]; cv_Ss(n_models,6)= 0;

% Inputs definition
x = x(:); y = y(:);rf = rf(:);
iso = 00; d_col = 1;

% Cross Validation
for i=1:n_models
```

```
    model.function = models{i,1};
    model.params = bmodel{i,1};
    model.r_ok = [22,4];

    [cv_scores{i,1}, cv_checks{i,1}, cv_matr{i,1}] =...
        crossval(x,y,rf,iso,d_col,model);
    cv_Ss(i,:) = table2array(cv_scores{i,1}(:,2:end));
end

% Cross Validation Scores
table_h = {'MeanAbsErr','MaxAbsErr','MSE','RMSE','rpearson','rspearman',
    'finalscore'};
table_r = {'Gexp';'Gaus';'Sphe';'Mate';'Spar'};

relMSE = cv_Ss(:,3)/min(cv_Ss(:,3)); %relative MSE
FinalScore = ((1./relMSE).^2).*cv_Ss(:,5).*cv_Ss(:,6); %finalscore
cv_Ss = [cv_Ss, FinalScore];
cv_Ssf = array2table(cv_Ss,'VariableNames',table_h,'RowNames',table_r);
clear relMSE FinalScore

%Trend addition and Boxcox Inversion
cv_St(n_models,6)= 0;
for i=1:n_models

    cv_matr{i,1}.Z_tr = Mx + cv_matr{i,1}.Z;

    if lambda==00
        cv_matr{i,1}.Z_ibt1 = cv_matr{i,1}.Z_tr;
    elseif lambda==0
        cv_matr{i,1}.Z_ibt1 = exp(cv_matr{i,1}.Z_tr);
    else
        cv_matr{i,1}.Z_ibt1 = (lambda*cv_matr{i,1}.Z_tr + 1).^(1/lambda)
    ;
    end
    cv_matr{i,1}.Z_ibt = real(cv_matr{i,1}.Z_ibt1);
    cv_realZ(i,1) = isreal(cv_matr{i,1}.Z_ibt1); %#ok<SAGROW>

    cv_St(i,:) = correlstats(v1,cv_matr{i,1}.Z_ibt);%total cv scores

end

% Total Cross Validation Scores
relMSE = cv_St(:,3)/min(cv_St(:,3)); %relative MSE
FinalScore = ((1./relMSE).^2).*cv_St(:,5).*cv_St(:,6); %finalscore
```

```
cv_St = [cv_St, FinalScore];
cv_Stf = array2table(cv_St,'VariableNames',table_h,'RowNames',table_r);
clear relMSE FinalScore

%Plots
for i=1:n_models

    % Stochastic Component's figures
    cc1 = [col,row,rf(:);qcol,qrow,zeros(Nu,1)];
    cc2 = [col,row,cv_matr{i,1}.Z(:);qcol,qrow,zeros(Nu,1)];
    Z1(max(cc1(:,2)),max(cc1(:,1)))=0; %#ok<SAGROW>
    Z2=Z1;
    for j = 1:size(cc1,1)
        Z1(cc1(j,2),cc1(j,1)) = cc1(j,3);
        Z2(cc2(j,2),cc2(j,1)) = cc2(j,3);
    end

    figure;pcolor(Z1);%title('Sample Stochastic Component');
    view(2);shading interp; colorbar;set(gca,'XTick',[],'YTick',[]);
    figure;pcolor(Z2);%title(sprintf('Estimation of Sample Stochastic
   Component \n%s',tit{i,1}));
    view(2);shading interp;colorbar;set(gca,'XTick',[],'YTick',[]);
    figure;scatter(rf(:),cv_matr{i,1}.Z(:),'filled','d');hold on;
    dvec1 = [rf(:);cv_matr{i,1}.Z(:)];
    plot([min(dvec1)-0.5,max(dvec1)+0.5],[min(dvec1)-0.5,max(dvec1)
   +0.5],'r');
    axis([min(dvec1)-0.5,max(dvec1)+0.5,min(dvec1)-0.5,max(dvec1)+0.5])
    %title('Scatter Plot')
    xlabel ('Observed Data'); ylabel ('Estimations');
    figure; h = histogram(rf(:),16,'EdgeColor',[0 0 1],'FaceAlpha',0.7);
    hold on
    histogram(cv_matr{i,1}.Z(:),'BinEdges',h.BinEdges,'EdgeColor',[0.2 1
    0]','FaceAlpha',0.7)
    %title('Histograms of Sample Stochastic Component')
    legend({'Original', 'Estimated'});
    clear h


    % Total Data figures
    cc3 = [col,row,v1(:);qcol,qrow,zeros(Nu,1)];
    cc4 = [col,row,cv_matr{i,1}.Z_ibt(:);qcol,qrow,zeros(Nu,1)];
    Z3(max(cc3(:,2)),max(cc3(:,1)))=0; %#ok<SAGROW>
    Z4=Z3;
    for j = 1:size(cc3,1)
```

```
        Z3(cc3(j,2),cc3(j,1)) = cc3(j,3);
        Z4(cc4(j,2),cc4(j,1)) = cc4(j,3);
    end
%     figure;pcolor(Z3);view(2);shading interp; %title('Original Sample
    ');
%     c = colorbar; c.Label.String = 'Normalised Velocity';set(gca,'
    XTick',[],'YTick',[]);
    figure;pcolor(Z4);view(2);shading interp; %title(sprintf('Estimation
     of Original Sample \n%s',tit{i,1}));
    c = colorbar; c.Label.String = 'Normalised Velocity';set(gca,'XTick'
    ,[],'YTick',[]);
    figure;scatter(v1(:),cv_matr{i,1}.Z_ibt(:),'filled','d');hold on;
    dvec2 = [v1(:);cv_matr{i,1}.Z_ibt(:)];
    plot([min(dvec2)-0.5,max(dvec2)+0.5],[min(dvec2)-0.5,max(dvec2)
    +0.5],'r');
    axis([min(dvec2)-0.5,max(dvec2)+0.5,min(dvec2)-0.5,max(dvec2)+0.5])
    %title('Scatter Plot')
    xlabel ('Observed Data')
    ylabel ('Estimations')
    figure;h = histogram(v1(:),16,'EdgeColor',[0 0 1],'FaceAlpha',0.7);
    hold on
    histogram(cv_matr{i,1}.Z_ibt(:),'BinEdges',h.BinEdges,'EdgeColor'
    ,[0.2 1 0],'FaceAlpha',0.7)
    %title('Histograms of Sample Data')
    legend({'Original', 'Estimated'});
    clear h

    clear Z1 Z2 Z3 Z4 dvec1 dvec2

end



% >>> Ordinary Kriging <<<

% Sort models based on cross validation scores
[~,ind] = sort(table2array(cv_Stf(:,7)),'descend');

% Matrices and Cells preallocation
Z{N_kr_mod,1}=[]; Z_error{N_kr_mod,1}=[];kr_checks{N_kr_mod,1}=[];
kr_matr{N_kr_mod,1}=[];
kr_Ss(N_kr_mod,6)= 0; table_r2{N_kr_mod,1} = [];
CI1{N_kr_mod,1}=[];UNC{N_kr_mod,1}=[];
```

```
% Inputs definition
xu = qcol; yu = qrow; iso = 00;

% Ordinary Kriging
for i=1:N_kr_mod
    model.function = models{ind(i),1};
    model.params = bmodel{ind(i),1};
    model.r_ok = [22,4];

    [Z{i,1},Z_error{i,1},kr_checks{i,1}, kr_matr{i,1}] =...
        ordkrig(x,y,rf,xu,yu,iso,model);
    kr_Ss(i,:) = correlstats(Z{i,1},qfluc);
    table_r2{i,1} = table_r{ind(i),1};

    %Confidence Intervals (95%)
    CI1{i,1}.low = Z{i,1} - 1.96*sqrt(Z_error{i,1});
    CI1{i,1}.up = Z{i,1} + 1.96*sqrt(Z_error{i,1});
    CI1{i,1}.uncer = 1.96*sqrt(Z_error{i,1});
    UNC{i,1} = real(CI1{i,1}.uncer);
    realCI(i,1) = isreal(CI1{i,1}.uncer); %#ok<SAGROW>
end

% Kriging Scores
relMSE = kr_Ss(:,3)/min(kr_Ss(:,3)); %relative MSE
FinalScore = ((1./relMSE).^2).*kr_Ss(:,5).*kr_Ss(:,6); %finalscore
kr_Ss = [kr_Ss, FinalScore];
kr_Ssf = array2table(kr_Ss,'VariableNames',table_h,'RowNames',table_r2);
clear relMSE FinalScore

%Trend addition and Boxcox Inversion
kr_St(N_kr_mod,6)= 0; Z_tr{N_kr_mod,1} = 0;
Z_ibt1{N_kr_mod,1} = 0;Z_ibt{N_kr_mod,1} = 0;
for i=1:N_kr_mod

    Z_tr{i,1} = qMx + Z{i,1};

    if lambda==00
        Z_ibt1{i,1} = Z_tr{i,1};
    elseif lambda==0
        Z_ibt1{i,1} = exp(Z_tr{i,1});
    else
        Z_ibt1{i,1} = (lambda*Z_tr{i,1} + 1).^(1/lambda);
    end
    Z_ibt{i,1} = real(Z_ibt1{i,1});
```

```
    kr_realZ(i,1) = isreal(Z_ibt1{i,1}); %#ok<SAGROW>

    kr_St(i,:) = correlstats(qv,Z_ibt{i,1});%total kriging scores

end

% Total Kriging Scores
relMSE = kr_St(:,3)/min(kr_St(:,3)); %relative MSE
FinalScore = ((1./relMSE).^2).*kr_St(:,5).*kr_St(:,6); %finalscore
kr_St = [kr_St, FinalScore];
kr_Stf = array2table(kr_St,'VariableNames',table_h,'RowNames',table_r2);
clear relMSE FinalScore

%Plots
for i=1:N_kr_mod

    % Stochastic Component's figures
    cc1 = [col,row,rf(:);qcol,qrow,qfluc(:)];
    cc2 = [col,row,rf(:);qcol,qrow,Z{i,1}];
    Z1(max(cc1(:,2)),max(cc1(:,1)))=0; %#ok<SAGROW>
    Z2=Z1;
    for j = 1:size(cc1,1)
        Z1(cc1(j,2),cc1(j,1)) = cc1(j,3);
        Z2(cc2(j,2),cc2(j,1)) = cc2(j,3);
    end
    figure;pcolor(Z1);%title('Original Stochastic Component');
    view(2);shading interp; colorbar;set(gca,'XTick',[],'YTick',[]);
    figure;pcolor(Z2); %title(sprintf('Estimation of Stochastic
   Component \n%s',tit{ind(i),1}));
    view(2);shading interp; colorbar;set(gca,'XTick',[],'YTick',[]);
    figure;scatter(qfluc(:),Z{i,1}(:),'filled','d');hold on;
    dvec1 = [qfluc(:);Z{i,1}(:)];
    plot([min(dvec1)-0.5,max(dvec1)+0.5],[min(dvec1)-0.5,max(dvec1)
   +0.5],'r');
    axis([min(dvec1)-0.5,max(dvec1)+0.5,min(dvec1)-0.5,max(dvec1)+0.5])
    %title('Scatter Plot')
    xlabel ('Observed Data')
    ylabel ('Estimations')
    figure;h = histogram(qfluc(:),16,'FaceColor',[0 0 1],'FaceAlpha'
    ,0.7);
    hold on
    histogram(Z{i,1}(:),'BinEdges',h.BinEdges,'FaceColor',[0.2 1 0],'
   FaceAlpha',0.7)
    %title('Histograms of Stochastic Component')
```

```
    legend({'Original', 'Estimated'});
    clear h

    % Total Data figures
    cc3 = [col,row,v1(:);qcol,qrow,Z_ibt{i,1}];
    cc4 = [col,row,zeros(size(col,1),1); qcol,qrow,UNC{i,1}];
    Z3(max(cc3(:,2)),max(cc3(:,1)))=0; %#ok<SAGROW>
    Z4=Z3;
    for j = 1:size(cc3,1)
        Z3(cc3(j,2),cc3(j,1)) = cc3(j,3);
        Z4(cc4(j,2),cc4(j,1)) = cc4(j,3);
    end
    figure;pcolor(Z3); view(2);shading interp; %title(sprintf('Estimation of Original Data \n%s',tit{ind(i),1}));
    c = colorbar; c.Label.String = 'Normalised Velocity';set(gca,'XTick',[],'YTick',[]);
    figure;scatter(qv1(:),Z_ibt{i,1}(:),'filled','d');hold on;
    dvec2 = [qv1(:);Z_ibt{i,1}(:)];
    plot([min(dvec2)-0.5,max(dvec2)+0.5],[min(dvec2)-0.5,max(dvec2)+0.5],'r');
    axis([min(dvec2)-0.5,max(dvec2)+0.5,min(dvec2)-0.5,max(dvec2)+0.5])
    %title('Scatter Plot')
    xlabel ('Observed Data')
    ylabel ('Estimations')
    figure;h = histogram(qv1(:),16,'FaceColor',[0 0 1],'FaceAlpha',0.7);
    hold on
    histogram(Z_ibt{i,1}(:),'BinEdges',h.BinEdges,'FaceColor',[0.2 1 0],'FaceAlpha',0.7)
    %title('Histograms of Data')
    legend({'Original', 'Estimated'});
    figure;pcolor(Z4); view(2);shading interp; %title('95% Confidence Interval');
    c1 = colorbar; c1.Label.String = 'Normalised Velocity'; set(gca,'XTick',[],'YTick',[]);
    clear h

    clear cc1 cc2 cc3 cc4 Z1 Z2 Z3 Z4 dvec1 dvec2

end

% >>>Correlation Coefficient of Indicators<<<
edges4 = (1500:4000/4:5500)/5500;
[~,~,ind_data4] = histcounts(qv1,edges4);
```

```
ind4_est{N_kr_mod,1}=[];Rpearson4(N_kr_mod,1)=0;Rspearman4(N_kr_mod,1)
    =0;
MCR4(N_kr_mod,1)=0;

edges16 = (1500:4000/16:5500)/5500;
[~,~,ind_data16] = histcounts(qv1,edges16);
ind16_est{N_kr_mod,1}=[];Rpearson16(N_kr_mod,1)=0;Rspearman16(N_kr_mod
    ,1)=0;
MCR16(N_kr_mod,1)=0;

for i=1:N_kr_mod
    [~,~,ind4_est{i,1}] = histcounts(Z_ibt{i,1},edges4);
    ind4_est{i,1}(Z_ibt{i,1}<=edges4(1)) = 1;
    ind4_est{i,1}(Z_ibt{i,1}>=edges4(end)) = length(edges4)-1;
    Rpearson4(i,1) = corr(ind4_est{i,1},ind_data4);
    Rspearman4(i,1) = corr(ind4_est{i,1},ind_data4,'type','Spearman');
    MCR4(i,1) = sum(ind4_est{i,1}~=ind_data4)/Nu;


    [~,~,ind16_est{i,1}] = histcounts(Z_ibt{i,1},edges16);
    ind16_est{i,1}(Z_ibt{i,1}<=edges16(1)) = 1;
    ind16_est{i,1}(Z_ibt{i,1}>=edges16(end)) = length(edges16)-1;
    Rpearson16(i,1) = corr(ind16_est{i,1},ind_data16);
    Rspearman16(i,1) = corr(ind16_est{i,1},ind_data16,'type','Spearman')
    ;
    MCR16(i,1) = sum(ind16_est{i,1}~=ind_data16)/Nu;

end

% Kriging Indicators Scores Table
table_h = {'MeanAbsErr','MaxAbsErr','MSE','RMSE','Rpearson','Rspearman'
    };
table_h2 = {'MeanAbsErr','MaxAbsErr','MSE','RMSE','Rpearson','Rspearman'
    ,'Rpearson4','Rspearman4','MCR4','Rpearson16','Rspearman16','MCR16'
    ,};
kr_iSsf = array2table(kr_Ss(:,1:end-1),'VariableNames',table_h,'RowNames
    ',table_r2);
kr_iStf = array2table([kr_St(:,1:end-1),Rpearson4,Rspearman4,MCR4,
    Rpearson16,Rspearman16,MCR16],'VariableNames',table_h2,'RowNames',
    table_r2);
%=====================================================================


%% ################## CHI2 ################################
```

```
%=====================================================================

load('chi1_iso.mat')

% >>> Fitting II and Estimation of xi1 & xi2 <<<

xi1 = R;xi2 = 1;

% Desired Models
models = {'Gexp';'Gaus';'Sphe';'Mate';'Spar'};
n_models = length(models);

% >>> Rescaling and Rotation of the random field

% (Inverse) Transformation Matrix
A = [cos(phi*pi/180)/xi1, sin(phi*pi/180)/xi1;
-sin(phi*pi/180)/xi2, cos(phi*pi/180)/xi2];


% Rescale and Rotate Coordinations
c_tr = A*[c{1,1}';c{1,2}']; %transformed coordinations of known points
x_tr = c_tr(1,:)';
y_tr = c_tr(2,:)';
qc_tr = A*[qc{1,1}';qc{1,2}']; %transformed coordinations of unknown points
qx_tr = qc_tr(1,:)';
qy_tr = qc_tr(2,:)';

% >>> Check isotropy <<<

% Experimental Variogram (anisotropic)
x = x_tr; y = y_tr; rf = fluc; iso = 0;
[~,~,~] = expvar(x,y,rf,iso,ncpc,nrbins,4,phitol,2); %exper. variogr. of high analysis
%[gexp_tr, nr_pairs_tr, c_centers_tr] = expvar(x,y,rf,iso,ncpc,nrbins,phistep,phitol,2);

%Initial Values and Limits for optimization
b = [gexpmax,maxdist*1/3,gexpmax/100]; % s2,xi & c0
b_lb = [eps,eps,eps]; b_ub = [gexpmax*1.5,maxdist,gexpmax/5]; %lower and upper limits
bsp = [1000,maxdist*1/3,gexpmax/100]; % eta0, xi, c0
bsp_lb = [eps,eps,eps]; bsp_ub = [inf,maxdist,gexpmax/5]; %lower and upper limits
```

```
%Summary cells
model_par0 = {[b,1.5];b;b;[b,1.5];[bsp,1]}; %initial parameters values
model_par_lb = {[b_lb,eps];b_lb;b_lb;[b_lb,0.3];[bsp_lb,-2+eps]}; %lower
      bounds
model_par_ub = {[b_ub,2-eps];b_ub;b_ub;[b_ub,3.5];[bsp_ub,inf]}; %upper
    bounds

clear b b_lb b_ub bsp bsp_lb bsp_ub

% Estimation of New Anisotropy
R_tr(n_models,1)=0;phi_tr(n_models,1)=0;xi1_tr(n_models,1)=0;xi2_tr(
    n_models,1)=0;
for i=1:n_models
    model.function = models{i,1};
    model.params0 = model_par0{i,1};
    model.paramslb = model_par_lb{i,1};
    model.paramsub = model_par_ub{i,1};
    [R_tr(i,1),phi_tr(i,1),xi1_tr(i,1),xi2_tr(i,1),~,~] = ...
        aniso_dvf(c_tr(1,:),c_tr(2,:),rf,model,'NWEr_m',20,0.4,nrbins,
    phistep,phitol,0);
end



% >>> Fitting III and Parameters of Correlation Estimation (s2,c0,v or
    eta1) <<<

% Experimental (Semi-)Variogram (isotropic)
x = x_tr; y = y_tr; rf = fluc; iso = 1; flag = 1;
[~,~,~] = expvar(x,y,rf,iso,ncpc,nrbins,4,phitol,2); %exper. variogr. of
      high analysis
[gexp2, nr_pairs2, c_centers2] = expvar(x,y,rf,iso,ncpc,nrbins,phistep,
    phitol,flag);
gexpmax2 = max(max(gexp2));

% Initial Values and Limits for optimization
[k,l] = find(triu(true(N)));
d = hypot(c_tr(1,k)-c_tr(1,l),c_tr(2,k)-c_tr(2,l));
maxdist2(i,1) = ncpc*max(max(d));
% maxdist2 = hypot(c_tr(1,1)-c_tr(1,N),c_tr(2,1)-c_tr(2,N))*ncpc;

b = [gexpmax2,maxdist2*2/3,gexpmax2/100]; % s2,xi & c0
```

```
b_lb = [eps,eps,eps]; b_ub = [gexpmax2*1.5,maxdist2*1.5,gexpmax2/5]; %
    lower and upper limits
bsp = [1000,maxdist2*2/3,gexpmax2/100]; % eta0, xi, c0
bsp_lb = [eps,eps,eps]; bsp_ub = [inf,maxdist2*1.5,gexpmax2/5]; %lower
    and upper limits

% Summary cells
model_par0 = {[b,1.5];b;b;[b,1.5];[bsp,1]}; %initial parameters values
model_par_lb = {[b_lb,eps];b_lb;b_lb;[b_lb,0.3];[bsp_lb,-2+eps]}; %lower
     bounds
model_par_ub = {[b_ub,2-eps];b_ub;b_ub;[b_ub,3.5];[bsp_ub,inf]}; %upper
    bounds

clear b b_lb b_ub bsp bsp_lb bsp_ub

% Estimation of Parameters (s2,c0,v or eta1)
bmodel2{n_models,1}=[]; fval2(n_models,1)=0; tit2{n_models,1}=[];
iso = 1;objmod = 'NWEr_m'; flag = 1;
for i=1:n_models
    model.function = models{i,1};
    model.params0 = model_par0{i,1};
    model.paramslb = model_par_lb{i,1};
    model.paramsub = model_par_ub{i,1};

   [bmodel2{i,1},fval2(i,1),tit2{i,1}] =...
        variogramfit(gexp2,nr_pairs2,c_centers2,iso,model,objmod,flag);
end


% >>> Cross Validation <<<

% Matrices and Cells preallocation
cv_scores{n_models,1}=[]; cv_checks{n_models,1}=[];
cv_matr{n_models,1}=[]; cv_Ss(n_models,6)= 0;

% Inputs definition
x = x_tr; y = y_tr; iso = 1;d_col = 1;

rx_tr = pdist2(x_tr(:),x_tr(:));
ry_tr = pdist2(y_tr(:),y_tr(:));

% Cross Validation
for i=1:n_models
    model.function = models{i,1};
```

```
    model.params = bmodel2{i,1};
    model.r_ok = [mean(rx_tr(:))/5,mean(ry_tr(:))/5];

    [cv_scores{i,1}, cv_checks{i,1}, cv_matr{i,1}] =...
        crossval(x,y,rf,iso,d_col,model);
    cv_Ss(i,:) = table2array(cv_scores{i,1}(:,2:end));
end

% Cross Validation Scores
table_h = {'MeanAbsErr','MaxAbsErr','MSE','RMSE','rpearson','rspearman',
    'finalscore'};
table_r = {'Gexp';'Gaus';'Sphe';'Mate';'Spar'};

relMSE = cv_Ss(:,3)/min(cv_Ss(:,3)); %relative MSE
FinalScore = ((1./relMSE).^2).*cv_Ss(:,5).*cv_Ss(:,6); %finalscore
cv_Ss = [cv_Ss, FinalScore];
cv_Ssf = array2table(cv_Ss,'VariableNames',table_h,'RowNames',table_r);
clear relMSE FinalScore

%Trend addition and Boxcox Inversion
cv_St(n_models,6)= 0;
for i=1:n_models

    cv_matr{i,1}.Z_tr = Mx + cv_matr{i,1}.Z;

    if lambda==00
        cv_matr{i,1}.Z_ibt1 = cv_matr{i,1}.Z_tr;
    elseif lambda==0
        cv_matr{i,1}.Z_ibt1 = exp(cv_matr{i,1}.Z_tr);
    else
        cv_matr{i,1}.Z_ibt1 = (lambda*cv_matr{i,1}.Z_tr + 1).^(1/lambda)
    ;
    end
    cv_matr{i,1}.Z_ibt = real(cv_matr{i,1}.Z_ibt1);
    cv_realZ(i,1) = isreal(cv_matr{i,1}.Z_ibt1); %#ok<SAGROW>

    cv_St(i,:) = correlstats(v1,cv_matr{i,1}.Z_ibt);%total cv scores

end

% Total Cross Validation Scores
relMSE = cv_St(:,3)/min(cv_St(:,3)); %relative MSE
FinalScore = ((1./relMSE).^2).*cv_St(:,5).*cv_St(:,6); %finalscore
cv_St = [cv_St, FinalScore];
```

```
cv_Stf = array2table(cv_St,'VariableNames',table_h,'RowNames',table_r);
clear relMSE FinalScore

%Plots
for i=1:n_models

    % Stochastic Component's figures
    cc1 = [col,row,rf(:);qcol,qrow,zeros(Nu,1)];
    cc2 = [col,row,cv_matr{i,1}.Z(:);qcol,qrow,zeros(Nu,1)];
    Z1(max(cc1(:,2)),max(cc1(:,1)))=0; %#ok<SAGROW>
    Z2=Z1;
    for j = 1:size(cc1,1)
        Z1(cc1(j,2),cc1(j,1)) = cc1(j,3);
        Z2(cc2(j,2),cc2(j,1)) = cc2(j,3);
    end

    figure;pcolor(Z1);%title('Sample Stochastic Component');
    view(2);shading interp; colorbar;set(gca,'XTick',[],'YTick',[]);
    figure;pcolor(Z2);%title(sprintf('Estimation of Sample Stochastic
   Component \n%s',tit{i,1}));
    view(2);shading interp;colorbar;set(gca,'XTick',[],'YTick',[]);
    figure;scatter(rf(:),cv_matr{i,1}.Z(:),'filled','d');hold on;
    dvec1 = [rf(:);cv_matr{i,1}.Z(:)];
    plot([min(dvec1)-0.5,max(dvec1)+0.5],[min(dvec1)-0.5,max(dvec1)
   +0.5],'r');
    axis([min(dvec1)-0.5,max(dvec1)+0.5,min(dvec1)-0.5,max(dvec1)+0.5])
    %title('Scatter Plot')
    xlabel ('Observed Data'); ylabel ('Estimations');
    figure; h = histogram(rf(:),16,'EdgeColor',[0 0 1],'FaceAlpha',0.7);
    hold on
    histogram(cv_matr{i,1}.Z(:),'BinEdges',h.BinEdges,'EdgeColor',[0.2 1
    0]','FaceAlpha',0.7)
    %title('Histograms of Sample Stochastic Component')
    legend({'Original', 'Estimated'});
    clear h


    % Total Data figures
    cc3 = [col,row,v1(:);qcol,qrow,zeros(Nu,1)];
    cc4 = [col,row,cv_matr{i,1}.Z_ibt(:);qcol,qrow,zeros(Nu,1)];
    Z3(max(cc3(:,2)),max(cc3(:,1)))=0; %#ok<SAGROW>
    Z4=Z3;
    for j = 1:size(cc3,1)
        Z3(cc3(j,2),cc3(j,1)) = cc3(j,3);
```

```
        Z4(cc4(j,2),cc4(j,1)) = cc4(j,3);
    end
%     figure;pcolor(Z3);view(2);shading interp; %title('Original Sample
    ');
%     c = colorbar; c.Label.String = 'Normalised Velocity';set(gca,'
    XTick',[],'YTick',[]);
    figure;pcolor(Z4);view(2);shading interp; %title(sprintf('Estimation
     of Original Sample \n%s',tit{i,1}));
    c = colorbar; c.Label.String = 'Normalised Velocity';set(gca,'XTick'
    ,[],'YTick',[]);
    figure;scatter(v1(:),cv_matr{i,1}.Z_ibt(:),'filled','d');hold on;
    dvec2 = [v1(:);cv_matr{i,1}.Z_ibt(:)];
    plot([min(dvec2)-0.5,max(dvec2)+0.5],[min(dvec2)-0.5,max(dvec2)
    +0.5],'r');
    axis([min(dvec2)-0.5,max(dvec2)+0.5,min(dvec2)-0.5,max(dvec2)+0.5])
    %title('Scatter Plot')
    xlabel ('Observed Data')
    ylabel ('Estimations')
    figure;h = histogram(v1(:),16,'EdgeColor',[0 0 1],'FaceAlpha',0.7);
    hold on
    histogram(cv_matr{i,1}.Z_ibt(:),'BinEdges',h.BinEdges,'EdgeColor'
    ,[0.2 1 0],'FaceAlpha',0.7)
    %title('Histograms of Sample Data')
    legend({'Original', 'Estimated'});
    clear h

    clear Z1 Z2 Z3 Z4 dvec1 dvec2

end



% >>> Ordinary Kriging <<<

% Sort models based on cross validation scores
[~,ind] = sort(table2array(cv_Stf(:,7)),'descend');

% Matrices and Cells preallocation
Z{N_kr_mod,1}=[]; Z_error{N_kr_mod,1}=[];kr_checks{N_kr_mod,1}=[];
kr_matr{N_kr_mod,1}=[];
kr_Ss(N_kr_mod,6)= 0; table_r2{N_kr_mod,1} = [];
CI1{N_kr_mod,1}=[];UNC{N_kr_mod,1}=[];

% Inputs definition
```

```
x = x_tr; y = y_tr; xu = qx_tr; yu = qy_tr; iso=1;

% Ordinary Kriging
for i=1:N_kr_mod
    model.function = models{ind(i),1};
    model.params = bmodel2{ind(i),1};
    model.r_ok = [mean(rx_tr(:))/5,mean(ry_tr(:))/5];

    [Z{i,1},Z_error{i,1},kr_checks{i,1}, kr_matr{i,1}] =...
        ordkrig(x,y,rf,xu,yu,iso,model);
    kr_Ss(i,:) = correlstats(Z{i,1},qfluc);
    table_r2{i,1} = table_r{ind(i),1};

    %Confidence Intervals (95%)
    CI1{i,1}.low = Z{i,1} - 1.96*sqrt(Z_error{i,1});
    CI1{i,1}.up = Z{i,1} + 1.96*sqrt(Z_error{i,1});
    CI1{i,1}.uncer = 1.96*sqrt(Z_error{i,1});
    UNC{i,1} = real(CI1{i,1}.uncer);
    realCI(i,1) = isreal(CI1{i,1}.uncer); %#ok<SAGROW>
end

% Kriging Scores
relMSE = kr_Ss(:,3)/min(kr_Ss(:,3)); %relative MSE
FinalScore = ((1./relMSE).^2).*kr_Ss(:,5).*kr_Ss(:,6); %finalscore
kr_Ss = [kr_Ss, FinalScore];
kr_Ssf = array2table(kr_Ss,'VariableNames',table_h,'RowNames',table_r2);
clear relMSE FinalScore

%Trend addition and Boxcox Inversion
kr_St(N_kr_mod,6)= 0; Z_tr{N_kr_mod,1} = 0;
Z_ibt1{N_kr_mod,1} = 0;Z_ibt{N_kr_mod,1} = 0;
for i=1:N_kr_mod

    Z_tr{i,1} = qMx + Z{i,1};

    if lambda==00
        Z_ibt1{i,1} = Z_tr{i,1};
    elseif lambda==0
        Z_ibt1{i,1} = exp(Z_tr{i,1});
    else
        Z_ibt1{i,1} = (lambda*Z_tr{i,1} + 1).^(1/lambda);
    end
    Z_ibt{i,1} = real(Z_ibt1{i,1});
    kr_realZ(i,1) = isreal(Z_ibt1{i,1});  %#ok<SAGROW>
```

```
    kr_St(i,:) = correlstats(qv,Z_ibt{i,1});%total kriging scores

end

% Total Kriging Scores
relMSE = kr_St(:,3)/min(kr_St(:,3)); %relative MSE
FinalScore = ((1./relMSE).^2).*kr_St(:,5).*kr_St(:,6); %finalscore
kr_St = [kr_St, FinalScore];
kr_Stf = array2table(kr_St,'VariableNames',table_h,'RowNames',table_r2);
clear relMSE FinalScore

%Plots
for i=1:N_kr_mod

    % Stochastic Component's figures
    cc1 = [col,row,rf(:);qcol,qrow,qfluc(:)];
    cc2 = [col,row,rf(:);qcol,qrow,Z{i,1}];
    Z1(max(cc1(:,2)),max(cc1(:,1)))=0; %#ok<SAGROW>
    Z2=Z1;
    for j = 1:size(cc1,1)
        Z1(cc1(j,2),cc1(j,1)) = cc1(j,3);
        Z2(cc2(j,2),cc2(j,1)) = cc2(j,3);
    end
    figure;pcolor(Z1);%title('Original Stochastic Component');
    view(2);shading interp; colorbar;set(gca,'XTick',[],'YTick',[]);
    figure;pcolor(Z2); %title(sprintf('Estimation of Stochastic
   Component \n%s',tit{ind(i),1}));
    view(2);shading interp; colorbar;set(gca,'XTick',[],'YTick',[]);
    figure;scatter(qfluc(:),Z{i,1}(:),'filled','d');hold on;
    dvec1 = [qfluc(:);Z{i,1}(:)];
    plot([min(dvec1)-0.5,max(dvec1)+0.5],[min(dvec1)-0.5,max(dvec1)
   +0.5],'r');
    axis([min(dvec1)-0.5,max(dvec1)+0.5,min(dvec1)-0.5,max(dvec1)+0.5])
    %title('Scatter Plot')
    xlabel ('Observed Data')
    ylabel ('Estimations')
    figure;h = histogram(qfluc(:),16,'FaceColor',[0 0 1],'FaceAlpha'
   ,0.7);
    hold on
    histogram(Z{i,1}(:),'BinEdges',h.BinEdges,'FaceColor',[0.2 1 0],'
   FaceAlpha',0.7)
    %title('Histograms of Stochastic Component')
    legend({'Original', 'Estimated'});
```

```
    clear h

    % Total Data figures
    cc3 = [col,row,v1(:);qcol,qrow,Z_ibt{i,1}];
    cc4 = [col,row,zeros(size(col,1),1); qcol,qrow,UNC{i,1}];
    Z3(max(cc3(:,2)),max(cc3(:,1)))=0; %#ok<SAGROW>
    Z4=Z3;
    for j = 1:size(cc3,1)
        Z3(cc3(j,2),cc3(j,1)) = cc3(j,3);
        Z4(cc4(j,2),cc4(j,1)) = cc4(j,3);
    end
    figure;pcolor(Z3); view(2);shading interp; %title(sprintf('
    Estimation of Original Data \n%s',tit{ind(i),1}));
    c = colorbar; c.Label.String = 'Normalised Velocity';set(gca,'XTick'
    ,[],'YTick',[]);
    figure;scatter(qv1(:),Z_ibt{i,1}(:),'filled','d');hold on;
    dvec2 = [qv1(:);Z_ibt{i,1}(:)];
    plot([min(dvec2)-0.5,max(dvec2)+0.5],[min(dvec2)-0.5,max(dvec2)
    +0.5],'r');
    axis([min(dvec2)-0.5,max(dvec2)+0.5,min(dvec2)-0.5,max(dvec2)+0.5])
    %title('Scatter Plot')
    xlabel ('Observed Data')
    ylabel ('Estimations')
    figure;h = histogram(qv1(:),16,'FaceColor',[0 0 1],'FaceAlpha',0.7);
    hold on
    histogram(Z_ibt{i,1}(:),'BinEdges',h.BinEdges,'FaceColor',[0.2 1 0],
    'FaceAlpha',0.7)
    %title('Histograms of Data')
    legend({'Original', 'Estimated'});
    figure;pcolor(Z4); view(2);shading interp; %title('95% Confidence
    Interval');
    c1 = colorbar; c1.Label.String = 'Normalised Velocity'; set(gca,'
    XTick',[],'YTick',[]);
    clear h

    clear cc1 cc2 cc3 cc4 Z1 Z2 Z3 Z4 dvec1 dvec2

end

% >>>Correlation Coefficient of Indicators<<<
edges4 = (1500:4000/4:5500)/5500;
[~,~,ind_data4] = histcounts(qv1,edges4);
ind4_est{N_kr_mod,1}=[];Rpearson4(N_kr_mod,1)=0;Rspearman4(N_kr_mod,1)
    =0;
```

```
MCR4(N_kr_mod,1)=0;

edges16 = (1500:4000/16:5500)/5500;
[~,~,ind_data16] = histcounts(qv1,edges16);
ind16_est{N_kr_mod,1}=[];Rpearson16(N_kr_mod,1)=0;Rspearman16(N_kr_mod
    ,1)=0;
MCR16(N_kr_mod,1)=0;

for i=1:N_kr_mod
    [~,~,ind4_est{i,1}] = histcounts(Z_ibt{i,1},edges4);
    ind4_est{i,1}(Z_ibt{i,1}<=edges4(1)) = 1;
    ind4_est{i,1}(Z_ibt{i,1}>=edges4(end)) = length(edges4)-1;
    Rpearson4(i,1) = corr(ind4_est{i,1},ind_data4);
    Rspearman4(i,1) = corr(ind4_est{i,1},ind_data4,'type','Spearman');
    MCR4(i,1) = sum(ind4_est{i,1}~=ind_data4)/Nu;

    [~,~,ind16_est{i,1}] = histcounts(Z_ibt{i,1},edges16);
    ind16_est{i,1}(Z_ibt{i,1}<=edges16(1)) = 1;
    ind16_est{i,1}(Z_ibt{i,1}>=edges16(end)) = length(edges16)-1;
    Rpearson16(i,1) = corr(ind16_est{i,1},ind_data16);
    Rspearman16(i,1) = corr(ind16_est{i,1},ind_data16,'type','Spearman')
    ;
    MCR16(i,1) = sum(ind16_est{i,1}~=ind_data16)/Nu;
end

% Kriging Indicators Scores Table
table_h = {'MeanAbsErr','MaxAbsErr','MSE','RMSE','Rpearson','Rspearman'
    };
table_h2 = {'MeanAbsErr','MaxAbsErr','MSE','RMSE','Rpearson','Rspearman'
    ,'Rpearson4','Rspearman4','MCR4','Rpearson16','Rspearman16','MCR16'
    ,};
kr_iSsf = array2table(kr_Ss(:,1:end-1),'VariableNames',table_h,'RowNames
    ',table_r2);
kr_iStf = array2table([kr_St(:,1:end-1),Rpearson4,Rspearman4,MCR4,
    Rpearson16,Rspearman16,MCR16],'VariableNames',table_h2,'RowNames',
    table_r2);
%
    ============================================================================
```